Vol. 17 • No. 2 • October 2023

JOURNAL OF GEOMATICS

ISSN: 0976 - 1330

An official publication of Indian Society of Geomatics

Journal of Geomatics

(A publication of the Indian Society of Geomatics)

Editorial Board

Advisory Board

Indian Society of Geomatics
Executive Council 2023-2026

Secretary: (address for correspondence)
4117, Space Applications Centre, ISRO, Ahmedabad-380058, India
Email: secretary@isgindia.org; cpsingh@sac.isro.gov.in

Journal of Geomatics

(A Publication of the Indian Society of Geomatics)

Vol. 17. No. 2 Research articles October 2023

Journal of Geomatics Vol. 17, No. 2, October 2023

Site Suitability Assessment for Petroleum hubs and Oil retail assets in the Jomoro District: A Hybrid Approach using Fuzzy AHP and VIKOR Method

D. Asenso-Gyambibi[1], Joseph Agyei Danquah[1], E. K. Larbi[1], N. Lamkai Quaye-Ballard[1], M.S. Peprah[2], B. Asamoah Asante[1], E.A Asamoah[1]
[1]Geo-Informatics Division, Building and Road Research Institute (CSIR-BRRI), Kumasi, Ghana
[2]IHTMOC Consulting Company Ltd, Kumasi, Ghana
*Email: edlarbi90@gmail.com

(Received: 17 November 2022; in final form 31 August 2023)

DOI- *https://doi.org/10.58825/jog.2023.17.2.59*

Abstract: The importance of petroleum infrastructure is undeniable in the face of both local and global energy needs. However, incidents such as explosions originating from these facilities often lead to tragic consequences, including the loss of life and property in nearby communities. This situation has raised significant concerns among government officials and citizens alike. This situation calls for a comprehensive study to identify tangible strategies for reducing the associated risks. Unlawful siting of oil refineries, petrochemical facilities, berthing terminals, pipelines, storage terminals, and oil and gas retail assets stems from a failure to evaluate the environmental impact on a growing human population, consumer competition, and a failure to enforce energy standards. The study aims to employ a multifaceted approach comprising of suitability, proximity and spatial statistical analysis in assessing viable areas for developing petroleum hubs in the district. Through validation using newly acquired land for petroleum hub and existing filling stations in the study area. This study investigated the efficiency of the method and level of adherence to established protocols by the Ministry of Energy, Environmental Protection Agency (EPA), and Town and Country Planning Department. The study relied on both primary and secondary data. The basic data set consists of the positions of filling stations as determined by the Garmin handheld GPS and the measured land border. The secondary data was gathered from Ghana's Land Commission's Survey and Mapping section. It consists of topographic data, geology, and pedology from which the area's soil types, lithology, road networks, terrain slope, water bodies and land use elements were extracted and utilised. Using Fuzzy AHP and VIKOR, the dataset was categorised and weighted. Spatial evaluations were performed using ArcGIS software to identify regions suitable or unsuitable for the placement of petroleum hubs in the research area. Results shows 67.44% of the area are highly suitable for establishment of petroleum hubs, 32.33% of the area falls within moderate suitability zones whereas the least suitability zones occupied 0.23% of the total area. The newly acquired government land for the petroleum hub project fell within the highly suitable zone confirming the validity of the studies in comparison with studies from field experts via environmental impact assessment. The proposed petroleum hub covered areas dominated by very high and high area suitability for its establishment constituting 75.9 km^2 (90.3%) of its entire area whereas the moderate suitability zones constituted 8.2 km^2 (9.7%) of the remaining areas. Towns situated in very high areas includes; Bakakole Nkwanta, Ahobre, Nawule, Allowule, Tikobo No.1, Edu, Damofu, Ave lenu and Ebonloa, Mpatabo. High areas comprises of Kengen Kpokezo, Alenda wharf, Tekyinta. Anwonakrom, Nkwamta, Elubo and Agege are among the moderate and low area zones for hub and oil retail assets establishment. 75% of the oil retail assets complied with the established protocols whiles 25% defaulted. The combination of GIS methodologies and multi-criteria decision analyses has proven to be an efficient method for highlighting acceptable areas for petroleum hubs, oil retail assets, and determining high-risk areas for adequate area planning. It is proposed that authorities and stakeholders implement efforts to educate, assess site suitability, and enforce specified standards in the construction of petroleum infrastructure.

Keywords: Multi-criteria decision analysis, petroleum infrastructure, Fuzzy AHP, VIKOR, petroleum hubs, oil retail assets

1. Introduction

Africa is endowed with large amounts of both fossil and renewable energy resources, with significant new oil and gas finds (Bank, 2009). Over the last 20 years, Africa's oil reserves have increased by more than 25%, with an expected growth rate of 6% per year. Africa's abundant oil reserves and the potential for future discoveries have positioned the continent as a significant contributor to global oil production and resource extraction (Bank, 2009). Recent years have witnessed more issues on licenses and unlawful siting of oil and gas infrastructure (Aslani and Alesheikh, 2011). The regular news of fuel explosions in the Republic of Ghana, as well as the resulting loss of life, property, and assets, necessitate quick involvement by the government, geospatial specialists, and numerous stakeholders in the energy industry (Peprah et al., 2018). The increasing number of petroleum hubs and oil retail assets operating along important roadways and habitat areas in several growing countries, like Ghana, necessitates the necessity to supervise and manage such activities in the country (Uzochukwu et al., 2018). As the human population grows, so does the number of vehicles on the road, resulting in increased demand for fuel (Njoku and Alagbe, 2015).

This creates the need for the establishment of petroleum hubs and fueling services within the communities. Furthermore, the use of natural gas for commercial and home reasons is increasing, making it critical to build a petroleum trading hub in order to assure national energy security (Xiaoguang et al., 2015). Petroleum trading hubs

are increasingly being established due to their pivotal role in transmitting price signals, facilitating price reductions, reducing import price premiums, and securing pricing power for both petroleum and natural gas (Xiaoguang et al., 2015).

In semi-urban environments such as the one under consideration, the indiscriminate placement of petroleum hubs and oil retail assets causes traffic disruptions due to insufficient parking space for tankers during product offloading, hampered vehicle accessibility, rampant parking along the station. Also, commercial activities in and around the vicinity, explosions from highly flammable products and fuel tankers along the way, pollution of underground and surface water (Njoku and Alagbe, 2015). The sustainability of fuel supply is critical in ensuring a country's energy security, the location of environmentally sensitive commercial and service activities in rural or urban areas needs to be guided by standards enforced by government and non-governmental organizations (Tah, 2017; Xiaoguang et al., 2015).

In Ghana, the permit required to operate petroleum hubs and oil retail assets is usually obtained from the Ministry of Energy, Environmental Protection Agency (EPA), Town and Country Planning Department (Peprah et al., 2018). However, some operators fail to get permits from these agencies before launching commercial initiatives, possibly to avoid paying the needed costs. According to literature, there have been multiple reported occurrences of wildfires and explosions related with filling stations in Ghana, resulting in countless deaths and millions of dollars in annual losses (Addai et al., 2016; Norman et al., 2015). In most urban areas in Ghana, poor planning and disregard for planning norms have resulted in illegal land use and slum development, as well as the placement of oil and gas assets in hazardous regions (Kusimi and Appati, 2012).

Because everyone is concerned about their health, safety, and protection, there is a need to conduct a site appropriateness assessment before doing these activities in the spatial context of the research area. Site suitability assessments encompass both qualitative and quantitative evaluations. Qualitative assessments involve the consideration of factors such as climate, drainage, topography, vegetation, geology, and soil properties. In contrast, quantitative evaluations provide more detailed and statistically estimated results. (Mosleh et al., 2017). Geographic Information Systems (GIS) have proven to be highly valuable in addressing geospatially connected issues that encompass both qualitative and quantitative data (Guler and Yomralioglu, 2017; Njoku and Alagbe, 2015). (Boolean logic, Weighted Linear Combination (WLC), Weighted Overlay (WO), Storie and Square root, Multiple Linear Regression models, Multivariate statistics) and other parametric methods are among the traditional methods frequently employed in site appropriateness (Ghanbarie et al., 2016; Mugiyo et al., 2021).

Except for the WLC and qualitative approaches, category data is limited in most traditional methodologies (Mugiyo et al., 2021). The fluctuation in the geo-environmental parameters can affect the accuracy of the site suitability maps in the traditional approach, which ignores the continuous nature of site occurrence, resulting in site misclassification, discrete and sharply defined boundaries. Furthermore, the usual approach is time-consuming and expensive (Behrens and Scholten, 2006; Taghizadeh et al., 2020). Also, numerous studies have employed spatial layers and decision-making algorithms to determine site suitability.

These techniques include; the Analytical Hierarchy Process (AHP), Technique for Order of Preference by Similarity to Ideal Solution (TOPSIS), and Weighted Overlay Analysis (Rahman et al.2021; Peprah et al., 2018; Jozaghi et al., 2018). Modern approaches such as machine learning (ML) based methods; (Random Forest(RF), Artificial Neural Networks (ANN), Logistic Regression (LR), Naïve Bayes classifier, Support Vector Machines(SVM)) and multi-criteria decision methods (MCDM) such as (Analytical Hierarchy Process (AHP), Elimination and Choice Expressing Reality (ELECTRE), Grey Relational Analysis (GRA) and Vlsekriterijumsko Kompromisno Rangiranje (VIKOR)) are gaining ground on traditional ways (Danvi et al., 2016; Mugiyo et al., 2021). In a study conducted by Taghizadeh et al. in 2020 on land suitability assessment for sustainable agricultural production, machine learning-based methods, specifically Random Forest (RF) and Support Vector Machine (SVM), outperformed traditional parametric land suitability maps. The ML-based maps demonstrated significantly higher Kappa index scores and overall accuracy, with values of 0.77 and 0.79 for RF and 0.69 and 0.73 for SVM, compared to the values of 0.45 and 0.50 for traditional parametric maps. This highlights the superior performance of ML-based approaches in land suitability assessment.

Based on the kappa index's specified class limitations; it was concluded that modern based methods for site suitability assessment have stronger levels of accuracy compared to traditional suitability assessment methods. Multi-criteria Decision Methods (MCDM) and Geographic Information Systems (GIS) are extremely important tools for solving spatial problems from the evaluation of decision variables (Peprah et al., 2018). When more than one MCDM approach (Fuzzy AHP and VIKOR) are used to construct a merged evaluation system in site suitability assessment, approximations of unclear, partial, and uncertain information observed in separate decision making methods are possible (Fazlollahtabar et al., 2009). Furthermore, rather than being discrete as in the classic Boolean approach, site suitability will be defined as continuous classes (Mugiyo et al., 2021).

The merging of fuzzy AHP with the VIKOR approach for site suitability analysis is an attempt to fill a gap in this regard. While both strategies have been employed alone, they must be combined to overcome the limits of each. A detailed assessment can be achieved from the merging of these methodologies, especially when data is partial or uncertain (Kumi-Boateng et al., 2020). GIS and MCDM procedures can give better appropriateness analysis than independent parametric approaches because they can accept attribute values and features near category

boundaries based on their respective importance to get the optimal selection (Broekhuizen et al., 2015; Kihoro et al., 2013). Furthermore, MCDM may judge both qualitative and quantitative criteria (Boroushaki and Malczewski, 2008). Furthermore, it is straightforward to grasp, simple to apply and adapt, and appropriate for problems with a hierarchical framework (Aslani and Alesheikh, 2011). GIS and MCDM has been applied in solving majority of problems in geo-scientific disciplines. Oil and gas station placement (Aslani and Alesheikh, 2011; Njoku and Alagbe, 2015; Tah, 2017), and forest risk mapping (Akay and Erdogan, 2017) are two examples. Selection of optimal rice-growing sites (Kihoro et al., 2013), landfill site selection (Guler and Yomralioglu, 2017), and planning of forest product primer transportation (Akay and Yilmaz, 2017).

Because numerous choice variables can be evaluated and weighted, multi-criteria decision methods (MCDM) and geographic information systems (GIS) are extremely effective tools for solving problems in a spatial context. Hence, MCDM and GIS techniques were adopted in the present study. The study aims to employ a hybrid approach of an MCDM technique comprising of Fuzzy AHP and VIKOR to investigate whether the newly proposed land for the development of the Ghana petroleum hub falls within a suitable area as well as provide locations of viable zones for future establishment of petroleum hubs and oil retail assets in the district.

Also, the study is to determine whether the oil and gas operators in Jomoro district adhere to the requirements established by Ghana's Ministry of Energy and Town and Country Planning Department for validation purposes. In addition, assess the spatial distribution pattern of current oil retail assets. This study will assist authorities in taking the right actions on existing filling stations that have not met the requirements set by Ghana's Ministry of Energy and Environmental Protection Agency (EPA). It will make it easier for the Town and Country Planning Department to verify and execute siting regulations for those yet to be built. Furthermore, due to limited literature on the subject, It will thus serve as a reference for future study and decision making for individuals, and all petroleum stakeholders (Njoku and Alagbe, 2015).

2. Study area

The research area is situated in Ghana's Western Region, encompassing latitudes 04° 80' N to 05° 21' N and longitudes 02° 35' W to 03° 07' W, as outlined by Andoh and Offei-Addo in 2014. The district's capital city is Half Assini. It shares its borders with Wassa-Amenfi and Aowin-Suaman to the north, Nzema East District to the east, La Côte D'Ivoire to the west, and the Gulf of Guinea to the south.

The district spans a total land area of 1,495 square kilometers, accounting for approximately 5.6 percent of the entire area of Ghana's Western Region (Ghana districts, 2013). The District's south-central region has rolling granite topography with several steep-sided tiny round hills reaching from 200 to 600 meters (Andoh and Offei-Addo, 2014). The relief is lower along the shore, with flat highland parts and plunging lowlands. There are formations of highland ridges running northwest to southeast from Tano to Bonyere and finishing on its northern side in the Nawulley scarp (Andoh and Offei-Addo, 2014).

The district can be categorized into five distinct geological formations: Lower Birimian, Upper Birimian, Granite Tertiary Sands, and Coastal Sands. The Lower Birimian is primarily composed of phyllites with injected quartz veins, while the Upper Birimian is characterized by volcanic rocks with limited amounts of phyllites. Notably, there are substantial deposits of limestone in Nawulley and significant reserves of Kaolin in areas like Bawia, Nvellenu, and Tikobo No. 2. Of significant economic importance is the discovery and development of oil and gas in the Tano Basin off the coast of Jomoro (Ackah et al. in 2018).

The current vegetation includes a forest reserve in Ankasa, which is recognized for its dense forest cover. The district also features designated fallow lands, tree crop areas, and farms or plantations (Damnyag et al. 2013). Additionally, there are extensive sections of swampy woodlands that are less utilized for farming due to their consistently wet conditions throughout the year.

Regarding climate, the district experiences substantial rainfall, occurring in two distinct wet seasons, coupled with consistently high temperatures. The climate is described as Equatorial Monsoon, with rains caused by low pressure zones over the Sahara that attract winds from the south of the Equator (Jomoro District Assembly, 2010). The monthly mean recorded temperature is 26 degrees Celsius. Relative humidity is also very high across the district, reaching 90% at night and falling to 75% as the temperature increases in the afternoon. The map in Figure 1 depicts the Jomoro district.

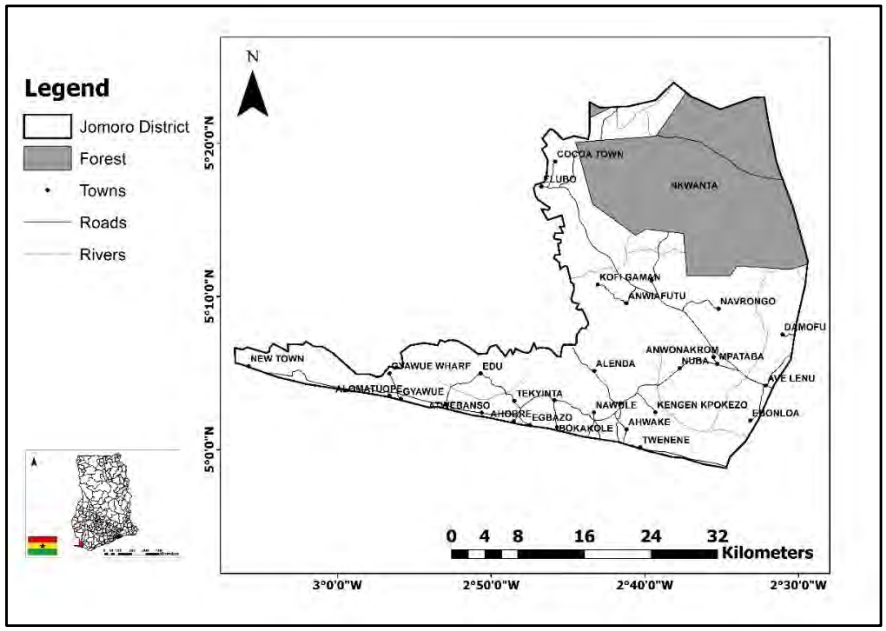

Figure 1. Map of the Study area

3. Resources and Approach

3.1 Resources

The study's input set includes both primary and secondary sources. The existing locations (Garmin Handheld GPS) of the filling stations formed the primary set, while the secondary set (topographic maps containing features such as contours, vegetation, roads, soil types, and water bodies) obtained from the Land Commission of Ghana's Survey and Mapping Division, Geological and Mineral Department of Ghana. The earth explorer website (https://earthexplorer.usgs.gov) was used to download the land use and land cover data (LULC). These characteristics were utilized as spatial criteria for determining site suitability. Table 1 shows a list of the data that was used and its repository. Table 2 depicts a selected set of the existing filling stations.

3.2 Methods

3.2.1 Field data collection

A preliminary inspection was conducted to investigate the area around the stations and to establish the best procedures to use for the survey. The government proposed land for the establishment of the petroleum hub in the study area was surveyed using static Trimble GPS. This was to determine its boundary location and area. Garmin Handheld GPS receivers were used to map the positions of the filling stations in the study region. Geographic features in each station's immediate vicinity were measured and documented. Green areas proximities, pump station to road proximity, filling stations perimeters, neighbouring stations proximities, and proximities of public facilities were all measured.

Table 1. Inputs and Repository

Inputs Used	Repository
1.Land Use and Land Cover (LULC)	https://earthexplorer.usgs.gov.
2.Geological and Soil data	Geological and Mineral Department of Ghana
3.Digital Elevation Model (DEM)	https://lpdaac.usgs.gov/product/astgtmv003/
4.Linear features (roads, rivers)	Survey and Mapping Division of Ghana

Table 2. A sample location of the fueling stations (meter units)

ID	Eastings (m)	Northings (m)	Fueling stations	Locations
1	550407	561170	JD station	Ave lenu
2	535141	559235	Petrol station	Tikobo No.1
3	528029	583824	Shell	Elubo
4	526481	584544	Blanko oil	Elubo
5	525863	584441	Pacific	Elubo
6	525246	584503	Total	Elubo
7	531073	556334	APCO	Nawule
8	513398	558178	Goil	Half Assini

3.2.2 Proximity analysis

In the ArcGIS environment, buffer assessments of fuel pump length to road, gap between neighboring stations, and distance between stations to any state facilities were performed. This was done to ensure that the stations met the standards stipulated by the Ministry of Energy and the Town and Country Planning Department. Filling stations that fell beyond the prescribed buffer limits met the standards and will offer less of a risk to the environment, but those that fell inside the defined buffer are projected to cause environmental risk, particularly in settlement areas (Njoku and Alagbe, 2015). The set guide for the pump stations and roadways gap is at least 100 m, so a buffer of 100 m was utilized in the ArcGIS environment. Generated buffers for the gap between filling stations, state facilities and water was at least (500 m to 1000 m) to assess the level of compliance (Peprah et al., 2018). Buffer analyses were also performed to check whether the proposed petroleum hub complied to the set standards necessary for its establishment. A distance-based analysis was performed to evaluate the spatial link between the filling stations and their neighboring characteristics. It also allowed spatial features that met the stated criteria to be categorized depending on distance (Aslani and Alesheikh, 2011; Peprah et al., 2018; Tah, 2017). Table 3 shows the criteria for selecting appropriateness.

3.2.3 Model generation

The approach employed in this study involves a weighted overlay of six thematic layers, which were derived from both the Survey and Mapping division and remotely sensed data. The resolution of these scores was achieved through the use of Fuzzy Analytic Hierarchy Process (AHP) and VIKOR methods. Initially, Fuzzy AHP was used to estimate the weights, and subsequently, the final weights were derived from the VIKOR method. Each parameter was ranked based on its relative importance, determined through the compromise solution offered by the VIKOR method. The Suitability and Proximity model was executed within the ArcGIS environment, following (Equation 1) as defined in Peprah et al. (2018). Figure 2 provides a visual representation of the methodology, illustrating the steps taken to generate suitability zones and validate the data.

$$S = \sum_{i=1}^{n} W_i C_i \prod_{j=1}^{n} p_j \quad (1)$$

where; S = Suitability sites for oil and gas establishments; W_i = variable scores; C_i = Criteria cost; p_j = proximity.

Table 3. Proximity standards for suitability assessment (Peprah et al., 2018)

Restriction source	Min. buffer (m)/degree	Max. buffer (m)/degree	Analysis buffer(m)/ degree
Slope	0^o	20^o	$\leq 20^o$
Built up areas	500m	1000m	500m
Roads	100m	500m	100m
Surface water	100m	500m	100m

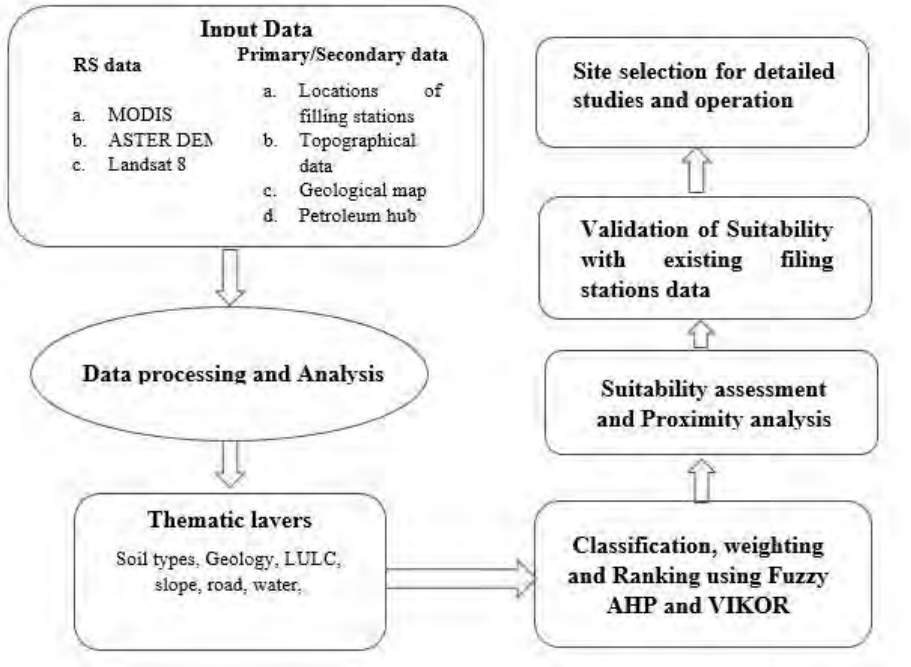

Figure 2. Flow Chart of Methods

3.2.4 Fuzzy AHP (FAHP)

The initial weights for variables were determined using Fuzzy AHP to address uncertainties and variations in judgment scales, which are common in traditional AHP. (Fazlollahtabar et al., 2009; Kumi-Boateng et al., 2020). Fuzzy AHP's computational complexity grows as the number of possibilities increases, influencing large-scale decision-making problems (Fazlollahtabar et al., 2009). The fuzzy members are represented as follows: $\tilde{q}_i = (e_{ij}, f_{ij}, g_{ij})$ and in geometric space as shown in Figure 3 (Firoozi et al., 2017). Equation (2) represents the fuzzy judgment matrix, which was created using feedback from respondents and experts (Kim et al., 2019):

$$\begin{bmatrix} (1,1,1) & (e_{12}, f_{12}, g_{12}) & \cdots & (e_{1n}, f_{1n}, g_{1n}) \\ (e_{21}, f_{21}, g_{21}) & (1,1,1) & \cdots & (e_{2n}, f_{2n}, g_{2n}) \\ (e_{n1}, f_{n1}, g_{n1}) & (e_{n2}, f_{n2}, g_{n2}) & \cdots & (1,1,1) \end{bmatrix} \quad (2)$$

Equation (3) is used to get the row geometric mean. (Kumi-Boateng et al., 2020):

$$\tilde{\sigma}_i = \left(\prod_{j-1}^{n} \tilde{q}_{ij} \right)^{\frac{1}{n}} \quad (3)$$

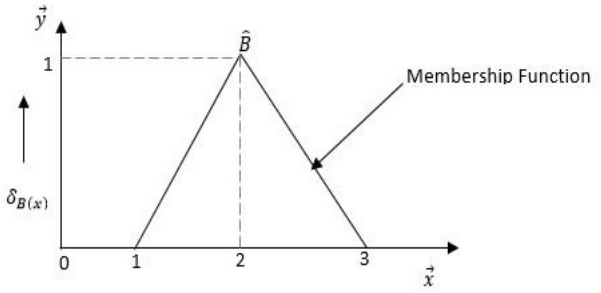

Figure 3. Triangular fuzzy membership

where; $\tilde{\sigma}_i$ = Geometric mean values, $\tilde{q}_{ij}$ = Triangular Fuzzy set, n = criteria number. The Fuzzy Geometric Mean is computed by adding the Geometric Means of each criterion as defined in Equation (4):

$$\Sigma_{i=1}^{n} \tilde{\sigma}_i = \tilde{\sigma}1 + \tilde{\sigma}2 + \tilde{\sigma}3 \cdots \tilde{\sigma}n \quad (4)$$

Normalization yields the Fuzzy weights as shown in Equation (5).:

$$\tilde{r}_{ij} = \tilde{w}_{ij} = \frac{\tilde{\sigma}i}{\Sigma_{i=1}^{n} \tilde{\sigma}i} \quad (5)$$

where; $\tilde{r}_{ij}$ = secondary variable normalized weights (option i weighted more than criterion j), $\tilde{w}_{ij}$ = main variable score. The final scores $\tilde{U}_i$ are thus determined using Eqn (6), which is represented as:

$$\tilde{U}_i = \Sigma_{i=1}^{n} \tilde{w}_{ij} \tilde{r}_{ij} \quad (6)$$

3.2.5 VIKOR

The final scores of the specified variable were generated using the VIKOR method, a well-known MCDM technique. The essence is to emphasize the ranking of alternatives sets of the conflicting criteria (Mardani et al., 2016). The VIKOR method may not be appropriate for complex problems with non-linear relationship (Rostami et al., 2010). First, the decision matrix between the criteria and alternatives is constructed using the AHP technique and the linguistic term in Table 4 given by Equation (7) (Abdullah, 2021; Akay and Erdogan, 2017).:

$$C^D = \begin{bmatrix} C_{11}^D & \cdots & C_{1y}^D \\ \vdots & \ddots & \vdots \\ C_{m1}^D & \cdots & C_{my}^D \end{bmatrix} \text{m=1,2,3…n;y=1,2,3…x} \quad (7)$$

Resolve the best and worst solution from the beneficial and non-beneficial variable as given by Equation (8) and Equation (9) respectively (Peleckis, 2022):

Best solution: $C_m^+ = (C_{my}) \max$ for beneficial criteria,

$C_m^+ = (C_{my}) \min$ for non-beneficial criteria; (8)

Worst solution: $C_m^- = (C_{my}) \min$ for beneficial criteria,

$C_m^- = (C_{my}) \max$ for non-beneficial criteria (9)

The utility S_i and regret measure R_i is calculated from Equation (10) and Equation (11) respectively (Mardani et al., 2016):

$$S_i = \sum_{y=1}^{x} \left[w_y \frac{(C_m^+ - C_{my})}{(C_m^+ - C_m^-)} \right] \quad (10)$$

$$R_i = \max_y \left[w_y \frac{(C_m^+ - C_{my})}{(C_m^+ - C_m^-)} \right] \quad (11)$$

The value of Q_i is calculated as shown in Equation(12) (Abdullah, 2021):

$$Q_i = \left[v \frac{(S_i - S^-)}{(S^+ - S^-)} \right] + \left[(1-v) \frac{(R_i - R^-)}{(R^+ - R^-)} \right] \quad (12)$$

where; $S^- = \max S_i; R^- = \max R_i (\max value)$;

$S^+ = \min S_i; R^+ = \min R_i (\min value)$; $(1-v)$ is the weight of the separate remorse, $0 \le v \le 1$

The criteria's are ranked in ascending order of Q_i based on the conditions in Equation (13) (Mardani et al., 2016);

$$\begin{cases} (Q(A_2) - Q(A_1) \ge \left(\frac{1}{(n-1)} \right) \\ (Q(A_m) - Q(A_1) < \left(\frac{1}{(n-1)} \right) \end{cases} \quad (13)$$

3.2.4 Cost criteria and Buffer Analysis

The Cost friction surface is a grid-cell-based pixel dataset established using predefined criteria. Multiple thematic maps were formed in the ArcGIS environment, utilizing these cost criteria to facilitate the identification of suitable locations. Its feasibility is contingent on various factors such as; slope, road, geological structures, soil types and rivers (Kumi-Boateng et al., 2020). For a more reliable suitability assessment, the interdependent nature of these factors needs to be considered. Six (6) main cost variables (geology, soil type, water, road, slope, land use and land cover (LULC)) were employed for the assessment. Buffer distance analysis was performed on the research area's drainage features (rivers), built-up areas, and paved surfaces (roads). This was done to establish the appropriate distance to build oil and gas structures near rivers, roadways, and settlement areas in order to avoid fires and contamination from surface runoffs. This process was undertaken to measure the level of adherence to the regulations set forth by the Ministry of Town and Country Planning, the Ministry of Energy, the Environmental Protection Agency (EPA), and the Ministry of Lands and Administration. A 100-meter analytical buffer was applied to rivers and roadways, while a 500-meter buffer zone was utilized for built-up areas. Figure 3 depicts the criteria's suitability model, while Figure 4 depicts the linear and built-up regions' proximity models.

Road buffer

The road closeness distance was measured across a 100-meter radius. This is significant since roads are a crucial factor in site appropriateness selection when accessibility is necessary. The Ghana Lands Commission's Survey and Mapping Division provided the road network. The network of roads is relevant in the transportation of oil and gas products from their production centres to their destination areas. Figure 5 represents the road proximity analysis applied in the studies.

Geology and Soil types

Geology and soil types of the area were considered and evaluated to see whether their physical and chemical properties will be suitable for siting of the petroleum infrastructure. Certain geological structures and soil types contain metallic constituents that form impurities in fuels. Furthermore, some soil types and their technical features are unsuitable for construction, which is a limitation because most filling stations have their oil reservoir in deep excavations (Peprah et al., 2018). The geology and soil data came from Ghana's Geological and Mineral Department. Figures 6 and 7 depict data on geology and soil types, respectively.

Slope

Slope is a key element in suitable site selection for petroleum hubs in decision making process. Areas of mild slopes are very suitable as compared to areas of steep slopes. This factor was considered because places of higher relief are not suitable for siting petroleum hubs due to stability and high fire risk reasons (Akay and Erdogan, 2017). The slope was formed using Aster DEM data obtained from the USGS archives (http://lpdaac.usgs.gov/products/astgtmv003/). The data has a resolution of 30 x 30 meters. Figure 8 depicts the slope of the research area.

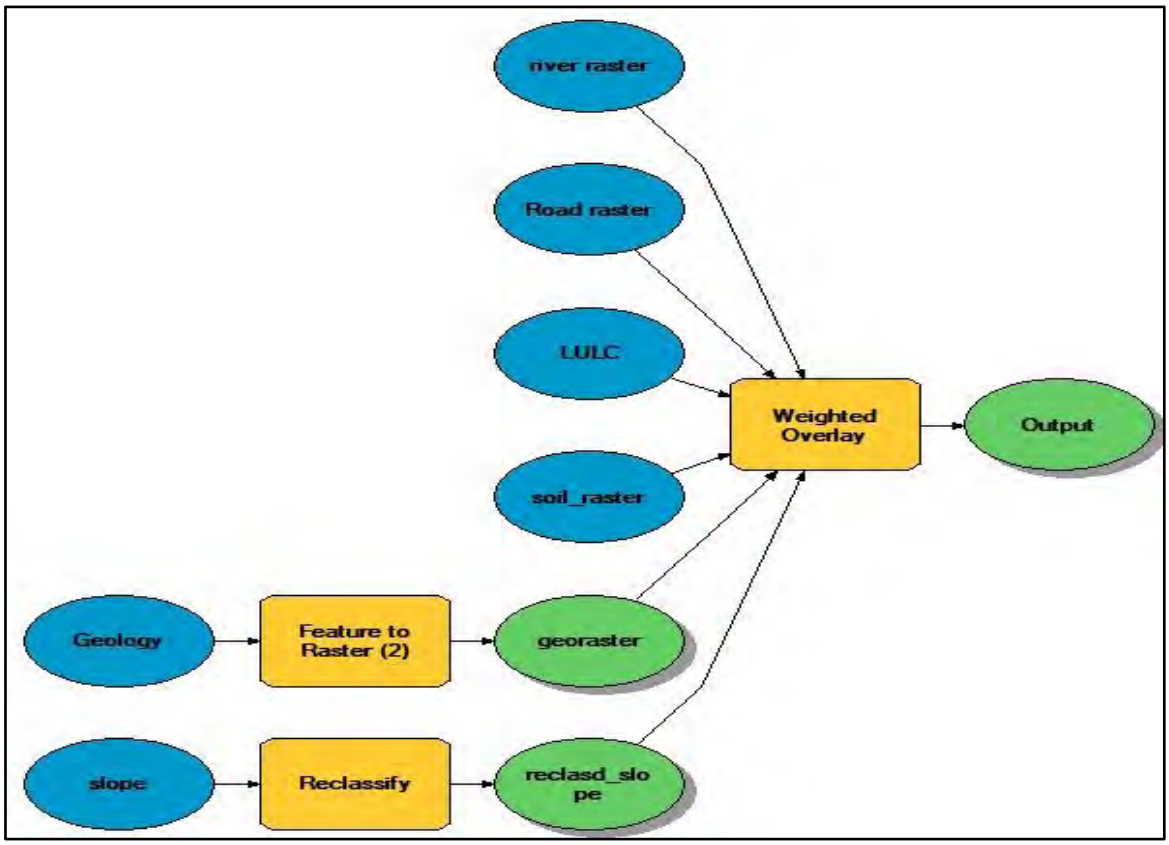

Figure 3. Suitability model

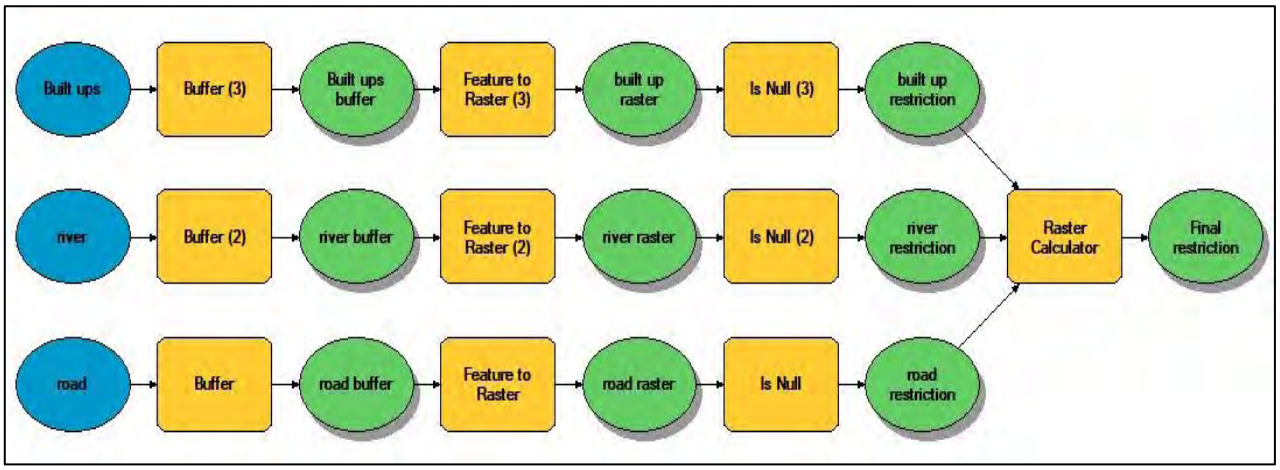

Figure 4: Restriction model

LULC

A very significant criterion to evaluate because it considers human safety, health, and settlement in the decision-making process. The land use and land cover was grouped into five (5) classes namely; dense forest, cropland, built/urban areas, barren/sparsely vegetated and water. The LULC data was gathered from MODIS satellite photography and identified using the IGBP classification scheme, which may be found at https://earthexplorer.usgs.gov. Figure 9 depicts land use and land cover data.

River buffer

Water bodies are indispensable factors to be considered in suitable site assessment. A buffer distance of 100m was established for the rivers in order to manage or avoid surface runoffs from petroleum hubs and filling stations into the water bodies in the event of rain. The river data were gathered from the Ghana Lands Commission's Survey and Mapping Division. The river proximity analysis used in the studies is depicted in Figure 10.

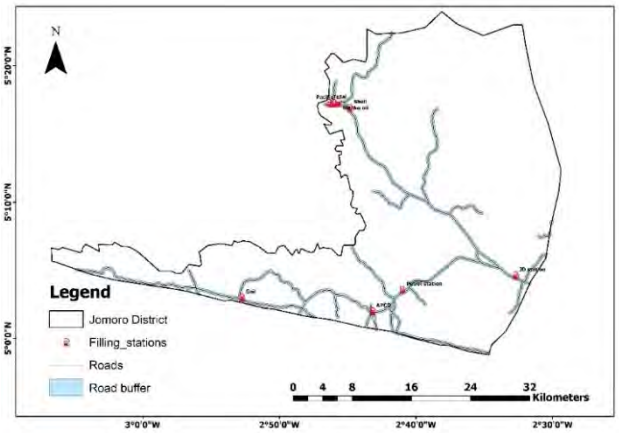

Figure 5. Road proximity analysis

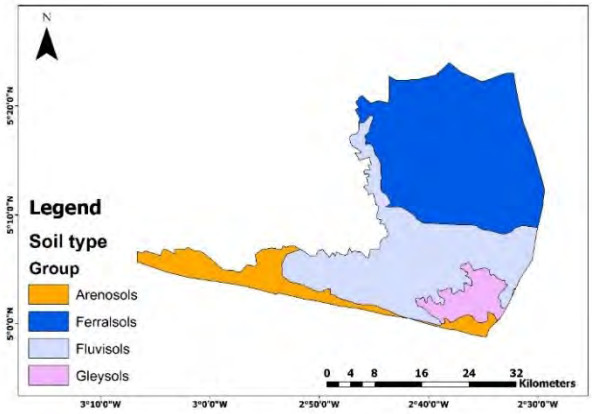

Figure 7. Soil type

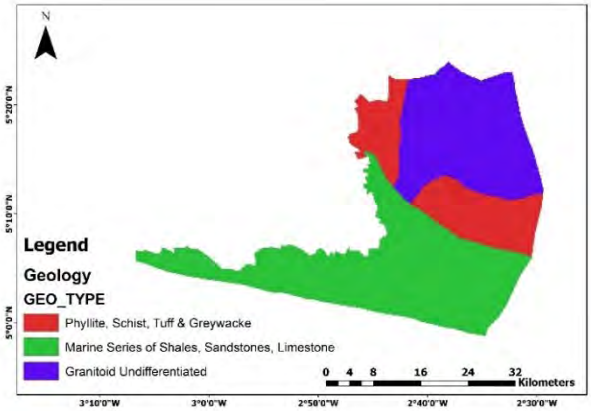

Figure 6. Geology map

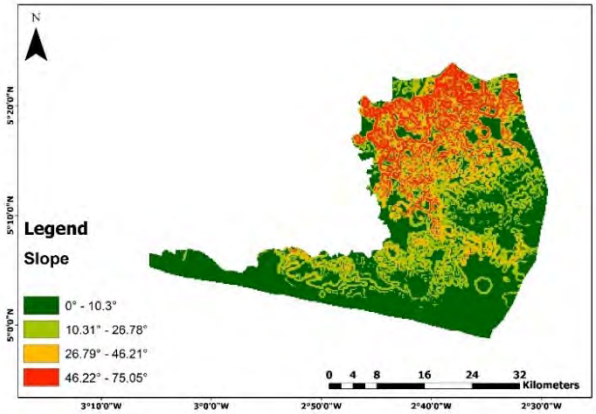

Figure 8. Slope map

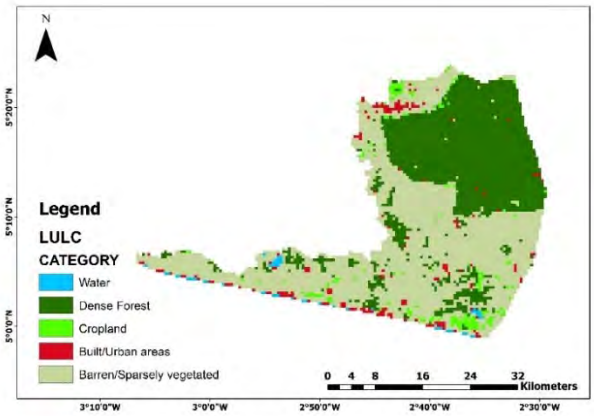

Figure 9. Land use Land cover (LULC)

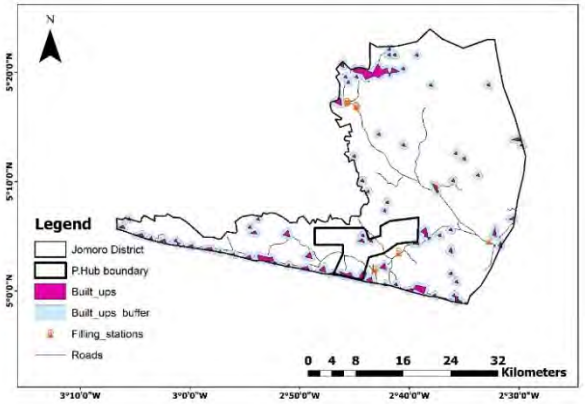

Figure 10. Built ups buffer

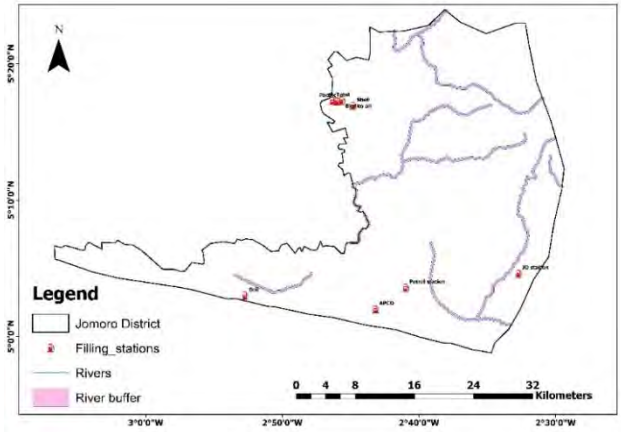

Figure 11. River proximity analysis

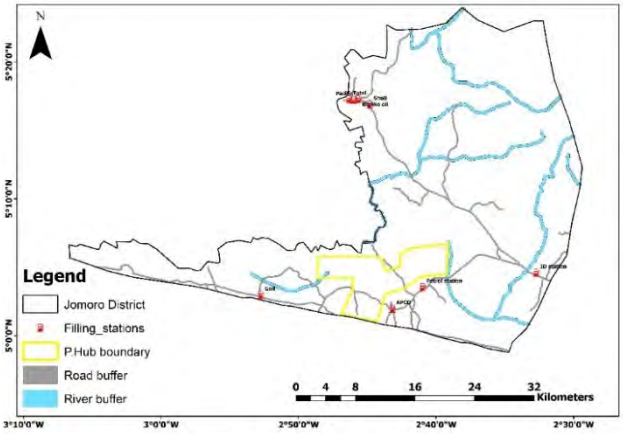

Figure 12. Proximity analysis for petroleum hub

Index Value Scoring

Index value scoring can be used to assess the relative importance of several options based on their weights. The susceptibility of observed values to ground water infiltration can also be scored and graded (Sharma et al., 2012). The Index score was computed using the scoring overlay tool within the ArcGIS environment. Table 4 displays the rating scores used for the different classes, and Table 5 presents the thematic layer categories.

4 Results and Discussions

The paper aims to perform a site suitability assessment prior to the establishment of a petroleum hub at the Jomoro district of Ghana as well as assess the suitability of the existing oil retail assets by integrating Fuzzy AHP, VIKOR, proximity analysis and remote sensing techniques in the GIS environment. The weights, selection criteria, and restriction model from Equation 1 comprise the Suitability model. Figure 2 depicts the methodological flow chart used in the research process. According to Equation 2, the initial weights were created using Fuzzy AHP from the fuzzy judgment matrix. This approach was adopted to mitigate the uncertainties and unequal judgment scales encountered in the traditional AHP, as defined in Equation 2. The decision matrix utilized in the research, as shown in Table 6, was derived from pairwise comparisons using the AHP method, ensuring a valid consistency ratio of 0. 09. This was done to eliminate any subjectivity in the cost criteria analysis. The VIKOR method was applied to determine the ultimate weights and rankings of the cost factors, taking into account the conditions set by the compromise solution as defined by Equation 12 and 13.

Table 4. Index Value Scoring (Source :(Sharma et al., 2012))

Index Score	Representation
1	Very Low
2	Low
3	Moderate
4	Moderate High
5	High
6	Very High

Table 5. Classification of Thematic layers

Variables	Classes	Rating	Representation
Roads (R_d)	1	3	Moderate
Land use and Land cover (L_u)	Cropland	3	Moderate
	Dense forest	1	Very Low
	Built/Urban areas	2	Low
	Barren/sparsely vegetated	5	High
	Water	1	Very Low
Rivers(R_i)	1	1	Very Low
Geology (G_e)	Granitoid undifferentiated	2	Low
	Marine series of shales, sandstone, limestone	1	Very Low
	Phyllite, schist, tuff, greywacke	1	Very Low
Slope (S_l)	0°- 10.3°	6	Very High
	10.31°- 26.78°	4	Moderate High
	26.79°- 46.21°	3	Moderate
	46.22°-75.05°	1	Very Low
Soil type (S_t)	Ferrasols	2	Low
	Fluvisols	4	Moderate High
	Arenosols	3	Moderate
	Gleysols	1	Very Low

The study' cost criteria include remotely sensed data, primary and secondary data received from Ghana's Survey and Mapping Division, and field data collecting. ArcGIS 10.4 software was employed to produce all the maps of the weighted alternatives. The cost criterion used in the studies include remotely sensed data as well as secondary data gathered from Ghana's Survey and Mapping Division. ArcGIS 10.4 software was used to create all maps of the weighted alternatives.

$$\begin{bmatrix} (n) & S_l & L_u & G_e & R_d & R_i & S_t \\ S_l & (1,1,1) & (1,1,1) & (1,1,1) & (1,1,1) & (1,1,1) & (1,2,3) \\ L_u & (1,1,1) & (1,1,1) & (1,1,1) & (1,2,3) & \left(\frac{1}{3},\frac{1}{2},1\right) & (1,1,1) \\ G_e & (1,1,1) & (1,2,3) & (1,1,1) & (1,2,3) & \left(\frac{1}{3},\frac{1}{2},1\right) & (1,1,1) \\ R_d & (1,1,1) & (1,1,1) & \left(\frac{1}{3},\frac{1}{2},1\right) & (1,1,1) & \left(\frac{1}{3},\frac{1}{2},1\right) & (1,1,1) \\ R_i & (1,1,1) & (1,2,3) & (1,2,3) & (1,2,3) & (1,1,1) & (1,2,3) \\ S_t & \left(\frac{1}{3},\frac{1}{2},1\right) & (1,1,1) & (1,1,1) & (1,1,1) & \left(\frac{1}{3},\frac{1}{2},1\right) & (1,2,3) \end{bmatrix} \begin{bmatrix} (n) & U & M & L & W_y \\ S_l & 1.000 & 1.122 & 1.201 & 0.181 \\ L_u & 0.833 & 1.000 & 1.201 & 0.167 \\ G_e & 0.833 & 0.891 & 1.000 & 0.149 \\ R_d & 0.833 & 0.891 & 1.000 & 0.149 \\ R_i & 1.000 & 1.587 & 2.080 & 0.262 \\ S_t & 0.693 & 0.794 & 1.000 & 0.137 \end{bmatrix}$$

where; n = criteria; U=Upper Values; M = Middle values; L= Lower values

Table 6. Decision matrix

criteria(n)	slope	LULC	geology	road	water	soil type
slope	1.0000	1.0000	1.0000	1.0000	1.0000	2.0000
LULC	1.0000	1.0000	1.0000	2.0000	0.5000	1.0000
geology	1.0000	2.0000	1.0000	2.0000	0.5000	1.0000
road	1.0000	1.0000	0.5000	1.0000	0.5000	1.0000
water	1.0000	2.0000	2.0000	2.0000	1.0000	2.0000
soil type	0.5000	1.0000	1.0000	1.0000	0.5000	1.0000
best	*0.5000*	*2.0000*	*2.0000*	*2.0000*	*0.5000*	*2.0000*
worst	*1.0000*	*1.0000*	*0.5000*	*1.0000*	*1.0000*	*1.0000*

Table 7. Calculation of unity measure, Si

criteria(n)	slope	LULC	geology	road	water	soil type	Si
slope	0.17	0.14	0.106667	0.15	0.25	0	0.8166667
LULC	0.17	0.14	0.106667	0	0	0.13	0.5466667
geology	0.17	0	0.106667	0	0	0.13	0.4066667
road	0.17	0.14	0.16	0.15	0	0.13	0.75
water	0.17	0	0	0	0.25	0	0.42
soil type	0	0.14	0.106667	0.15	0	0.13	0.5266667

Table 8. Compromise solution, ranking and weighting

Si	Ri	Qi	Rank	W_y (%)
0.81667	0.25	1	6	39
0.54667	0.17	0.27073	3 A(m)	11
0.40667	0.17	0.1	1 A(1)	4
0.75	0.17	0.51869	5	20
0.42	0.25	0.51626	4	20
0.52667	0.15	0.14634	2	6
$S_{min;}$ *(0.4067)*	$R_{min;}$ *(0.15)*	*2.552*		
$S_{max;}$ *(0.8167)*	$R_{max;}$ *(0.25)*			

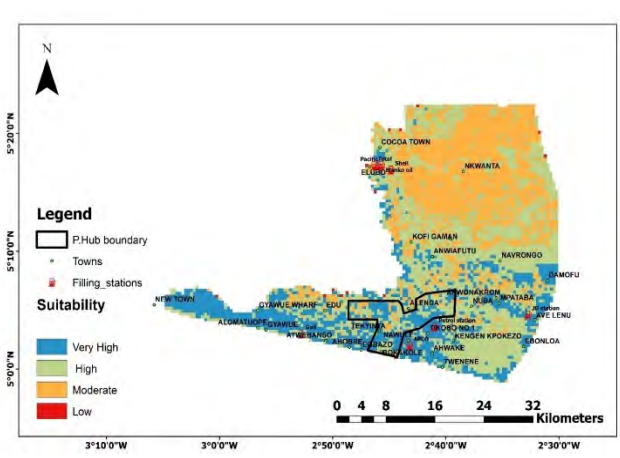

Figure 13. Suitability map

Table 9. Distance to neighbouring stations

From	To	Linear distance (km)
JD station	Petrol station	15.39
Petrol station	APCO	4.99
APCO	Goil	17.77
Total	Pacific	0.62
Pacific	Blanko oil	0.63
Blanko oil	shell	1.71

Table 10. Area and percentage coverage (Suitability)

Description	Area (Km^2)	Coverage (%)
Very High	300.521	22.90
High	584.513	44.54
Moderate	424.200	32.33
Low	3.010	0.23

The fuzzy judgment matrix is represented by Equation 2, and the Geometric mean is calculated using Equation 3. A triangular fuzzy membership function, illustrated in Figure 3, was used to define the fuzzy set, as outlined in Equation 4. The initial fuzzified weights are thus obtained from Equation 5. The VIKOR method was used for the final ranking of the alternative set. The essence is to emphasize the ranking of alternatives sets of the conflicting criteria (Mardani et al., 2016). The decision matrix utilized in the VIKOR method is specified by Equation 7 and Table 6. The best and worst solution (Equation 8 and Equation 9) is factored from the beneficial and non-beneficial criteria as shown in Table 6. The unity measure is computed using Equation 10, as shown in Table 7. The regret measure is determined through Equation 11. The values of Qi were derived from the results of the utility and regret measures, as presented in Table 7. The values of Qi are calculated as given in Equation 12. The criteria are then sorted in ascending order based on the Qi values shown in Table 8. In VIKOR, a compromised solution is proposed according to Equation 13. This is to satisfy two conditions an acceptable advantage and an acceptable stability in decision making. These conditions needs to be satisfied for the method to be valid. Six (6) main cost factors namely;

water, road, geology, slope, soil types, land use and land cover (LULC) were selected and used for mapping the suitability sites. Buffer distance analysis was performed on the research area's drainage features (rivers), built-up areas, and paved surfaces (roads). This was done to establish the appropriate distance to build oil and gas structures near rivers, roadways, and settlement areas in order to avoid fires and contamination from surface runoffs. This process was carried out to assess compliance with regulations set by the Town and Country Planning, Ministry of Energy, Environmental Protection Agency (EPA), and Ministry of Lands and Administration. The suitability and restriction models are depicted in Figure 3 and 4, respectively. Figure 6 depicts the geological nature of the research area. Figure 7 depicts the soil map of the study area, which is divided into four (4) classes: fluvisols, ferrasols, gleysols, and arenosols. The slope analysis is given by Figure 8. Areas of mild slopes are very suitable as compared to areas of steep slopes. Previous studies show areas with steep slopes have a high risk of fire spread compared to areas with gentle slopes. The land use and land cover was grouped into five (5) classes namely; dense forest, cropland, built/urban areas, barren/sparsely vegetated and water as shown in Figure 9. The classification of the various thematic layers and index scores are tabulated in Table 5. Figures 5, 10, 11 and 12 shows the proximity analysis carried out in the study area. Figure 5 represents road proximity analysis which is the distance of the pump station to the roads. All oil retail assets were found sited along the major highway. All stations fell outside the 100m buffer zone implying stations complied to the set standards by the Ministry of Energy with regard to roads. APCO filling station recorded 129m distance to the road which is the closest station to the road whiles JD station recorded the farthest distance of about 329m. The river buffer analysis is demonstrated in Figure 11. In the analysis, it was observed all available stations were sited away from the 100m set standard away from existing water bodies. Goil station had the closest proximity of 1 865m to the rivers whereas Total station had the farthest distance from the nearest water body available which was 11 195.154m. The set standard was to guard oil spillage and water pollution in the event of flooding. The analysis for the built up areas were carried out as seen in Figure 10. Two (2) of the oil and gas stations defaulted in the 500m buffer analysis, forming 25% of the available oil and gas stations. Total and Goil station recorded a distance of 314.29m and 60.33m respectively from the built up areas. Table 7 elaborates on the distance between the neighbouring stations. The minimum set distance between the neighbouring stations should be at least 400m. All stations complied with the standard. Total and Pacific recorded the least distance of 620m whereas Goil and APCO recorded the largest distance of 17 770m (Table 9). The proposed land for the development of the petroleum hub had an area of 20 513.83 acres (84.25km^2). Figure 12 shows the proximity analysis performed on the siting of the petroleum hub. The closest proximity of the existing stations to the hub was 1937.39m and 1475.86m occupied by Petrol station and APCO station respectively. The boundary of the hub went through as well as enclosed few built up areas as observed in Figure 12. The hub comprises of a network of roads running through the proposed land. An 11.5 km river stretch extended 1km of its length into the hub. The Suitability analysis of the map is represented in Figure 13. The suitability map was formed from the suitability and restriction model as depicted in Figure 3 and 4 respectively. The suitability was divided into four (4) categories: extremely high, high, moderate, and low. The area and percentage coverage of the suitability classes are shown in Table 8. Very high areas occupied 22.9%, high areas occupied 44.54%, moderate areas occupied 32.33% and low areas scored 0.23% of the suitability of the total area (Table 10). From Figure 13, the proposed petroleum hub felled on areas dominated by very high and high area suitability for its establishment constituting 75.9 km^2 (90.3%) of its entire area whereas the moderate suitability zones constituted 8.2 km^2 (9.7%) of the remaining areas. Towns situated in very high areas includes; Bakakole Nkwanta, Ahobre, Nawule, Allowule, Tikobo No.1, Edu, Damofu, Ave lenu and Ebonloa, Mpatabo. High areas comprises of Kengen Kpokezo, Alenda wharf, Tekyinta. Anwonakrom, Nkwamta, Elubo and Agege are among the moderate and low area zones for hub and oil retail assets establishment. The need for the establishment of a petroleum hub continues to remain a major concern due to increasing importation of petroleum products from year to year. Figure 14 represents the trend of import of petroleum products from 2007 to 2016.

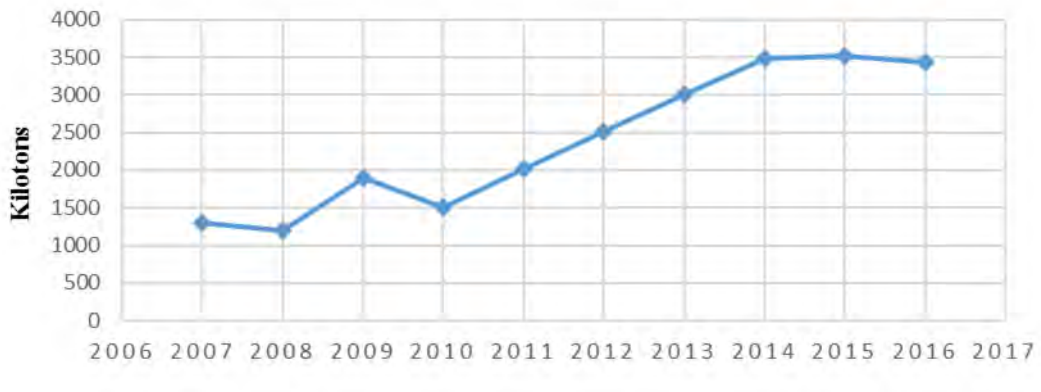

Figure 14. Petroleum products imports from 2007 to 2016 (Source: Abudu and Sai, 2020)

5 Conclusions and Recommendations

The Ministry of Energy has regulatory responsibility on behalf of the State under Act 84. All petroleum operations must be carried out in a manner without adverse effects on Ghana's environment, resources, or people (Ten, 2014). The paper aims to perform a site suitability assessment prior to the establishment of a petroleum hub at the Jomoro district of Ghana as well as assess the suitability of the existing oil retail assets by integrating Fuzzy AHP, VIKOR, proximity analysis and remote sensing techniques in the GIS environment in compliance with the policies by the Ministry of Energy and Environmental Protection Agency (EPA). The weights, selection criteria, and restriction model comprise the Suitability model. Fuzzy AHP was used to construct the initial weights from the fuzzy judgment matrix. This was done to address the uncertainties and imbalanced scale of judgment that existed in classical AHP. The decision matrix used in the studies was employed from the pairwise comparison of the AHP method with a valid consistency ratio of 0.09. This was done to eliminate any subjectivity in the cost criteria analysis. VIKOR method was used to generate the final weights and ranking of the cost factors based on the conditions set by the compromise solution. The essence is to emphasize the ranking of alternatives sets of the conflicting criteria (Mardani et al., 2016). The study' cost criteria include remotely sensed data, primary and secondary data received from Ghana's Survey and Mapping Division, and field data collecting ArcGIS 10.4 software was used to create all maps of the weighted alternatives. The suitability was divided into four (4) categories: extremely high, high, moderate, and low. Very high areas occupied 22.9%, high areas occupied 44.54%, moderate areas occupied 32.33% and low areas scored 0.23% of the suitability of the total area. From the study, the proposed petroleum hub felled on areas dominated by high area suitability for its establishment constituting 75.9 km^2 (90.3%) of its entire area whereas the moderate suitability zones constituted 8.2 km^2 (9.7%) of the remaining areas.

75% of the filling stations complied with the established protocols by Ghana's Ministry of Energy and Town and Country Planning Department, but 25% fell short in terms of proximity to public services. For future planning objectives, the study unveiled the geographical spread of filling stations along the major road. The proximity evaluation point demonstrates that some of the existing stations found expressions in an unsuitable setting, posing a risk to the people and properties in their neighborhood. The non-existence of firefighting stations was also observed in the vicinity. The study has once again proved the utility of multi-criteria decision analysis (MCDA) and geographic information system (GIS) techniques in handling spatially associated topical problems (Peprah et al., 2018). Furthermore, this report indicated that Ghana is reliant on petroleum imports (Abudu and Sai, 2020). It is recommended that the suitability map produced for the study area should be used and further environment impact assessment should be carried out by the authorities to assess the significant impacts the sited stations have on the environment. It is also recommended that site suitability analyses be incorporated in the Town and Country Department's planning scheme for future development and policy formulation. Measures should be put in place to enforce the set standards and prosecute offenders to bring sanity in the oil and gas projects. This study should be duplicated in other parts of the country or used for future redevelopment of the study area. Furthermore, for stations located in inappropriate zones, the authorities must conduct a proper environmental impact assessment to identify the substantial implications they may have on the ecosystem and the steps that may be implemented to mitigate those impacts (Njoku and Alagbe, 2015).

Acknowledgement

The authors wish to express their profound gratitude to the reviewers for their useful remarks that helped to improve this paper. Our heartfelt gratitude also goes to the CSIR-Building and Road Research Institute, Ghana's Lands Commission's Survey and Mapping Division and Geological Survey Department for supplying us with the essential data and equipment for the research.

References

Abdullah A.S. (2021). An Integrated Neutrosophic SWARA and VIKOR Method for Ranking Risks of An Integrated Neutrosophic SWARA and VIKOR Method for Ranking Risks of Green Supply Chain. Neutrosophic Sets and Systems, 40, 114–126. https://doi.org/10.5281/zenodo.4625690

Abudu H. and R. Sai. (2020). Examining prospects and challenges of Ghana ' s petroleum industry : A systematic review. Energy Reports, 6, 841–858. https://doi.org/10.1016/j.egyr.2020.04.009

Ackah I., E. Osei, F. Xavier, D. Tuokuu and C. Bobio (2018). Oiling the wheels of sub-national development : An overview of development plan implementation in the Western region of The Extractive Industries and Society. December. https://doi.org/10.1016/j.exis.2018.12.002

Addai E.K., S.K. Tulashi, J. Annan and I. Yeboah (2016). Trend of fire outbreaks in Ghana and ways to prevent these incidents, Safety and Health at Work. 7, 284–292.

Akay A.E. and A. Erdogan (2017). GIS-Based multi-criteria decision analysis for forest fire risk mapping ISPRS Annals of the Photogrammetry, Remote Sensing and Spatial Information Sciences. 2017 4th International GeoAdvances Workshop, Vol. IV-4/(Safranboln, Karabuk, Turkey), 25–30.

Akay A.E. and B. Yilmaz (2017). Using GIS and AHP for planning primer transportation of forest products", ISPRS Annals of the Photogrammetry, Remote Sensing and Spatial Information Sciences. 2017 4th International GeoAdvances Workshop, Vol. IV-4/(Safranboln, Karabuk, Turkey), 19–24.

Andoh G.G. and E. Offei-Addo (2014). 2010 Population and Housing Census District Analytical Report Jomoro district. https://doi.org/www.statsghana.gov.gh

Aslani M. and A.A. Alesheikh (2011). Site selection for small gas stations using GIS. Scientific Research and Essays, 6(15), 3161–3171.

Bank A.D. (2009). Oil and Gas in Africa. https://doi.org/ISBN 978-0-19-956578-8

Behrens T. and T. Scholten (2006). Digital soil mapping in Germany. A Review. J. Soil Sci. Plant Nutr, 169, 434–443.

Boroushaki S. and J. Malczewski (2008). Implementing and extension of the analytical hierarchy process using ordered weighted averaging operators with fuzzy quantifiers in ArcGIS. Comput. Geosci, 34, 399–410.

Broekhuizen H., C.G.M. Groothuis-Oudshoorn, J. A. Van Til, J. M. Hummel and M.J. Ijzerman (2015). A review and classification of approaches for dealing with uncertainty in multi-criteria decision analysis for healthcare decisions. Pharmaco Economics, 33, 445–455.

Damnyag L., O. Saastamoinen, D. Blay, F.K. Dwomoh, L.C.N. Anglaaere and A. Pappinen (2013). Sustaining protected areas: Identifying and controlling deforestation and forest degradation drivers in the Ankasa Conservation Area, Ghana. Biological Conservation, 165, 86–94.

Danvi A., T. Jütten, S. Giertz, S.J. Zwart and B. Diekkrüger (2016). A spatially explicit approach to assess the suitability for rice cultivation in an inland valley in central Benin. Agric. Water Manag, 177, 95–106.

Fazlollahtabar H., H. Eslami and H. Salmani (2009). Designing a fuzzy expert system to evaluate alternatives in fuzzy analytic hierarchy process. Journal of Software Engineering and Applications, 3, 409–418. https://doi.org/doi:10.4236/jsea.2010.34046

Firoozi M.A., M. Goodarzi and R. Shirali (2017). Assessment and potential survey of lands in Khuzestan Province using the Buckley Geometric Mean Model and Geographic Information System (GIS). Open Journal of Geology, 7, 234–241.

Ghana districts (2013). Jomoro Western Region. accessed from www.ghanadistricts.gov.gh/districts on 06/05/2022

Ghanbarie E., A.A. Jafarzadeh, F. Shahbazi and M. Servati (2016). Comparing Parametric Methods (the Square Root and the Storie) with the Fuzzy Set Theory for Land Evaluation of Chase Region for Wheat. Int. J. Adv. Biotechnol. Res, 7, 343–351.

Guler D. and T. Yomralioglu (2017). A GIS-Based landfill site selection approach using spatial multi-criteria decision-making methods, International Symposium on GIS Applications in Geography and Geosciences. Istanbul, Turkey, 1–8.

Jomoro District Assembly (2010). District Medium Term Development Plan, under the Ghana Shared and Development Growth Agenda 1. accessed on May 6, 2022

Jozaghi A., B. Alizadeh, M. Hatami, I. Flood, M. Khorrami, N. Khodaei and T.E. Ghasemi (2018) A comparative study of the AHP and TOPSIS techniques for dam site selection using GIS: a case study of Sistan and Baluchestan province. Iran Geosci 8(12):494

Kihoro J., N.J. Bosco H. and Murage (2013). Suitability analysis for rice growing sites using a multi-criteria evaluation and GIS approach in Great Mwea Region. Springer Plus, 365(2), 1–9.

Kim S., H. Lee and Y. Lin (2019). Geometric mean block matrices, Linear Algebra and its Applications. 575, 299–313. https://doi.org/https://doi.org/10.1016/j.laa.2019.04.008

Kumi-Boateng B., M.S. Peprah and E.K. Larbi (2020). The integration of Analytical Hierarchy Process (AHP), Fuzzy Analytical Hierarchy Process (FAHP), and Bayesian Belief Network (BBN) for flood-prone areas identification – A Case study of the Greater Accra region , Ghana. Journal of Geomatics, 14(2), 138–154.

Kusimi J.M. and J. Appati (2012). Bushfires in the Krachi District: The socio-economic and environmental implications, International Archives of the Photogrammetry. Remote Sensing and Spatial Information Sciences, XXXIX-B8, 2012 XXII ISPRS Congress, 25 August(Melbourne, Australia), 39–44.

Mardani A., E.K. Zavadskas and K. Govindan (2016). VIKOR Technique : A Systematic Review of the State of the Art Literature on Methodologies and Applications. Sustainability. 2016, 8(37), 1–38. https://doi.org/10.3390/su8010037

Mosleh Z., M.H. Salehi, A.A. Fasakhodi, A. Jafari, A. Mehnatkesh and I. Borujeni (2017). Sustainable allocation of agricultural lands and water resources using suitability analysis and mathematical multi-objective programming. Geoderma, 303, 52–59.

Mugiyo H., V.G.P. Chimonyo, M. Sibanda, R. Kunz, C.R. Masemola, A.T. Modi and T. Mabhaudhi (2021). Evaluation of Land Suitability Methods with Reference to Neglected and Underutilised Crop Species : A Scoping Review. 1–24.

Njoku C.G. and A.O. Alagbe (2015). Site Suitability Assessment of Petrol Filling Stations (PFSs) in Oyo Town , Oyo State , Nigeria : a Geographic Information Systems (GIS) Approach. IOSR Journal of Environmental Science, Toxicology and Food Technology (IOSR-JESTFT), 9(12), 8–19. https://doi.org/10.9790/2402-091230819

Norman I.D., B.M. Awiah, M.K. Aikins and F.N. Binka (2015). Review of catastrophe fires and risk communication, Ghana. Advances in Applied Sociology, 5, 167–177.

Peleckis K. (2022). Application of the Fuzzy VIKOR Method to Assess. Energies. 2022, 15(1349), 1–16. https://doi.org/. https:// doi.org/10.3390/en15041349

Peprah M.S., C. Boye, P.O. Appau and E.K. Larbi (2018). Suitability analysis for siting oil and gas filling stations using multi-criteria decision analysis and GIS approach – A case study in Tarkwa and its environs. Journal of Geomatics,12(2), 158–166.

Rahman N.F.A., A.A.H. Awangku, V.C. Tai, M. Mohammad, S.H. Haron, K. Khalid, M. Rasid and S.M. Shariff (2021) Sıte selection of water reservoir based on weighted overlay in ArcGIS (case study: Bachok,Kelantan). Sci Int (lahore) 33(2):135–139.

Rostami M., R. Tavakkoli-Moghaddam, R. and B. Zahiri (2010). Extended VIKOR as a new method for solving

Multiple Objective Large-Scale Nonlinear Programming problems. RAIRO - Operations Research, 44(4), 287-300. https://doi.org/10.1051/ro/2010013

Sharma L.K., S. Kanga, S. Nathawat, S. Sinha and P.C. Pandey (2012). Fuzzy Ahp for forest fire risk modelling, Disaster Prevention and Management. 2(21), 160–171. https://doi.org/10.1108/09653661211219964

Taghizadeh R., K. Nabiollahi, R. Kerry and T. Scholten (2020). Land Suitability Assessment and Agricultural Production Sustainability Using Machine Learning Models. April.

https://doi.org/10.3390/agronomy10040573

Tah D.S. (2017). GIS-Based locational analysis of petrol filling stations in Kaduna Metropolis. Science World Journal, 12(2), 8–13.

Ten (2014). Tweneboa, Enyenra, Ntomme (TEN) Project, Ghana. Final Environmental Impact Statement, I(September). https://doi.org/00002-E78-ES-RPT-0007 – REV 1

Uzochukwu O.C., O.O. Lilian, O.T. Uchenna and U.O. Ugbomhe (2018). Business development and sustainability of selected petrol stations in Anambra State of Nigeria. Africa Journal of Business Management, 12(1), 11–20.

Xiaoguang T., Z. Jiong and F. Bo (2015). ScienceDirect Strategic analysis on establishing a natural gas trading hub in China. Natural Gas Industry B, 1(2), 210–220. https://doi.org/10.1016/j.ngib.2014.11.0

Generation and Validation of Digital Elevation Model Using RISAT-1 SAR Interferometry

Ritesh Agrawal
Space Applications Centre / ISRO, Ahmedabad
Email: ritesh_agrawal@sac.isro.gov.in

(Received: 17 November 2022; in final form 31 August 2023)

DOI: *https://doi.org/10.58825/jog.2023.17.2.6*

Abstract: SAR Interferometry is one of the techniques used for generating three-dimensional information about the Earth's surface, which converts the absolute interferometric phase data of complex radar signal into topographic information. The prime objective of the study was to explore the potential of the RISAT-1 data for interferometric analysis. In this study, an attempt has made to generate the DEM of the part of Bharatpur region, Rajasthan using InSAR techniques using FFT based instead of the conventional approach due to non-availability of precise orbits. The analysis was carried out using FRS-1 data of 3 m resolution and 25 km swath corresponding to 21 February 2015 and 18 March 2015 having temporal separation of 25 days. The accuracy assessment of the generated DEM was compared with the extracted reference elevation information over 52 points from the Cartosat-1 DEM. The accuracy of the Generated DEM observed as 11.8 m and mean error of 2.3 m.

Keywords: RISAT-1, FRS, InSAR, Validation, Standard Deviation

1. Introduction

After the availability of initial Space-borne system, the generation of DEM performed using optical imagery and photogrammetric techniques (Crosetto and Aragues, 1999). The globally available elevation datasets cannot be used for the assessment of the local scale processes and on their impacts. The vertical error in the globally DEM datasets is the orders of magnitude higher than the magnitude at the estimate of the local level, such as in the case of river gradients, where the variation is much smaller than the vertical error. Urban flooding (Xu et.al, 2021; Jain et. al 2016) and 3-D city modelling (sharma et.al, 2016) is one of the examples where the precise DEM is more importance, which requires high resolution and accurate terrain. (Schumann & Bates, 2018). With the advancement in technology, Spaceborne imaging Synthetic Aperture radar (SAR) data gained and demonstrated high potential in generation of digital elevation model (DEM) of land surfaces (Mercer 1995; Bamler 1999; Das et al. 2014, Agrawal. et al., 2018). SAR datasets have two different approach for DEM generation (Gelautzet al, 2003). The radargrammetric approach works similar to photogrammetric approach using SAR amplitude image in place of optical image (Gelautz et al, 2003, Agrawal et al., 2018). The interferometric approach utilizes the phase information of the SAR image instead of the amplitude information for the generation of the DEM (Das et al. 2014, Abdelfattah and Nicolas, 2002, Zhouet al, 2005).
Two images from the coherent sources of the same region are required to form a phase difference images called as interferrogram (Zhou et al., 2009). The all-weather capability of techniques makes it powerful and cost effective data acquisition over a larger area (Zhou et al, 2005). The first InSAR results published by Goldstein et al. (1988) from the SEASAT L-band SAR data. In subsequent years, the ERS tandem mission provided a unique opportunity for the generation of the high-resolution DEM using repeat track interferometry. (Eldhuset et. al., 2003). Studies have demonstrated the potential of the interferometric technique to produce high-resolution topographic maps with relative height errors of 5m using repeat pass ERS imagery (Rufino, 1998, Eldhuset et. al., 2003, Jayaprasad et al, 2008, Shipping 2000). The standard approach for the generation of the DEM using InSAR includes image registration, interferogram calculation and filtering, phase unwrapping, elevation computation, and geocoding (Zhou et. Al, 2012; Geymen 2014), in which flat-earth removal has to rely on accurate orbital modeling to avoid long wavelength errors (Francis, 2006). The imaging quality, spatial and temporal baseline and atmospheric artifacts influence the accuracy of DEM. InSAR data processing also influence the DEM accuracy such as phase unwrapping, trends and planimetric errors. The image selection was carried out using baseline length and the minimization of the time-period of image acquisition to avoid baseline and temporal decorrelation (Arora and Patel, 2009).

RISAT-1 Synthetic Aperture Radar (SAR) is India's first indigenous, active, antenna-based microwave radar sensor in space, which was launched on 26 April 2012 from SDSC, SHAR, by Indian Space Research Organization (ISRO) (Valarmathi et al, 2013, Mahadevan et al, 2013). The spacecraft is 3-axis stabilized operating from an altitude of 536 km in sun synchronous orbit (Misra et al, 2013). It carrying a multi-mode Synthetic Aperture Radar (SAR) system provides complementary imaging capability in C-band with variety of resolution and swath requirements (Mahadevan et al, 2013). The resolutions from 3 to 50 m achieved with swath ranging from 25 to 223 km. In all the imaging modes, a novel polarimetry mode called circular or hybrid polarimetry also imagined (Misra et.al,2013). FRS-1 is a Stripmap mode while as MRS, CRS and FRS-2 are the ScanSAR-imaging mode.

This paper deals with generation of the DEM using repeat pass interferometry using FRS-1 Stripmap imaging mode

from the RISAT-1 satellite data. InSAR processing carried out using RH polarization from the circular polarimetric data. The datasets selected by keeping the minimum temporal and optimum baseline.

2. Study Area

Bharatpur district, Rajasthan covers an area of 5044.1 Km^2 and located between 26°40' and 27°50' latitude and 76°53' and 77°45'. The city of Bharatpur is popularly known as eastern gateway of Rajasthan. The city is enclosed between Gurgaon, Mathura, Agra, Dholpur, Dausa and Alwar. It is drained by three seasonal rivers viz., Gambhir River, tributaries of the Yamuna River, Ban Ganga River and Rooparel River. Limited availability of water resources confined the agriculture into traditional kharif cultivation and rabi cultivation is prevalent where irrigation facilities are available.

3. Data used

The RISAT-1 data has very limited datasets for the interferometric analysis due to less and non-systematic coverage of FRS-1 and the acquisition has limited data availability in terms of the similar geometry and baseline requirement. The data is selected from the pool of the FRS datasets by making the criteria having temporal separation of less than 2 month and variation in the look angle should be less than 0.2 deg. The FRS-1 Stripmap mode of RISAT-1 data (Table 1) is used in this study. InSAR analysis of data acquired on 21February and 18March of 2015 carried out having a time difference of 25 days (figure 1) is carried out.

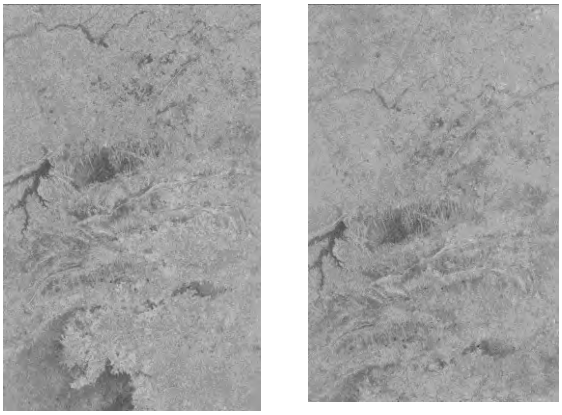

Figure 1. a) Master image (21st February), b) Slave image (18th march)

4. Methodology

The processing of SAR interferometric data is a complex issue. Based on the quality of the data sets, the performance of each single processing step has its influence on the final product. The basic steps involved in the derivation of topographic information from SAR images are shown in figure 2. The InSAR processing steps involves data importing, Orbit modelling, image co-registration, interferrogram generation, phase unwrapping to DEM generation. The precise orbital data plays an important role in the image co-registration error and flat earth correction and inaccurate orbital information can lead to misregistration of the image and inclusion of long wavelength error. In this study FFT based approach is used instead of the orbital based process to avoid misregistration and inclusion of the long wavelength error.

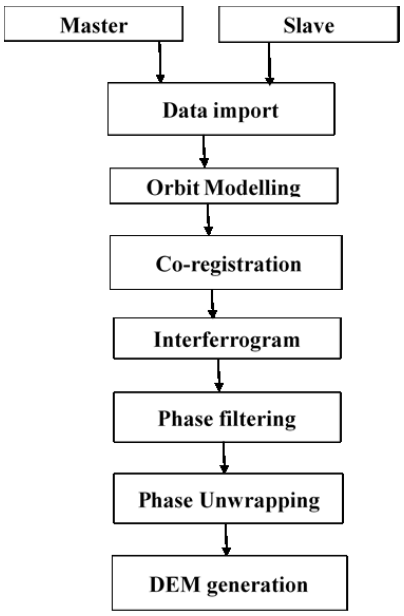

Figure 2. InSAR processing for the DEM generation.

5. Orbit Modelling

Importing of the data involves the importing of the SLC image along with the sensor parametrs, Image geometry parameters, orbital parameters along with the geolocational information of the scene centre and its extents. The extracted orbital information available in ECI co-ordinate system in RISAT-1 needs its conversion in ECEF co- ordinate system as shown in figure 3.

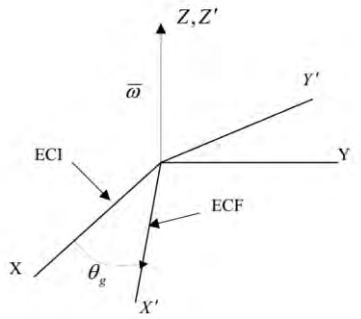

Figure 3. Conversion of ECI to ECF co-ordinate system

Since the state vectors consists of position and velocity,it is more appropriate to represent the trajectory as function of time so that the velocity will be the time derivative of the position; in this approach, the 2nd degree of polynomial takes the form as below:

$$X(t) = a_{x0} + a_{x1}.t + a_{x2}.t^2 \quad (1)$$
$$Y(t) = a_{y0} + a_{y1}.t + a_{y2}.t^2 \quad (2)$$
$$Z(t) = a_{z0} + a_{z1}.t + a_{z2}.t^2 \quad (3)$$

5.1. Image co-registration

Image co-registration is one of the key step for the interferometric processing. Variation in viewing geometry

of satellite from two parallel orbits cause small shift in one image with respect to other image. Image co-registration performs the geometrical alignment of the two SAR images covering same region. Image registration is performed in two steps as 1) coarse co-registration and 2) Fine co-registration.

The coarse co-registration computes the offset using orbital parameter by considering the centre co-ordinate of the master and estimate its location in the image grid for the master and slave image and its difference is considered the initial offset, which is further used for the estimation of the fine co-registration process.

Due to the unavailability of the precise ephemeris information of RISAT-1 orbital data, the computation of the offset between the two images may provide wrong estimation based on orbital parameter, which may yield in the wrong co-registration results in non-generation of interferogram. Estimation of the correct offsets computed by employing phase correlation (PC) approach, which utilizes the phase shift property of the Fourier transform to estimate large image offset. The purpose of the PC algorithm is to estimate the translation (Δx, Δy) between a pair of images sharing some common support: Let I1 (x, y) and I2 (x, y) be the images, then their common support satisfies.

$$I1\ (x + \Delta x, y + \Delta y) = I2\ (x, y) \quad (4)$$

The equation can be transformed in the FFT domain as

$$\widehat{I_1}(\omega_x, \omega_y) e^{j(\omega_x \Delta x + \omega_y \Delta y)} = \widehat{I_2}(\omega_x, \omega_y) \quad (5)$$

$$\frac{\widehat{I_2}(\omega_x, \omega_y)}{\widehat{I_1}(\omega_x, \omega_y)} = e^{j(\omega_x \Delta x + \omega_y \Delta y)} \quad (6)$$

The translation (Δx, Δy) can estimated by taking the inverse FFT

$$Corr\ (x, y) \triangleq \mathfrak{F}^{-1}\left\{e^{j(\omega_x \Delta x + \omega_y \Delta y)}\right\} = \delta(x - \Delta x, y - \Delta y) \quad (7)$$

Therefore, the translation values one estimated by maximum correlation in the image location:

$$(x, y) = arg\left\{\max_{(\tilde{x}, \tilde{y})} \{Corr\ (\tilde{x}, \tilde{y})\}\right\} \quad (8)$$

The fine co-registration process performs sub pixel level registrations. This process involves the selection of the multiple window in x and y direction within master image and corresponding smaller image segments selected in slave image over same locations. A search for the proper two-dimensional shift conducted using the correlation coefficient as the measure of goodness. In the oversampled image and the final image offset is estimated by the under sampled of the image offset with the same factors. The estimated offset parameters from the multiple windows modeled in the affine transformation model are given by the equations and used for the resampling of the slave image.

$X=\alpha_{00}+ \alpha_{10}X+ \alpha_{01}Y+ \alpha_{11}XY$
$Y=\beta_{00}+ \beta_{10}Y+ \beta_{01}X+ \beta_{11}XY$

5.2 Interferogram

Interferogram is defined as the product of the complex SAR values of a slave image and the complex conjugate of a master image. Flattening of the interferogram is carried out to remove the azimuth and range phase trends expected for a smooth curved Earth (Ellipsoid, height constant) from the interferogram.Adaptive filtering is carried out to reduce the phase noise in the flattened interferogram and thereby reducing the number of residues. The program reads the complex valued interferogram and filters the interferogram. The boxcar filter is applied for filtering the interferrogram to eliminate the noise present in the fringes. The filtered interferrogram is shown in Figure 4.

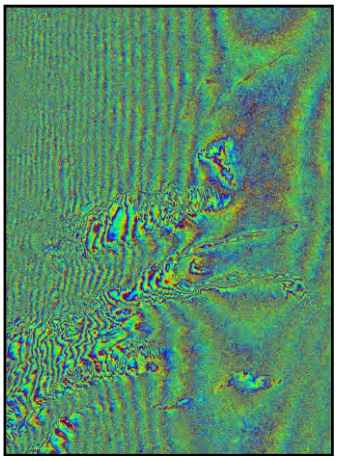

Figure 4. Filtered interferogram

$$R_i = \begin{Bmatrix} \frac{1}{w} \sum_{j=0}^{w-1} A_{i+j-w/2} & if\ \frac{w-1}{2} \le i \le N - \frac{w+1}{2} \\ A_i & Otherwise \end{Bmatrix} \quad (9)$$

5.3 DEM generation

For the computation of the absolute phase from the interferrogram, there is need for the computation of correct integer number of phase cycles that needs to add to each phase measurement in order to obtain the correct slant range distance. The process of computation of such absolute phase in terms of addition of integer multiple of 2π, is referred to as phase unwrapping. Absolute phase together with the precision baseline is used to compute topographic heights.

$$d\phi = -\frac{4\pi B}{\lambda H}\cos(\alpha - \theta)\sin\theta\cos\theta dz \quad (10)$$

where,

$d\phi$ is change in phase difference corresponding to change in elevation (dz)

B is the baseline length; H is the flying height of the satellite

θ is look angle; α is the angle made by the baseline vector. The computed elevation information refers in the image geometry. Geocoding is a process, which converts the image geometry in the map geometry. Conversion of such process is called geocoding. Geocoding removes all the distortions (Local, Global) and provides the end user a distorted free image in map coordinates. InSAR geocoding provides topographic information (DEM) in the map geometry by resampling using bilinear interpolation techniques.

6. DEM validation

Accuracy assessment for the DEM is normally performed by its comparison with the available topography maps or by collecting the elevation data from the field. The Cartosat-1 10 m DEM used as a reference DEM in this study and elevation points were collected randomly with suitable spatial and as well as the topographical distributed.

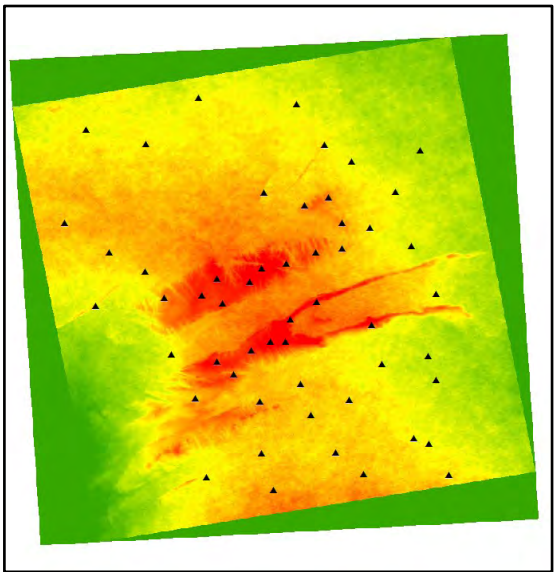

Figure 5. Points overlaid for accuracy assessment

These reference points used for the validation of the Generated DEM and the elevation value of the RISAT-1 Generated DEM compared with it. The figure 5 shows the distribution of control points used for evaluation of the DEM accuracy on the DEM generated by the RISAT-1 FRS datasets. Error analysis shows mean error of 2.23 m, while the RMSE observed is 11.8 m. The reference elevation values and the generated elevation values were compared at 52 points and shown as in the figure 6.

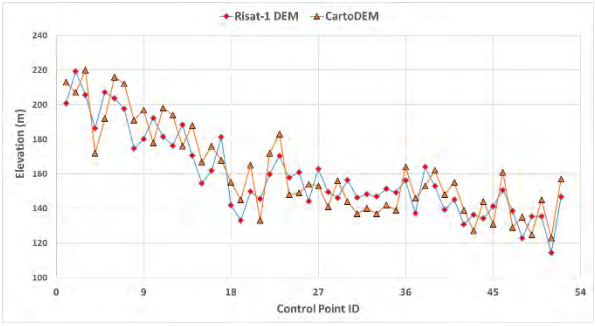

Figure 6. Comparison of the RISAT-1 DEM with CARTODEM

From the figure it is clear that the elevation values between the two DEMs are quite matching.

7. Conclusion

InSAR processing is described over the parts of the Bharatpur region, Rajashtan. An Improved FFT based co-registration approach used in this study instead of the conventional orbital-based approach, which is used for the avoid of the image mis-registration due to inaccuracy of the orbit. The study can perform the generation of the DEM even in the absence of the precise orbit. The accuracy of the generated DEM is compared with the Cartosat-1 DEM by comparing the elevation over 52 points. Error analysis shows mean error of 2.23 m, while the RMSE observed is 11.8 m. This study shows the potential of the FRS-1 datasets for the generation of the DEM with the required accuracy and the future Indian SAR satellite such as RISAT series FRS mode has capabilities for the interferometric applications.

Acknowledgement

Author express their sincere gratitude to Nilesh Desai, Director SAC. The author wishes sincerely thank the reviewers for their critical comments and suggestion for improving the quality of the paper

References

Abdelfattah R. and J.M. Nicolas (2002), Topographic SAR Interferometry Formulation for High-Precision DEM Generation, IEEE Transactions on Geoscience and Remote Sensing, 40(11), 2415- 2426

Agrawal R., A. Das and A.S. Rajawat (2018), Accuracy Assessment of Digital Elevation Model Generated by SAR Stereoscopic Technique Using COSMO-Skymed Data, Journal of the Indian Society of Remote Sensing, 46(10):1739–1747, doi: 10.1007/s12524-018-0835-6

Arora M.K. and V. Patel (2009), SAR Interferometry for DEM Generation, Geospatial world

Bamler R (1999). The SRTM mission—A worldwide 30 m resolution DEM from SAR interferometry in 11 days. In D. Fritsch & R. Spiller (Eds.), Photogrammetric week' 99 (pp. 145–154). Heidelberg, Germany: WichmannVerlag.

Crosetto M. and F. Aragues (1999), Radargrammetry and SAR Interferrometry for DEM generation: validation and data fusion, Proc. of the CEOS SAR Workshop, Toulouse, 26-29 October

Das A., R. Agrawal and S. Mohan (2014). Topographic correction of ALOS-PALSAR images using InSAR derived DEM. Geocarto International. https://doi.org/10.1080/10106049.2014.883436

Eldhuset K., P.H. Andersen, S. Hauge, E. Isaksson and D. Weydahl (2003), ERS tandem InSAR processing for DEM generation, glacier motion estimation and coherence analysis on Svalbard, International Journal of Remote Sensing, 24(7), 1415-1437

Francis I.O. (2006) InSAR Operational and Processing Steps for DEM Generation, Promoting Land Administration and Good Governance, 5th FIG Regional Conference Accra, Ghana, March 8-11, 2006

Gelautz M., P. Paillou, C.W. Chen, H.A. Zebker (2003), A Comparative Study of Radar Stereo And Interferometry For DEM Generation, Proc. of FRINGE 2003 Workshop, Frascati, Italy,1 – 5 December 2003

Geymen A. (2014) Digital elevation model (DEM) generation using the SARinterferometry technique, Arab J Geosci (2014) 7:827–837 DOI 10.1007/s12517-012-0811-3

Goldestein R.M., H.A. Zebker and C.L. Werner (1988), Satellite radar interferometry: Two-dimensional phase unwrapping. Radio Science, 23, 713–720

Jain G.V., R. Agrawal, R.J. Bhanderi, P. Jayaprasad, J.N. Patel, P.G. Agnihotriy and B.M. Samtani (2016) Estimation of sub-catchment area parameters for Storm Water Management Model (SWMM) using geo-informatics, Geocarto International 31 (4), 462-476

Jayaprasad P, B. Narender, S.K Pathan and Ajai (2008), Generation and Validation of DEM Using SAR Interferometry and Differential GPS Supported by Multispectral Optical Data, Journal of the Indian Society of Remote Sensing, 36, 343-352

Li S., H.P. Xu and Q. Zhang (2011), An Advanced DSS-SAR InSAR Terrain Height Estimation Approach Based on Baseline Decoupling, Progress In Electromagnetics Research, 119, 207-224

Mahadevan V., K. Prasad, D.S. Jain, S. Chowdhury, M. Pitchamani and N.M. Desai (2013), Ground segment for RISAT-1 SAR mission, Current Science, 104(4), 477-489

Mercer B. (1995). SAR technologies for topographic mapping. Photogrammetric week. Heidelberg, Germany: WichmannVerlag.

Misra T., S.S. Rana, N.M. Desai, D.B. Dave, R. Jyoti, R.K. Arora, C.V.N. Rao, B.V. Bakori, R. Neelakantan and J.G. Vachchan (2013), Synthetic Aperture Radar payload on-board RISAT-1: configuration, technology and performance, Current Science, 104(4), 446-461

Rufino G., A. Moccia and S. Esposito (1998), DEM Generation by Means of ERS Tandem Data, IEEE Transactions on Geoscience and Remote Sensing, 36 (6), 1905-1912

Schumann GJ-P and P.D. Bates (2018) The Need for a High-Accuracy, Open-Access Global DEM. Front. Earth Sci. 6:225. doi: 10.3389/feart.2018.00225

Sharma S.A., R. Agrawal and P. Jayaprasad (2016) Development of '3D city models' using IRS satellite data, Journal of the Indian Society of Remote Sensing 44,187-196

Shiping S., 2000, DEM Generation Using ERS-1/2 Interferometric SAR Data, In Proceeding of IGARSS2000, Honololu USA, 24-28 July 2000, 788-790

Valarmathi N, R.N. Tyagi, S.M. Kamath, B.T. Reddy, M.V. Ramana, V.V. Srinivasan, C. Dutta, N.V. Venketesh, Raveendranath, G.N. Babu, S. Prasad, R. Rajeev, P. Badagandi, S. Natarajan. J. Sudhakar, S.S. Rao and M.K. Reddy (2013), RISAT-1 spacecraft configuration: architecture, technology and performance, Current Science, 104(4), 462-471

Xu K., J. Fang, Y. Fang, Q. Sun, C. Wu and M. Liu, (2021) The Importance of Digital Elevation Model Selection in Flood Simulation and a Proposed Method to Reduce DEM Errors: A Case Study in Shanghai, Int J Disaster Risk Sci (2021) 12:890–902, DOI: 10.1007/s13753-021-00377-z

Zhou C., G.E. Linlin, E. Dongchen and H. Chang (2005), A Case Study of Using External DEM in InSAR DEM Generation, Geo-spatial Information Science, Volume 8, No. 1, 14-18

Zhou H., J. Zhang, L. Gong and X. Shang (2012) Comparison and Validation of Different DEM Data Derivedfrom InSAR, Procedia Environmental Sciences 12, 590 – 597

Zhou X., N. B. Chang and S. Li (2009), Applications of SAR Interferometry in Earth and Environmental Science Research, Sensors,9, 1876-1912; doi:10.3390/s9030187

Sediment yield from a tropical mountainous watershed by RUSLE model: An insight for sediment influx into the tropical estuary

Diksha Karapurkar[1]*, V. S. Hegde[1,2&3]
[1]Sri Dharmasthala Manjunatheshwara College of Engg and tech., Dharwad
[2]National Institute of Advanced Studies, IISc Bangalore
[3]Vishvanathrao Deshpande Institute of Technology, Haliyal
*Email: dkarapurker@sdmcet.ac.in

(Received: 25 November 2022; in final form 24 March 2023)

DOI: *https://doi.org/10.58825/jog.2023.17.2.7*

Abstract: Sediment yield is the possible volume of sediments that a basin is capable of delivering to its watershed outlet. It is a function of the topography of the drainage basin, climate, including precipitation, land use- land cover, soil characteristics, and other factors associated with the rate of soil formation and its transportation. Modeling sediment yield from a watershed enables quantitative computing estimates of sediments generated from a watershed. The Revised Universal Soil Loss Equation (RUSLE) is an efficient model for the assessment of annual soil loss from a basin using remotely sensed data in the Geographical Information System (GIS) platform. In the present study, the assessment of sediment yield from the Gangolli river basin of Karnataka, located on the central west coast of India, is carried out based on satellite data, processed in the GIS platform following the RUSLE model. The basin has a relief of 1360 m and a total catchment area of 1,51,927 hectares, spread on the western face of the Western Ghat region of the South Kanara district. The basin is located in a tropical environment and experiences a hot humid climate and annual precipitation of ~ 355 cm. Physiographically, the basin is divided into three subdivisions; the high-relief mountainous region of the Western Ghats, the residual hilly region with low relief, and the coastal plains. The basin has a high circularity Index (0.25) and a moderately high elongation ratio (0.51). The total actual sediment yield from the basin has been estimated to be 1,98,774.06 tons/yr-1 and the potential yield is 12,32,868.17 tons/yr-1, implying high sediment flux into the estuarine system. The results of this study help to strategize inland soil conservation planning as well as estuarine management.

Keywords: RUSLE, Sediment yield, Tropical catchment, Hypsometry, Gangolli watershed

1. Introduction

Globally, tropical rivers and some large rivers of the subtropical region contribute ~80% of sediments to the world's oceans (Eisma, 1988; Milliman, 1991) of which ~92% of the sediments are trapped in estuaries and nearshore (Gibbs, 1981; Schubel and Kennedy, 1984). This sediment is then utilized in the formation of estuarine islands, spits, beaches, dunes, and modification in the bottom bathymetry, which leads to many sediment-related problems such as siltation of the estuarine channel (Gopinathan and Quasim, 1971; Kuang et al., 2014), spit growth across river mouths (Hegde et al., 2012, Pradhan et al., 2015), narrowing and migration of river mouths, and morphological changes in estuarine islands (Kumar et al., 2010; 2012). These problems can be addressed by studying the quantum and sources of sediments arriving at the estuarine system. Different approaches include studying hydrographic conditions across the estuaries (Hegde et al., 2004), sediment sink and movement in the estuarine beaches (Hegde et al., 2007, 2009; Nayak et al., 2010; Karapurkar et al., 2022), provenance and sediment transport pathways are determined through heavy mineral constituent studies (Shalini et al., 2019; Paltekar et al., 2021). Lalomov (2003), Frihy (2007), and Shalini et al. (2019) based on the mineralogical and geochemical studies of heavy minerals from the estuarine beach sands identified alongshore currents as well as offshore sources for sediments on the modern shores. The presence of paleo-beaches off the coast (Rao and Wagle, 1997) is identified as one of the potential sources. Tamura et al. (2010) recognized fluvial sediment input sources on tropical monsoon-influenced beaches. Hitherto, the role of the fluvial influx of sediments from a mountainous tropical catchment to the estuarine system has not been emphasized. Assessment of fluvial input of sediment load from the catchment becomes a very difficult task due to its strong dependency on rainfall input, land use land cover change, and variations in soil conservation practices (Lam-Hoai et al., 2006). Lack of sediment discharge data at the watershed outlet and large-scale variations in topology leads to an improper understanding of sediment source and budget, which hinders the management of sediment-related issues such as siltation.

Sediment influx into the estuarine system can come from different sources to the estuary from its catchment, alongshore drift finally entering into the estuary by tidal surges, or from offshore sources (Shankar and Manjunatha, 1997; Evans et al., 2001; Dai et al., 2018; Kinsela et al., 2022). There are several methods to assess and compute the sediments coming from the basin, viz Universal Soil Loss Equation (USLE), Modified Universal Soil Loss Equation (MUSLE), and Revised Universal Soil Loss Equation (RUSLE). RUSLE is an efficient user-friendly model for estimating sediment yield. The parameters required can easily be obtained using remotely sensed data and it can take into account more complex combinations of tillage practices and cultivation practices as well as a wider variety of slope forms and is successfully employed for catchments of tropical mountain systems (Renard, 1997; Ganasri & Ramesh, 2016; Markose & Jayappa, 2016). The Results of the RUSLE model in combination with GIS can generate long-term results of

soil erosion estimation, even for the steep slope regions when the physical parameters are known (Rangsiwanichpong et al., 2018; Ullah, 2018).

Soil erosion models Integrated with GIS and remote sensing technology are considered the most powerful tools to measure soil erosion and sediment yield at various spatial scales. Estimation of soil loss using conventional methods are both costly and time-consuming (Amin and Romshoo, 2019) especially for tropical mountain watersheds due to inadequate gauged discharge data, forest cover, and inaccessibility. In the present study, an attempt is made to assess sediment yield from the Western Ghats' mountainous tropical catchment using the RUSLE model. Although many rivers originating from the Western Ghats, flowing across the Central west coast of India and joining the Arabian Sea experience many sediment-related problems like siltation in navigational channels, the potential of the sediment yield from the catchment in siltation is not understood and the results are not integrated with the morphometric characteristics of the watershed for possible management options.

Therefore, the objective of the present study is to estimate the volume of sediments that can be released by the basin, annually and the process responsible for high erosion in mountainous tropical catchment giving high sediment yield, which is capable of delivering maximum sediments into the estuarine environment.

For this purpose, the Gangolli River basin of Kundapur Taluk in the Udupi District of Karnataka is selected. Among the other coastal districts of Karnataka, Udupi is a rapidly urbanizing area, therefore large-scale land use land cover modification is taking place, such as urbanization due to highway projects, railway projects, and watershed projects like the Chakra dam. The proposed Nethravati diversion scheme is likely to alter land use and land cover of the adjacent river basin (Djoukbal et al., 2018).

2. Study area

The Gangolli River basin (Latitudes 13^0 30' to 13^0 55'N and longitudes 74^0 40' to 75^0 10'E) is a major drainage system of Kundapur Taluk with a total drainage area of 1513.04 km^2, in Udupi district, Karnataka state, India, that debauches its sediment and water load into the Arabian sea through the Gangolli estuary (Figure 1)**.** The basin experiences a tropical environment, a hot and humid climate, and an annual rainfall of 300-350cm. Of this, 85% of the precipitation is received from the southwest monsoon from June to September and the remaining 15% of the precipitation is received throughout the northeast and inter-monsoon months. Maximum discharge through the river is observed during the monsoon season. The average temperature of the region is 26.5^0C and it experiences typical maritime weather.

The Gangolli River system is a multichannel watershed with the Kollur River, the Chakra River, and the Haladi River as the major tributaries of the Gangolli. The Haladi, Chakra, and Kollur (Souparnika) rivers originate at an altitude of 760 m above MSL at Kaveri, 820 m above MSL near Kattinahole, and 1100 m above MSL at Kodachadri, Kollur respectively, in the Western Ghats. The Haladi River flows northwesterly from its origin for about 83 km, whereas the Chakra and Kollur Rivers flow southwesterly for about 68 km and 70 km respectively, and join together near Kundapur and finally flow as the Gangolli River before its discharge into the Arabian Sea. The major tributaries of the Haladi River are the Varahi, Dasanakatte, and Kubja Rivers and the tributaries of the Chakra River include the Savehaklu Hole, and Kattinahole whereas the Kollur River has the Halkal Hole, the Jadkal hole and the Souparnika hole as major tributaries.

Several reservoirs (Bhadra, Savehaklu, and Mani) are developed on the major tributaries of the river which also work as entrapment for sediments. The river Kollur flows along the Maravathe coast parallel to the shore for 300m without meeting the sea, then takes a sharp turn landward and further flows southwards to intersect with the river Haladi at Gangolli, forming a confluence point before debauching its water-sediment load into the Arabian Sea. The river forms a wide estuary with a braided confluence system and finally forms a narrow river mouth before it enters the Arabian Sea.

Figure 1. Location map of the Gangolli watershed.

3. Methodology

3.1. Morphometric analysis

Morphometric analysis of the drainage basin is carried out for the basin as summarized in table 1. For the generation of the Hypsometric curve, the Digital Elevation Model (DEM) of the study area is obtained from Shuttle Radar Topographic Mission (SRTM) (data obtained from usgs.gov.in dated 2005), using the Hydrology tool of ArcGIS 10.3. The same data is utilized to derive drainage and slope maps of the basin to generate a percentage hypsometric curve as given by Strahler (1954a).

3.2. Working of the RUSLE model

Sediment yield (A) in the RUSLE model (Renard, 1997) is expressed as:

$$A = R \times K \times LS \times C \times P \quad (1)$$

Where R is the Rainfall Erodibility factor, an expression of soil loss from an area due to the frequency, intensity, and duration of rainfall; K is the Soil Erodibility Factor

which is determined by the texture of the soil and represents the susceptibility of soil to erosion by the impact of rain and runoff.; LS is the Topographic Factor that determines the rate of infiltration and runoff over the ground surface; C represents Cover Management Factor (C). It depends on the degree of coverage such that it is protected from the direct impact of precipitation and hence splash erosion; P is the Conservation Practice Factor determined by the land use and land cover pattern. Various data used in the present study are presented in Table 1. A brief workflow of the methodology is given in figure 2.

Table 1. Type of data used in the study.

Data Type	Source	Details
SRTM Data	www.usgsglovis.org	Digital elevation model; 2000; 30m resolution
Landsat 8	www.usgsglovis.org	Multispectral image; 12th February 2015; 30m resolution
Rainfall Data	Indian Meteorological Department, Bangalore	Rainfall data for period 1985-2014; Kundapur rain gauge station
Soil map	The National Bureau of Soil Survey and Land Use Planning, India	Soil map for the year 2003; scale: 1:2,50,00,000

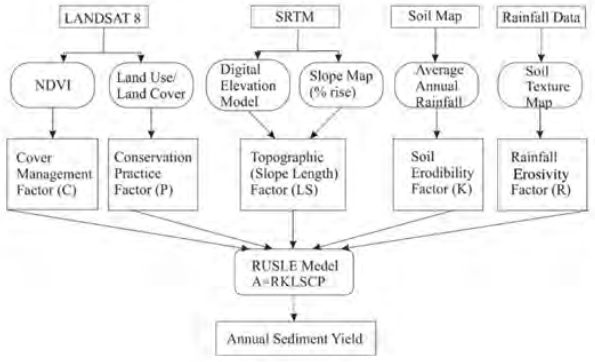

Figure 2. Workflow chart for the RUSLE model

3.2.1 Rainfall Erodibility Factor (R)

Rainfall Erodibility Factor (R) is determined by Babu et al. (2004) over the Indian subcontinent bears a relation of:

$$R = 81.5 + 0.38\,Ra \quad (2)$$

where Rα is the average annual rainfall in mm.

Rainfall data for the study area were collected from the Kundapur rain gauge for the period 1985 to 2015 and were used to determine average annual precipitation (355 cm for the study area). The Rainfall Erodibility Factor (R) is computed following the above relation.

3.2.2. *Soil Erodibility Factor (K)*

Soil Erodibility Factor (K) is dependent on the texture of the soil, organic matter content, structure, and permeability (Wischmeier and Smith, 1978) and is given by the equation:

$$K = 27.66 \times m^{1,14} \times 10^{-8} \times (12 - a) + 0.0043 \times (b - 2) + 0.0033 \times (c - 3) \quad (3)$$

where,

m is (silt%+sand%*(100-clay%)),

α is organic content (%),

b is the structure code used in classifying soils and

c is the soil permeability class.

Details of b and c are provided in table **2**. A soil map of the study area prepared by the National Bureau of Soil Survey and Land Use Planning (NBSS & LUP), India is used.

Table 2. Details of soil structural codes and soil permeability class as given by Wischmeier and Smith (1978).

b/c	Soil structural code	Soil Permeability class
1	Very fine granular	Very slow
2	Fine granular	Slow
3	Medium or coarse granular	Slow to moderate
4	Blocky, Platy, or massive	Moderate
5		Moderate to rapid
6		Rapid

3.2.3 Topographic Factor (LS)

Topographic factor (LS) is calculated using the following equation given by Ganasri and Ramesh, 2016:

$$LS = \left[\frac{Q_a M}{22.13}\right] \times (0.065 + 0.045 \times S_g + 0.0065 \times S_g^2) \quad (4)$$

where,

Q_a is the flow accumulation map,

M is the cell size,

S_g is slope rise in percentage

3.2.4 Cover Management Factor (C)

The Cover Management Factor is derived usingNormalized Differential Vegetation Index (NDVI) map of the region generated using LANDSAT-8 image where,

$$NDVI = \frac{\text{NIR Band} - \text{RED Band}}{\text{NIR Band} + \text{RED Band}} \quad (5)$$

NDVI values exhibit a non-collinear relationship with that of the C-factor. It is assumed close to 1 for the densely vegetated area and 0 for barren or water-logged areas. The majority of the area in the basin is occupied by forested land followed by water bodies and the minor area is covered by agricultural land, barren land, and suburban area. Considering the above conditions, the C-factor is obtained using the equation proposed by Jong et al. (1998).

$$C = 0.431 - 0.805 \times NDVI \quad (6)$$

3.2.5 Conservation Practice Factor (P)

The Conservation Practice Factor (P) depends on the type of land use/land cover in the region. Perfect soil conservation is represented by a value of 0, and 1 represents no conservation in the region. Land use land cover map of the area is generated using the same LANDSAT 8 image processed in a GIS environment.

3.2.6 Method for calculating Potential and Actual Sediment Yield

Actual Sediment Yield analysis is carried out following Renard 1997 as given by equation 1 and is called the Revised Universal Soil Loss Equation (RUSLE). The results obtained were processed and classified using ArcGIS 10.3. The classifications used are based on the natural slope break function, following which the areal coverage of each class is quantified. To determine the Potential Sediment Yield from the basin upon complete loss of vegetation is quantified by eliminating Cover Management Factor from the RUSLE equation (Figure 3). Hence the resulting equation can be expressed as:

$$A = R \times K \times LS \times P \quad \textbf{(7)}$$

The results were then classified upon importing the class breaks from that used for Actual Sediment Yield and Potential Sediment Yield quantified.

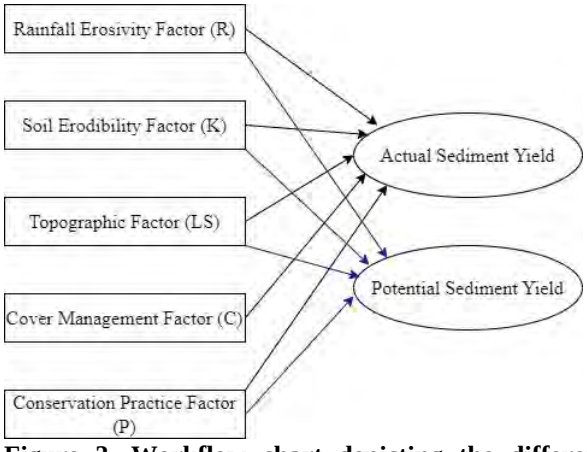

Figure 3. Workflow chart depicting the difference between actual and potential sediment yield calculation

4. Results

4.1 Morphometric parameters

The watershed of the river Gangolli is characterized by a dendritic drainage pattern, typical of humid tropical drainage basins. River Haldi and River Kollur are fifth-order streams whereas River Chakra is the fourth-order stream. River Kubja which forms the major tributary of river Haladi flows roughly parallel to river Chakra and is also a fourth-order stream. River Chakra originates on the eastern face of the Western Ghats and flows due west whereas the river Kubja originates on the western face of the Western Ghats, and flows roughly parallel to the course of river Chakra then after. River Kollur originates on the western face and river Haldi on the Eastern face of the Western Ghats. East-West is the most dominant trend of streams followed by North-South, suggesting strong structural control on the morphometry of the drainage system (Figure 4). Similar observations come from Subrahmanya (1996), Ajaykumar et al. (2017), and more. Higher-order streams show deep, narrow valleys and entrenching processes in the coastal and midlands.

Morphometry data for the Gangolli indicates that the basin is elongated with a high elongation ratio (0.51) (Schumm, 1956), a low Circularity ratio of 0.25, and a Form Factor value of 0.21 (Sukristiyanti et al., 2018). The drainage density of the basin (0.35km/km^2) is however low due to seasonal rainfall (June to October) and residual hills in coastal plains. High relief of the basin (1360m) suggests increased runoff and minimum infiltration (Akhil et al., 2022). The relief ratio of the basin (15.46m/km) together with the high ruggedness number (458.55) are suggestive of elevated runoff, hence high erosive potential.

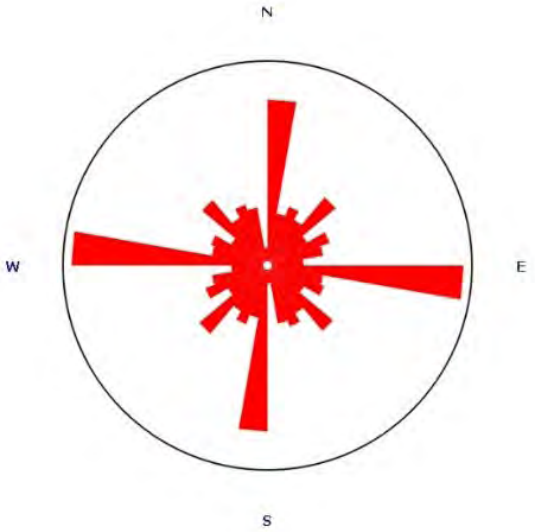

Figure 4. Rose diagram showing the dominant trends of stream flow

4.2 Hypsometric curve

The hypsometric curve for the drainage basin is generated at an interval of 25m following **Strahler (1952)**. The curve has shown a coefficient of determination of 0.849 (**Figure 5**). The hypsometric curve showed five phases of its nature based on the slope and the corresponding area.

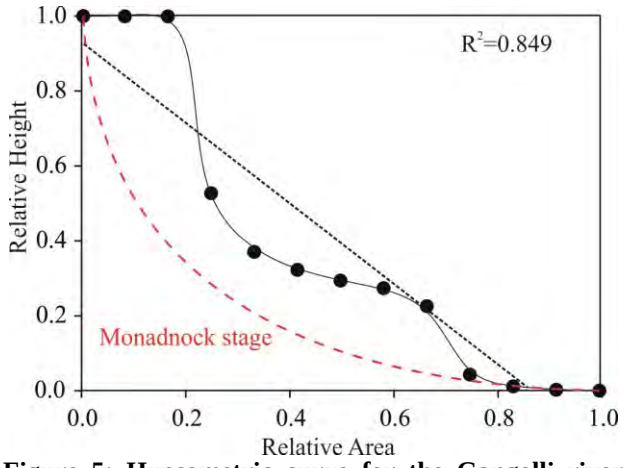

Figure 5: Hypsometric curve for the Gangolli river basin

Three steeper slopes are seen in the hilly regions of the Western Ghats (1360 to 875m and 725 to 350m) and the coastal plains (175 to 0m) with two phases of gentler slopes separating the three steep phases. Steeper phases which comprise 23.36% of the total basin area facilitate high runoff and low infiltration resulting in high sediment yield. The basin is in an inequilibrium stage as indicated by the hypsometric curve (Strahler 1954b).

4.3 Rainfall Erosivity Factor (R)

Rainfall is the major force facilitating the erosion of a landscape. Rainfall in the western tropical Indian coast increases towards the western face of the Western Ghats from the coastal plains. Continuous rainfall data helps to estimate a more representative value of R for a region.
Since the rainfall data from the study area is from one station, average rainfall over 30 years has been considered. The region under study has an average annual rainfall of 355cm during the period 1985-2015 and the value of R is worked out to be 2905.92 MJ mm ha^{-1} hr^{-1} $year^{-1}$.

4.4 Soil Erodibility Factor (K)

The soil erodibility Factor for the present study is obtained from the soil map of the area (Figure 6). The values of soil erodibility for soils in the region range from 0.001 to 0.1 (Figure 7). The mountainous region of the Western Ghats and residual hills are occupied by clayey (0.001 to 0.008) and Gravelly clay (0.003 to 0.01) soils with minor rocky outcrops (0.002). Coastal areas are occupied by diverse textured soils, dominated by Sandy over loamy around fluvial channels (0.07 to 0.08) Gravelly clay, followed by loamy over sandy (0.036), sand (0.1), and mud (0.01). With an increase in the sand portion of the soil, its susceptibility to erosion is increased. Clays however resist erosion due to cohesive forces among particles.

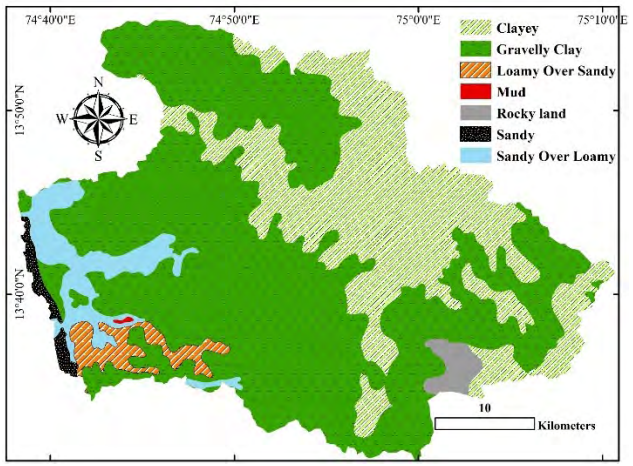

Figure 6: Soil map of the watershed derived from Karnataka soil cover map (2003) prepared by The National Bureau of Soil Survey and Land Use Planning, India on a scale of 1:2,50,00,000

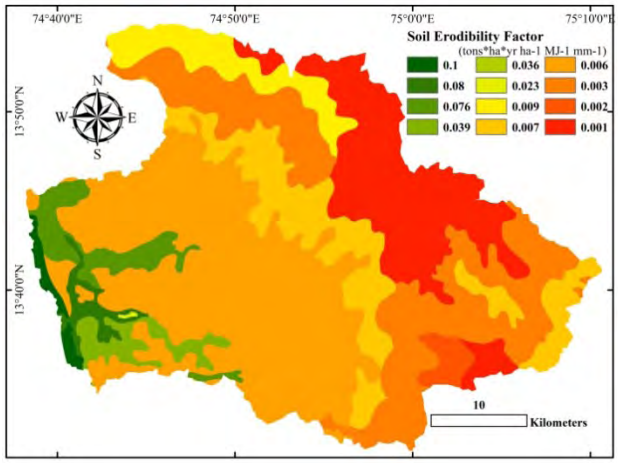

Figure 7: Soil Erodibility Factor (K) map

4.5 Topographic Factor (LS)

The study area has higher Topographic factor values in the Western Ghats (4.25 to 135.74) an attribute of a large elevation drop within a small area. It decreases further west towards the residual hills (0.53 to 4.25) and coastal plains (0 to 0.53) of the catchment (Figures 8 and 9). Since the streams draining higher relief areas have high velocity, they are capable of eroding more than those flowing in the lower reliefs in the coastal plains.

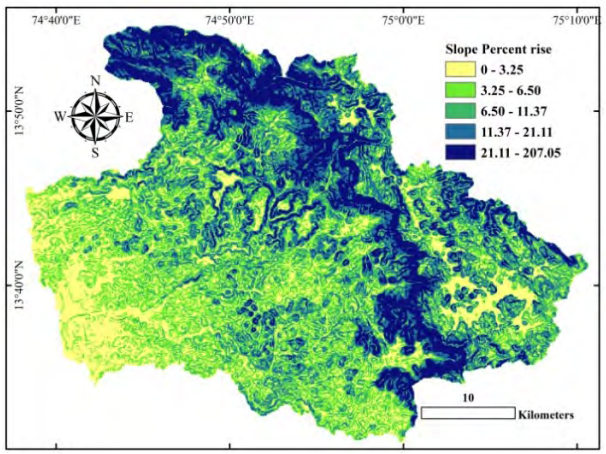

Figure 8. Slope map of the basin

4.6 Cover Management Factor (C)

The results (Table 3) suggest forest in the area is the dominant land cover (71.96%) followed by agricultural and fallow land (23.38%) (Figure 10).Value of C range from 0 to 0.59 for the study area (Figure 11). Higher values indicate water bodies, agricultural land, or poor vegetal cover. The evergreen and semi-evergreen forest-covered areas show lower C values. The direct impact of rain on the surface is thus reduced and prevents soil from being eroded due to flash erosion caused by precipitation.

Table 3. Classification of land use land cover.

Sr. No.	Class Name	Area (ha)	Area (%)
1	Water Body	6190.2	4.09
2	Forest land	73705.6	48.65
3	Scanty vegetation	33795.4	22.31
4	Suburban Area	2136.87	1.41
5	Barren Land	228.78	0.15
6	Agricultural Land	35433.1	23.39
Total		**151490***	**100**

* The observed difference between total areas of the basin pertains to geometric approximation.

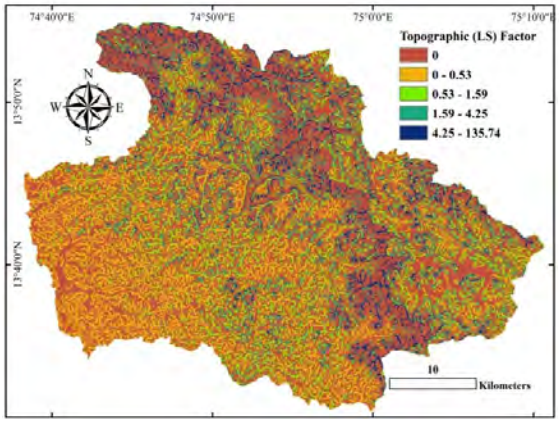

Figure 9.Topographic factor (LS) map

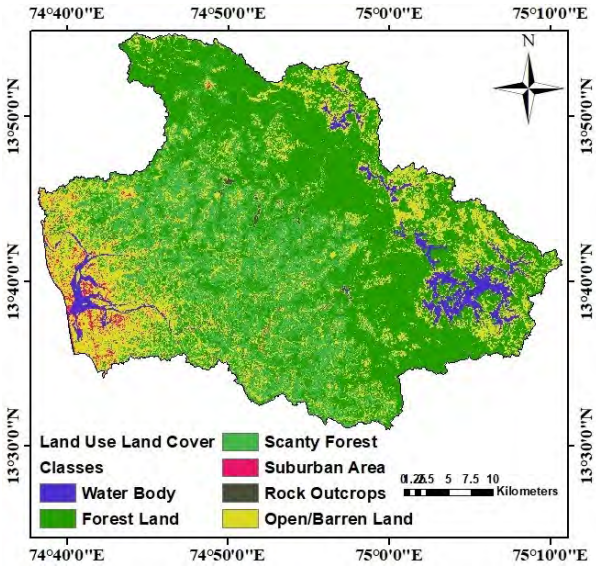

Figure 10. Land use land cover of Gangolli basin

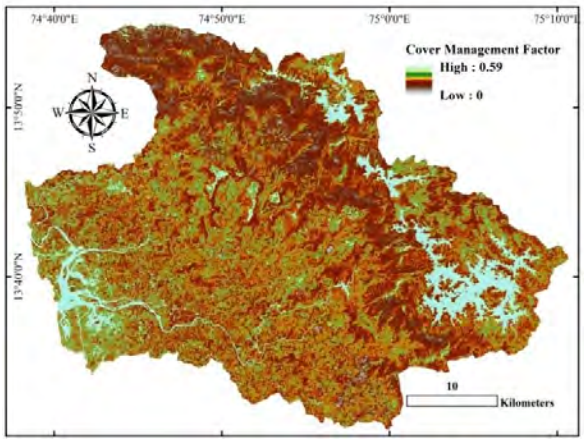

Figure 11. Crop Management factor (C) map4.7 Conservation Practice Factor (P):

Total forested land in the area together with thick and scanty vegetation account for 71.96%, whereas, of the remaining area 23.38% is covered by agricultural land, 4% by water bodies and the remaining is minor built-up land and barren area. Of the 71.96% vegetation cover, 48.65% is permanent forest land that occupies steep slopes of the Western Ghats. Hence P is considered to be 0.5 (USDA Handbook 1981). Due to the forest cover, the effect of the increase in velocity of runoff over steep slopes of the Western Ghats is reduced.

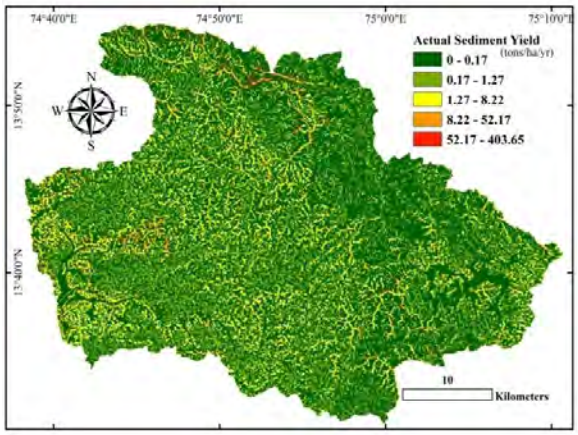

Figure 12. Map showing the actual sediment yield of the watershed

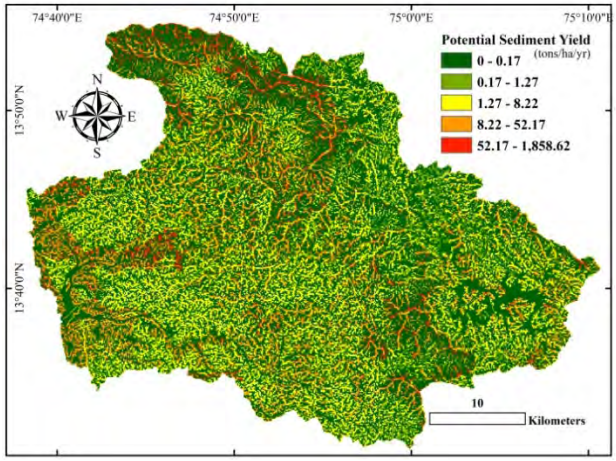

Figure 13. Map showing the potential of the watershed to yield sediments

.8 Sediment influx in the estuarine environment

The estimated sediment influx into the Gangolli estuary through the catchment using the RUSLE model revealed an annual sediment discharge of 1,98,774.06 tons (Table 4) (Figure 12). High erosive potential zones are located in the coastal plains of the basin, where most of the agricultural and urban areas exist. In the absence of the Cover Management factor, using the RUSLE model, the estimate reveals that the basin is capable of releasing 12,32,868.17 tons (Table 5) of sediments into the estuarine environment annually (Figure 13). Upon comparing the actual soil loss with the potential soil loss of the study area, it is clear that the basin is capable of releasing 10,34,094.11 tons of soil more in the absence of vegetation cover. The land use land cover map reveals that the erosive hotspots are concentrated around the estuary/lower catchment where the agricultural area and the sub-urban areas lie.

5. Discussion

A hot and humid climate facilitates soil formation processes in the tropical region, while the high precipitation and relief help in the transportation of sediments to the sea. The Gangolli River has a shorter flow length and hence has high erosive strength. This is reflected in deep entrenching valleys and high sediment output through the catchment outlets of the nearby rivers (Ganasri & Ramesh, 2016).

Higher erosive strength combined with high basin relief (1360m), high drainage density (0.35km/km^2), and high ruggedness number (458.55) and cohesive sediments in the high relief regions leads to increased sediment yield, lowered infiltration, and high runoff. These factors thus together overcome lower circularity (0.25) and high elongation (0.51) of the basin (Gajbhiye et al., 2014).

The present study revealed an estimate of 1,98,774.06 tons of annual sediment yield through the Gangolli basin of an area of 151357.08 hectares with an average sediment yield of 1.12 tons/ hectare area of the basin. Basins with a low circularity ratio have high channel storage and low sediment yield–delivery ratio (Singh et al., 2009, Bhagwat et al., 2011). Elongation ratios nearer to 1.0 are typical of regions of very low time of concentration resulting in peak flow and flood (Bhagwat et al., 2011). Since the river has a low Circularity ratio and high elongation ratio, sediment influx to the estuarine environment is high.

The sediments are mostly concentrated in the nearshore region and continental shelf, with only ~8% of the terrestrial sediment input reaching the deep ocean (Gibbs, 1981; Schubel & Kennedy, 1984). The release of sediments into the estuarine environment, coupled with sediment influx/out fluxes through tidal surges are evident from the morphological changes in the estuarine islands and their banks (Mahapatra et al., 2014). Sediment yields through the basin hence help in the effective management of the estuarine and coastal morphology.

The potential of the basin to yield sediments in the absence of vegetation cover in the area using RUSLE (Renard, 1997) gave an estimate of 12,32,868.17 tons of sediments that can be delivered into the Gangolli estuary. This suggests an average of 10,34,094.11 tons of sediments is annually held by the vegetation cover in the basin. Therefore, any change in land use land cover in the basin will alter the quantum of sediments that can be yielded from the basin.

Table 4. Categorization of the actual degree of soil erosion, and soil loss

Erosion Categories	Class Interval	Area (ha)	Area (%)	Soil Loss (tons yr-1)
Very slowly eroding	0-0.17	89,795.87	59.33	1.18
Slightly eroding	0.17-1.27	34,925.87	23.08	22,694.86
Moderately eroding	1.27-8.22	22,567.62	14.91	84,915.63
Highly eroding	8.22-52.17	3,867.49	2.56	69,683.84
Severely eroding	>52.17	200.23	0.13	21,478.55
Total		**1,51,357***		**1,98,774.06**

*The observed difference between total areas of the basin pertains to geometric approximation.

Table 5. Categorization of potential degree of soil erosion, and soil loss

Erosion Categories	Class Interval	Area (ha)	Area (%)	Soil Loss (tons yr-1)
Very slowly eroding	0-0.17	89,748.15	59.30	18.6
Slightly eroding	0.17-1.27	5,511.11	3.64	5,330
Moderately eroding	1.27-8.22	30,341.80	20.05	1,42,503.9
Highly eroding	8.22-52.17	21,646.54	14.30	5,24,948.8
Severely eroding	>52.17	4,109.48	2.72	5,60,066.8
Total		**1,51,357***		**12,32,868.17**
Sediments held by basin				**10,34,094.11**

*The observed difference between the total areas of the basin pertains to geometric approximation.

6. Conclusion

Extensive coastal conservation projects like seawall construction and breakwater construction along the Maravanthe coast imply beach erosion problems. At the same time, training of the river mouth with breakwaters and dredging to maintain the navigational depth in the estuarine channel indicates siltation. The building of several dam reservoirs and vented dams in the upstream basin has rendered low fluvial sediment influx to the coastal environment. These observations necessitate the estimation of sediment yield through the basin. This study employed the Revised Universal Soil Loss Equation to model the soil yielded from the Gangolli watershed. The basin yielded 1,98,774.06 tons of soil during the year 2015. In the complete absence of vegetation cover, the basis has the potential of yielding 12,32,868.17 tons/yr soil. With continued deforestation, erosion of soil will concentrate along the residual hills and coastal plains. This huge quantity of sediments can reduce the storage capacity of reservoirs upstream as well contribute to the siltation of the estuarine navigable channel. Knowledge of the quantum of sediment yield through the basin will provide valuable insight and a basis for the management of estuary and the adjacent beaches.

Watersheds with fairly good permanent vegetation cover, low relief, and well-developed soil cover for a high infiltration rate with low runoff, and low elongation ratio with favorable conservation practices will thus yield lower sediments in a given tropical climate. Whereas a decrease in forest covers, high relief with lower flow length leads to higher susceptibility of soil to erosion in the same climate. Availability of temporally distributed sediment discharge data at the outlet of a river, rainfall data over the basin, and field surveyed soil texture data can help to predict an accurate estimate of sediment yield through a basin. The present study is based on readily available data in the public domain and with limited ground-truth surveys. The study concludes that the Revised Universal Soil Loss Equation is an efficient and effective method for estimating sediment yield through a tropical river basin.
This study helps in understanding the role of vegetation cover in conserving soil and the potential of fluvial sediments in controlling the configuration of the coast. RUSLE has proved to be an effective tool in the quantification of sediment yield through the watershed. It is an efficient method to locate erosional hotspots and hence its management. A yearly sediment yield estimation is required to establish the trend in.

Acknowledgment
The study has been carried out as a part of the Space Applications Centre-funded ISRO-RESPOND project (No.B.19012/50/2017 Sec 2). The authors are grateful to the Indian Meteorological Department and Indian National Bureau of Soil Survey and Land use planning for providing us with rainfall data and soil maps. Facilities extended to carry out the study at the Geology Laboratory, SDMCET, are sincerely acknowledged.

References

Ajayakumar P., S. Rajendran and T.M. Mahadevan (2017). Geophysical lineaments of Western Ghats and adjoining coastal areas of central Kerala, southern India and their temporal development. Geoscience Frontiers, 8(5), 1089–1104. https://doi.org/10.1016/j.gsf.2016.11.005

Akhil R., T.K. Prasad and V. Vineethkumar (2022). Analyzing the significance of morphometric parameters in runoff efficiency: A case study in Valakkayi Tode tropical watershed, Valapattanam River, Kerala, India. Journal of Sedimentary Environments, 7, 67–78. https://doi.org/10.1007/s43217-021-00083-2

Amin M. and S.A. Romshoo (2019). Comparative assessment of soil erosion modelling approaches in a Himalayan watershed. Modeling Earth Systems and Environment, 5(1), 175–192. https://doi.org/10.1007/s40808-018-0526-x

Babu R., B.L. Dhyani and N. Kumar (2004). Assessment of erodibility status and refined iso-erodent map of India. *Indian Journal of Soil Conservation*, *32*(3), 171–177.

Bhagwat T.N., A. Shetty and V.S. Hegde (2011). Spatial variation in drainage characteristics and geomorphic instantaneous unit hydrograph (GIUH); implications for watershed management—A case study of the Varada River basin, Northern Karnataka. *CATENA*, *87*(1), 52–59. https://doi.org/10.1016/j.catena.2011.05.007

Dai Z., X. Mei, S.E. Darby, Y. Lou and W. Li (2018). Fluvial sediment transfer in the Changjiang (Yangtze) river-estuary depositional system. Journal of Hydrology, 566, 719–734. https://doi.org/10.1016/j.jhydrol.2018.09.019

Djoukbala O., M. Mazour, M. Hasbaia and O. Benselama (2018). Estimating of water erosion in semiarid regions using RUSLE equation under GIS environment. Environmental Earth Sciences, 77(9), 345. https://doi.org/10.1007/s12665-018-7532-1

Eisma D. (1988). Transport and Deposition of Suspended Matter in Estuaries and the Nearshore Sea. In A. Lerman & M. Meybeck (Eds.), *Physical and Chemical Weathering in Geochemical Cycles* (pp. 273–298). Springer Netherlands. https://doi.org/10.1007/978-94-009-3071-1_13

Evans P., D. Hanslow, A. Coutts-Smith and Z.J. You (2001). Nearshore—Inner Shelf Sediment Exchange on the NSW Central Coast. In Coastal Engineering 2000—Proceedings of the 27th International Conference on Coastal Engineering, ICCE 2000 (Vol. 276, p. 3164). https://doi.org/10.1061/40549(276)245

Frihy O. E. (2007). Chapter 2 The Nile Delta: Processes of Heavy Mineral Sorting and Depositional Patterns. In M. A. Mange & D. T. Wright (Eds.), Developments in Sedimentology (Vol. 58, pp. 49–74). Elsevier. https://doi.org/10.1016/S0070-4571(07)58002-7

Gajbhiye S., S.K. Mishra and A. Pandey (2014). Prioritizing erosion-prone area through morphometric analysis: An RS and GIS perspective. Applied Water

Science, 4(1), 51–61. https://doi.org/10.1007/s13201-013-0129-7

Ganasri B.P. and H. Ramesh (2016). Assessment of soil erosion by RUSLE model using remote sensing and GIS - A case study of Nethravathi Basin. *Geoscience Frontiers*, *7*(6), 953–961. https://doi.org/10.1016/j.gsf.2015.10.007

Gibbs R.J. (1981). Sites of river-derived sedimentation in the ocean. *Geology*, *9*(2), 77–80.

Gopinathan C.P. and S.Z. Qasim (1971). Silting In Navigational Channels Of The Cochin Harbour Area. Journal of the Marine Biological Association of India, 13(1), Article 1.

Hegde V.S., G.D. Kanchanagouri, P.T. Hanamgond, G.K. Huchchannavar, G. Shalini and M.S. Bhat (2004). Depositional environment and silting in the Sharavati estuary, central west coast of India. *IJMS Vol.33(3)*. http://nopr.niscair.res.in/handle/123456789/1683

Hegde V.S., B.K. Koti, P. Hanamgond, G. Shalini and K.H. Girish (2007). Depositional environment of a tropical estuarine beach near Sharavati River mouth, Central West Coast of India. *Journal of the Geological Society of India*, *69*, 1279–1284.

Hegde V.S., S. Nayak, G. Shalini, P.A. Krishnaprasad, A.S. Rajawat, K.H. Girish and T. Bhagwat (2012). Spit Dynamics along the Central West Coast of India: Implications for Coastal Zone Management. *Journal of Coastal Research*, *28*, 505–510. https://doi.org/10.2307/41509948

Hegde, V.S., G. Shalini, S. Nayak, A.S. Rajawat, A. Suryanarayana, J. Seelam, B.K. Koti and G.K. Girish (2009). Low-Scale Foreshore Morphodynamic Processes in the Vicinity of a Tropical Estuary at Honnavar, Central West Coast of India. *Journal of Coastal Research*, *25*. https://doi.org/10.2112/07-0902.1

Jong S.M. de, l.C. Brouwer and H.T. Riezebos (1998). *Erosion hazard assessment in the La Peyne catchment, France.*

Karapurkar D., V.S. Hegde and R. Ramakrishnan (2022). Sediment dispersal pattern along an engineered micro-tidal tropical estuarine beach. *Journal of Earth System Science*, *131*(1), 13. https://doi.org/10.1007/s12040-021-01767-z

Kinsela M.A., D.J. Hanslow, R.C. Carvalho, M. Linklater, T.C. Ingleton, B.D. Morris, K.M. Allen, M.D. Sutherland and C.D. Woodroffe (2022). Mapping the Shoreface of Coastal Sediment Compartments to Improve Shoreline Change Forecasts in New South Wales, Australia. Estuaries and Coasts, 45(4), 1143–1169. https://doi.org/10.1007/s12237-020-00756-7

Kuang C., W. Chen, J. Gu and L. He (2014). Comprehensive analysis on the sediment siltation in the upper reach of the deepwater navigation channel in the Yangtze Estuary. Journal of Hydrodynamics, 26(2), 299–308. https://doi.org/10.1016/S1001-6058(14)60033-0

Kumar A., K.S. Jayappa and P. Vethamony (2012). Evolution of Swarna estuary and its impact on braided islands and estuarine banks, Southwest coast of India. *Environmental Earth Sciences*, *65*(3), 835–848. https://doi.org/10.1007/s12665-011-1128-3

Kumar A., K.S. Jayappa and B. Deepika (2010). Application of remote sensing and geographic information system in change detection of the Netravati and Gurpur river channels, Karnataka, India. *Geocarto International*, *25*(5), 397–425. https://doi.org/10.1080/10106049.2010.496004

Lalomov A.V. (2003). Differentiation of Heavy Minerals in the Alongshore Debris Flow and Modeling of Processes of Coastal-Marine Placer Formation. Lithology and Mineral Resources, 38(4), 306–313. https://doi.org/10.1023/A:1024607628886

Lam-Hoai T., D. Guiral and C. Rougier (2006). Seasonal change of community structure and size spectra of zooplankton in the Kaw River estuary (French Guiana). Estuarine, Coastal and Shelf Science, 68(1), 47–61. https://doi.org/10.1016/j.ecss.2006.01.009

Mahapatra, M., R. Ramakrishnan and A.S. Rajawat (2014). *Monitoring long-term morphological changes of Narmada estuary using remote sensing and GIS techniques*. *8*.

Markose V.J. and K.S. Jayappa (2016). Soil loss estimation and prioritization of sub-watersheds of Kali River basin, Karnataka, India, using RUSLE and GIS. Environmental Monitoring and Assessment, 188(4), 225. https://doi.org/10.1007/s10661-016-5218-2

Milliman J.D. (1991). Flux and fate of fluvial sediment and water in coastal seas. *Ocean Margin Processes in Global Change. Report, Dahlem Workshop, Berlin, 1990*, *9*, 69–89.

Nayak S., V.S. Hegde, G. Shalini, A.S. Rajawat, K.H. Girish, J. Seelam and A. Suryanarayana (2010). Geomorphic Processes in the Vicinity of the Venkatapur River Mouth, Central West Coast of India: Implications for Estuarine Sedimentation. *Journal of Coastal Research*, *265*. https://doi.org/10.2307/40863894

Paltekar M., V.S. Hegde, S. Hulaji, A.R. Pratihari and M.M. Korkoppa (2021). Geochemistry of heavy minerals from Uttara Kannada beach sediments, West Coast of India: An insight into provenance studies. *Journal of Sedimentary Environments*, *6*(4), 693–705. https://doi.org/10.1007/s43217-021-00078-z

Pradhan U., P. Mishra, P.K. Mohanty and B. Behera (2015). Formation, Growth and Variability of Sand Spit at Rushikulya River Mouth, South Odisha Coast, India. Procedia Engineering, 116, 963–970. https://doi.org/10.1016/j.proeng.2015.08.387

Rangsiwanichpong P., S. Kazama and L. Gunawardhana (2018). Assessment of sediment yield in Thailand using revised universal soil loss equation and geographic information system techniques. River Research and Applications, 34(9), 1113–1122. https://doi.org/10.1002/rra.3351

Rao V.P. and W.G. Wagle (1997). Geomorphology and surficial geology of the western continental shelf and slope of India: A review. *Current Science*, *73*(4), 330–350.

Renard K.G., G.R. Foster, G.A. Weesies, D.K. McCool and D.C. Yoder (1997). *Predicting soil erosion by water: A guide to conservation planning with the Revised Universal Soil Loss Equation (RUSLE)*. Washington, DC (USA) ARS.

Schubel J.R. and V.S. Kennedy (1984). The Estuary as a Filter: An Introduction. In V. S. Kennedy (Ed.), *The Estuary As a Filter* (pp. 1–11). Academic Press. https://doi.org/10.1016/B978-0-12-405070-9.50007-4

Schumm S.A. (1956). Evolution of Drainage Systems and Slopes in Badlands at Perth Amboy, New Jersey. GSA Bulletin, 67(5), 597–646. https://doi.org/10.1130/0016-7606(1956)67[597:EODSAS]2.0.CO;2

Shalini G., V.S. Hegde, M. Soumya and M.M. Korkoppa (2019). Provenance and Implications of Heavy Minerals in the Beach Sands of India's Central West Coast. *Journal of Coastal Research*, *36*(2), 353–361. https://doi.org/10.2112/JCOASTRES-D-19-00046.1

Shankar R. and B.R. Manjunatha (1997). Onshore Transport of Shelf Sediments into the Netravati-Gurpur Estuary, West Coast of India: Geochemical Evidence and Implications. Journal of Coastal Research, 13(2), 331–340.

Singh J.P., D. Singh and P.K. Litoria (2009). Selection of suitable sites for water harvesting structures in Soankhad watershed, Punjab using remote sensing and geographical information system (RS&GIS) approach—A case study. Journal of the Indian Society of Remote Sensing, 37(1), 21–35. https://doi.org/10.1007/s12524-009-0009-7

Strahler A.N. (1952). Hypsometric (Area-Altitude) Analysis of Erosional Topography. *GSA Bulletin*, *63*(11), 1117–1142. https://doi.org/10.1130/0016-7606(1952)63[1117:HAAOET]2.0.CO;2

Strahler A.N. (1954a). Statistical Analysis in Geomorphic Research. The Journal of Geology, 62(1), 1–25. https://doi.org/10.1086/626131

Strahler A.N., (1954b) Quantitative geomorphology of erosional landscapes, C.-R. 19th Intern. Geol. Conf, Algiers, sec. 13, pt. 3, pp. 341-354.

Subrahmanya K.R. (1996). Active intraplate deformation in south India. Tectonophysics, 262(1), 231–241. https://doi.org/10.1016/0040-1951(96)00005-4

Sukristiyanti S., R. Maria and H. Lestiana (2018). Watershed-based Morphometric Analysis: A Review. IOP Conference Series: Earth and Environmental Science, 118, 012028. https://doi.org/10.1088/1755-1315/118/1/012028

Tamura T., K. Horaguchi, Y. Saito, V.L. Nguyen, M. Tateishi, T.K.O. Ta, F. Nanayama and K. Watanabe (2010). Monsoon-influenced variations in morphology and sediment of a mesotidal beach on the Mekong River delta coast. Geomorphology, 116(1), 11–23. https://doi.org/10.1016/j.geomorph.2009.10.003

Ullah S., A. Ali, M. Iqbal, M. Javid and M. Imran (2018). Geospatial assessment of soil erosion intensity and sediment yield: A case study of Potohar Region, Pakistan. Environmental Earth Sciences, 77(19), 705. https://doi.org/10.1007/s12665-018-7867-7

United States & Department of Agriculture. (1981). 1981 handbook of agricultural charts. 101: charts, maps 28 cm.- USDA.

Wischmeier W.H. and D.D. Smith (1978). Predicting rainfall erosion losses—A guide to conservation planning. *Predicting Rainfall Erosion Losses - a Guide to Conservation Planning.*https://www.cabdirect.org/cabdirect/abstract/19786726437

Journal of Geomatics Vol. 17, No. 2, October 2023

Evaluation of Slope Correction Methods to Improve Surface Elevation Change Estimation over Antarctic Ice Sheet using SARAL/AltiKa

Priyanka Patel[1, *], Purvee Joshi[2], Tarang Patadiya[3], Sushil Kumar Singh[2], Kunvar Yadav[1], Sandip R Oza[2]
[1] Ganpat University, Mehsana
[2] Space Applications Center, ISRO, Ahmedabad
[3] Gujarat University, Ahmedabad
[*]Correspondence E-mail: pyankap@gmail.com

(Received: 30 December 2022; Accepted: 9 July 2023)

DOI: *https://doi.org/10.58825/jog.2023.17.2.23*

Abstract: Antarctic Ice Sheet (AIS) surface elevation change plays a crucial role in understanding the ice sheet mass balance. The present study focuses on improving AIS surface elevation estimations by incorporating slope correction methods called Direct Method (DM) using SARAL/AltiKa 40 Hz geophysical data record for 2013 (Exact Repeat Mission) and 2020 (Drifting Phase) with terrain slope ranges from 0° to 0.85°. The NASA's Ice, Cloud, and Land Elevation Satellite (ICESat) Digital Elevation Model (DEM) has been utilized as a priori topography model to retrieve slope of the AIS terrain. While comparing the two direct methods (DM1 & DM2) based slope corrected elevations with Operation Ice Bridge (OIB) elevation data of November 2013, the RMSE resulted in 0.35 and 0.37 m and biases of the order of 0.26 and 0.28 m for DM1 and DM2 respectively. Moreover, comparison with ICESat DEM showed the RMSE of the order of 1.81 and 2.09 m, and biases of the order of 0.95 and 0.99 m for DM1 and DM2, respectively. It has been observed that DM1 is the most suitable method for correcting terrain slope with the lowest RMSE and bias. Moreover, the slope induced error correction methods show utmost importance in estimating accurate elevation, especially over undulating terrain of AIS.

Keywords: SARAL/AltiKa, Antarctic Ice Sheet, Surface Elevation, Slope Correction Method

1. Introduction

The study of changes in Antarctic Ice Sheet (AIS) surface elevation serves as a significant response of ice dynamics and is crucial for understanding global climatic variations (Helm et al., 2014; Felikson et al., 2017; Suryawanshi et al., 2019). A satellite altimetry is a key measurement tool for monitoring polar ice sheets (Remy et al., 1989). Zwally et al. (1975) first proposed the use of the satellite altimetry to measure ice sheet surface elevation changes. Several studies used altimeter due to its capability to provide almost complete and homogeneous coverage of the ice sheets, which makes it useful for understanding and analysing elevation over ice sheets (Bamber, 1994; Davis et al., 2004; Roemer et al., 2007; Pritchard et al., 2009; Flament and Remy, 2012; Helm et al., 2014; Mcmillan et al., 2019; Suryawanshi et al., 2019; Hai et al., 2021).

Both laser and radar altimeters have been widely used to observe polar elevations remotely (Pritchard et al., 2009; Smith et al., 2009; Sorensen et al., 2011; Ewert et al., 2012). For example, to examine the AIS elevation changes between 1995 and 2000, Davis et al. (2004) used ERS-2 radar altimeter data. Another study by Pritchard et al. (2009) utilized ICESat laser altimeter data to monitor AIS elevation changes. However, there are certain advantages and disadvantages of both laser and radar altimeters. For instance, in a laser altimeter the divergence of the beam is narrow, resulting in a fine resolution footprint. Due to this the slope-induced error in estimating elevation can be ignored (Fricker et al., 2005; Brenner et al., 2007). On the other hand, the processing of radar altimeter data over ice sheet surface is complicated due to its large radar footprint, causing the slope-induced error (SE) in elevation estimations. This requires slope correction in radar altimeter as the essential data processing step for correcting the range of the satellite for the corresponding ground location (Bamber, 1994; Schroder et al., 2019; Hai et al., 2021).

There are certain slope correction methods such as Direct Method (DM), Intermediate Method (IM) and Relocation Method (RM). The IM (Remy et al., 1989) does not deal with correcting the range of the satellite, instead, it focuses on finding the exact location so that the measured range becomes accurate. The RM (Brenner et al., 1983; Roemer et al., 2007; Hai et al., 2021) locates the closest point to the satellite using surface slope magnitude and direction and calculates the correction required to determine surface elevation. The DM (Brenner et al., 1983) calculates the corrected range to the nadir position using the surface slope magnitude between the closest point and nadir. Based on the previous studies (Brenner et al., 1983; Cooper, 1989; Bamber, 1994; Roemer et al., 2007; Hurkmans et al., 2012; Helm et al., 2014; Hai et al., 2021), two mathematical approaches of the direct method have been noticed, which helps in retrieving the elevation in a more accurate manner. Here, the approaches have been termed as Direct Method 1 (DM1) (Roemer et al., 2007; Hai at al., 2021) and Direct Method 2 (DM2) (Brenner et al., 1983; Suryawanshi et al., 2019).

DM1, a study by (Brenner et al., 1983; Bamber, 1994; Roemer et al., 2007) have introduced the consideration of quadratic function to fit the varying DEM surface as the effective surface. This function helps in calculating the local slope angle and direction, which further minimizes much of a slope-induced error in estimating elevation (discussed in detail in section 4). DM2 incorporated by (Brenner et al., 1983; Suryawanshi et al., 2019) measured the elevation impacted due to terrain slope. Therefore, the

present study aims to implement slope correction methods (DM1 and DM2) for further improving the elevation and elevation change over AIS. SARAL/AltiKa, a radar altimeter has been used in this study, which is principally a nadir-looking altimeter that transmits and receives microwave pulses (Ka-band frequency, 35.75 GHz) as backscattered signals (Suryawanshi et al., 2019; Verron et al., 2021). In the present study, the surface elevation has been estimated for 2013 from the Exact Repeat Mission (ERM) and 2020 from the Drifting Phase (DP) of SARAL/AltiKa (discussed in section 3) over AIS. In addition, a-priori available Digital Elevation Model (DEM) from NASA's Ice, Cloud and Land Elevation Satellite (ICESat) was then used to apply slope corrections on the retrieved elevations mainly for regions having slope less than or equal to 0.85°. The limit on the slope has been applied to avoid vertical error which can reach more than 80 m above the surface slope 0.85° (Brenner et al., 1983; Hurkmans et al., 2012; Fei et al., 2017). In order to deduce the best approach out of the two methods (DM1 and DM2), the estimations obtained from SARAL/AltiKa have been compared with NASA's Airborne Topographic Mapper (ATM) of the Operation Ice Bridge dataset for the period 26 November, 2013 and ICESat DEM for the period 2003-2005 over Vostok subglacial lake. The paper also includes the estimation of elevation change between 2013 and 2020 of SARAL/AltiKa slope-corrected datasets over entire AIS, obtained using the best approach out of two (DM1 and DM2).

2. Study Areas

The Antarctic Ice Sheet has been chosen to implement direct method-based slope correction for estimating corrected elevation as shown in Figure 1. A green colored rectangle over East Antarctic Ice Sheet covering Vostok subglacial lake has been selected for finding range correction magnitude (ΔR) associated with terrain slope (θ) for comparison of two methods DM1 and DM2, respectively.

3. Data used

The joint altimetry mission of ISRO and CNES, called as SARAL (Satellite with ARgos and AltiKa) followed initially 35-day repeat cycle, known as Exact Repeat Mission mode (ERM) from launch i.e. February 2013 to July 2016. Thereafter it entered into a new orbit called the Drifting Phase (DP) on July 4, 2016. Both, ERM and DP phases acquisition of SARAL/AltiKa have been depicted for one cycle in Figures 2a and 2b. SARAL/AltiKa 40Hz geophysical data records have been utilized from the FTP link ftp://avisoftp.cnes.fr/AVISO/pub/saral/gdr_f for the years 2013 and 2020 in ERM mode and DP mode respectively as listed in Table 1 to estimate the AIS surface elevation change. The 500 m high resolution NASA's, ICESat DEM (1 February 2003 to 30 June, 2005) downloaded from the US National Snow and Ice Data Centre (NSIDC) website http://nsidc.org/data/nsidc-0304 to estimate the terrain slope of AIS. Further, the ATM of OIB data for the year 2013 have been downloaded from https://nsidc.org/data/ilatm2/versions/2 to compare the slope-corrected dataset of SARAL over Vostok Lake.

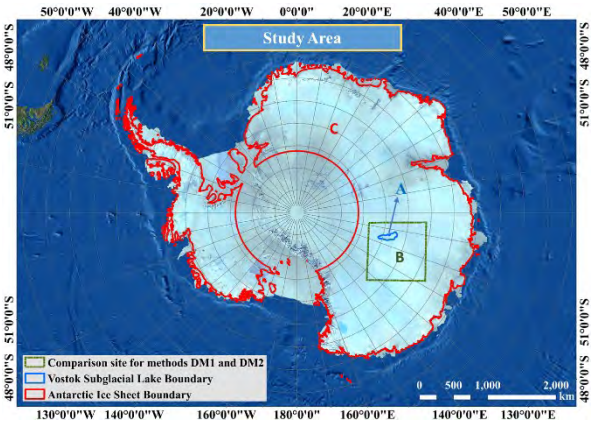

Figure 1: A) Region selected for Comparison of Direct Methods (DM1 & DM2) derived using SARAL/AltiKa with ATM and ICESat DEM over Vostok Lake (shown in blue color), EAIS, B) Region selected for depicting graph of Slope induced elevation correction (ΔR) (metres) vs. Slope (Degrees) (shown in green color) and C) Antarctic Ice Sheet (red color boundary) selected for estimating elevation change by incorporating DM1 based slope correction method

Table 1: Details of altimeter data utilized for applying slope correction methods and improving surface elevation estimations over AIS.

Sr. No.	Acquisition Duration	Data
1	(i) cycles 136 to 146 (16 Dec 2019 - 04 Jan 2021) (ii) cycles 01 to 09 (14 March 2013 - 23 Jan 2014)	SARAL/AltiKa
2	2003-2005	ICESat DEM
3	26 November, 2013	Airborne Topographic Mapper (ATM)

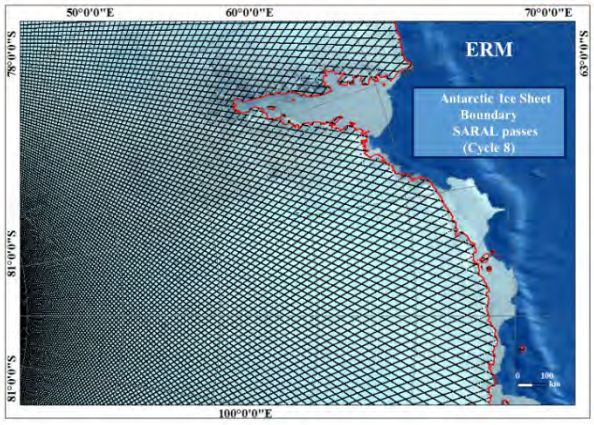

Figure 2a: SARAL/AltiKa passes of cycle 008 (14 Nov-19 Dec, 2013) in ERM mode

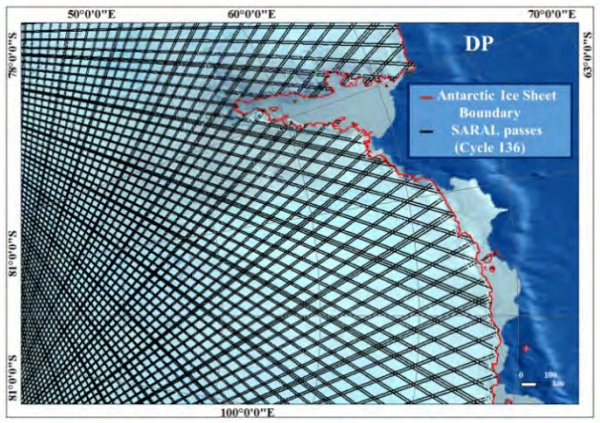

Figure 2b. cycle 136 (16 Dec-20 Jan, 2020) in DP mode over EAIS

4. Methodology

4.1 Ice Surface Elevation Estimation over AIS

The formula suggested by Helm et al. (2014) has been applied to derive the elevation over AIS.

$$\text{Elevation}=H-R_m-\text{DTC}-\text{WTC}-\text{IC}-\text{SETC}-\text{PTC} \quad (1)$$

where,
H is altitude of a satellite,
R_m is measured range of a satellite,
DTC and WTC are Dry and Wet Troposphere Corrections
IC is Ionosphere Correction
SETC is Solid Earth Tide Correction
PTC is Pole Tide Correction

Ice-2 is a physical retracker on board SARAL, which adapts brown model (Brown, 1977) with slight modification, where the concept is to fit the return waveform especially for the ice sheet region to coincide with the brown shape model. In the present study, elevation change between 2013 [cycles 01 to 09 (14 March 2013 - 23 Jan 2014)] and 2020 [cycles 136 to 146 (16 Dec 2019 - 04 Jan 2021)] have been derived using ice-2 retracker range.

4.2 Slope Induced Elevation Correction Methods

Due to complicated and non-linear surface topography, the altimeter measures range from the Point Of Closest Approach (POCA) instead of nadir view, which makes it difficult to process altimeter data for retrieving the correct estimation of surface elevation. Several hundred meters of vertical error can be introduced by a slope of 0.85˚ when measured at 800 km altitude of satellite (Brenner et al.,1983). In order to estimate correct elevation over such surfaces, it becomes very crucial to incorporate terrain slope information. This can be achieved by applying slope correction methods. Slope correction methods can be broadly categorized as (i) Direct Method (DM) (ii) Intermediate Method (IM) and (iii) Relocation Method (RM).

In present study, we have employed direct methods in order to incorporate the slope information and thereby improved surface elevation. Direct method for correcting slope induced error calculates the corrected range from the Center Of Gravity (COG) of satellite to the nadir point, which is normal to the local ellipsoid surface. The assumption for the direct method is such that the terrain surface between the originally measured position (P) and satellite nadir point (S) is a simple inclined plane as shown in Figure 3. Plane slope angle θ has been used for the range correction estimation.

The two direct methods suggested by (i) Hai et al. (2021) (here after named as Direct Method 1 (DM1)) (ii) Brenner et al. (1983) (here after named as Direct Method 2 (DM2)) have discussed in detail in subsequent sub sections for the terrain slope range 0 to 0.85°. A python based module has been developed to implement the slope correction methods over AIS surface elevation and ESRI's ArcGIS was used to analyze the outputs of the study.

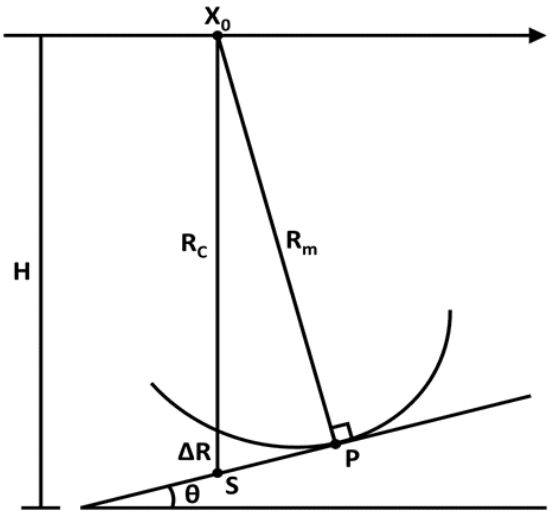

Figure 3: Schematic diagram of direct method.

4.2.1 Direct Method 1 (DM1)

Within the radar Pulse Limited Footprint (PLF), the topography surface can either be complex or flat region. In the present case we have utilized the first study approached by Hai et al. (2021) for the terrain slope range 0 to 0.85°. In this case, a quadratic function has been introduced to fit the varying DEM surface as the effective surface. Explicitly, the method was expressed by Roemer et al. (2007) as follows:

$$h_i = \overline{h} + \theta_x x_i + \theta_y y_i + \theta_{xx} x_i^2 + \theta_{xy} x_i y_i + \theta_{yy} y_i^2 \quad (2)$$

$$\theta = \sqrt{\theta_x^2 + \theta_y^2} \quad (3)$$

$$c = \frac{2(\theta_x^2\theta_{xx} + \theta_x\theta_y\theta_{xy} + \theta_y^2\theta_{yy})}{\theta^2} \quad (4)$$

$$R_c - R_m = \Delta R \quad (5)$$

$$\Delta R = \frac{R_m\theta^2}{2\left(1 - R_m\left(c - \frac{1}{r_E + \overline{h}}\right)\right)} \quad (6)$$

In the final expression of correct elevation, the R_m (measured range) will be replaced by the corrected range R_c (measured from eq. 5) in the equation 1.

where,
h_i,x_i , y_i are vertical & horizontal Cartesian coordinates of each DEM pixel
$\overline{h}$ is fitted model elevation in meters (m)
θ_x, θ_y,θ_{xx},θ_{xy},θ_{yy} are 1st and 2nd order coefficients of topography (need to be estimated)
c is curvature is measured in (m^{-1})
θ is slope angle measured in radians
R_c is corrected range measured in meters (m)
$\Delta R = R_c - R_m$ measured in meters (m)
r_E is mean radius of Earth that is equal to 6371 km = 6371000 m

To implement the direct method 1, there are two key points which need to be noted. First, determining the fitting area within the nadir (S) and POCA (P) points. A technique called the Euclidean distance, is used to search a fitting area within the footprint between the COG of the satellite and DEM cells. Secondly, a linear least-square technique is adopted to successfully estimate at least six DEM cells ($\bar{h}, \theta_x, \theta_y,\theta_{xx},\theta_{xy},\theta_{yy}$). Also, in this method, the slope angle is estimated by PLF (Pulse-Limited Footprint) which is determined using the quadratic and spatial scale fitting. This improves the quality of slope and curvature parameters (Roemer et al., 2007).

4.2.2 Direct Method 2 (DM2)

Initially, this method was introduced by Brenner et al. (1983) with the assumption that terrain slope θ is very small. Using this approach Suryawanshi et al. (2019) have shown the slope-induced elevation correction over AIS for the terrain slope range 0 to 1°. We have incorporated the slope-induced elevation correction (Brenner et al., 1983) using ICESat DEM-derived slope (θ) information for the terrain slope range 0 to 0.85°. The formulae used in the calculations are given below:

$$\Delta R = H - H\cos\theta \quad (7)$$

$$\Delta R = H(1 - \cos\theta) \quad (8)$$

If θ (measured in radians) is small, then

$$\Delta R = \frac{H\theta^2}{2} \quad (9)$$

where,
ΔR is slope induced elevation correction magnitude

$$Correct\ Elevation = Elevation - \Delta R \quad (10)$$

5. Results and Discussion

From the study, it has been observed that in radar altimetry data, slope-induced elevation correction is important. This is because the radar altimeter does not measure the distance between the satellite and the sub-satellite point (nadir), instead, it measures from the POCA in case of an inclined surface, where the measurement taken is shifted upward, resulting in an error, which depends on the square of the slope (Hurkmans et al., 2012). The relationship between correction magnitude (ΔR) and surface slope (θ) has been shown in Figure 4. The statistical trend of the graph shown in Figure 4 has been aligned with the previous studies (Brenner et al., 1983; Suryawanshi et al., 2019; Hai et al., 2021). For example, Brenner et al. (1983) mentioned as "For a radar altimeter with an altitude of 800km and surface slope of 0.8° can cause up to 80 m of vertical error". Therefore, the slope-induced elevation correction has been applied for regions having a slope less than or equal to 0.85° over AIS. However, the graph of (ΔR) vs. slope (θ) has been displayed for the East Antarctic Ice Sheet (EAIS) shown in Figure 1, which shows that the correction magnitude (ΔR) is smaller in DM1 compared to DM2.

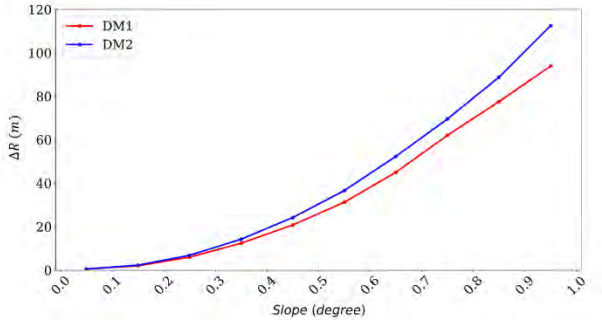

Figure 4: Slope induced elevation correction (ΔR) vs. Slope (Degrees)

5.1 Comparison of DM1 and DM2 over Vostok subglacial Lake

To realize the best approach between the two (DM1 and DM2) in terms of slope correction, slope-corrected surface elevation of SARAL/AltiKa cycle 008 (14 November – 19 December, 2013) data have been compared with the NASA's Airborne Topographic Mapper (ATM) (26 November, 2013) over Vostok subglacial Lake, EAIS (shown in figure 5) because of its flat topography (Richter et al., 2014). The ATM data available over AIS for the year 2013 is available from 18 to 28 November, but we have used 26 November, 2013 in order to compare and overlap the dataset in terms of temporal context with cycle 8 of SARAL/AltiKa over Vostok subglacial lake. The bias and root mean square error for DM1 and DM2 derived from the SARAL/AltiKa dataset with ATM and ICESat DEM are shown in Tables 2 and 3. While comparing DM2 with ATM resulted in RMSE of the order of 0.37 m. On the other hand, the comparison of DM1 with ATM resulted slightly better RMSE of the order of 0.35 m compared to DM2 over Vostok lake. Furthermore, the statistical comparison of DM1 and DM2 (for cycle 8 of SARAL) with DEM (2003-2005) also yielded better RMSE and bias of DM1 (1.81 and 0.95 m) compared to DM2 (2.09 and 0.99 m), respectively. It is to be noted that the above error estimations may also be partially contributed by interpolated products of SARAL/AltiKa. Moreover, Remy et al. (1989) demonstrated in their study that the results of the refined direct method which are termed here as DM1 significantly improve because it accounts for the surface curvature in addition to the slope of the surface. Therefore, based on the computations shown in Table (2, 3) and the graph shown in Figure 4, and also by considering an additional parameter "curvature" along with slope, it can

be inferred that DM1 is better than DM2 in terms of RMSE and bias.

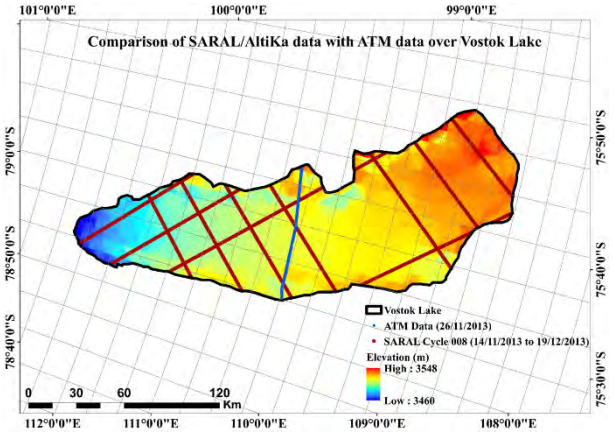

Figure 5: Comparison of Direct Method derived using SARAL/AltiKa with ATM over Vostok Lake

Table 2: Comparison of DM1 and DM2 with ATM over Vostok Lake

Direct Method	Bias (m)	RMSE (m)
DM1	0.26	0.35
DM2	0.28	0.37

Table 3: Comparison of DM1 and DM2 with ICESat DEM over Vostok Lake

Direct Method	Bias (m)	RMSE (m)
DM1	0.95	1.81
DM2	0.99	2.09

5.2 Estimation of elevation over Antarctic Ice Sheet

Figure 6 shows the slope-induced elevation correction map derived using DM1 with an elevation contour of 200 m over the AIS for the year 2020. The elevation has been found to vary between 0 and ~4092 metres. In the inner part of AIS, high elevation is observed (~4092 m) that keeps on decreasing towards the coast.

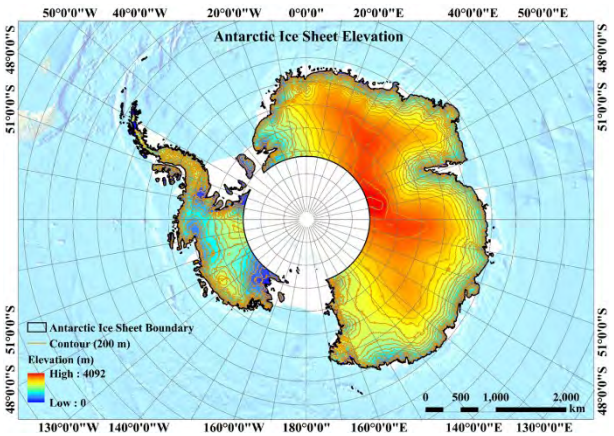

Figure 6: Direct Method 1 based slope corrected map of elevation over Antarctic Ice Sheet for the period 2020

5.3 Elevation change between 2013 and 2020 from SARAL/AltiKa dataset using the DM1 approach

To examine elevation change, the year 2020 [cycle 136 to 146 (16 Dec 2019 - 04 Jan 2021)] has been subtracted from year 2013 [cycle 1 to 9 (14 March 2013 - 23 Jan 2014)] over AIS. It has been observed that the elevation change ranges from -2 to 2 metres per year as shown in figure 7. Moreover, as observed in Figure 2, DP data (2020) represents higher geographic coverage, whereas in ERM mode (2013) same track has been repeated, limiting its capability to cover a larger area on the ground. This yields a higher number of distributed observations per 500m grid cell, which could provide a robust representation of elevation at 500m grid resolution.

It has been noted that in the coastal region, the thinning of ice is more compared to the inner part where the local surface topography is flat. Elevation change obtained between 2013 and 2020 of SARAL/AltiKa over AIS shows the mean loss of -0.26m/yr. It can be inferred from figure 7 that various parts of AIS show different elevation change behaviour. For example, Pine Island and Thwaites glaciers in WAIS show much of elevation loss, shown in blue colour in Figure 7. This may be due to the reasons mentioned by (Davies, 2020) and Darji et al. (2019) that mainly the ice stream is heavily crevassed and dangerous, which results in calving when studied using Sentinel-1A data. There are many other factors also responsible for the calving events, such as earthquakes, which occur at the plate boundaries of the Antarctica Plate (Winberry et al., 2020). In addition, grounding lines in WAIS extend down to 2000 metres below sea level, making the ice sheet intrinsically unstable and susceptible to melting, causing it to move quickly (Schoof, 2007; Davies, 2020). Moreover, stable elevation changes were observed in the EAIS. This may be due to the local surface topography which is the flat terrain, which is mostly located above sea level (An et al., 2022).

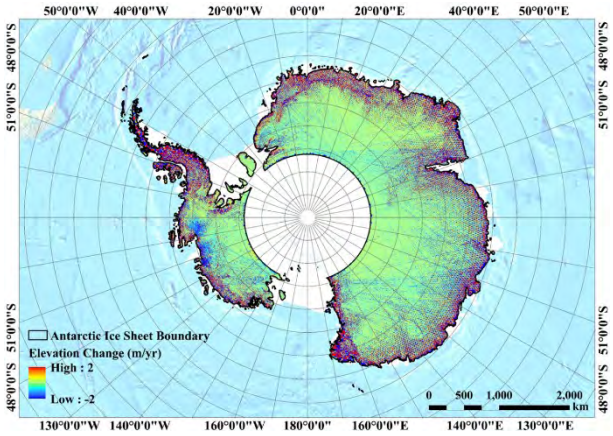

Figure 7: Elevation change between 2013 and 2020 of SARAL/AltiKa in metres per year over AIS

6. Conclusions

The current study is focussed on the detailed discussion and implementation of two approaches of direct methods (DM1 and DM2) to improve elevation and elevation change over the Antarctic Ice Sheet (AIS) for regions having slopes less than or equal to 0.85°. The ICESat DEM

has been used as a priori topography model to retrieve the slope of the surface. Thereafter, in order to check the slope corrected dataset the DM1 and DM2 (for cycle 8 of SARAL) have been compared with ATM (for 26 Nov, 2013) and DEM (2003-2005) over Vostok subglacial Lake.

The study reveals the applicability of DP mode data to assess the average elevation change over ice sheet. Based on the RMSE and bias values obtained on the comparison, it has been observed that DM1 is the appropriate method for slope correction. Therefore, the DM1 method has been utilized to obtain elevation and elevation change between 2013 (Exact Repeat Mission) and 2020 (Drifting Phase) of the SARAL/AltiKa dataset over AIS. This resulted in a mean loss of -0.26 m/yr. Various parts of AIS show different behavior of elevation change. To observe and infer the detailed topography changes, we have to consider a long time series of radar altimeter data. Hence, the study can further continue to estimate and improve the elevation estimations over ice sheets by incorporating the most suitable slope correction technique.

Acknowledgement
We gratefully acknowledge Shri Nilesh M. Desai, Director, (SAC-ISRO) Ahmedabad, for his encouragement and support. We are also thankful to Dr. Parul Patel, Dr. S.P. Vyas and Dr. Sharad Chander from SAC providing the necessary technical support. Authors are also thankful to Dr. Amit Parikh, Head & Principal, MUIS College, Ganpat University for always motivating and supporting.

References

An J., S. Huang, X. Chen, T. Xu and Z. Bai (2022). Research progress in geophysical exploration of the Antarctic ice sheet. Earthquake Research Advances, 100-203.

Bamber J.L. (1994). Ice sheet altimeter processing scheme. International Journal of Remote Sensing, 15(4), 925-938.

Brenner A.C., R.A. Blndschadler, R.H. Thomas and H.J Zwally (1983). Slope-induced errors in radar altimetry over continental ice sheets. Journal of Geophysical Research: Oceans, 88(C3), 1617-1623.

Brenner A.C., J.P. DiMarzio, H.J. and Zwally (2007). Precision and accuracy of satellite radar and laser altimeter data over the continental ice sheets. IEEE Transactions on Geoscience and Remote Sensing, 45(2), 321-331.

Brown G. (1977). The average impulse response of a rough surface and its applications. IEEE transactions on antennas and propagation, 25(1), 67-74.

Cooper A.P.R. (1989, July). Slope correction by relocation for satellite radar altimetry. IEEE, In 12th Canadian Symposium on Remote Sensing Geoscience and Remote Sensing Symposium, 4, 2730-2733.

Davis C.H. and A.C. Ferguson (2004). Elevation change of the Antarctic ice sheet, 1995-2000, from ERS-2 satellite radar altimetry. IEEE Transactions on Geoscience and Remote Sensing, 42(11), 2437-2445.

Darji S., R. Shah, S. Oza and I.M. Bahuguna (2019). Is the Pine Island glacier, Antarctica calving triggered by earthquakes and tsunamis?. Current Science, 116(7), 1057-1059.

Davies B. (2020). Pine Island Glacier, AntarcticGlaciers.org. Retrieved Jan 01, 2023, from https://www.antarcticglaciers.org/antarctica-2/west-antarctic-ice-sheet-2/pine-island-glacier/

Ewert H., A. Groh and R. Dietrich (2012). Volume and mass changes of the Greenland ice sheet inferred from ICESat and GRACE. Journal of Geodynamics, 59, 111-123.

Fricker H.A., A. Borsa, B. Minster, C. Carabajal, K. Quinn and B. Bills (2005). Assessment of ICESat performance at the salar de Uyuni, Bolivia. Geophysical Research Letters, 32(21).

Flament T. and F. Rémy (2012). Dynamic thinning of Antarctic glaciers from along-track repeat radar altimetry. Journal of Glaciology, 58(211), 830-840.

Fei L.I., X.A.I.O.Feng, Z.H.A.N.G. Sheng-Kai, E. Dong-Chen, C.H.E.N.G. Xiao, H.A.O. Wei-Feng, Y.U.A.N. Le-Xian and Z.U.O. Yao-Wen (2017). Dem Development and Precision Analysis for Antarctic Ice Sheet Using Cryosat-2 Altimetry Data. Chinese Journal of Geophysics, 60(3), 231-243.

Felikson D., T.J. Urban, B.C. Gunter, N. Pie, H. D. Pritchard, R. Harpold and B.E. Schutz (2017). Comparison of elevation change detection methods from ICESat altimetry over the Greenland Ice Sheet. IEEE Transactions on Geoscience and Remote Sensing, 55(10), 5494-5505.

Hurkmans R.T.W.L., J.L. Bamber and J.A. Griggs (2012). Brief communication Importance of slope-induced error correction in volume change estimates from radar altimetry. The Cryosphere, 6(2), 447-451.

Helm V., A. Humbert and H. Miller (2014). Elevation and elevation change of Greenland and Antarctica derived from CryoSat-2. The Cryosphere, 8(4), 1539-1559.

Hai G., H. Xie, W. Du, M. Xia, X. Tong and R. Li (2021). Characterizing slope correction methods applied to satellite radar altimetry data: A case study around Dome Argus in East Antarctica. Advances in Space Research, 67(7), 2120-2139.

McMillan M., A. Muir, A. Shepherd, R. Escolà, M. Roca, J. Aublanc, P. Thibaut, M. Restano, A. Ambrozio and J. Benveniste (2019). Sentinel-3 delay-Doppler altimetry over Antarctica. *The Cryosphere, 13*, 709–722.

Pritchard H.D., R.J. Arthern, D.G. Vaughan and L.A. Edwards (2009). Extensive dynamic thinning on the margins of the Greenland and Antarctic ice sheets. Nature, 461(7266), 971-975.

Remy F., P. Mazzega, S. Houry, C. Brossier and J.F. Minster (1989). Mapping of the topography of continental ice by inversion of satellite-altimeter data. Journal of Glaciology, 35(119), 98-107.

Roemer S., B. Legrésy, M. Horwath and R. Dietrich (2007). Refined analysis of radar altimetry data applied to

the region of the subglacial Lake Vostok/Antarctica. Remote sensing of environment, 106(3), 269-284.

Richter A., S.V. Popov, M. Fritsche, V.V. Lukin, A.Y. Matveev, A.A. Ekaykin, V.Y. Lipenkov and R. Dietrich (2014). Height changes over subglacial Lake Vostok, East Antarctica: insights from GNSS observations. Journal of Geophysical Research: Earth Surface, 119(11), 2460-2480.

Schoof C. (2007). Ice sheet grounding line dynamics: Steady states, stability, and hysteresis. Journal of Geophysical Research: Earth Surface, 112(F3).

Smith B.E., H.A. Fricker, I.R. Joughin and S. Tulaczyk (2009). An inventory of active subglacial lakes in Antarctica detected by ICESat (2003–2008). Journal of Glaciology, 55(192), 573-595.

Sorensen L.S., S.B. Simonsen, K. Nielsen, P. Lucas-Picher, G. Spada, G. Adalgeirsdottir, R. Forsberg and C.S. Hvidberg (2011). Mass balance of the Greenland ice sheet (2003–2008) from ICESat data–the impact of interpolation, sampling and firn density. The Cryosphere, 5(1), 173-186.

Schroder L., M. Horwath, R. Dietrich, V. Helm, M.R. Van Den Broeke and S.R. Ligtenberg (2019). Four decades of Antarctic surface elevation changes from multi-mission satellite altimetry. The Cryosphere, 13(2), 427-449.

Suryawanshi M.R., S. Chander, S.R. Oza and I.M. Bahuguna (2019). Variability in the ice sheet elevations over Antarctica derived from repetitive SARAL/AltiKa radar altimeter data (2013–2016). Journal of Earth System Science, 128, 1-11.

Verron J., P. Bonnefond, O. Andersen, F. Ardhuin, M. Bergé-Nguyen, S. Bhowmick, D. Blumstein and E.D. Zaron (2021). The SARAL/AltiKa mission: A step forward to the future of altimetry. Advances in Space Research, 68(2), 808-828.

Winberry J.P., A.D. Huerta, S. Anandakrishnan, R.C. Aster, A.A. Nyblade and D.A. Wiens (2020). Glacial earthquakes and precursory seismicity associated with Thwaites Glacier calving. Geophysical Research Letters, 47(3), e2019GL086178.

Zwally H. (1975). General discussion: the state of the art–and where do we go from here. J. Glaciology, 15(73), 444.

WebGIS-Based Road Crash Information System: A Case Study

Saran M S[1,*], Manju V S[2] and Vishnu V P[1]
[1]KSCSTE - NATPAC, Trivandrum, Kerala
[2] Professor, Dept. of Civil Engineering, College of Engineering Trivandrum, Kerala
Email: saran.ms@gmail.com

(Received: 16 January 2023; in final form 27 April 2023)

DOI: https://doi.org/10.58825/jog.2023.17.2.29

Abstract: Road crashes in India is showing progressive growth since COVID time, despite many road safety measures and programs the rate of crashes is not declining. Many times, road safety measures are not implemented in proper geographical locations owing to a lack of proper crash information, which includes crash information from the past. Road crash information is thus a vital support for the road safety assessment programs that eye for a reduction in road crashes. In India, as in other developing countries, very little effort is taken to provide enough road crash information conveniently and systematically. The identification of road crash locations, analysis, and treatment of road accident black spots are widely regarded as one of the most effective approaches to road accident prevention. By incorporating these approaches, a user-friendly web Geographic Information System (GIS) based Road Crash Information System (RCIS) is developed in the present study for Kerala State, India. An online platform to add, update and maintain the database of road accident black spots is offered by the system, including analysis functionalities. The database maintains a standard guideline for road crash reporting thereby reducing data redundancy. Integration of all crash data from accident locations and filtering data based on different criteria are the core objectives of this study. The study also focused on systematically sharing the accident black spot details to the public user through an online platform.

Keywords: Accident Black Spot, Road Safety, Transportation, Vehicle Crash Data, Web-based Geographic Information System

1. Introduction

World Health Organization (WHO) statistics reveal that about 1.35 million people die worldwide annually in road accidents and leaving between 20 and 50 million people with non-fatal injuries. A higher number of road traffic injuries are recorded in developing countries, with 93% of fatalities coming from low and middle-income countries. In 2018, the reported number of road traffic deaths in India was around 1.5 lakhs and it was estimated that more than 3 lakh people are killed in road traffic crashes in India every year (WHO, 2018). The diverse mix of traffic with high-speed vehicles sharing road space with vulnerable road users, unsafe road infrastructure, and poor condition of vehicles all contribute to India's high mortality rates. Accidents are a major cause of concern in Kerala as well. According to Kerala Police in 2019, a total of 41,111 accidents occurred which caused 4,440 deaths and 46,055 injuries *(https://keralapolice.gov.in).*

It is important for traffic safety programs to identify high-risk areas. In the literature on highway traffic safety, these areas are mentioned as “black spots.” According to the Ministry of Road Transport and Highways (MoRTH), Government of India, black spots on National Highways is a road about 500m in length in which either 5 road accidents (involving fatalities/grievous injuries) occurred during the last three calendar years or 10 fatalities occurred in the last three calendar years. The identification of accident location, analysis, and treatment of road accident black spots are widely considered one of the most effective approaches to preventing road accidents.

Geographic Information System (GIS) is one of the most inseparable Geoinformatics tools which are used ubiquitously in almost all the disciples of studies, whether it is Geography, Wild Life, Engineering, etc. The useful aspect of GIS as a management tool is its ability to associate spatial objects such as street names, mileposts, route numbers, etc. with attribute information such as road crashes, causes, etc. Web-based GIS or WebGIS is a part of Internet GIS that enables accessibility of geographic or non-geographic data over the web via communication protocol e.g., WWW (World Wide Web). A web GIS-based information system for road crashes for the state will be highly beneficial for society, it will be highly beneficial for law enforcers and other road-related agencies to keep a tab on the vulnerable location and take adequate measures to prevent road crashes in the future.

2. Related Work

GIS technology is been used ubiquitously in many fields of study, and a significant number of works are carried out in road crash identification. Very few studies have attempted to understand the analysis of black spots associated with road crashes in India. Srinivasan et al. (1987), in their study to identify and improve road crash vulnerable areas on the NH in Kerala, used three methods to point out the black spots viz., Quantum of road crash method, Accident prone index method, and Accident severity index (ASI) method. The study concluded that the ASI method was the most suitable for identifying black spot. A study on the application of GIS to analyze the causes of road traffic crashes in Kenya by Mwatelha (2001) has suggested measures to alleviate the problem of road traffic crashes through the inclusion of advanced technology like GIS. Krishnamurthy et al.(2011), conducted a study on the identification, analysis, and improvement of Black Spots on three selected National

Highway stretches in Kerala. Road crash details about the study region were analyzed for the purpose. Road crash frequency and severity index methods were applied to identify road crash black spots. AutoTURN 6.1 and AUTOCAD 2008 software were used for simulations. Improvement measures were suggested to avert road crashes in the future. The road crash study of Ajmer City in India by Bhalla et al.(2014), made use of GIS technology to derive the peak time for the road crash occurrence, its position, and the reason for the crash.

WebGIS have proven to work well in addressing transportation problems, especially road safety. Hassan and Al-Amayreh (2005), in their study, have developed an algorithm for optimal path routing and a traffic control system to alert drivers about the optimal route based on high/low traffic volume road width, road crashes, snow and flooding and dynamic changes of road density (Hassan and Al-Amayreh, 2005). Evangelidis et al.(2006), proposed a WebGIS-based Traffic Accident Information System (TAIS) application by utilizing the advantages of the Database Management System (DBMS) and WWW server merged with the high capabilities provided by contemporary Internet Map Services (IMS). GIS development packages - ESRI ArcIMS and ArcSDE were used to exhibit this attempt and try to establish that proper analysis of spatial and temporal patterns, easy information retrieval, faster communication, and fast response system can only reduce the probability of road crash occurrence.

Yusoff et al. (2014), has introduced an open-source web-based GIS software to reduce development or maintenance costs by proposing an effective road management system for maintaining and controlling road conditions on the web. Accident hot spot analysis for spatial and temporal clustering of data using GIS for the city of Thiruvananthapuram was done by Prasannakumar et al, 2011. The result of the study shows temporal accident clustering near educational institutions during the monsoon season. Deepti and Ganesh (2010), developed a GIS database for the identification of accident hot spots in the Kannur district of Kerala. The “Density” function is available in the spatial analyst extension of the ArcGIS software was applied. Simple and Kernel densities were used to identify the accident patterns. In 2009, the Government of Tamil Nadu introduced a user-friendly software program called Road Accident Data Management System (RADMS) as part of the Road Safety Action Plan. The GIS-based system records the details of each accident occurring in the state, geographically locates it, identifies accident-prone locations, and displays crash trends (*https://morth-roadsafety.nic.in*)

3. Objectives

Road controlling authorities put a lot of effort and expense into collecting large amounts of data related to road asset management, including data related to road safety. Data is the basis of all road safety activities and is important for interpreting the problems of a road crash and suggesting road safety measures. Authentic and well-organized data enables road safety auditors to accurately identify issues, priority areas, and risk factors, plan effectively, set goals, and improve performance. Without data-led diagnosis and management, it will be hard to attain remarkable and sustainable scaling of crash risk or severity of crashes.

The core objective of this study is to develop an accident information system highlighting road crash black spots in the study area. The specific objectives include the development of a Road Crash Information system (RCIS) using GIS as a backend application, highlighting the road accident scenarios, and updating the accident scenario on a public website periodically.

4. Study Area

Kerala State in India is taken as the study area. Kerala falls within the graticules of 8°17'30" N and 12°47'40" N and 74°27'47" E and 77°37'12" E. The state is located between the Lakshadweep Sea to the west and Western ghats to the east (Figure 1). Topography of Kerala consist of coastal plains, midlands and high lands. The state has a good transportation network, with good air, rail, road and water connectivity. Road related crashes in the state are on the rise and proper assimilation and dissemination of information is vital to spread awareness of road safety.

Figure 1. Study Area

5. Methodology

The GIS-based road crash information system was developed for the State of Kerala. This study focused on developing a web-based road crash information system. The road accident data in Kerala was collected from the Kerala Crime Records Bureau for the years 2017, 2018, and 2019. The information system lets the users visualize the road crash black spots for all the districts in Kerala during these three years. Provisions are provided to query the road crash database based on user preferences such as district-wise, police station-wise, and based on fatalities. The information system was developed based on the database and programming. The methodology of RCIS involves the steps shown in figure 2. The whole process of web-based RCIS can be divided into three stages; Login, Insert data, and Fetch data.

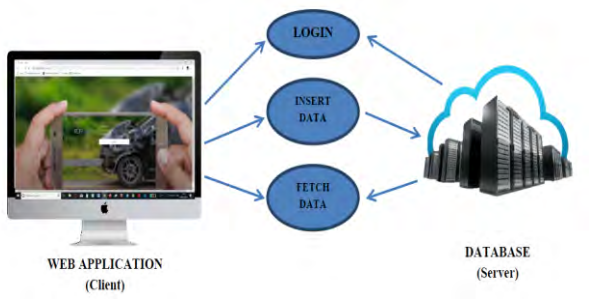

Figure 2. Methodology of RCIS

5.1 Web Application Development

The information system is developed based on client-server architecture, where the server is a Geospatial Information System database server and the client is a web browser. The web application was developed using the programming languages HTML 5, core JavaScript, Cascading Style Sheets3 (CSS3), and PHP with the help of Visual Studio Code software. HTML is the standard markup language for creating web pages and web applications. Visual Studio Code is one of the best editors for PHP development. Features like extensions, syntax highlighting, bracket matching, code completion, and out-of-the-box snippets make Visual Studio Code more efficient than simple Notepad++. The software Visual Studio Code with the latest version 1.77 was used for developing and debugging the web application.

The web application displays the location of road crash spots on a customizable map technology named Leaflet Open Street Map (OSM). Leaflet are used as it is the leading open-source JavaScript library for mobile-friendly interactive maps. It Weighs about 38 KB of JavaScript and has all the mapping attributes that the developers require. Leaflet API helps developers to integrate Leaflet OSM Maps into their web applications. It includes static map image recovery services, geocoding web services, driving direction creation, and the acquisition of elevation profiles. Using these services, the web application developed by us was integrated with the locations of the road crash black spots and displayed as markers on the map. A responsive HTML5 Charting Library named CanvasJS was used in the web application to visualize the Data as charts. CanvasJS offers 30 different types of Charts and generates across devices including iPhone, Android, Mac, and PC. Without compromising the maintenance or functionality of the web application, it allows to create rich dashboards that work across any device. Graphs include many great themes and are 10 times faster than traditional Flash / SVG-based Charting Libraries – resulting in lighter, more attractive, and more responsive dashboards.

5.2 Database of the Web Application

MySQL database was used to implement the system; it is open source and completely embedded within the PHP. WampServer software was used to create MySQL databases and tables for the system. WampServer is a software stack for the Microsoft Windows operating system, consisting of the Apache web server, OpenSSL for Secure Sockets Layer (SSL) support, MySQL database, and PHP programming language. Four tables were created in the database in which three tables are used to store the details of accident spots and the other table is used to store the login information of the user. The Spatial data and attribute data collected about the road crash spots in the study area were inserted into the corresponding table of the database (Figure 3). Spatial data including the starting and ending latitude-longitude pairs of the accident data are stored as string data in MySQL database. This data is used to represent locations of the accident hotspots by performing appropriate conversions and operations. Since only point data is represented in the web application, Geometry details in the database include only the coordinate pairs to represent points.

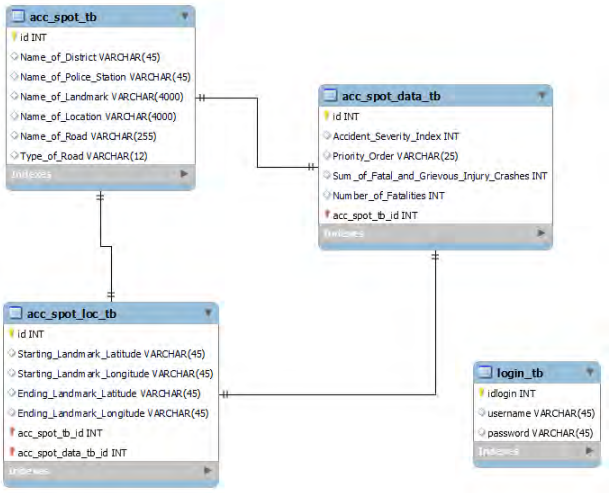

Figure 3. EER diagram of the database

6. Web-Based Road Crash Information System

The web application mainly consists of four web pages – Login page, Home page, View data page, and Insert data page.

6.1 Login and Home Page

The web application at the initialization leads the user to the Login page. Authorized persons with valid usernames and passwords are allowed to access the system. The login page prompts the user to enter the login credentials - username and password. A signup section is also available on the login page for new users to register in the web application. New users can register by entering their name, email/username, and password. While registering for the administrative privilege user needs to enter the one-time password (OTP) that will be sent to the registered Email address. After successful registration, the user can login to the system. Based on the privileges of the user the web application redirects them to the corresponding Home page of the web application. The user with administrative privilege will be redirected to the Home page with options to view and insert data. The user without administrative privilege can only view the system. The home page of the web application consists of a customized Leaflet OSM highlighting the Kerala state and a control panel as shown in figure 4.

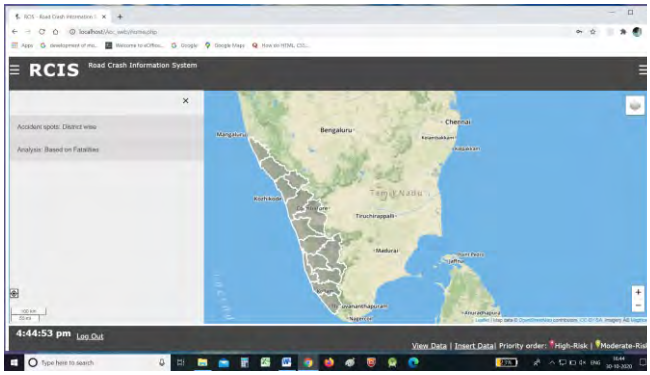

Figure 4. Home page of web application

Geographic locations of road crash black spots were geocoded on the map with the help of a database and Leaflet API. The control panel on the left side of the map consists of different options to filter the result from the database. The first section in the control panel displays the district-wise road crash spots in Kerala. A dropdown list of districts in Kerala is provided from which users need to select the district and click on the 'View Road crash Spots' button to view the road crash spots in the district. A dropdown list of police stations within the district is available in the panel. The user needs to select the district and the corresponding police station to see the hotspots matching the user-defined criteria in the selected area. ASI is calculated for each accident data based on the number of fatal and grievous injury crashes. Based on the ASI, road crash spots are classified into High-Risk, Moderate-Risk, and Low-Risk priority orders. Road crash spots are displayed as markers on the map with two different colors indicating the priority order. The marker with red color indicates the road crash spots having the High-Risk priority order and yellow indicates Moderate-Risk. On clicking the marker, a pop-up window consisting of information such as Name of Location, Name of Landmark, and ASI values is displayed. Pie charts are provided for a graphical representation of several road crashes based on the type of road – NH, State Highway (SH), and Other roads (OR). Figure 5 shows the Home page of the Web Application displaying the road crash spots in the Kollam district along with the pie chart based on the type of road.

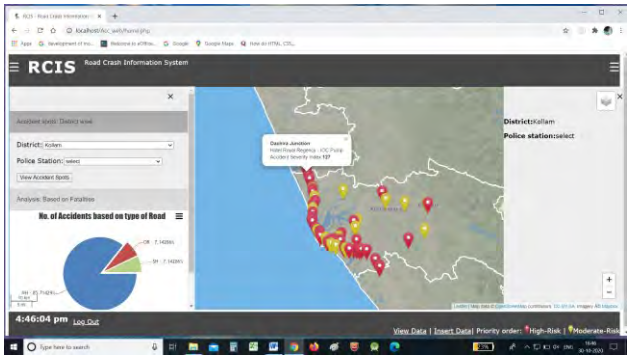

Figure 5. Home Page Displaying Road Crash Spots in Kollam District

The second section in the control panel is used to display the analysis based on the number of fatalities in road crashes in Districts of Kerala. To view the analysis based on the Sum of Fatal and Grievous Injury Crashes, the user needs to click on the 'Sum of Fatal and Grievous Injury Crashes in Kerala' button. A column chart showing the analysis based on the Sum of Fatal and Grievous Injury Crashes will be displayed in the control panel. To view the analysis based on the number of fatalities in road crashes in the study area, the user needs to click on the 'Number of Fatalities' button. A column chart showing the analysis based on the Number of Fatalities will be displayed in the control panel. A live clock is also provided in the footer section of the Home page along with the Logout option.

6.2 View and Insert data page

The user with administrative privilege can view and insert data in the database using the 'View Data' and 'Insert Data' options in the footer of the Home page. When the user clicks on the View Data option, the web application redirects to the web page that shows the list of accident hotspots in the study area. The options to filter the data based on the district and the corresponding police station are available for the administrator along with data Edit and Delete options (Figure 6).

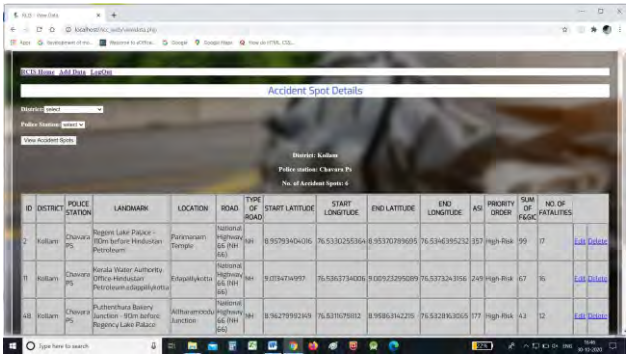

Figure 6. View Data page of the Web Application displaying the list of road crash spots in the Kollam district

Insert Data option redirects the web application to the web page to add details of new accident hotspots in Kerala. The user needs to enter details in the corresponding fields on the Insert Data page. After entering data, the user needs to click on the Save Data button at the bottom of the form (Figure 7). Validation rules such as required field validation, number format validation, dropdown list validation, digit validation, etc. are incorporated in the client side of the web page to check the validity of data entered by the user. PHP form validation rules such as required field validation, number format validation, digit validation, etc. are included on the server side and not null, primary key validations are set in MySQL database to avoid duplication of data. The user with administrative privilege can enter the details of new accident hotspots using this web page. Newly inserted data will be readily available to the public through the web application.

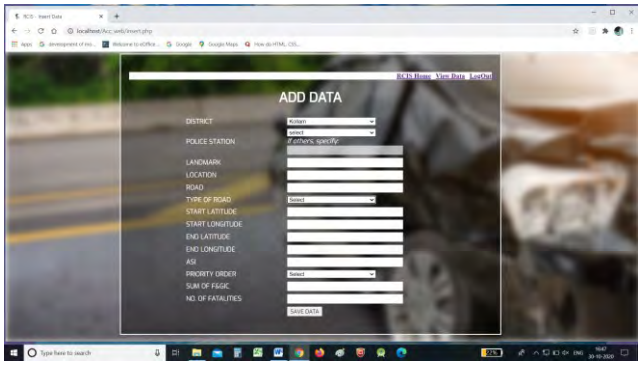

Figure 7. Insert Data page of the Web Application

7. Conclusion

Reliable and precise data are required in each phase of road safety management to properly identify problems, risk factors, and priority treatments, formulate strategy, set goals, and monitor performance. Road safety information, especially road crash data is collected every day. This data should be useful for road safety practices only if it is properly coded, visualized, processed, and analyzed systematically. The analyzed data provide meaningful results, especially the road crash black spots. The vulnerable locations thus identified the need to display to a wider audience rather limited to the researchers and bureaucrats. The present study was an attempt in this direction. The study developed a Road Crash Information System (RCIS); the web application shows the first and second-order road crash black spots within the State of Kerala. Tools and graphical interfaces are given to the application to facilitate facile analysis and visualization of the road crash details by a common man. The web application can provide a common online platform for reporting accidents to selected organizations such as the Regional Transport Offices (RTO), the Police Department, and the Motor Vehicle Department (MVD). This common platform can overcome any shortcomings such as loss of data, repetitive data collection, and inconsistencies in results and leads to high reliability in data collection and accident management systems. In addition, such a system would provide road users with valuable information on the location of accident black spots all over the area and the trends of road crashes. The developed system will be hosted publicly soon. For recording the road black spots details, a map-based interface for capturing the location coordinates can be provided instead of manual entry, and bulk data uploading utility could be included in the future. A mobile and desktop application for the system can be developed in the future.

Acknowledgments

We would like to express our sincere gratitude to Kerala State Council for Science, Technology, and Environment (KSCSTE) - National Transportation Planning & Research Centre (NATPAC) for providing technology materials and financial support for this study.

References

Bhalla P., S. Tripathi and S. Palria, "Road Traffic Accident Analysis of Ajmer City Using Remote Sensing and GIS Technology," The ISPRS TC VIII International Symposium on "Operational Remote Sensing Applications: Opportunities, Progress and Challenges," 2014, no. 545.

Deepti K. and B. Ganesh, "Identification of Accidents Hotspots: A GIS based Implementation for Kannur District, Kerala," International Journal of Geomatics and Geosciences, 2010, vol. 1, no. 1, pp. 51–56.

Evangelidis K., S. Basbas and P. Papaioannou, "A GIS web-based traffic accident information system," WIT Transactions on Information and Communication Technologies, 2006, vol. 36, pp. 363-372. doi: 10.2495/IS060341.

Hassan M. and M. Al-Amayreh, "Web Based Traffic System," International Arab Journal of Information Technology, 2005, vol. 2, no. 3, pp. 234-238.

Kerala Police (2019), Available at: https://keralapolice.gov.in/crime/road-accidents). Accesses on 06 June 2021.

Krishnamurthy K., M.V.L.R. Anjaneyulu and R. Rakesh, "Black Spot Identification, Analysis and Improvement Measures on Selected National Highway Stretches in Kerala, India", Proc. TRB 2011 Annual Meeting, 2011, pp. 1-15.

Morth Road Safety, Available at: morth-roadsafety.nic.in/WriteReadData/LINKS/Tamil%20Nadu%20RADMS48011e76-eee8-487e-99ea-b8cb34fc68b7.pdf. Accessed on 19 July 2021.

Mwatelha J.K.Z., "Application of Geographical Information Systems (GIS) to Analyze Causes of Road Traffic Accidents (RTAs) – Case Study of Kenya," Proc. In. Con. On Spatial Info. for Sustainable Dvpt, 2001, pp. 1 -7.

Prasannakumar V., H. Vijith, R. Charuthaa and N. Geetha, "Spatio-Temporal Clustering of Road Accidents: GIS Based Analysis and Assessment," Procedia Social and Behavioral Sciences, 2011, vol. 21, pp. 317–325.

Srinivasan N.S., V.S. Iyer, C. Mahesh and K. Srinath, "Scientific identification and improvement of accident prone locations on national highways in Kerala," J. Indian Roads Congress, 1987, vol. 48, no. 3, pp. 1 – 10.

World Health Organization, *Global status report on road safety 2018*. Geneva, Switzerland: World Health Organization, 2018.

Yusoff N.M.R.N., H.Z.M. Shafri and R. Muniandy, "An effective road management system using web -based GIS software," IOP Conf. Series Earth and Environmental Science, 2014, pp. 1-8. doi: 10.1088/1755-1315/20/1/012025.

Journal of Geomatics Vol. 17, No. 2, October 2023

Fog / visibility forecast and verification at IGI Airport, New Delhi during the winter seasons of 2020-21 & 2021-22

C. Anuradha[1], S.H Arun [1,*], S. Charan[1] and J. Sebin[2]

[1] Meteorological Watch Office, India Meteorological Department, New Delhi
[2] India Meteorological Department, Ministry of Earth Sciences, New Delhi
*Email: arunshphysics05@gmail.com

(Received: 20 January 2023; in final form 26 April 2023)

DOI: https://doi.org/10.58825/jog.2023.17.2.33

Abstract: The reduction in visibility due to fog leads to cancellation of flights, delays and diversions at Indira Gandhi International (IGI) Airport, New Delhi during the winter season. Accurate prediction of fog/ visibility is required within sufficient lead time to make the flight operations safer, economical and more convenient. This study attempts to improve the fog/visibility forecast at IGI airport for the months of December and January during the winter seasons of 2020-21 and 2021-22. Various meteorological parameters required to predict the fog/visibility are obtained from India Meteorological Department- Global Forecasting System (IMD-GFS) forecasted meteorological information which are valid for the next 24 and 48-hours. Forecast verification was performed using Meteorological reports (METAR) and synoptic observations. The results for 2020-21 fog/visibility forecast for 24-hours are promising with a Percentage of Detection (POD) of 0.92, Critical Success Index (CSI) as 0.68, and False Alarm Ratio (FAR) as 0.28. Moreover, the 2021-22 results for 24-hours fog /visibility forecast are also observed to be promising with a POD of 0.73, CSI of 0.54 and FAR at 0.32. This method gives fairly accurate predictions in point locations and can also be used for a larger spatial area. However, the 48-hours forecast performance needs further improvement. The method also predicted the wind speed and relative humidity which were found to be in agreement with the observed data to a great extent. In the upcoming years, the fog/visibility forecast method will be more robust with better prediction accuracy of meteorological parameters from model outputs and observations.

Keywords: Fog, Visibility, Forecast, IMD GFS, IGI Airport

1. Introduction

Indo-Gangetic Plains (IGP) experiences widespread fog episodes and associated low visibility conditions in every winter season (November- February) which acts as a major hazard to surface, marine and aviation transportation activities. Gultepe et al. 2007 have reported that the total economic loss which affects aviation, marine, and surface transport is comparable to those of tornadoes. The accidents during the winter months have been increased significantly in recent years (Singh et al., 2004). Moreover, Singh et al. (2012) reported that the number of accidents in the month of January is very high due to foggy weather and associated low visibility conditions.

Flight cancellations and diversions are more frequent at the IGI airport during the winter season which can cause huge economic losses to the aviation industry (Kulkarni et al., 2019). For an improved understanding of fog physics, variability of fog events, its duration and intensity need to be studied in detail which can further lead to better fog/visibility prediction for safer aviation, marine and surface transportation activities during the winter season.

In recent years, significant research contributions have been added in the field of fog detection, monitoring, nowcasting and forecasting over the IGP using various satellites, models and *in-situ* based observations (Bhushan et al., 2003; Mitra et al., 2008; Saraf et al., 2011; Singh et al., 2011; Chaurasia et al., 2011; Jenamani 2012; Srivastava et al., 2017; Dey 2018; Arun et al., 2018a; Arun et al., 2018b; Kutty et al., 2020; Arun et al., 2022). Mohapatra et al., 1998 examined the performance of four different fog forecasting methods i.e., persistence, modified Taylor, synoptic, statistical and composite methods during the winter months of 1993-94 over the Bangalore airport. In addition, the detailed statistical analysis also showed that the composite method has better accuracy in fog forecasting over the study area. The spatial extent of fog over the IGP for the winter season 2002-03, 2003-04 and 2004-05 has been examined by Choudhury et al. (2007) in which fog prone areas are classified according to the intensity derived from fog maps. Moreover, an attempt has also been made for fog forecasting by using the available information on meteorological parameters such as temperature, humidity, wind speed etc. Syed et al. (2012) investigated the climatology, inter annual variability and trends in fog to understand the fog characteristics over the Indian sub-continent by using the observation data from 82 stations during the period from 1976-2010. The results of their study indicated that the trends in fog frequency are positive but not gradual. An attempt has been made by Bhowmik et al., 2004 in which an objective method consisting of statistical multiple discriminating analysis was implemented for the fog prediction over the Delhi region. In their analysis, synoptic observations and sounding have been used to find out the trend in fog occurrence over the Delhi region. Multi Rule based Diagnostic (MRD) approach using Weather and Research Forecast (WRF) model data has been used for the fog prediction over the Delhi region (Payra et al., 2014). In this approach, foggy and non-foggy days are distinguished in 94% of cases and the onset of fog is well captured within an accuracy of 30-90 minutes. The spatial visibility

forecast over the Kolkata airport has been performed by Dutta et al., 2015 by using an Artificial Neural Network (ANN). The study reported that visibility categorization is possible with the ANN in which the best visibility forecast has been observed in the range of 0-50 m where very dense fog conditions have been occurred. An analogue model has been introduced by Goswami et al., 2017 for the fog prediction over the IGP in which fog occurrence is represented in terms of visibility. The study investigated the performance of the model and found to have more success whenever the visibility is less than 500m and the duration of the fog event is more than 04 hours.

Further, Jayakumar et al. (2018) introduced a high resolution (~330m) unified model for the fog/visibility prediction over Delhi. Moreover, the study suggested that the visibility prediction by the model is highly sensitive to aerosols. The ability of various Numerical Weather Prediction (NWP) models such as the National Centre for Medium Range Weather Forecasting (NCMRWF) Unified model (NCUM) in visibility forecast over the IGP has been examined (Singh et al., 2018). In their study, Indian National Satellite (INSAT-3D) fog maps and visibility observations from METAR data have been used for verification purposes. The study indicated that the performance of NCUM is reasonably well in predicting the spatial extent of fog over the IGP with a lead time of one day. Further, Dey (2018) provided the theoretical explanation to the new Brightness Temperature Difference (BTD) threshold to improve the fog prediction over the IGP. Moreover, the study also discussed about the quantification of minimum droplet concentration for the identification of fog and also performed the sensitive study of critical droplet concentration on liquid water content. An Adaptive Neuro-Fuzzy Inference System (ANFIS) has been used for visibility prediction with a lead time of 12 hours over Delhi during the fog season (Goswami et al., 2020). The study reported that the forecast error of ANFIS is the least, i.e., 9.09%, as compared to other existing neural networks and forecast models and hence can be adopted as an alternate option for the fog/visibility forecast purposes. A high resolution (~330m) fog/visibility forecast model known as DM-CHEM and the aerosol scheme has been introduced by Jayakumar et al. (2021) which has been operational since 2020 and the performance of the model is reasonably well with the observed visibility.

The fog/visibility forecast over the IGP has been significantly improved with the introduction of the Winter Fog Experiment (WiFEx) campaign at the IGI airport since 2016 (Ghude et al., 2017). The main objectives of the project are to better understand the fog characteristics, fog microphysics, variability of fog events and associated thermodynamics to improve the fog prediction over the IGP. In addition, the sensitivity of the WRF model to simulate the life cycle of dense fog events has been investigated during the WiFEx campaign (Pithani et al., 2019). The study reported that the performance of quasi-normal scale elimination (QNSE) and MYNN 2.5 Planetary Boundary Layer (PBL) schemes in the simulation of fog life cycle is reasonably well as compared to the other schemes. Further, Pithani et al., 2020 investigated the performance of the Weather Research & Forecasting (WRF) model in 43 very dense fog events in real time forecasts at 2km horizontal grid spacing. The results indicated that the model has reasonably well predictive accuracy with a hit rate of 0.78 whereas the FAR (0.19) and missing rate (0.32) are low. Furthermore, Dhangar et al. (2021) extensievely studied the physical and chemical structure of fog as well as the variability of fog events which can further be used to improve the fog prediction over the IGP. Moreover, to improve fog prediction and other surface meteorological parameters, the role of high resolution land data assimilation has been investigated (Parde et al., 2022). Later, the three dimensional structure of dense fog events has been studied with the help of the WRF model and other ground based observations during the WiFEx campaign (Yadav et al., 2022). The study indicated that the complexity and physical process during dense fog events are well captured by the WRF model.

Even though a large number of research activities are going on in the field of fog detection and prediction using satellite, model and in-situ based observations, it still needs improvement, especially in the field of accurate fog/visibility predictions during the winter seasons. In this article, the authors made an attempt to give fog/visibility predictions at the IGI airport with a lead time of 24-hours and 48-hours which is followed by a detailed forecast verification with the observed data.

2. Data Used

The study has been performed during the months of peak winter season i.e. December and January of year 2020-21 and 2021-22 over the IGI Airport. Half hourly METAR and 3 hourly synoptic observations available at https://olbs.amssdelhi.gov.in provided the current weather information. IMD-GFS model runs with a horizontal resolution of ~12 km and 64 hybrid sigma pressure levels. The four-dimensional (4D) ensemble variational data assimilation (DA) system (4DEnsVar) of NCMRWF is used to generate the initial conditions of IMD-GFS models. The 4DEnsVar data assimilation is capable of assimilating various conventional and polar/geostationary satellite observations including the radiance values. The analysis is performed four times a day, i.e. 0000,0600,1200 and 1800 UTC and 10 days forecast is generated in each run. The IMD-GFS based specific aviation products are available in airport wise also. This includes charts, wind and temperature chars, wind and temperature numerical values and meteograms. These products include all weather parameters required for fog/visibility purposes. From a forecaster's point of view, these IMD-GFS specific aviation products are very much useful for generating fog/visibility forecasts in a more accurate way. For forecasting purpose, IMD GFS forecasted meteorological parameters which have a validity period of 24-hours and 48-hours have been used (https://internal.imd.gov.in and https://nwp.imd.gov.in). Currently, IMD-GFS model outputs are not available in the open domain for research purposes.

3. Methodology

The prime goal of this study is to enhance the prediction of fog/visibility forecast over IGI Airport during the winter season of 2020-21 & 2021-22. On a daily basis, current weather information obtained from METAR and synoptic observations were studied diligently to understand the trend in the present weather. The other meteorological parameters which have a significant role in fog formation such as minimum air temperature, dew point depression, wind speed and direction, backing and veering of wind, relative humidity, surface temperature inversion, cloud cover and Western Disturbance (WD) or any other significant synoptic system surrounding Delhivalid for next 24-hours & 48-hours are collected from IMD GFS Model outputs. The values of above mentioned parameters favorable for fog formation are mentioned in Table 1. The output of 24 and 48-hours IMD GFS model are used to predict fog/visibility over the IGI airport.

Table 1. Favourable conditions of meteorological parameters for fog formation (Singh, 2011; Arun et al., 2022).

Weather parameter	Favorable conditions for fog formation
Minimum air temperature (°C)	< 8 °C
Dew point depression (°C)	< 3°C
Relative humidity (%)	>75%
Wind speed (Knots)	02 to 04 knots
Wind direction	Depends up on wind speed
Wind veering/backing	Backing
Surface temperature information (°C)	>2 °C
Cloud information	Clear sky
Location of WD/other synoptic system over and around Delhi	Approaching or passing over IGP

There are a total of 9 meteorological parameters which are mentioned in Table 1 where each of the parameters has an equal weightage of 11%. The total percentage after combining all the favorable parameters gives the 24-hours and 48-hours probability forecast of fog formation and the corresponding lowest visibility as shown in Table 2. If all the parameters are favorable, then it indicates a 99% chance of fog formation with the lowest visibility of 00 m. Similarly, if 8 out of 9 parameters are favorable, then it indicates 88% chance of fog formation with a lowest visibility of 200m and so on. The complete analysis has been performed in a similar manner.

Table 2. Classification of probability of fog formation and corresponding visibility

Probability of fog formation (%)	Visibility (m)
99	00
88	200
77	400
66	600
55	800
44	1000
33	>1000
22	>1000
11	>1000
00	>1000

4. Results and Discussion

The present study has been carried out during the December and January months of the winter seasons of 2020-21 & 2021-22. The probability of fog formation and the corresponding lowest visibility have been calculated on daily basis with a lead time of 24-hours and 48-hours. The tabular format of the fog/visibility forecast issued on 8th Jan 2022 is shown in Table 3. Firstly, METAR and synoptic observations provided the present weather conditions on 8th Jan 2022. Considering the present weather and using the 24-hours and 48-hours forecasted meteorological parameters information, the probability of fog formation and lowest visibility expected for the next 24 and 48-hours are forecasted. According to data mentioned in Table 3, five & eight out of nine weather parameters are favorable for fog formation for 9th & 10th Jan 2022 respectively. Since, an equal weightage of 11% has been given to each favorable parameter, the probability of fog formation is 55% for 9th Jan 2022 & 88% for 10th Jan 2022 respectively. According to Table no. 3, the lowest visibility is forecasted as 800 m & 200 m for 9thand 10th of January 2022 respectively. The fog/visibility forecast for the entire season has been carried out in a similar manner.

Fog is classified into various categories depending upon the visibility which is discussed as follows. When visibility is ≤50m, it is a very dense fog event; a dense fog event implies that visibility is ranging from 51 m to 200m, further if visibility is observed between 201 m to 500m, it is identified as a moderate fog event; shallow fog occurs when visibility is in between 501m to 800m and mist occurs if visibility is greater than 800m. In addition, runways are classified into different categories (i.e. CAT I, CAT II, CAT IIIA, CAT IIIB and CAT IIIC) based on the Runway Visual Range (RVR). When the visibility reported is above 800 m, it is classified as CAT I category whereas CAT II is defined when the visibility is above 350 m. CAT IIIA and CAT IIIB have visibility range of 200 m and 50-200 m respectively, whereas CAT IIIC have no visibility range. Currently, IGI airport is equipped with CAT IIIB facility on all the runways.

Table 3. General format of fog/visibility forecast issued at IGI Airport on 08.01.2022

Weather parameter at surface	**08/01/22 00UTC**		**09/01/22 00 UTC**		**10/01/22 00 UTC**	
Minimum air temperature (°C)	15.8	U	13	U	09	U
Dry bulb temperature (°C)	15	-	-		-	
Dew point temperature (°C)	15	-	-		-	
Dew point depression (°C)	00	F	00	F	00	F
Relative humidity (%)	100	F	95	F	95	F
Wind speed (knots)	05	U	06	U	04	F
Wind direction	E	U	SE	U	NW	F
Wind veering/backing	B	F	B	F	B	F
Surface temperature inversion (°C)	02	U	06	F	08	F
Cloud conditions	Cloudy Sky	U	Cloudy sky	U	Clear sky	F
Locationof Western disturbance/any other synoptic system over and around Delhi	68°E 28°N	F	72°E 28°N	F	76°E 28°N	F
Present fog conditions	TSRA	U	-	-	-	-
Visibility (m)	1500	U	-	-	-	-

The time series plots of 24-hours forecast visibility and 48-hours forecast visibility with the observed visibility for the years 2020-21 & 2021-22 are shown in Figure 1 (a-d). In addition, the corresponding predicted surface wind speed (knots) and relative humidity (%) along with the observed data are shown in Figure 2 (a-d) and Figure 3 (a-d) respectively. The performance between observed and forecasted visibility, wind speed, relative humidity etc. are in agreement. For example, 24-hours forecast for 31.12.2020 and 01.01.2021 predicted a very dense fog event with the lowest visibility of 50 m. The predicted wind speed was also favorable for31.12.2020and 01.01.2021 being 04 and 02 knots respectively. The wind speed observed was 02 knots on both days which favored the fog formation. Similarly, the relative humidity was predicted to be 90% and 95% for 31.12.2020 and 01.01.2021 respectively. The relative humidity observed was also favorable at 94% for both days. Hence these events were correctly predicted and the observed lowest visibility was 50m only on both days.

Very dense fog with the lowest visibility of 50m was predicted in 24-hours forecast for 13.01.2022. The observed lowest visibility on 13.01.2022 was also observed to be 50m which is in accordance with the predicted visibility. The parameters like Western Disturbance, relative humidity, wind category, and surface temperature inversion were predicted to be 78˚E, 95%, backing wind & 6˚C respectively. The observed meteorological parameters such as WD at 83˚E, relative humidity of 100%, backing wind, and surface temperature inversion of 6˚C were in agreement with the predicted data and also contributed in the formation of very dense fog. Moderate fog was predicted for 07.01.2022 in 24-hours forecast with the lowest visibility of 400 m. The predicted parameters like relative humidity (95%), WD (74 ˚E), inversion temperature (6˚C), and minimum air temperature (12 ˚C) were in agreement with the observed values of relative humidity (98%), WD(67 ˚E), inversion temperature (6˚C), minimum air temperature (13.2˚C) which led to the formation of moderate fog with visibility of 500m. The 24-hours forecast for 14.12.2021 predicted shallow fog with the lowest visibility of 600m. Few predicted parameters such as clear sky, inversion temperature of 8˚C, backing wind, relative humidity(95%) etc. were favorable for fog formation.

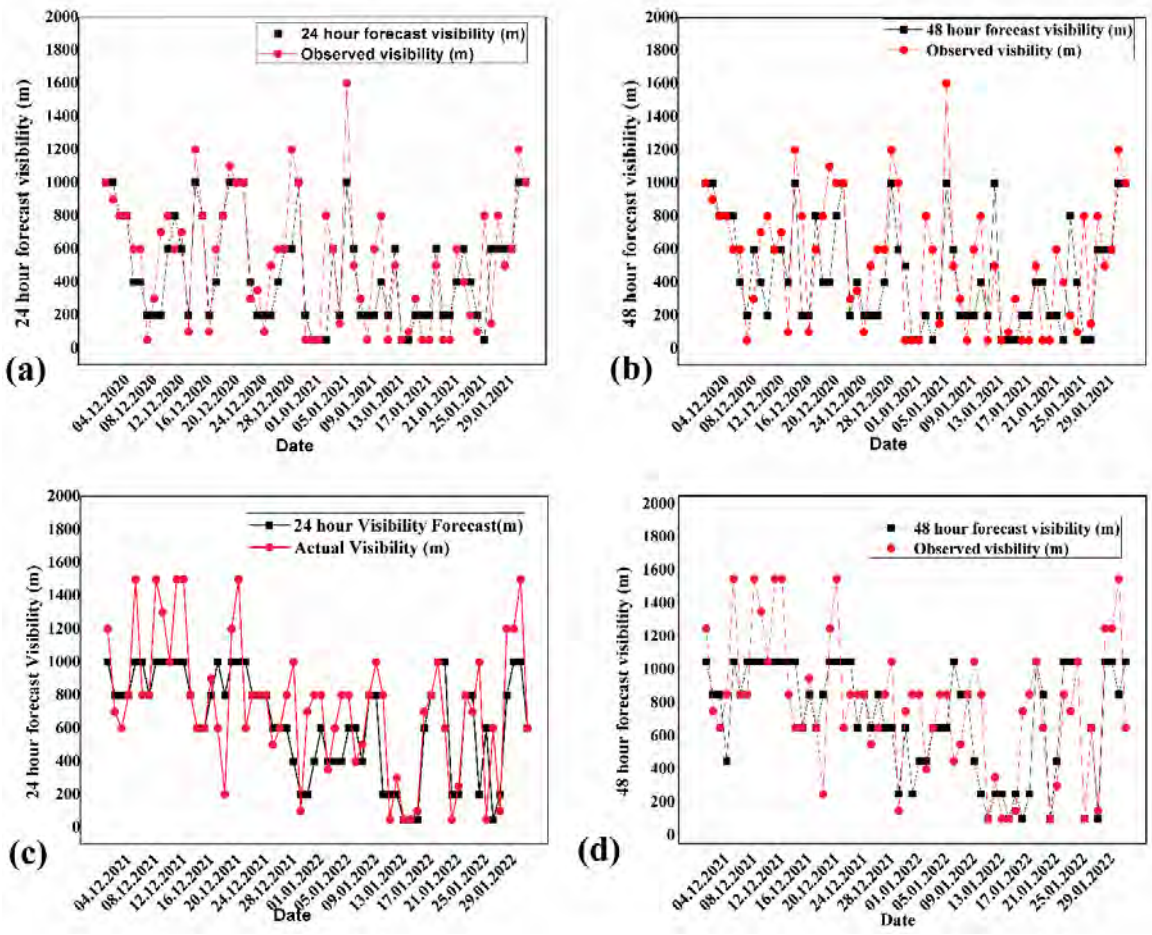

Figure 1 (a-d). Time series plots of forecast visibility and observed visibility. (a) 24- hours forecast, 2020-21, (b) 48- hours forecast, 2020-21, (c) 24- hours forecast, 2021-22 and (d) 48-hours forecast, 2021-22.

Later, observed meteorological conditions like clear sky, inversion temperature of 8˚C, backing wind, relative humidity (98%) were also in favourable positions. Moreover, other parameters that were predicted to be unfavorable like wind speed (0 Knots), and minimum air temperature (9 ˚C) were also observed to be in unfavorable state only with reported wind speed of 0 knots & minimum air temperature of 10.5 ˚C. All of the above factors led to the formation of shallow fog with the lowest visibility of 600 m as predicted. Similarly, the 24-hours forecast for 15.12.2021 predicted the parameters as WD (70 ˚E), clear sky, inversion temperature (8˚C), backing wind, relative humidity (95%), wind speed (0 knots), minimum air temperature (9 ˚C). Moreover, these parameters were in accordance with the observed values of WD (67˚E), clear sky, inversion temperature (6˚C), backing wind, relative humidity (91%), wind speed (0 knots), minimum air temperature (11.2 ˚C). Hence the observed visibility of 600m was in agreement with the predicted lowest visibility of 600m.The fog predicted for 17.01.2022 in 24-hours forecast was shallow fog with the lowest visibility as 800 m. The predicted parameters like relative humidity (90%), WD(90˚E), inversion temperature (2˚C), minimum air temperature (8˚C), backing wind etc. were in agreement with the observed values of relative humidity (92%), WD (90 ˚E), inversion temperature (2 ˚C), min air temperature (7.8˚C), backing wind, clear sky etc. which led to the formation of shallow fog with visibility of 800m as predicted.

The 48-hours visibility forecast were also predicted accurately in a substantial number of cases. For example, 48-hours forecasts for 04.01.2021 and 07.01.2021 predicted a dense fog event with the lowest visibility of 200m. Later on, the lowest visibility of 150m and 300m in dense fog conditions were reported on 04.01.2021 and 07.01.2021 respectively. The wind speed of 02 knots and 03 knots predicted for 04.01.2021 and 07.01.2021, respectively were highly in agreement with the observed wind speeds of 04 and 03 knots for the corresponding days. Similarly, the observed relative humidity of 98% on both days were close to the predicted value of 95% for both days. A very dense fog of 50 m was accurately predicted for 11.01.2022 in 48-hours forecast and the observed lowest visibility reported on 11.01.2022 was also 50 m. The predicted parameters like relative humidity (95%), wind speed 4 knots, WD (79˚E), inversion temperature (6 ˚C), clear sky, backing wind etc. were in agreement with the observed values of relative humidity (100%), wind speed 3 knots, WD (75 ˚E), inversion temperature (6 ˚C), clear sky & backing wind etc.

Even though the predictions of fog/visibility are noticed to be in agreement with the observations in the majority of the events, there were some cases observed in which discrepancies were reported. Some examples are discussed as follows. The 24-hours forecast for 07.01.2021 predicted dense fog with the lowest visibility of 200 m as the wind

speed was predicted to be 6 knots which is in the unfavorable range. However, the actual wind speed observed on that day was 04 knots which is in the favourable range for fog formation which leads to the lowest visibility of 50 m in very dense fog conditions on 07.01.2021. The analysis revealed that the wrong prediction of wind speed led to an error in fog/visibility prediction. Similarly, the wrong prediction of wind speed of 06 knots for 08.01.2021 in 24-hours forecast is identified as the reason for the discrepancy as the observed wind speed was 02 knots. Thus, the very dense fog event (visibility 50 m) was observed on 08.01.2021 instead of the predicted visibility of 200 m in dense fog conditions. Furthermore, the 24-hours forecast predicted dense fog with the lowest visibility of 200m on both the days on 19.01.2021 and 20.01.2021. Later, very dense fog of lowest visibility of 50m was observed even though the WD was in the unfavorable range on both days. Dense fog with the lowest visibility of 200 m was predicted in the 24-hours forecast for 11.01.2022. Even though all parameters were predicted to be in the favourable range except the wind was predicted to be unfavorable being veering in nature. In actual observation, a very dense fog was observed at the IGI Airport with the lowest visibility of 50 m. This discrepancy may be due to the observed backing nature of wind which is favorable for fog formation, whereas it was predicted as veering in nature. Similarly, dense fog (visibility 200 m) was predicted in 48-hours forecast for 13.01.2022. All parameters were predicted to be in the favourable range except minimum air temperature (8˚C) which was in the unfavorable range. Even though all other parameters were observed as predicted but discrepancies were observed in the value of minimum air temperature (6.6 ˚C) which came under the favourable range. This led to the formation of very dense fog on 13.01.2022 instead of dense fog. Shallow fog with the lowest visibility of 800m was predicted in 24- hours forecast for 18.12. 2021. However, dense fog with the lowest visibility of 200 m was observed. This may be due to the prediction error in WD and minimum air temperature, i.e., no WD was predicted for 18.12. 2021, but a WD was observed at 74˚E. In addition, the minimum air temperature was predicted in the unfavorable range being 9˚C, but the observed value of minimum air temperature was 6.2˚C. All of these favorable factors result in the formation of dense fog instead of shallow fog.

In some cases, an opposite scenario happened in which the predicted visibility was less, but the actual visibility was found to be sufficient for aviation requirements. For example, all meteorological parameters except cloud conditions were predicted to be favourable for 25.12.2020 which led to a prediction of a dense fog event with the lowest visibility of 200 m. But in actual observation, along with the cloud conditions, wind speed and wind direction were also observed to be in an unfavorable state causing shallow fog with the lowest visibility of 700 m which is not hazardous for aviation activities. Similarly, for 02.01.2021 and 25.01.2021, very dense fog with the lowest visibility of 50 m forecasts were issued. The predicted values of all meteorological parameters were in the favourable range for very dense fog formation. However, shallow fog with the lowest visibility of 800 m was recorded on both days. Further analysis revealed that the minimum air temperature and wind speed on both days were unfavorable which led to the formation of shallow fog instead of very dense fog. Moderate fog with the lowest visibility of 400m was predicted in 24-hours forecast for 31.12.2021. However, the observed visibility was 800m in shallow fog. The reason for shallow fog instead of moderate fog may be due to the observed cloudy sky, WD (89˚E) which has already been passed Delhi 3 days ago and due to which the impact of WD was low & relative humidity(88%) was also observed to be on the lower side. All of these conditions led to a low moisture supply which led to the formation of shallow fog only. 24-hours forecast of 30.12.2021 predicted dense fog with visibility of 200m. However, certain observed parameters like wind speed (0knots), wind direction and surface temperature inversion(2˚C) were not found in the favourable range as predicted. These weather conditions contributed to the formation of shallow fog (visibility of 700m) instead of dense fog.

The 48-hour fog/visibility forecast is a more challenging task and more vulnerable to errors as compared to 24-hours forecast. The following section briefly discusses the discrepancies observed in those events where the predicted and observed visibility are not in agreement. Forecasts for 13.12.2020, 30.12.2020 and 19.01.2021 was of moderate fog with the lowest visibility of 400 m. The WD predicted was to be in the unfavourable range for 13.12.2020 & 19.01.2021, whereas the surface temperature inversion and wind speed predicted were in unfavourable range for fog formation on 30.12.2020. Still, in all the cases, a very dense fog of the lowest visibility of 50 m was observed. Very dense fog was predicted for 03.01.2021 and 25.01.2021 as all the parameters were predicted to be favourable for very dense fog formation. However, minimum air temperature & wind speed was observed to be unfavourable for both days. In addition, the WD and dew point depression were also observed as unfavourable for 25.01.2021 whereas for 03.01.2021, the unfavourable parameter was surface temperature inversion. All of the above parameters were related to the occurrence of shallow fog with the lowest visibility of 600 m on both 03.01.2021 and 25.01.2021 instead of very dense fog as predicted. Very dense fog (visibility of 50m) was predicted in 48-hours forecast for 16.01.2022 i.e. all the parameters were predicted to be favourable for fog formation. However, observed values of surface temperature inversion (2 ˚C), minimum air temperature (8.1 ˚C), wind speed (6knots) and wind direction were found to be unfavourable which leads to a shallow fog (700m) instead of very dense fog on 16.01.2022. Further, 48-hours forecast for 10.01.2022 predicted dense fog with a visibility of 200 m. However, the observed visibility was 800 m in shallow fog. This discrepancy may be due to the parameters like cloud conditions (clear sky), backing wind, surface temperature inversion (6 ˚C) were predicted to be favourable for fog formation. However, cloudy sky, veering wind, surface temperature inversion (2 ˚C) which were observed on 10.01.2022 were unfavourable for fog formation. This led to the formation of shallow fog instead of dense fog.

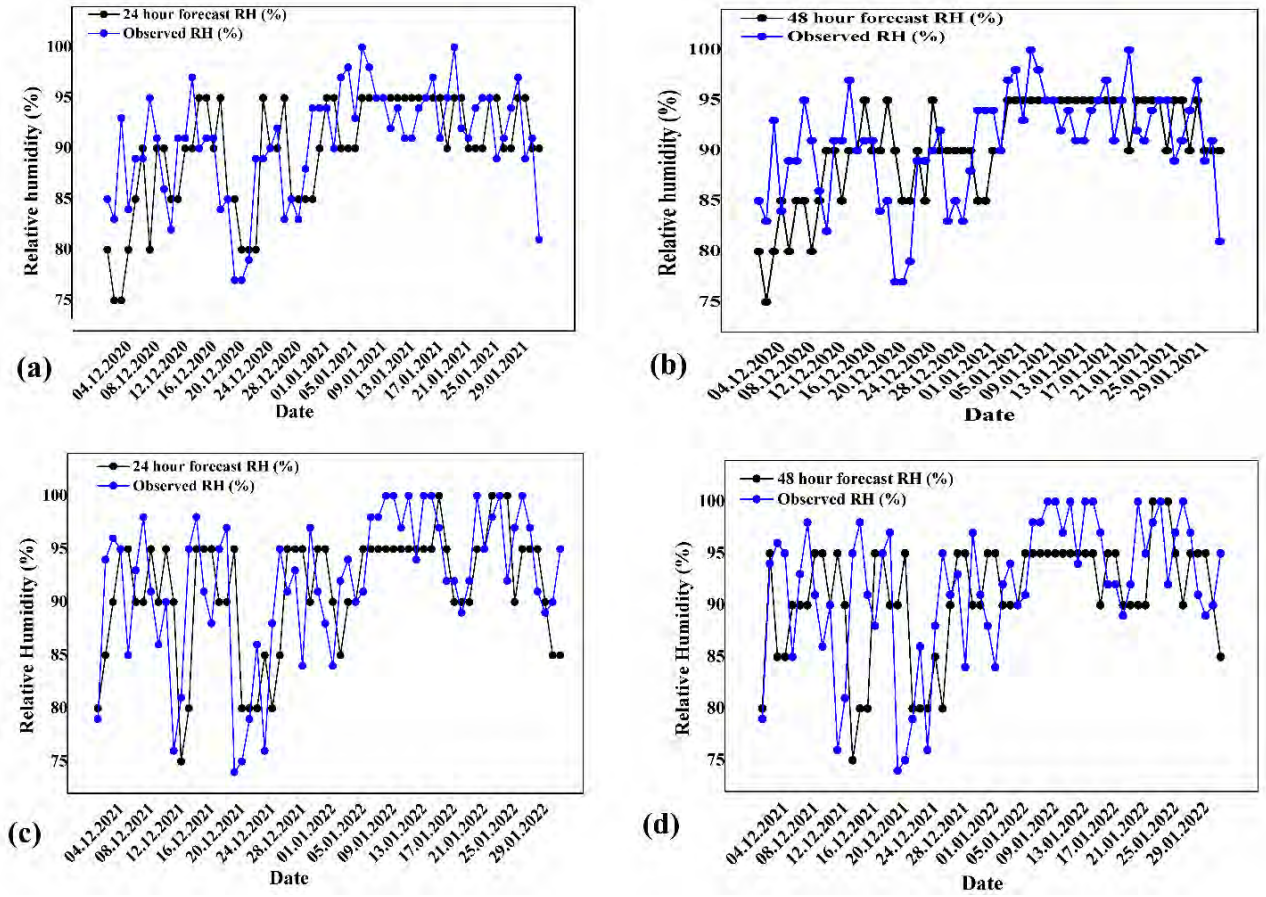

Figure 2 (a-d). Time series plots of forecast relative humidity and observed relative humidity. (a) 24-hour forecast, 2020-21, (b) 48-hour forecast, 2020-21, (c) 24-hour forecast, 2021-22 and (d) 48-hour forecast, 2021-22.

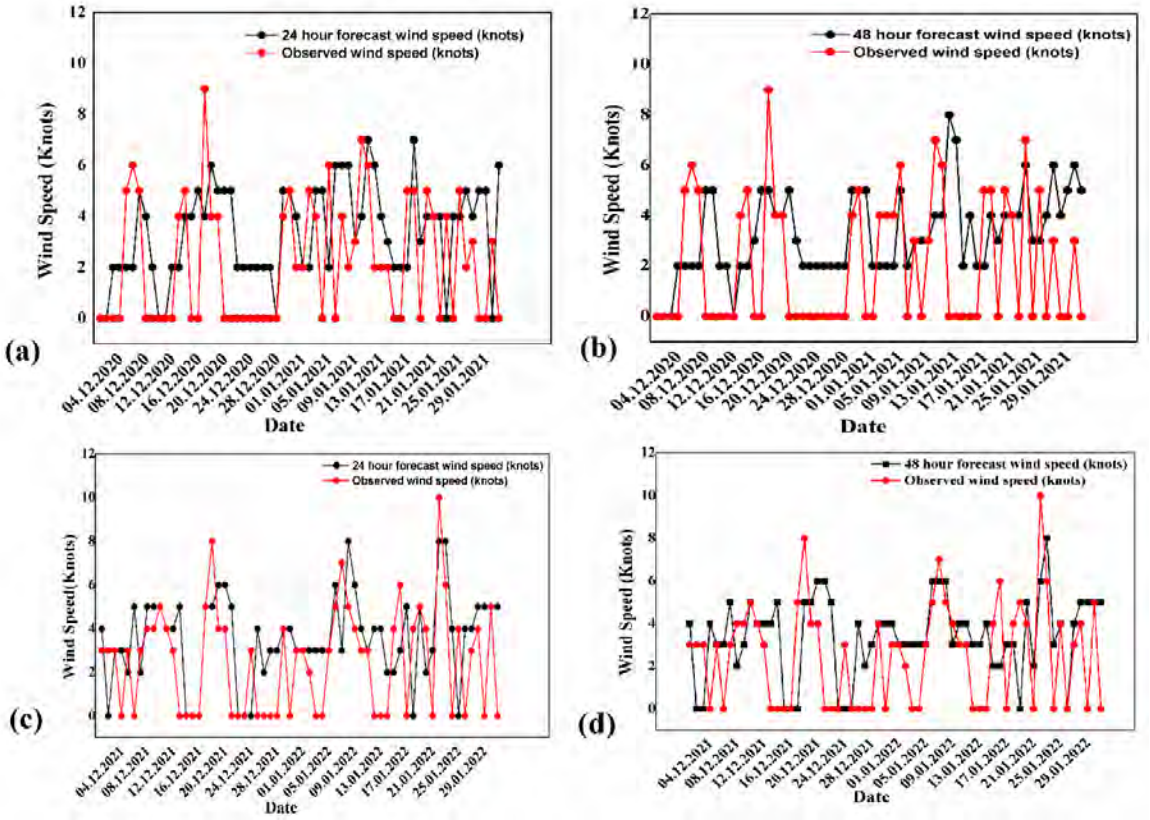

Figure 3 (a-d). Time series plots of forecast wind speed and observed wind speed. (a) 24-hour forecast, 2020-21, (b) 48-hour forecast, 2020-21, (c) 24-hour forecast, 2021-22 and (d) 48-hour forecast, 2021-22.

Furthermore, it has also been observed that in some events (13.01.2022 and 14.01.2022), very dense fog has been reported even though the observed wind speed was 0 knots which is considered to be unfavorable for fog formation in the present analysis. This may be due to the error in reporting the wind speed i.e., wind speed of 1-2 knots may sometimes be reported as calm (0 knots). Hence the range of wind speed favorable for fog formation may be changed in the future course from 2-4 knots to 0 - 4 knots. It has also been noticed in few cases like on 11.01.2022 that even though the temperature was reported to be slightly higher than 8 ˚C, still very dense fog was observed on that day. Air temperature is generally reported on the higher side for safety purposes in aviation meteorology. This is because engine efficiency is lower & lift is less with higher temperatures and thus reporting temperature on the higher side enables the adequate planning of fuel and load in the aircraft. Hence the range of minimum air temperature favorable for fog formation might be changed from less than 8 ˚C to less than 10˚C. Overall analysis showed that the role of each meteorological parameter should be given different weightages instead of giving equal weightage to each of them.

This is because throughout the winter season, the parameters like relative humidity, dew point depression, cloud conditions and backing of wind are mostly in favourable ranges for fog formation and hence do not impact the variations in fog intensity significantly. However, the remaining parameters like wind speed, WD, surface temperature inversion, minimum air temperature affect the genesis and dissipation of fog in a dominant way throughout the winter season. Hence depending upon the supremacy, the weightage must be changed accordingly. This factor will be taken into consideration in the upcoming fog/visibility forecast studies. Finally, the present study also revealed that the 24-hours forecast has better accuracy as compared to 48-hours forecast. Normally, 6-hours lead time forecast is sufficient for the proper management of aviation transportation activities at the IGI airport. However, considering the complete requirements of the aviation sector, 24-hours forecasts can also play a crucial role. Therefore, in future studies, 24-hours fog/visibility forecast which will be updated in every 06 hours will be implemented which can further increase the accuracy of the fog/visibility predictions at the IGI airport.

The bar diagrams in Figure 4 (a-d) represent the overall number of types and occurrence of various fog events observed along with the 24-hours and 48-hoursfog forecasts for 2020-21 and 2021-22 winter seasons. In 2020-21, 12 very dense fog events, 8 dense fog, 8 moderate fog, 23 shallow fog and 11 mist events were reported. In 2021-22, the number of observed events of very dense fog, dense fog and moderate fog were 5, 4 and 6 respectively which were less as compared to 2020-21 data. But the reported shallow fog and mist events in 2021-22 were 30 and 17 respectively which were higher than that in 2020-21 data.

The following section briefly discusses about the statistics between the predicted and observed fog events over the IGI airport. In 2020-21, 12 very dense fog events were occurred. The 24-hours and 48-hour forecasts of 2020-21 accurately predicted 8 out of them but missed out the remaining 4 events. However, in 2021-22, 24 and 48-hours forecasts predicted 4 & 6 very dense fog events respectively which were very close to the observed no of 5 very dense fog events. Further, in 2020-21, the number of dense fog events predicted were 17 and 19 respectively for 24 and 48-hours forecasts, but dense fog occurred only 8 times out of them which indicates the overestimated dense fog predictions in 2020-21. Similar scenario was observed in 2021-22 as well in which the predicted dense fog events for 24 and 48-hour forecasts were 9 and 7 respectively, but the actual occurrence of dense fog was observed only on 4 events out of them.

The prediction of moderate fog was quite near to the actual observations for both the years. The 24-hours and 48-hours forecast predicted 10 and 12 moderate fog events respectively for 2020-21 in which moderate fog was observed on 8 times out of them. Similarly, in 2021-22, the 24-hours and 48-hours forecasts predicted 6 & 5 moderate fog events respectively. in which moderate fog was observed on 6 times out of them. The shallow fog events were predicted to be 17 & 14 in 24-hours and 48-hours forecasts respectively for year 2020-21. However, shallow fog was observed in 23 events in 2020-21. Similarly, in 2021-22, the shallow fog was observed in 30 events, but it was predicted only for 27 & 23 events in 24-hours and 48-hours forecasts. Overall, underestimation in shallow fog prediction was observed in both the years 2020-21 and 2021-22. Finally,11 mist events were observed in 2020-21. Moreover, 24-hours and 48-hours forecasts of 2020-21 were quite near to the actual number of events i.e., 10 and 9 mist events respectively. In 2021-22, 17 mist events were reported and 24-hours & 48-hours forecasts predicted 16 and 21 events respectively.

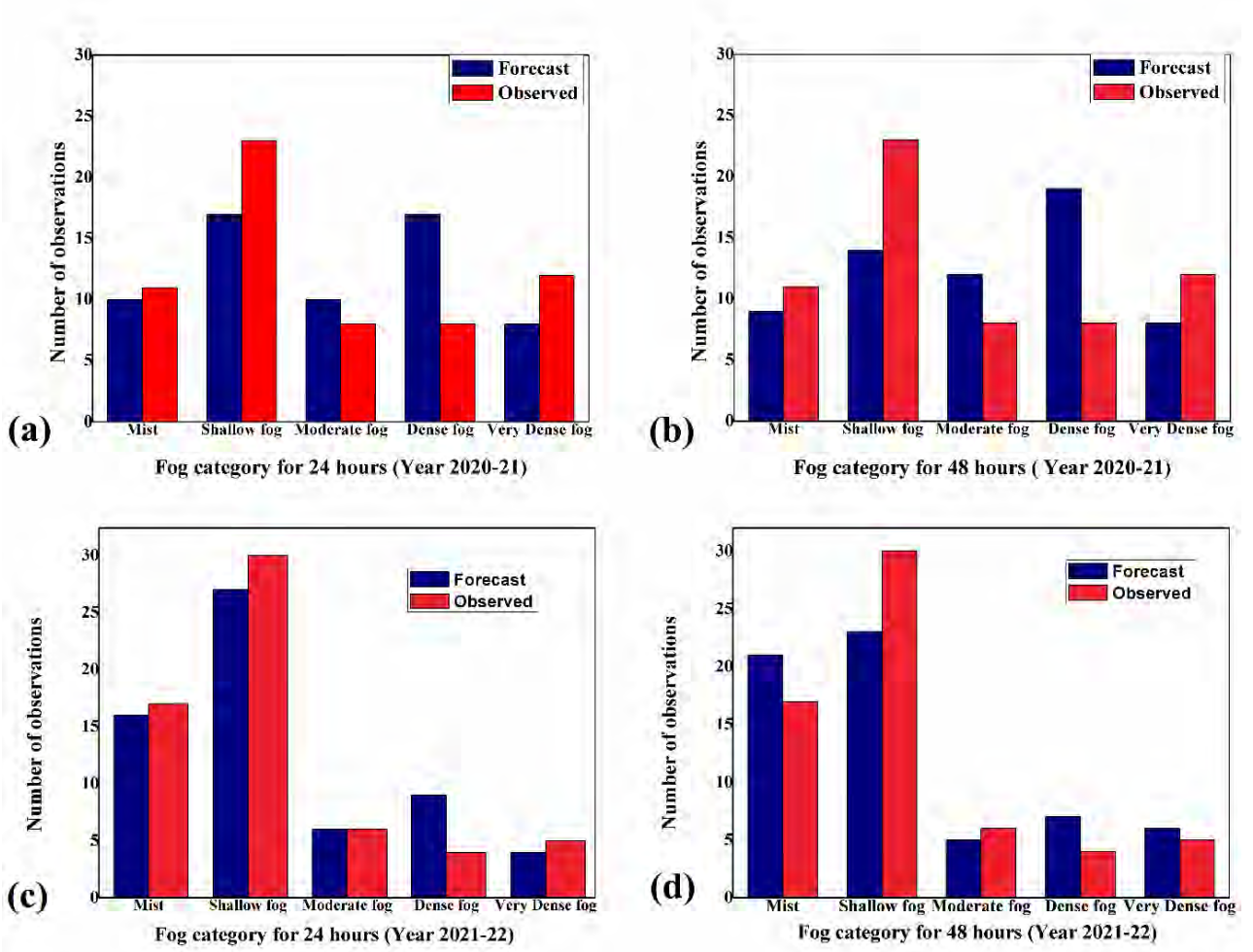

Figure 4 (a-d). Bar diagram plots between forecasted and observed fog events at IGI airport. (a) 24-hour forecast, 2020-21, (b) 48-hour forecast, 2020-21, (c) 24-hour forecast, 2021-22 and (d) 48-hour forecast, 2021-22.

In the present study, the 24-hours and 48-hours forecasts of visibility for 2020-21 and 2021-22 have been compared with the corresponding observed visibility from METAR and synoptic observations which are indicated as scatter plots shown in Figure 5(a-d). From Figure 5(a-d), the correlation between the forecasted and observed data sets were estimated. The correlation coefficient for 24-hours forecast is promising with values of 0.79 & 0.70 for 2020-21 & 2021-22 respectively. However, the correlation coefficient for 48-hours forecast is 0.65 & 0.66 for 2020-21 & 2021-22 respectively which is lower than 24-hours forecast.The most probable reason may be as the lead time of forecast increases, accuracy of various meteorological parameters from the model outputs which were used to predict the visibility may decrease. This implies that the 48-hours forecast is a challenging task as compared to 24-hours forecast.

To get more insights to the statistical analysis, the 24-hours and 48-hours visibility forecast were categorized further into two categories i.e. visibility with an error of ±100m & ±200m for the years 2020-21 (Table 4) & 2021-22 (Table 5). The Probability of Detection(POD) of 24-hours forecast is excellent with values of 0.92 & 0.98 for visibility error of ±100 m & ±200 m respectively for 2020-21. The POD for 48-hours forecast of 2020-21 is lower as compared to 24-hours forecast as it is 0.79 & 0.85 for visibility error of ±100m & ±200m respectively. Similarly, the POD of 24-hours forecast for 2021-22 also observed to be high i.e., 0.73 & 0.87 for visibility error of ±100 m & ±200 m respectively. However, the POD for 48-hours forecast of 2021-22 is comparatively lower than 24-hours forecast i.e., 0.61 & 0.81 for visibility error of ±100 m & ±200 m respectively.

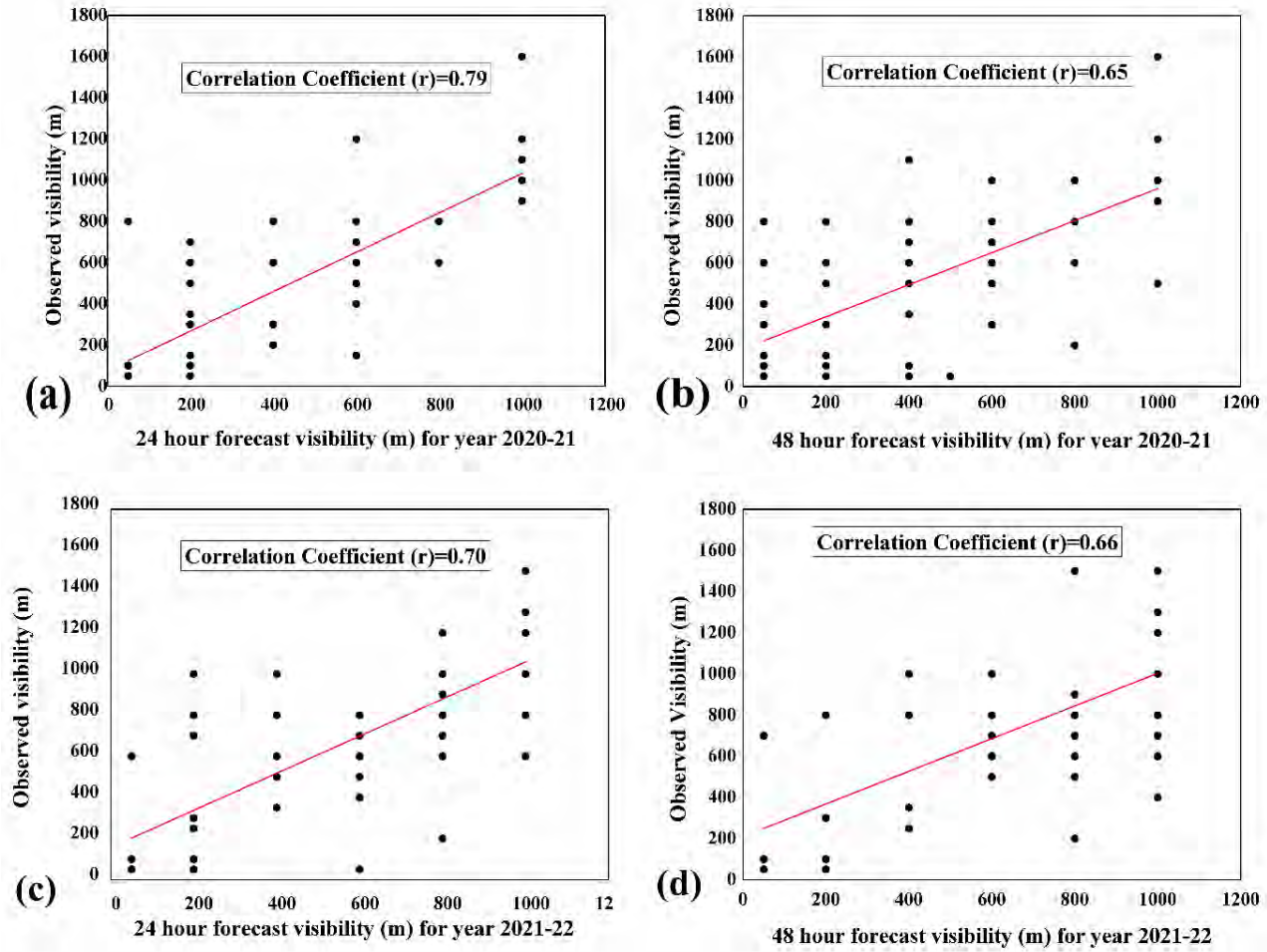

Figure 5(a-d). Scatter plots of forecast and observed visibility. (a) 24-hours forecast, 2020-21 (b) 48-hours forecast, 2020-21, (c) 24-hours forecast, 2021-22 and (d) 48-hours forecast, 2021-22.

Overall analysis indicated that the accuracy is highest in 24-hours forecast (visibility±200 m), i.e., 0.89 & 0.79 in 2020-21 & 2021-22 respectively. The lowest accuracy is observed in 48-hours forecast (visibility ±100 m), i.e., 0.54 & 0.56 in 2020-21 & 2021-22 respectively. Accuracy of 24-hours forecast (visibility±100 m) & 48-hours forecast (visibility±200 m) are observed to be in moderate range i.e., 0.73 & 0.68 respectively for the year 2020-21. Similarly, for 2021-22, the accuracy of 24-hours forecast (visibility±100 m) & 48-hours forecast (visibility±200 m) are noticed to be in the moderate range i.e., 0.63 & 0.74 respectively. It has also been observed that the accuracy of 24-hours forecast for both visibility errors of ±100 m & ±200 m for year 2020-21 is greater than that of 2021-22. However, opposite trend is observed for 48-hours forecast accuracy as it is found to be greater in 2021-22 than that in 2020-21 for both visibility errors of ±100m & ±200m. The general trend observed in accuracy analysis is followed in success ratio analysis as well. Out of all the four cases, the success ratio is highest in 24-hours forecast (visibility±200 m) i.e., 0.88 & 0.82 in 2020-21 & 2021-22 respectively. The lowest success ratio is observed in 48-hours forecast (visibility ±100m) i.e., 0.56 & 0.63 in 2020-21 & 2021-22 respectively. Success ratio of 24-hours forecast (visibility±100m) & 48-hours forecast (visibility±200m) are observed to be in moderate range i.e., 0.72 & 0.71 respectively for the year 2020-21. Similarly, for 2021-22, success ratio of 24 -hoursforecast (visibility±100m) & 48-hours forecast (visibility±200 m) are also observed to be in moderate range i.e., 0.68 & 0.76 respectively.

Table 4. Statistical report of 24-hours and 48-hours visibility forecast for the years 2020-21

Statistical Term	24-hour forecast		48-hour forecast	
	Visibility ± 100 m	Visibility ± 200m	Visibility ± 100m	Visibility ± 200m
Probability of Detection (POD)	0.92	0.98	0.79	0.85
Accuracy	0.73	0.89	0.54	0.68
Success ratio	0.72	0.88	0.56	0.71
Critical Success Index (CSI)	0.68	0.87	0.49	0.63
False Alarm Ratio (FAR)	0.28	0.12	0.44	0.29
Bias score	1.28	1.10	1.41	1.20
Heidke skill score	0.35	0.65	0.05	0.23

Table 5. Statistical report of 24-hours and 48-hours visibility forecast for the years 2021-22

Statistical Term	24-hour forecast		48-hour forecast	
	Visibility±100m	Visibility±200m	Visibility±100m	Visibility±200m
Probability of Detection (POD)	0.73	0.87	0.61	0.81
Accuracy	0.63	0.79	0.56	0.74
Success ratio	0.68	0.82	0.63	0.76
Critical Success Index (CSI)	0.54	0.73	0.45	0.64
False Alarm Ratio (FAR)	0.32	0.18	0.37	0.24
Bias score	1.08	1.07	1.18	1.05
Heidke skill score	0.22	0.55	0.11	0.20

The Critical Success Index (CSI) is also calculated and found to be highest in 24-hours forecast (visibility±200 m) i.e., 0.87 & 0.73 for 2020-21 & 2021-22 respectively. The lowest CSI is observed in 48-hours forecast (visibility ±100 m) i.e., 0.49 & 0.45 in 2020-21 & 2021-22 respectively. However, the performance of CSI has been observed to be in the moderate range for 24-hours forecast (visibility±100 m) & 48-hour forecast (visibility±200 m), i.e., 0.68 & 0.63 respectively for 2020-21 and 0.54 & 0.64 respectively for 2021-22. Furthermore, the False Alarm Ratio (FAR) over all the seasons were investigated and it is observed to be lowest in 24-hours forecast (visibility±200 m), i.e., 0.12 & 0.18 for years 2020-21 & 2021-22 respectively. However, the highest FAR are observed in 48-hours forecast (visibility±100 m), i.e., 0.44 & 0.37 for the year 2020-21 & 2021-22 respectively. However, 24-hour forecast (visibility±100 m) & 48-hours forecast (visibility±200 m) cases have moderate FAR, i.e., 0.28 & 0.29 respectively for 2020-21 and 0.32 & 0.24 respectively for 2021-22. In addition, the bias score of all forecasts is calculated and found to be above one for all the cases in 2020-21 & 2021-22 which implies an over forecast scenario. The best bias score is observed in 24-hours forecast (visibility±200 m), i.e., 1.10 & 1.07 for the year 2020-21 & 2021-22 respectively. Finally, the Heidke Skill score is also estimated and give reasonably good values, i.e., 0.65 & 0.55 for 24-hours forecast (visibility±200 m) for the year 2020-21 & 2021 -22 respectively.

The overall statistical analysis shows that 24-hours forecast (visibility ±200 m) gives the best statistical results having the highest POD, accuracy, SR, CSI & Heidke skill score and lowest FAR, bias score in both the years of 2020-21 & 2021-22. However, an opposite scenario was observed in 48-hours forecast (visibility±100 m), i.e., the statistical results like the lowest POD, accuracy, SR, CSI, Heidke skill score and highest FAR and bias score in both the years of 2020-21 & 2021-22. Moreover, the 48-hours forecast (visibility±100 m) performance needs to be improved. The study also indicated that the improvement in accuracy of visibility to an error of ±100 m over a long

period of 48 hours is a challenging task, whereas the shorter period (24 hours) with a greater range in visibility (±200m) gives promising results. As the lead time required to make a decision for aviation purposes is approximately 06 to 08 hours, then 24-hour fog/visibility forecasts can fulfil aviation requirements in any aspect. Further, fog is also categorized based on the visibility range as well. Combining all the factors, a 24-hours (visibility ±100 m) fog/ visibility forecast which will be updated in every 06 hours, can fulfil the aviation requirements during the winter seasons at IGI airport. In the upcoming years, as the accuracy of the model output improves, correspondingly, the fog/visibility forecast will also be more accurate.

5. Conclusion

The primary objective of the present study is to improve the accuracy of fog/visibility forecast over the IGI Airport during the winter seasons of 2020-21 and 2021-22. Various meteorological parameters collected from IMD GFS model outputs have been used to innovatively predict the 24-hours and 48-hours fog/visibility over the IGI Airport. Daily forecasts are issued which are valid for the next 24 hour and 48 hours consist of information on fog, visibility, wind speed and relative humidity etc. The verification of these forecasts is carried out using the METAR and synoptic observations prepared at IGI Airport by the Meteorological Watch Office. Results have show that the 24-hours forecast has the highest hit rate of 0.92, accuracy (0.73), success ratio (0.72), CSI (0.68) and fairly low FAR (0.28) & bias score (1.10) for the 2020-21 winter season. Similarly, the results of 24-hours forecast of 2021-22 also encouraged a hit rate of 0.73, accuracy (0.63), success ratio (0.68), CSI (0.54) and low FAR (0.32) & bias score (1.08). However, the 48-hours forecast of all seasons has lesser accuracy than 24-hours forecast. The 48-hours forecast scheme needs further improvement for better results. In future, the revised weightage criteria for each parameter instead of equal weightage can also have a scope to improve the fog/visibility forecast. The study has also suggested various findings that can be implemented in the future course to improve the fog/visibility forecast over the IGI airport during the upcoming winter seasons.

Author Statement

AC: Conceptualization, formal analysis, investigation, methodology, validation, visualization and writing original draftASH: Conceptualization, formal analysis, investigation, methodology, validation, visualization, writing-review and editing and supervision. CS: Conceptualization, formal analysis, supervision and writing-review and editing and supervision. SJ: Visualization and writing-review and editing.

Acknowledgement

The authors are grateful to Dr. Mrutyunjay Mohapatra, Director General of Meteorology, India Meteorological Department for the immense guidance and support needed to carry out the present study. The authors are thankful to all the Met Officials of MWO Palam for their assistance throughout the study.

References

Arun S.H., S.K. Sharma, S. Chaurasia, R. Vaishnav and R. Kumar (2018a). Fog/low clouds detection over the Delhi Earth Station using the Ceilometer and the INSAT-3D/3DR satellite data. Int. J. Remote Sens. 39(12) 4130-4144.

Arun S.H., S. Chaurasia, A. Misra and R. Kumar (2018b). Fog Stability Index: A novel technique for fog/low clouds detection using multi-satellites data over the Indo-Gangetic plains during winter season. Int. J. Remote Sens. 39(22)8200-8218.

Arun S.H., C. Singh, S. John, S.K. Diwakar, D.K. Sankhala, N. Nigam, C.S. Tomar and G. Kumar (2022). A study to improve the fog/visibility forecast at IGI Airport, New Delhi during the winter season 2020–2021. Journal of Earth System Science, 131(2), pp.1-11.

Bhowmik S.K.R, A.M. Sud and C. Singh (2004). Forecasting fog over Delhi-An objective method. Mausam. 55(2)313-322.

Bhushan B., H.K.N. Trivedi, R.C. Bhatia, R.K. Dube, R.K. Giri and R.S. Negi (2003). On the persistence of fog over northern parts of India. Mausam. 54(4)851-860.

Chaurasia S., V. Sathiyamoorthy, B. Paul Shukla, B. Simon, P.C. Joshi and P.K. Pal P K (2011). Night-time fog detection using MODIS data over Northern India. Meteorol Appl.18(4)483-494.

Choudhury S., H. Rajpal, A.K. Saraf and S. Panda (2007). Mapping and forecasting of North Indian winter fog: an application of spatial technologies. Int. J. Remote Sens. 28(16)3649-3663.

Dey S. (2018). On the theoretical aspects of improved fog detection and prediction in India. Atmos Res. 20277-80.

Dhangar N.G., D.M. Lal, S.D. Ghude, R. Kulkarni, A.N. Parde,P. Pithani, K. Niranjan, D.S. Prasad, C. Jena, V.S. Sajjan and T. Prabhakaran (2021). On the Conditions for Onset and Development of Fog Over New Delhi: An Observational Study from the WiFEX. Pure Appl. Geophys.178(9) 3727-3746.

Dutta D. and S. Chaudhuri (2015). Nowcasting visibility during wintertime fog over the airport of a metropolis of India: decision tree algorithm and artificial neural network approach. Nat Hazards (Dordr). 75(2)1349-1368.

Ghude S.D., G.S. Bhat, T. Prabhakaran, R.K. Jenamani, D.M. Chate, P.D. Safai, A.K. Karipot, M. Konwar, P. Pithani, V. Sinha and P.S.P. Rao (2017). Winter fog experiment over the Indo-Gangetic plains of India. Curr. Sci. 767-784.

Goswami P. and S. Sarkar (2017). An analogue dynamical model for forecasting fog- induced visibility: validation over Delhi. Meteorol Appl. 24(3)360-375.

Goswami S., S. Chaudhuri, D. Das, I. Sarkar and D. Basu (2020). Adaptive neuro- fuzzy inference system to estimate the predictability of visibility during fog over Delhi, India. Meteorol Appl. 27(2)1900.

Gultepe I., M. Pagowski and J. Reid (2007). A satellite-based fog detection scheme using screen air temperature.

Weather Forecast.22(3) 444-456.

Jayakumar A., E. N. Rajagopal, I.A. Boutle, J.P. George, S. Mohandas, S. Webster and S. Aditi (2018). An operational fog prediction system for Delhi using the 330 m Unified Model. Atmospheric Sci. Lett. 19(1), p. e796.

Jayakumar A., H. Gordon, T. Francis, A.A. Hill, S. Mohandas, B.S. Sandeepan, A. Mitra and G. Beig (2021). Delhi Model with Chemistry and aerosol framework (DM- Chem) for high- resolution fog forecasting. Q J R Meteorol Soc.

Jenamani R.K. (2012). Development of intensity based fog climatological information system (daily and hourly) at IGI airport, New Delhi for use in fog forecasting and aviation. Mausam. 63(1)89-112.

Kulkarni R., R.K. Jenamani, P. Pithani, M. Konwar, N. Nigam and S.D. Ghude(2019). Loss to aviation economy due to winter fog in New Delhi during the winter of 2011–2016. Atmosphere. 10(4)198.

Kutty S.G., A.P. Dimri and I. Gultepe (2020). Climatic trends in fog occurrence over the Indo- Gangetic plains. International Journal of Climatology, 40(4), pp.2048-2061.

Mitra A.K., S. Nath and A.K. Sharma (2008). Fog forecasting using rule-based fuzzy inference system. J. Indian Soc. Remote Sens. 36(3) 243-253.

Mohapatra M and A.T. Das (1998). Analysis and forecasting of fog over Bangalore airport. Mausam. 49135-142.

Parde A.N., S.D. Ghude, A. Sharma, N.G. Dhangar, G. Govardhan, S. Wagh, R.K. Jenamani, P. Pithani, F. Chen, M. Rajeevan and D. Niyogi (2022). Improving simulation of the fog life cycle with high-resolution land data assimilation: A case study from WiFEX. Atmospheric Research, 278, p.106331.

Payra S. and M. Mohan (2014). Multirule based diagnostic approach for the fog predictions using WRF modelling tool. Adv. Meteorol., 2014.

Pithani P., S.D. Ghude, V.N. Chennu, R.G. Kulkarni, G.J. Steeneveld, A. Sharma, T. Prabhakaran, D.M. Chate, I. Gultepe, R.K. Jenamani and R. Madhavan (2019). WRF model prediction of a dense fog event occurred during the winter fog experiment (WIFEX). Pure Appl. Geophys. 176(4) 1827-1846.

Pithani P., S.D. Ghude, R.K. Jenamani, M. Biswas, C.V. Naidu, S. Debnath, R. Kulkarni, N.G. Dhangar, C. Jena, A. Hazra and R. Phani (2020). Real-time forecast of dense fog events over Delhi: The performance of the wrf model during the wifex field campaign. Weather and Forecasting, 35(2)739-756.

Saraf A.K., A.K. Bora, J. Das, V. Rawat, K. Sharma and S.K. Jain (2011). Winter fog over the Indo-Gangetic Plains: mapping and modelling using remote sensing and GIS. Nat Hazards (Dordr). 58(1)199-220.

Singh H. and S.K. Dhattarwal (2004). Pattern and distribution of injuries in fatal road traffic accidents in Rohtak (Haryana). JIAFM, 26(1), pp.20-23.

Singh C. (2011). Unusual long and short spell of fog conditions over Delhi and northern plains of India during December–January 2009–2010. Mausam. 62(1)41-50.

Singh R.K. and S.K. Suman (2012). Accident analysis and prediction of model on national highways. Int. J. Civ. Eng. Technol.1(2)pp.25-30.

Singh A., J.P. George and G.R. Iyengar (2018). Prediction of fog/visibility over India using NWP Model. J Earth Sci. 127(2)1-13.

Srivastava S.K., A.R. Sharma and K. Sachdeva (2017). An observation- based climatology and forecasts of winter fog in Ghaziabad, India. Weather. 72(1)16-22.

Syed F.S., H. Körnich and M. Tjernström (2012). On the fog variability over south Asia. Climate dynamics, 39(12), pp.2993-3005.

Yadav P., A.N. Parde, N.G. Dhangar, G. Govardhan, D.M. Lal, S. Wagh, D.S. Prasad, R. Ahmed and S.D. Ghude (2022). Understanding the genesis of a dense fog event over Delhi using observations and high-resolution model experiments. Modeling Earth Systems and Environment, pp.1-12.

Geospatial Application for Dairy Supply Chain Management

Sukalpa Changmai*, Sameer Saran, and Prasun Kumar Gupta
Geoinformatics Department, Indian Institute of Remote Sensing, Dehradun, India
*Email: sukafa.5609@gmail.com

(Received: 23 March 2023; in final form 31 July 2023)

DOI: https://doi.org/10.58825/jog.2023.17.2.63

Abstract: The broad availability of geospatial data has changed how we think about solving problems. There are numerous uses for GIS and remote sensing in a variety of fields. Such a field is supply chain management where GIS is used to map various stages like producers, consumers, processing facilities, suppliers, distribution centers, and transportation routes for better decision making and optimization of flow of goods. This study integrates geospatial technology to map raw material sources, processed product delivery routes, areas served by processing sectors, and ultimately to model the relationships between different elements of the dairy industry. Parameters taken involve import-export data of milk and milk products, roads network, service areas, and satellite derived vegetation index. Aanchal Dairy in Dehradun district of Uttarakhand is considered for this study. The primary data was collected through field visits and the raw data was structured for further analysis. Secondary data was obtained from various verified internet sources. Results indicate certain regions with high quantity of raw milk supply and areas where processed products are delivered. Optimised routes and the areas where Aanchal Dairy provides its services are also defined. Vegetation index shows that places with high raw milk supply have better fodder for dairy cows. Finally, the results are geospatially mapped and various relationships are presented in graphical form.

Keywords: Geospatial technology, supply chain management, dairy industry, network analysis

1. Introduction

The Indian dairy sector has evolved significantly with technological advancements playing a key role in this transformation. The establishment of National Dairy Development Board in 1965 and Operation Flood in 1969-70 was aimed at modernizing and developing the dairy sector using cooperatives. These developments enabled the considerable growth of milk output, from 21.2 million tonnes in 1968-1969 to 121 million in 2010-11, and then to 209.96 million tonnes in 2020-21 (Ministry of Finance, 2021). This makes dairy the most important agricultural commodity, contributing 5% to India's economy and supporting over eight crore farmers. With 23% of the global milk production, India now holds the top spot(Ministry of Finance, 2021).

The dairy sector is, however, susceptible to a variety of losses, including physical, economic, quality, and environmental losses. These losses can be caused by a number of factors, such as spills, breakage, contamination, oversupply, competition, and changes in consumer demand. Globally up to 8.2% of the milk is lost causing damages worth billions of dollars each year (March et al., 2019). As reported by FAO, just 37% of the milk produced in India is processed or packaged, with the remaining consumed as fresh or as unpasteurized milk through informal channels (Punjabi, 2009). This risks adulteration, harmful bacteria growth, and subsequent loss of milk without any further utilization for producing dairy products.

Here, supply chain management plays a critical role towards development of an integrated strategy to unite different entities in solving problems related to the movement of commodities and information. This improves the quality, shelf life, and consumer accessibility of dairy products.Supply chains comprise of upstream and downstream linkages, including commodities, services, and customers (Schmitz, 2011). A supply chain is described as a network of facilities with distribution options that fulfils the tasks of acquiring raw materials, transforming those materials into intermediate and final items, and delivering finished goods to customers. Thus, in order to reduce cost, increase sales and improve customer service, supply chain management organizes and controls the flow of goods, information, and finances among a network of producers, distributors, suppliers, and customers (Leistritz et al., 2009).To ensure that goods are produced and delivered at the appropriate times, in adequate quantities and at the proper locations while minimizing the cost factor and satisfying consumer expectations, supply chain management connects sources, manufacturers, distributors, and retailers (Kumar & Agrawal, 2011).Supply Chain Management has four major decision areas, viz. location, production, inventory and transportation.

The term "Supply Chain Management" first appeared in the early 1990s, though proper integration of GIS and Remote Sensing in Supply Chain Management started in recent years. GIS must be considered a geographic decision support system to improve the existing decision-making (Durga Prasad et al., 2009). These interactive computer-based solutions assist decision makers in data modeling and resolving unstructured issues (Subhas & Sambrani, 2009; Yusianto et al., 2020). Geographic Information Systems are a valuable tool for managing supply chain risks as GIS analysis allows graphical portray of the information. The analysis also lets the firm view the complete profile of the organization, including the location of raw material suppliers, processing units, manufacturers, office and warehouse locations, as well as the locations of distributors, retailers and consumers. Geospatial technologies are also used to map producers, consumers, processing facilities, suppliers, distribution centers, and

transportation routes, facilitating better supply chain management decision-making (Kumar & Agrawal, 2011; Bosona et al., 2013).Some specific examples of the use of GIS in supply chain management are (1) Retail companies (such as Walmart) use GIS to track the location of its products in real time. This information helps to ensure that products are always available in the right quantities at the right stores; (2) Companies dealing with shipping and logistics (such as UPS) use GIS to optimize its delivery routes. This helps to reduce fuel consumption and emissions, and to improve delivery times; and (3) Food industries (such as the Coca-Cola Company) use GIS to manage its global supply chain. GIS helps to track the movement of its products, to identify potential risks, and to plan for future growth.

Uttarakhand, unlike other prime milk-producing states having milk surpluses, produces enough only towards fulfilling its own needs. In addition, the dairy industry continues to face challenges such as low productivity, low quality, erratic supply, varying consumer requirements and natural causes, such as natural calamities disrupting timely supply. Aanchal Dairy is one of the top brands in Uttarakhand serving all 13 districts. It is an apex level State association, administered by Uttarakhand Co-operative Dairy Federation Limited (UCDF). UCDF under the brand name 'Aanchal Dairy' continues to increase milk production despite selling an average of 1 lakh 65 thousand liters of liquid milk per day. Since, such huge production requires an utmost supply chain management system for uninterrupted milk and dairy products supply, therefore through this study use of geospatial applications for a better supply chain is been presented.

This research focuses to integrate the spatial analytical capabilities of remote sensing into a suitable supply chain management system. The purpose is to model relationship between different parameters of a dairy industry and to incorporate geospatial technology towards optimal route finding, planning and scheduling for different regions of the study area.

2. Study Area, Datasets and Software

2.1 Study Area

Dehradun district has been taken as the study area, as shown in figure 1. Dehradun, the capital city of Uttarakhand lies at 30.3165° N and 78.0322° E, and is one of the largest cities in the Himalayas. It is also the most populous city of Uttarakhand, with a population of 16,96,694 (as of Census 2011), known for its scenic landscape, pleasant year-round weather and provides a gateway to the Himalayas.

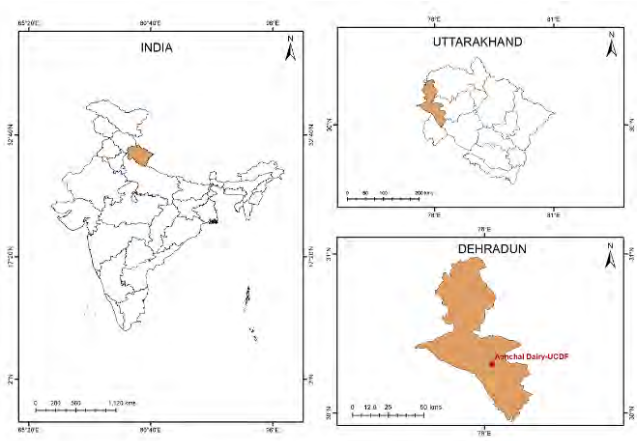

Figure 1. Study Area Map; The point marked with red shows the location of the regional head office of UCDF located in Dehradun district.

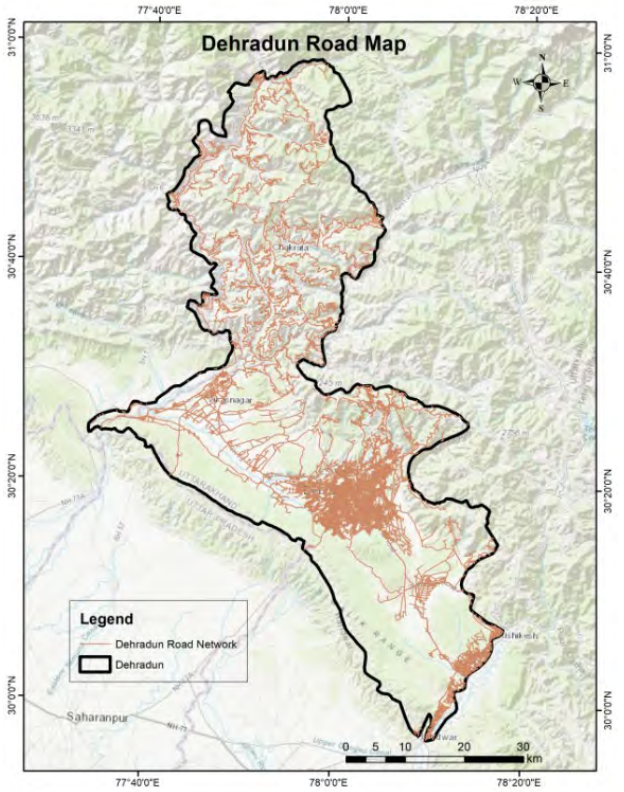

Figure 2. Dehradun Road Network

The primary source of the economy is tourism and the largest profession followed in the region is agriculture.

2.2 Datasets

2.2.1 Primary Dataset

The primary dataset (Table 1) includes names, pin-codes and coordinates of the import-export locations, details of the processing unit is included, along with daily and monthly import-export quantities of raw and processed milk respectively.

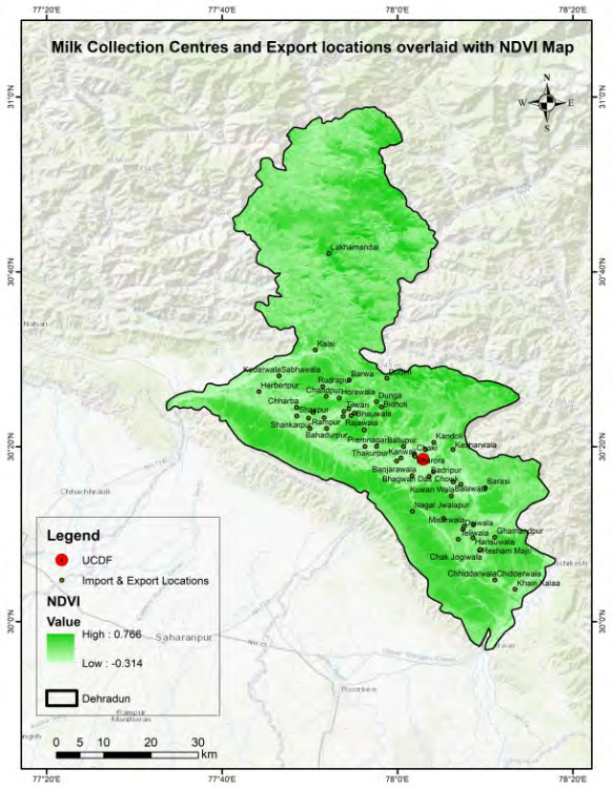

Figure 3. Milk collection centers and export locations overlaid with NDVI

2.2.2 Spatial Data

Various spatial data were used in the study. District boundary and road network for central India were collected from Open Street Map (OSM; https://www.geofabrik.de/) as shown in figure 2. It was then clipped in ArcGIS to acquire only the road network of Dehradun district. Total area of the district is 3088 km². Coordinates of 59 milk collection centers (also referred to as import locations) were collected through field visit conducted during June 2022 (Figure 3) and the satellite based Normalized Difference Vegetation Index (NDVI) of 10m spatial resolution is also acquired using Google Earth Engine figure 3. The NDVI is calculated from the median composite of Sentinel 2 images for the year 2021, using the standard normalized difference of visible and near-infrared bands (Weier &Herring, 2000). The NDVI value of the study area ranges from -0.31 to 0.76.

Table 1 includes data such as geographical coordinates and pin codes of the locations that supply raw milk. Import quantities of raw milk and export quantities of processed milk and dairy products are also recorded in the table. These data are in daily and monthly basis measured in liters. Data of only 14 locations out of 59 milk collection centers are shown in the table due to space constraint. The first seven rows show top 7 raw milk import locations and the last seven rows indicates places with least raw milk supply to UCDF.

2.2.3 Software Used

Different tasks were performed using the software given below to complete the study.

1. Google Earth Engine: It is a cloud-based geospatial analysis platform used to carry out large-scale geospatial processing, visualization and analysis of different satellite images. In this study NDVI cloud free median composite is acquired using Earth engine.

2. Tableau Public: It is a web tool for exploring, generating and distributing data visualizations. In this study, it is used to analyze the data, creating geospatial data view through Tableau Maps.

3. ArcGIS (v10.3) enables users to interact with maps and geographic data. It is used to handle numerous applications, compile and evaluate the mapped data, and creating maps of the research area.

4. Google Earth Pro: It is powerful mapping software providing a 3D interactive globe that aids planning, analysis and decision making. It was used for acquiring online geo-referenced address.

3. Methodology

This study primarily focuses on the integration of geospatial capabilities and relating various parameters with ground truth data. Quantitative data is generalized to model the relationship between different factors and illustrate the results of location and route analysis. Figure 4 gives a brief outline of the overall methodology used in the study.

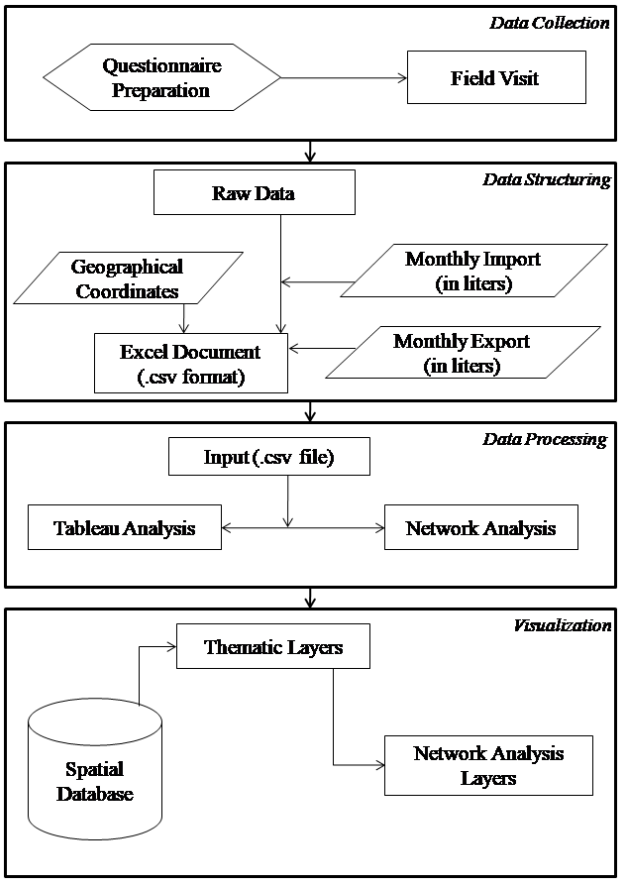

Figure 4. Proposed Methodology

3.1. Data Collection

The process includes a field survey conducted at UCDF, Dehradun, to collect ground truth data. A structured questionnaire was designed, which consisted of 3 phases. Phase 1 emphasized the sources, i.e., places supplying the raw milk. Phase 2 involved the processing details, and Phase 3 had questions related to the export of the processed materials. The survey included a total of 5 queries.

1. Details of the sources from where the raw milk is imported, along with the location coordinates.
2. Quantities of raw milk imported daily and monthly from each source.
3. Total processed items, i.e., processed milk and other milk products.
4. Quantities exported daily and monthly from the processing center.
5. Export Locations of the processed items.

3.2. Data Cleaning

Before analyzing, the gathered data was structured and checked for any anomalies and outliers. The data was structured into .csv format, which is also the desired format for further analysis in the study. The data involved coordinates of the import, processing unit and export locations. Daily and monthly dairy data was also an input in the excel sheet. Collection and distribution of milk and dairy products are measured in kilograms (kg) since the weights of transport vehicles were considered. The unit was converted to liters to ease the understandings of further analysis. Conversion involved the formula:

1 kg of milk = 0.9708 liters milk (for density of milk = 1033 kg/m3).

Once the primary data was structured, secondary data were collected from different sources involving verified websites.

3.3. Data Processing

The primary data were analyzed using the Tableau Public software, wherein comparisons and relations were analyzed and represented in map form including import and export localities. Integrated primary and secondary data were used for Network Analysis in ArcGIS software. Evaluation of the road layers helped in determining the shortest path from processing unit to the export locations. Also, service areas of the processing unit were demarcated. Single delivery stages were identified wherein the raw material collection and processed material distribution follows different approaches. Graphical representation showing the import-export variations was also carried out.

3.4 Experimental Setup

This section briefly explains about NDVI, network analysis, analysis using Tableau and finally visualization of the acquired results.

3.4.1 NDVI

NDVI shows the density of greenery in an area. It is computed using the reflected energy in near-infrared and visible electromagnetic spectrum.
The formula is:

$$NDVI = \frac{NIR-Red}{NIR+Red} \quad (1)$$

Since the most important food source for dairy cows involves green fodder, thus NDVI helps in identifying the places with better fodder density. Subsequently, validation using ground truth was done. The NDVI satellite imagery product of Sentinel 2 used in the study was collected using Google Earth Engine and had 10m spatial resolution. Point based sampling on import locations was done for the analysis.

3.4.2 Network Analysis

Various network issues include determining the best path through the study area, locating the nearest processing facility, determining the service area, and solving vehicle routing problems were analyzed using the ArcGIS Network Analyst extension (Patel et al., 2019).

3.4.3 Tableau Analysis

This analysis helped in locating the prime milk import locations. Fleets from UCDF collects milk from these locations which serve as a center point for a locality. Private dairy farms and farmers bring the milk to these locations set by Aanchal Dairy. Thus, milk is collected from a particular point wherein milk from the nearby localities is stocked. Import localities of raw milk and export localities for processed milk and processed dairy products were analyzed and geospatially viewed using Tableau.

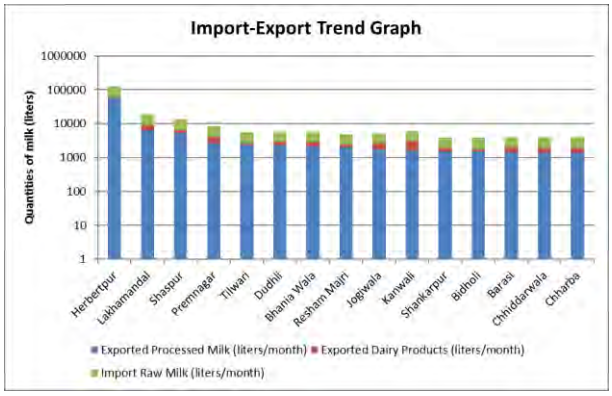

Figure 5. Import vs Export Trend Graph of 15 top locations receiving processed milk from UCDF; Export centers with monthly consumption/ sale of more than 1000 liters have been shown here; Y axis is in log-scale.

Table 1. Sample of field data collected; Coordinates of milk collection centers and monthly quantities of import-export of milk and milk products; The data sample has been sorted based on the 'Import Raw Milk (monthly)' column showing likely location of low and high production/ collection patterns. All quantities are in liters, unless mentioned otherwise.

Place	Pin code	Latitude (ºN)	Longitude (ºE)	Import Raw Milk (daily)	Import Raw Milk (monthly)	Export Processed Milk (daily)	Exported Processed Milk (monthly)	Exported Dairy Products (daily)	Exported Dairy Products (monthly)
Herbertpur	248142	30.4383	77.7366	2194.95	65848.5	1963.1	58893.3	87.4	2621.1
Lakhamandal	248124	30.7016	77.8695	319.90	9597.0	213.9	6407.7	93.2	2796.0
Shaspur	209743	30.3919	77.8087	236.61	7098.3	174.8	5245.5	38.8	1164.9
Premnagar	248001	30.3340	77.9602	149.41	4482.3	87.4	2621.4	49.5	1485.3
Kanwali	248001	30.3118	78.0067	101.26	3037.8	52.4	1572.6	46.6	1398.0
Tilwari	248197	30.4010	77.8982	98.45	2953.5	77.7	2329.8	10.7	320.1
Bhania Wala	248161	30.1842	78.1443	98.45	2953.5	69.9	2097.0	24.3	728.1
…….	……	…….	……	……	……	……	……	……	……
Sabhawala	248197	30.4683	77.7749	11.46	343.8	16.5	495.0	4.9	145.8
Khairi Kalaa	249204	30.0614	78.2234	11.35	340.5	5.8	174.6	6.8	203.7
Bhauwala	248007	30.3972	77.9182	10.97	329.1	6.7	201.0	2.9	87.0
Bhagwan Das Chowk	248001	30.2616	78.1204	10.79	323.7	8.7	261.0	4.9	145.5
Namkeen Bhandar	248001	30.3060	77.9984	9.82	294.6	11.7	349.5	6.8	203.7
Chaki	248001	30.3191	78.0325	5.30	159.0	12.6	378.6	6.8	203.7
Kharora	248001	30.3164	78.0321	3.50	102.0	17.3	519.9	7.3	219.0

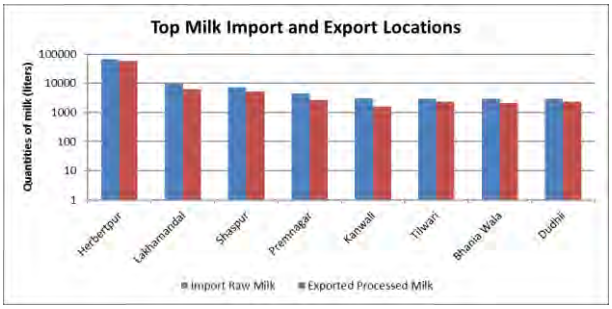

Figure 6. Top raw milk import and pasteurized milk export locations; Y axis is in log-scale

3.5 Data Visualization

Spatial data involving district map and road map was used to create thematic layers of road network and location of source-destination. NDVI overlay upon the import locations was visualized to determine the areas with suitable fodder for dairy cows. Finally, various network analysis layers were developed and evaluated to acquire the results.

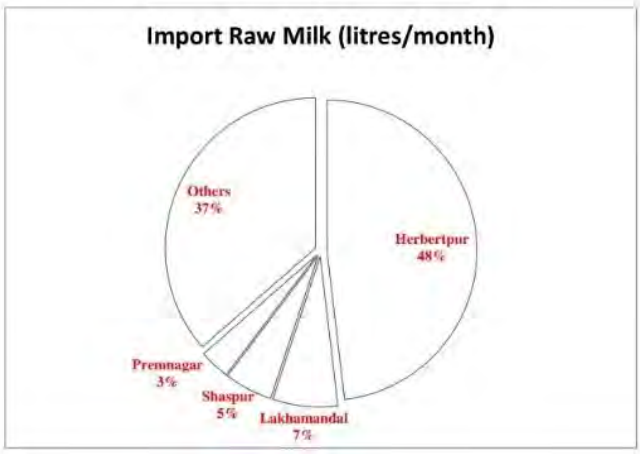

Figure 7. Percentage of raw milk import

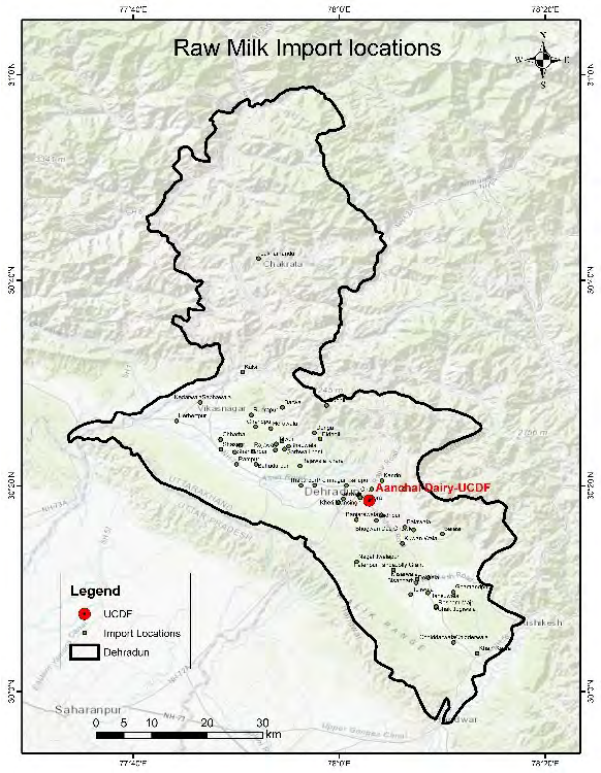

Figure 8. Import Locations of raw milk

4. Results and Discussion

4.1 Data Analysis in Graphical Form

Figure 5 shows import versus export trend of the different locations across Dehradun. This graph shows centers receiving processed milk greater than 1000 liters per month (i.e., 15 centers). The complete data (not shown) contains information from 59 milk collection centers. It can be clearly noticed that places such as Herbertpur, Lakhamandal, Shaspur, Premnagar, etc. receive highest quantity of processed milk and dairy products. In all the 15 centers shown, there is a net surplus of imported milk i.e., the quantity of imported raw milk is greater than the sum of the quantities of exported processed milk and exported dairy products. The data for 59 milk collection centers shows that 34 centers are in surplus, and 25 centers are in deficit. However, the quantity of milk in surplus 34 centers (~8100 liters) far exceed the deficit (~2600 liters) in the remaining 25 centers.

Figure 6 shows eight locations that supplies bulk quantities milk. Bhaniawala and Kanwali supplies around 100 liters milk per day which totals around 3000 liters a month from each source. Premnagar supplies around 4500 liters milk per month. Shaspur and Lakhamandal supply a total of 16000 liters per month whereas Herbertpur supplies highest raw milk with 2194 liters milk per day and a total of 66000 liters milk per month. The graphs in figure 5 and figure 6 are plotted using logarithmic scale in MS Excel by talking a base of 10 for a better visualization.

From figure 7 it is observed that 50% of raw milk is supplied by Lakhamandal and Herbertpur, whereas the other half is imported from the remaining sources. In the pie-chart others (40%) constitutes of 30 collection centers which contributes less than 1% each.

4.2 Interpretation of the Map Layouts

The maps given below shows the analysis of import locations, shortest path to export locations, service areas and NDVI generation for fodder required to the cattle.

4.2.1 Import Locations of Raw Milk to UCDF

Figure 8 shows 59 import locations of raw milk to UCDF. The initial process of the supply chain management in this paper shows the import of raw milk from various locations across the study area. The processing plant is marked in red whereas the black dots refer various raw milk collection centers.

4.2.2 Shortest Path to Export Locations

Once the raw milk is processed it is then packed and the milk products are exported to various locations across Dehradun. This is done by the transport facilities of UCDF which takes various routes to the export locations. The routes involve different road networks and through this study an analysis was done to determine the shortest path from the processing center to those export locations. Figure 9 shows the road network expansion across Dehradun while the highlighted line in the figure shows the shortest path. This is the optimized path from UCDF to various export locations receiving end products of Aanchal Dairy across Dehradun region.

4.2.3 Service Areas of Exported Products

Figure 10 shows the regions where the processed products (processed milk and dairy products) are delivered by UCDF. The service area of UCDF and its distributors were determined by field observations. Figure 10 shows three buffer zones around UCDF and the export locations. The 500m buffer zone is the one where UCDF vehicles deliver the products. In the 1000m buffer zone, UCDF distributors are located. These distributors deliver the products to retail shops within 2000m buffer zone under the brand name 'Aanchal Dairy'. It should be noted that the distances were calculated based on straight line distance, and not distance by road.

4.3 Fodder Map

The fodder map or NDVI Map shows the NDVI of Dehradun (Figure 11). The range of NDVI varies from -0.31 to 0.76 in the entire study area. There is strong evidence to suggest NDVI and livestock productivity are linked (Manning et al., 2017; Pearson et al., 2021).The NDVI at collection center points range from 0.2 to 0.4. This indicates the nearby localities of these regions have high density of shrubs and grasslands (Weier & Herring, 2000), which is also the best fodder for dairy cows. In return the raw milk production is also high in these regions supplying more than 80 liters per day as indicated by the field data.

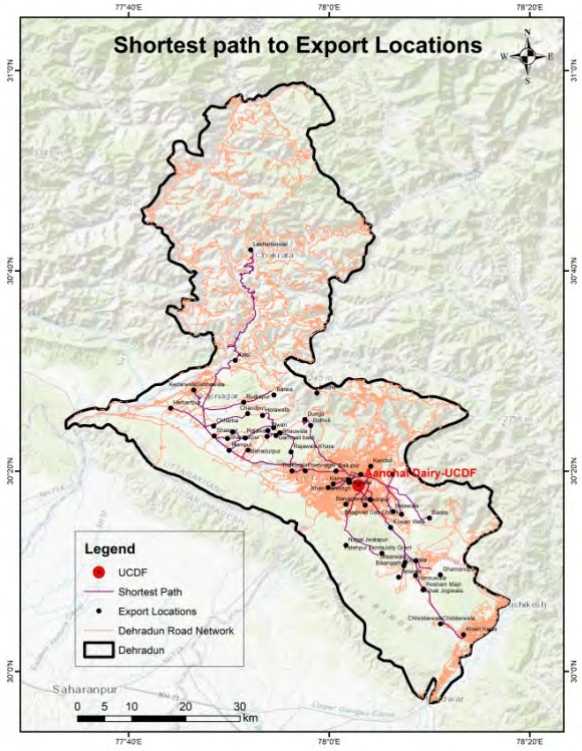

Figure 9. Shortest Path Map from UCDF to export locations

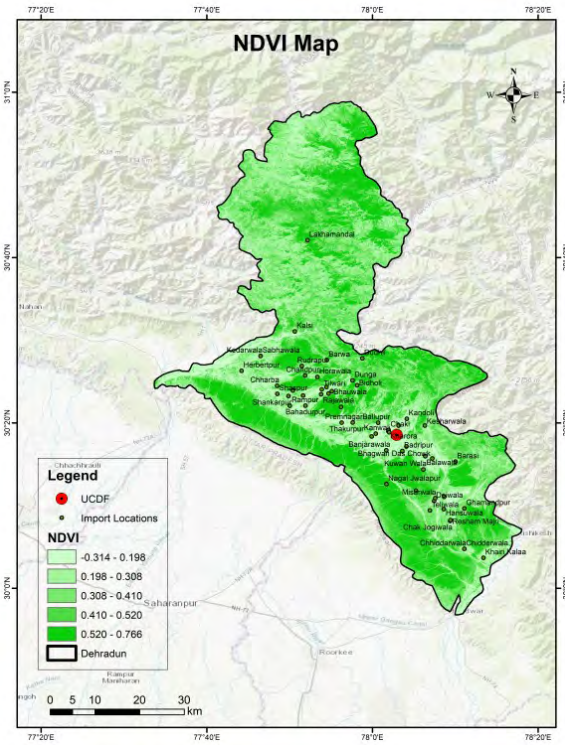

Figure 11. NDVI Map

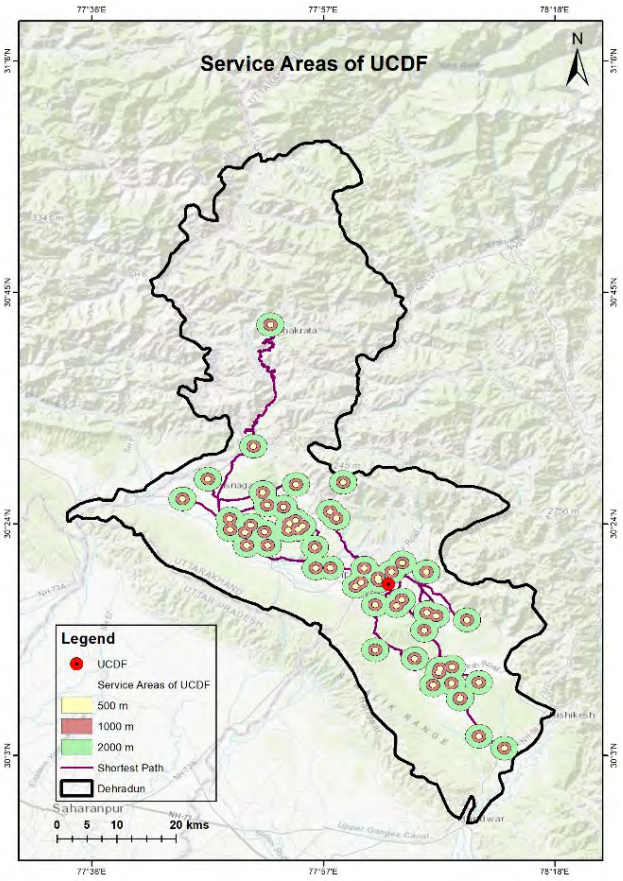

Figure 10. Service area map of Aanchal dairy

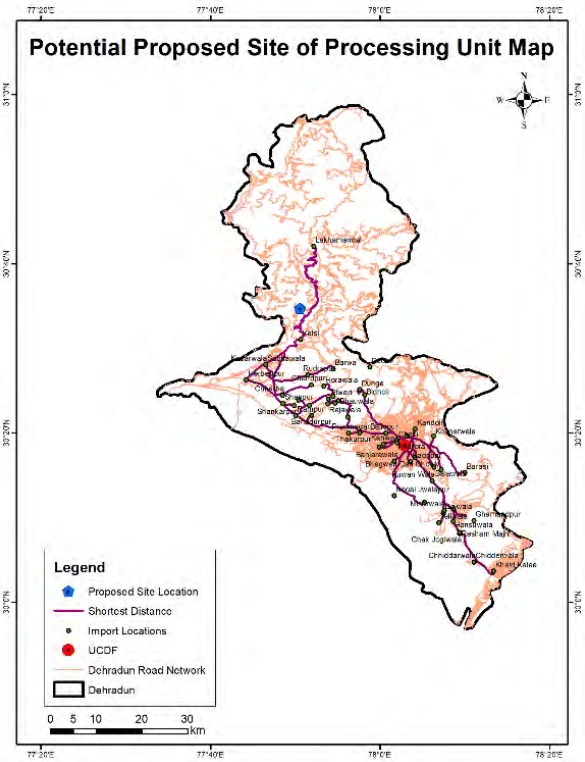

Figure 12. Potential proposed site for a new milk processing plant map

4.4 Proposed New Sites

The primary dataset in the study shows that some places supply raw milk to a larger extent compared to other places. The places are Lakhamandal and Herbertpur which account for more than 50% raw milk supply to the present processing unit. Figure 12 proposes a new processing plant near places supplying high quantity of raw milk so that the efficiency of the federation and supply of end products is

not hampered. The site was decided based on factors such as connectivity, terrain and distance from high yield collection centers. The proposed site does not include socio-economic factors and only focuses upon accessibility from the above-mentioned locations.

Figure 13. Prime milk import locations

4.5 Import-Export Relationship

Figure 13 shows the different locations which supply better quantities of milk than other locations in the region. 11 milk collection centers provide better quantities of milk than the rest. The milk is collected in these centers and then it is transported to the processing unit. The locations are Lakhamandal, Herbertpur, Premnagar, Tilwari, Kanwali, Bidholi, Bhaniawala and Shaspur. Analysis on Tableau helps in locating areas supplying raw milk (Figure 14). In the map dark brown indicates more quantity of raw milk supply and lighter the color lesser the quantity of milk supplied to UCDF. Raw milk is collected from the localities and collected in a location set by UCDF.

Figure 15 shows the areas receiving processed milk from UCDF. The analysis shows Herbertpur as the top export location. Various dairy products such butter, cheese, ghee etc. are also supplied to these areas under the brand name 'Aanchal dairy'.

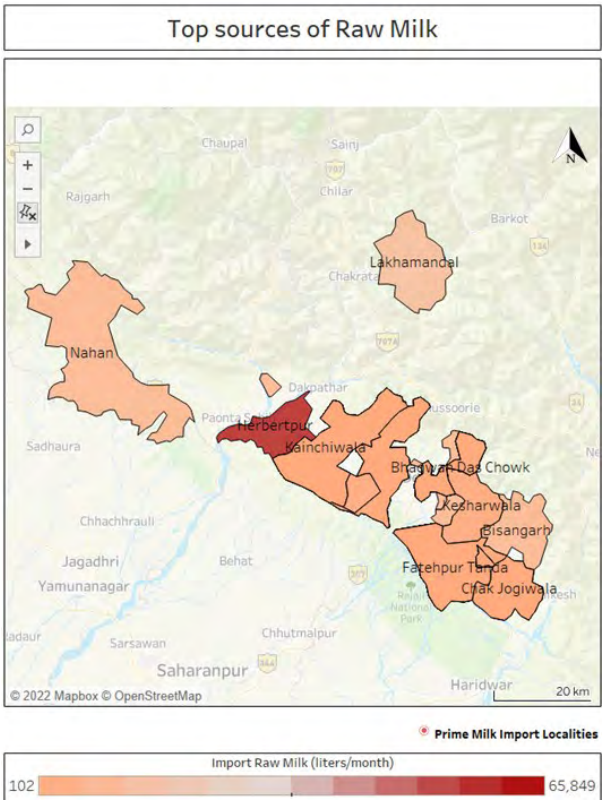

Figure 14. Raw milk import localities

4.6 Validation of the results

After validation it was observed that the fleet delivering the processed products take different routes to different locations. Also, there are various localities where deliveries with a single vehicle are possible as the locations fall in the same route. Taking the shortest path and managing the fleet accordingly can save a considerable amount of time and money while satisfying consumer needs. Also ground truth validation of NDVI shows that the area where NDVI ranges from 0.2 - 0.4 supply more quantity of milk than the other locations. These locations have a high density of grasslands and shrubs, which is an important fodder for dairy cows as well. Therefore, better the fodder for lactating cows more is the raw milk procurement.

5. Conclusion

The objective of this study was to integrate various spatial analytical capabilities of remote sensing into a suitable supply chain management. Graphical analysis of the import-export data shows areas providing milk to Aanchal Dairy (UCDF). Qualitatively, it was found that, milk collection centres having higher milk imports also had NDVI values ranging from 0.2 - 0.4. This implies that the regions also had a better fodder density for dairy cows. Once the milk is procured, it is then processed into packed milk and other dairy products.

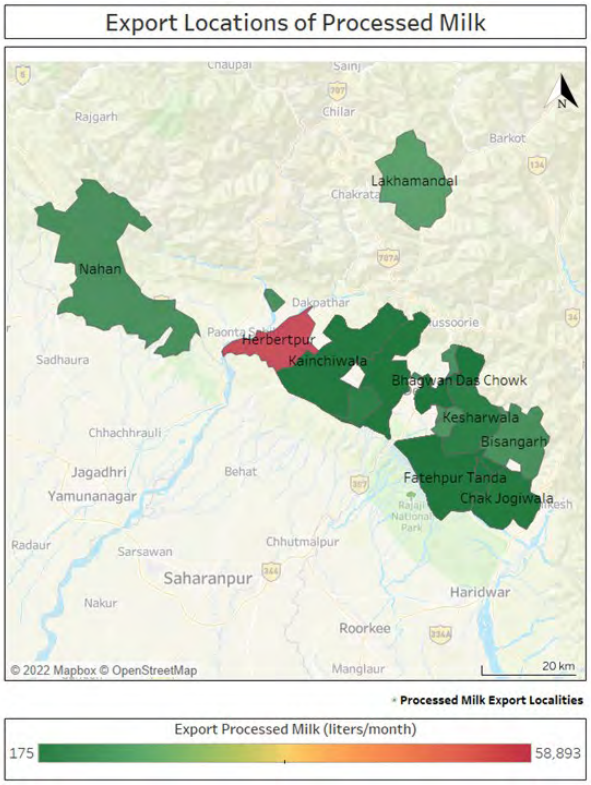

Figure 15. Processed milk and dairy products export localities

The processed products are then supplied to different places and through this study route analysis was conducted towards finding an optimized route for an efficient supply chain. The areas where Aanchal Dairy provides their services were also analyzed. Some regions supply more raw milk than they acquire the processed products. This was due to unbalanced import-export of raw milk and processed products.

The study finally helped in answering the research questions which involved various parameters of a dairy industry, their inter-relationship and the use of geospatial technologies for a practical and improved Supply Chain Management.

6. Recommendation

This study can include other secondary variables such as location of distributors, time frame and fleet size. Time frame can include total time required for the delivery of products from the processing unit to export locations. Loading-unloading parameter can also be included. Fleet size can answer the vehicle capacity related queries. It was difficult to incorporate the fleet in this research as the firm consisted vehicles with different dimensions and carrying capacity. Pollution parameter can also be included which will led to queries related to reduction in emissions and environmental benefits (Elasseri et al., 2020). Additional data on factors affecting milk production such as cattle breed, age, milking frequency, health, dry period, diet and accommodation could enhance predictability of supply.

Considering the rural-urban demarcations, analysis can be done to understand the impacts of a better supply chain management on rural development. Demand-Supply data can also be incorporated which can give a better insight to the trends of high and low season productivity and availability. Since, the main focus of this study was on the integration of spatial capabilities of GIS and Remote Sensing, further research can be done considering various socio-economic factors, especially for identification of new sites, and by applying these techniques to another study area.

Acknowledgements

This study is part of P.G. Diploma course carried out by the first author. Thanks to the Director, Indian Institute of Remote Sensing, Indian Space Research Organization (ISRO), Dehradun, India for his support. Sincere thanks to Uttarakhand Cooperative Dairy Federation (UCDF) for providing the necessary data and timely assistance.

References

Bosona T., I. Nordmark, G. Gebresenbet and D. Ljungberg (2013). GIS-based analysis of integrated food distribution network in local food supply chain. *International Journal of Business and Management*, *8*(17), 13.http://dx.doi.org/10.5539/ijbm.v8n17p13

Durga Prasad M.V. and P.K. Singh (2009). Applying AHP and GIS techniques for locating milk-chilling facilities in a backward tribal district of Gujarat. *Institute of Rural Management*, Working paper 209.

Elasseri J., V.V. Panicker and R. Sridharan (2020). Environmental friendly route design for a milk collection problem: the case of an Indian dairy. *International Journal of Production Research*, 60(3), 912-941. https://doi.org/10.1080/00207543.2020.1846219

Kumar S. and S. Agarwal (2011). GIS as a decision support for supply chain management. Geospatial World Forum, Hyderabad, January 18-22,2011.

Leistritz F.L., N.M. Hodur, D.M. Senechal, M.D. Stowers, D. McCalla and C.M. Saffron (2009). Use of agricultural residue feedstock in north dakota biorefineries. *Journal of Agribusiness*, *27*(345-2016-15314), 17-32. http://dx.doi.org/10.22004/ag.econ.90655

Manning J., G. Cronin, L. González, E. Hall, A. Merchant and L. Ingram (2017). The behavioural responses of beef cattle (Bos taurus) to declining pasture availability and the use of GNSS technology to determine grazing preference. *Agriculture*, 7(5), 45. https://doi.org/10.3390/agriculture7050045

March M.D., L. Toma, B. Thompson and M. J. Haskell (2019). Food waste in primary production: Milk loss with mitigation potentials. *Frontiers in Nutrition*, *6*, 173. https://doi.org/10.3389/fnut.2019.00173

Ministry of Finance, Government of India (2022). Economic Survey 2021-22. Viewed on 09 September 2022.

Patel S.S., R. Pandey and H. Misra (2019). An Optimisation Model for a Dairy Cooperative for promoting sustainable operations for milk collection.*Institute of Rural Management*, Working paper 293.

Pearson C., P. Filippi and L.A. González (2021). The relationship between satellite-derived vegetation indices and live weight changes of beef cattle in extensive grazing conditions. *Remote Sensing*, *13*(20), 4132.https://doi.org/10.3390/rs13204132

Punjabi M. (2009). India: Increasing demand challenges the dairy sector. In N. Morgan (Ed.), *Smallholder dairy development: Lessons learned in Asia*. FAO.ISBN 978-92-5-106187-9.

Schmitz P. (2011). Using Supply Chain Management as a tool to manage GIS projects. Viewed on 16 September 2022 Available: https://sensorsandsystems.com/using-supply-chain-management-as-a-tool-to-manage-gis-projects/

Subhas M.S. and V.N. Sambrani (2009). Geographic Information System (GIS) and Supply Chain Management (SCM)- A manager's perspective. 10th ESRI India User Conference (2009).

Yusianto, R., S. Marimin and H. Hardjomidjojo (2020). Intelligent spatial decision support system concept in the potato agro-industry supply chain. In *2020 International Conference on Computer Science and Its Application in Agriculture (ICOSICA)* (pp. 1-7). IEEE.https://doi.org/10.1109/ICOSICA49951.2020.9243233

Analytical study of relation between Land surface temperature and Land Use/Land Cover using spectral indices: A case study of Chandigarh

Yamini Agrawal[1]*, Hina Pandey[1], Poonam S. Tiwari[2]
[1]Photogrammetry and Remote Sensing Department, IIRS, Dehradun
[2] Geoweb Services, Information Technology and Distance Learning Department, IIRS, Dehradun
* Email: yamini.agrawal0510@gmail.com

(Received: 31 March 2023; in final form 6 October 2023)

DOI: *https://doi.org/10.58825/jog.2023.17.2.65*

Abstract: Rapid urbanization is the major cause for Land Use and Land Cover changes globally. The urbanization alters the land surface dynamics and affects the surface temperature, which gives rise to urban heat island effect. In the present study, spatial correlation analysis has been done between Land Surface Temperature (LST) and Land Use and Land Cover (LULC) for the city of Chandigarh. The LST is retrieved from Landsat-8 thermal band using Mono-Window algorithm and shows 2.5°C increase of temperature from 2016 to 2022. The LULC has been derived using Maximum Likelihood Classifier (MLC) which shows an increase in built-up of 7.56% and decrease in forest cover by 32%. Spectral indices belonging to major LULC classes have been derived using Sentinel-2 optical bands and spatially correlated with LST using linear regression analysis. The results show a strong positive correlation (r=0.988) between built-up and LST and a negative correlation (r=-0.625) between urban vegetation cover and LST. The mean correlation coefficient for LST-NDVI for vegetation and forest cover, LST-NDWI for water bodies, LST-NDBI for built-up and LST-NBLI for bare land is -0.3, 0.116, 0.51 and 0.392 respectively. The results indicate that vegetation and water bodies mitigate the rise of LST, whereas built-up areas and bare lands sustain in the rise of LST. The statistical analysis will be helpful for policy makers and urban planners for prevention of further degradation of urban environment and surface dynamics.

Keywords: LST, LULC, spectral indices, change detection, correlation, regression, mono-window algorithm

1. Introduction

Chandigarh is a planned city in India with rapidly developing urbanisation. Urbanisation is caused by increase in demographic density in the suburbs of the cities (Nimish et. al, 2018) which causes the built-up regions to spread out. The modifications in the land use change the local climatic conditions like radiative and energy balance (Alexander and Mills 2014). Various studies conducted previously suggests that (Jiang et.al., 2015; Awuh et al. 2018) rapidly changing land use and land cover affects and contributes to increased land surface temperature (LST).
Urban sprawl leads to expansion of LULC, which further affects the air quality of the region, soil degrading (Nimish et al. 2018), which in turn makes the fertile land barren. The urban growth pattern of Chandigarh and its relation to Land surface temperature was studied by (Nimish et al. 2018). A time series analysis for monitoring the urban sprawl of Chandigarh was carried out by (Saini and Tiwari 2019) to see the changes in the land use pattern. (Awuh et al. 2019) established that a strong positive correlation exists between the built-up class and land surface temperature. Cooling effects of water bodies like on land surface temperature was carried out by (Gupta et.al., 2019). (Chang et.al., 2007) studied the effects of urban green spaces and local water bodies form urban cool island (UCI) which helps in mitigating the urban heat Island (UHI). Urban microclimate analysis and its effects on Land surface temperature for Chandigarh was assessed by (Gupta et.al., 2017). The study indicates that the heavy industrial areas exhibit highest LST followed by high-rise compact buildings. (Li et.al, 2017b) evaluated indices like EBBI (Enhanced built-up and Bareness Index), DBI (Dry Built-up index) and DBSI (Dry Bare Soil Index) for differentiating the dry areas and built-up regions. (Pandey and Joshi 2015) tried to model spatial patterns of urban growth by utilising a multi agent system.

Spectral indices provide an efficient alternative to the classical classification algorithms like supervised classification or neural nets to distinguish between different surface cover features (He et al. 2010; Li et al. 2015). (Li et. al., 2017b)] proposed a method to classify LULC using unsupervised classification by employing spectral indices as inputs to the classifier. (Faridatul and Wu 2018) proposed three new indices namely modified normalised difference bare- land index (MNDBI) for differentiating impervious surfaces and bare land, tasseled cap water and vegetation index (TCWVI) for enhanced separation of vegetation and water areas and shadow index (ShDI) to separate water from shadows. (Guha and Govil 2020) observed that normalized difference built-up index (NDBI) and normalized difference bareness index (NDBaI) are mixing the built-up and fallow or bare lands during dry climates, so they proposed new indices, namely the dry built-up index (DBI) and dry bare-soil index (DBSI) to distinguish between built-up areas and bare lands using Landsat-8 satellite imagery.

2. Study Area and Dataset

2.1 Study Area

Chandigarh is a city which is located in Northern India and works as a capital for the states of Punjab and Haryana. Being a planned city, it is located at 30.7333° N and 76.7794° E with an average elevation of 335 m above mean sea level (Nimish et al. 2018; Saini and Tiwari 2019) as shown in Figure 1. According to census of India, 2011, the population of city is 10.55 Lakhs, with a growth rate of 17.19%

2.2 Dataset Used

For correlation analysis of land surface temperature and Land use land cover, the month of May for the years 2016-2022 has been chosen as it represents the peak of summer season in Chandigarh. During this period, the weather is relatively stable with minimal rainfall and cloud cover. The description of datasets utilised in the study has been given below.

(a) Sentinel-2A optical data

Sentinel-2 Level-2A atmospherically corrected data with 10 m spatial resolution for Chandigarh city was used for processing and generating Land Use Land Cover maps. The details of the Sentinel dataset used for the current study are given in Table 1. Since there was unavailability of cloudless optical data for May 2016, the latest available cloudless data acquired on 4th June, 2016 was used for producing LULC map.

Table 1: Optical data acquisition from Sentinel-2

Satellite	Acquisition Date	Tile Number	Cloud cover
Sentinel-2A	04/06/2016	T43RFQ	0.24260
Sentinel-2A	20/05/2018	T43RFQ	0.00400
Sentinel-2A	07/05/2020	T43RFQ	0.02370
Sentinel-2A	14/05/2022	T43RFQ	0.00000

(b) Landsat-8 thermal data

Landsat-8 resampled 30 m spatial resolution thermal data (Band-10) acquired by the TIRS sensor was used for generating Land- surface temperature (LST) maps. The average/mean data for the month of May 2016, May 2018, May 2020 and May 2022 was acquired and downloaded from Google earth Engine (GEE) from the Landsat-8 Data collection.

3. Methodology:

The approach for this study is depicted in figure 2.

3.1 Mono-window algorithm for the retrieval of Land Surface Temperature

For LST retrieval, mono-window algorithm was first proposed by (Qin et. al, 2010). Three major variables are required for this algorithm: emissivity, transmittance, and mean ambient temperature. This algorithm utilizes Band 10 of TIRS sensor of Landsat-8 which records the radiation in the spectral range from 10.60 µm to 11.19 µm.

In order to retrieve LST, first, the DN values are converted into spectral radiance at the sensor aperture, otherwise known as Top of the Atmospheric (TOA) radiance (Equation 1).

$$L_\lambda = \frac{L_{max}-L_{min}}{QCAL_{max}-QCAL_{min}}(D - QCAL_{min}) + L_{min} \quad (1)$$

where L_λ is Top of the Atmospheric radiance at the sensor's aperture in W/ (m^2 sr µm), $QCAL_{max}$ (= 65535) and $QCAL_{min}$ (= 0) for Landsat-8. After calculating the radiance values, the brightness temperature values are obtained by applying the inverse of the Plank function.

$$BT = \frac{K_2}{\ln(\frac{K_1}{L}+1)} - 273.15 \quad (2)$$

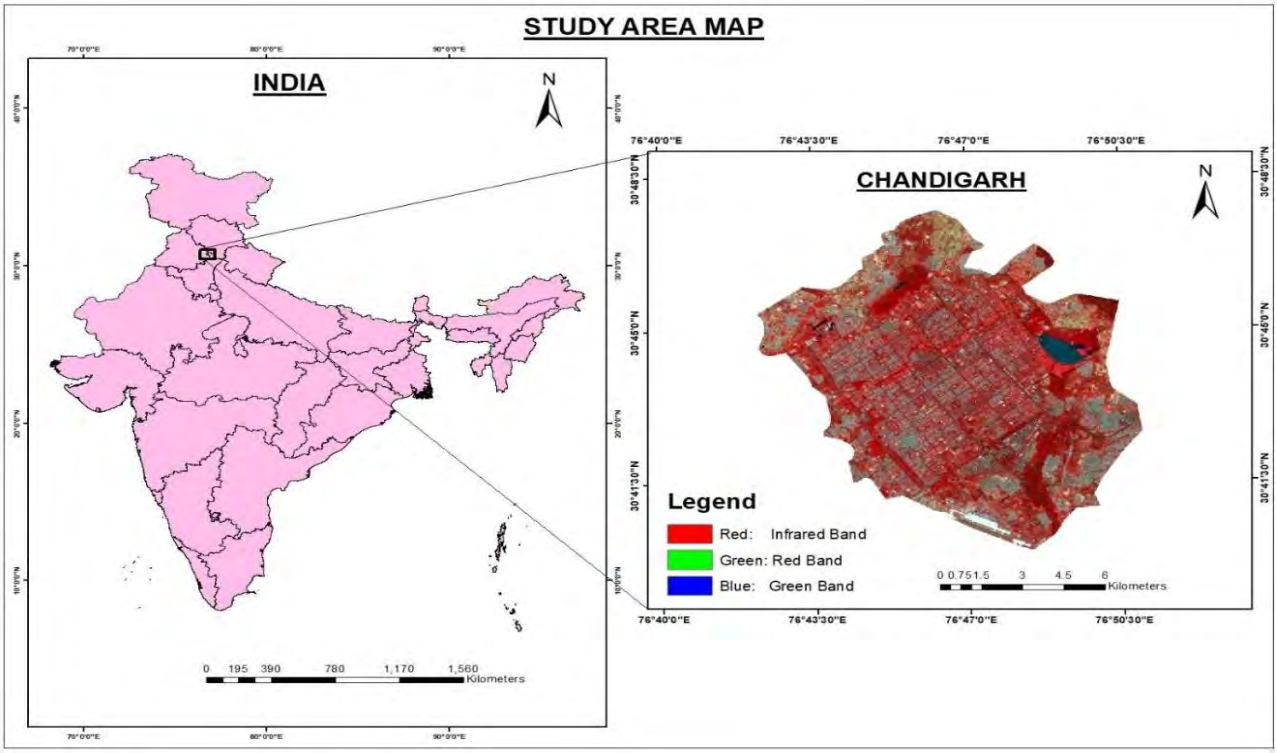

Figure 1. Study area map of Chandigarh represented by FCC (Sentinel-2)

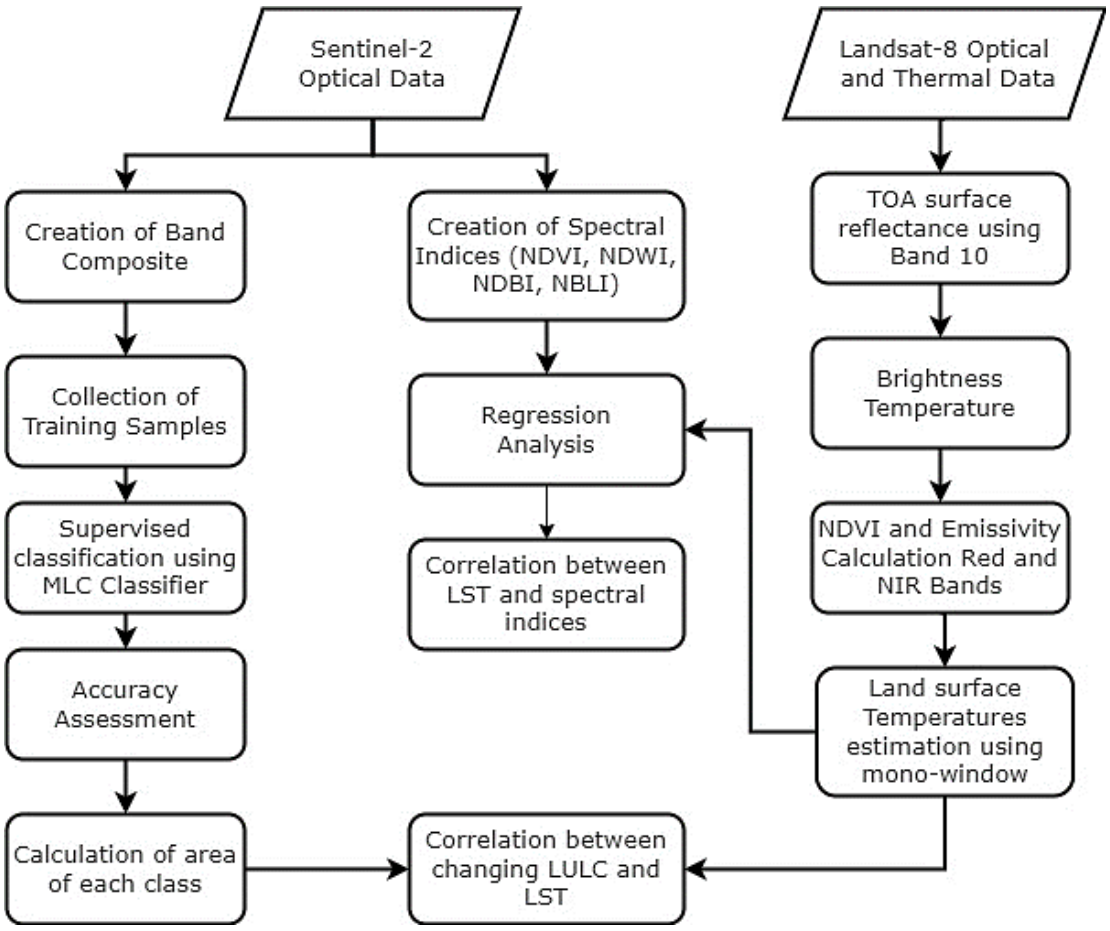

Figure 2. Flowchart depicting the methodology

Where BT is the temperature in Celcius (°C), K_1 is the pre-launch calibration constant in W/(m^2 sr μm) and K_2 is the pre-launch calibration constant in Kelvin. for Landsat 8 ETM+, K_1 = 774.89 W/(m^2 sr μm) and K_2 = 1321.08 K. The next step was to correct the BT from the effects of atmosphere and ground emissions. For this, Normalized Difference Vegetation Index (NDVI), Proportion of Vegetation (P_v) and Emissivity (ε) are derived.

$$NDVI = \frac{NIR-Red}{NIR+Red} \quad (3)$$

$$P_v = \left(\frac{NDVI-NDVI_{min}}{NDVI_{max}-NDVI_{min}}\right)^2 \quad (4)$$

$$\varepsilon = 0.004 * P_v + 0.986 \quad (5)$$

$$LST = \frac{BT}{1+\left(\frac{\lambda \times BT}{P_v} \times \ln \varepsilon\right)} \quad (6)$$

Where, LST is in Celsius (℃), BT is the brightness temperature in (℃), λ is the average wavelength (m).

3.2 Maximum-Likelihood Classification for Land Use Land Cover Map

Maximum-Likelihood classifier (MLC) for LULC classification is a parametric algorithm based on Bayesian theory of probability. MLC assumes that each class in every band is normally distributed. It is a supervised classification algorithm which is an extension of Bayes theorem (Norovsuren et al. 2019). In MLC, probability for each pixel belonging to *m* classes is calculated. Maximum likelihood classifier assigns every pixel *i* to a class w_i if the probability for the class w_i is maximum for that pixel (Shivakumar and Rajashekararadhya 2018). The probability density function for each class is calculated using:

$$P(x|w_i) = \frac{1}{\sigma_i\sqrt{2\pi}}\, e^{-\left(\frac{x-\mu_i}{2\sigma_i}\right)^2} \quad (7)$$

The MLC algorithm required a homogenous collection of training samples for the classes to be mapped, that is, Water, Bare Land, Healthy Vegetation, Forest and Built-Up. It assigns each cell to one of the classes of the signature file. With the help of mean vector and covariance matrix, membership of each cell to all the classes was calculated and each cell was assigned a class which has maximum likelihood of being a member of that class.

3.3 Retrieval of Land Surface Parameters

Normalized Difference Vegetation Index (NDVI) for vegetation and forested areas was proposed by (Tucker 1979). It takes reflectance values for near-infrared and red band in consideration. For water bodies surface retrieval, Normalized Difference Water Index (NDWI) was proposed by (McFeeters 1996) which uses spectral reflectance of near infrared and green bands. Normalised Difference Built-Up Index (NDBI) for retrieval of settlements and concrete structures was proposed by (Zha et al. 2003) which uses short-wave infrared and near infrared bands. For bare and fallow land retrieval, Normalised Bare Land Index (NBLI) was proposed by (Li et.al., 2017a) which uses reflectance values of thermal infrared and red bands. The spectral indices used in the study are summarized in Table 2.

Table 2. Indices derived using remote sensing for each major class

Surface Feature type	Index	Description	Formula	Reference
Vegetation	NDVI	Normalised Difference Vegetation Index	NIR-Red/NIR + Red	(Tucker 1979)
Water bodies	NDWI	Normalised Difference Water Index	Green-NIR/Green + NIR	(McFeeters 1996)
Built-Up	NDBI	Normalised Difference Built-Up Index	SWIR1-NIR/SWIR1+NIR	(Zha et al. 2003)
Bare/Fallow Land	NBLI	Normalised Bare Land Index	Red-TIR/Red + TIR	(Li et.al., 2017a)

4. Results and Discussion

The spatial-temporal assessment of LST, LULC and various spectral indices conducted for the study area are discussed below.

4.1 Spatial-Temporal Analysis of LST

Land surface temperature of Chandigarh city was derived using mono-window algorithm as shown in Figure (3). The statistical parameters including minimum and maximum temperatures, mean and standard deviation are summarized in Table (3). The mean temperature of the city varies between 34-36 °C in the month of May. There has been a slight rise in the minimum and maximum temperatures from 2016 to 2022.

The built -up has risen by almost 8% from 2016 to 2022 (Table 3) which can be accounted for the increase in the ranges of temperature. Though the vegetation area has increased by almost 8%, but the mean temperature of the area has been increased by almost 2.5 °C.

The highest temperature can be observed in the outskirts of the city where the concentration of bare and open land is highest. Sukhna lake and Dhanas lake shows least temperature (around 25- 27 °C). The Patiali Roa reserved forest and the Sukhna lake reserved forest shows less temperature compared to surrounding areas.

4.2 Spatial-Temporal Analysis of LULC

Multitemporal LULC mapping was done using MLC classifier as shown in Figure (4) and the results are summarized in Figure (5). Built-up and vegetation class have shown an increase of 7.56% and 8.19% respectively from 2016 to 2022. The forest cover has reduced by almost 32% and bare land has seen an overall decrease of about 16% as more urbanisation has covered the bare land. The net water content doesn't show much variation over the years. The increase in vegetation cover can be accounted by plantation activities. The outskirt of the city has seen major urban densification in the last few years due to urban sprawl.

The analysis shows that there is a high positive correlation (0.9886) between built up class and LST, which suggests that increased urbanisation strongly affect the land surface temperature.

Table 3. Multi-temporal LST changes and statistical summary for Chandigarh

Time Period	Minimum Temperature °C	Maximum Temperature °C	Mean °C	Standard Deviation
May 2016	25.74	40.48	34.21	1.641
May 2017	24.98	39.64	34.06	1.42
May 2018	25.11	40.96	35.22	1.22
May 2019	25.25	40.76	35.56	1.54
May 2020	25.84	41.56	35.88	1.915
May 2021	26.19	41.24	36.41	1.56
May 2022	27.04	41.60	36.94	1.641

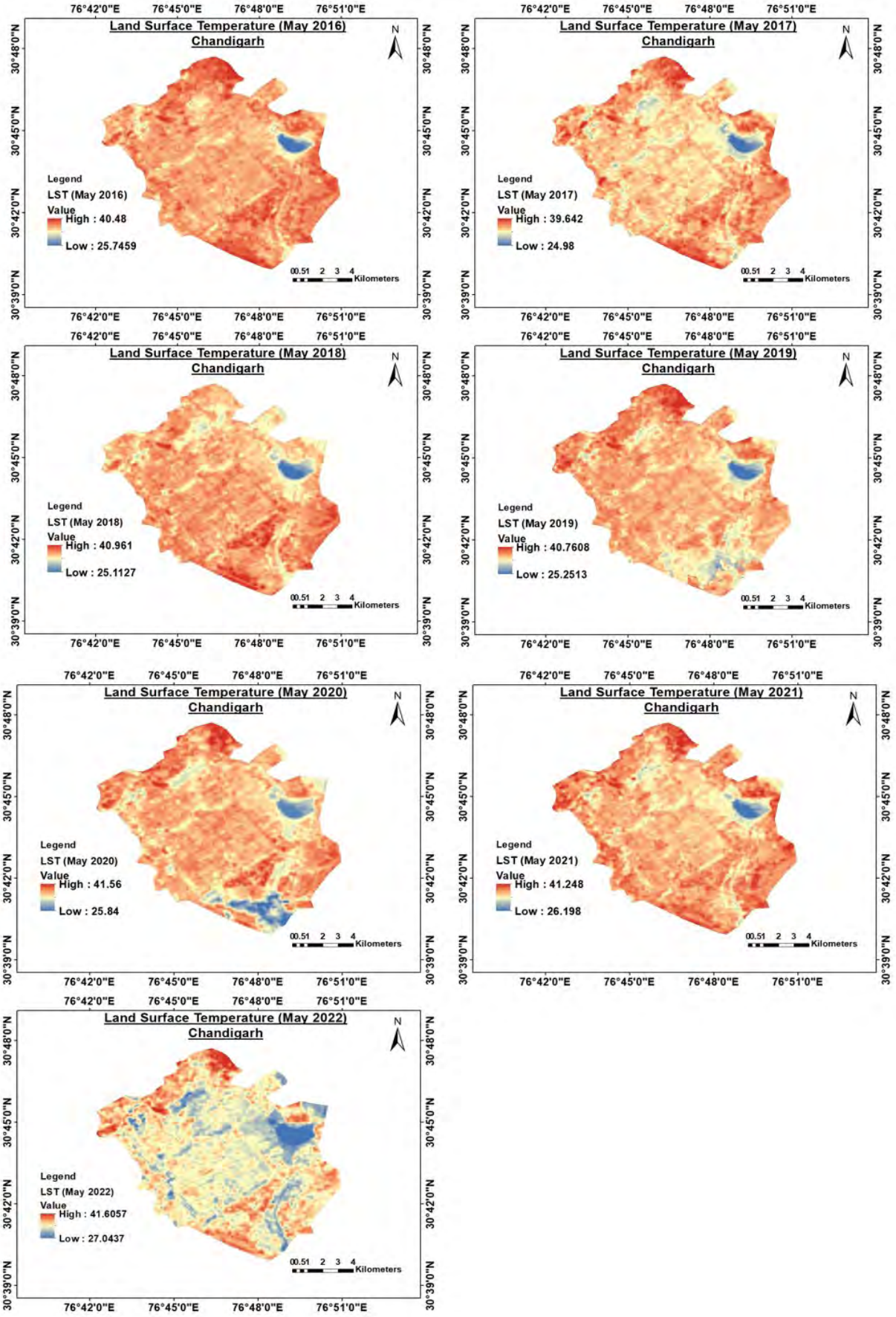

Figure 3. Land-surface temperature estimation using mono-window method for May 2016, May 2017, May 2018, May 2019, May 2020, May 2021 and May 2022

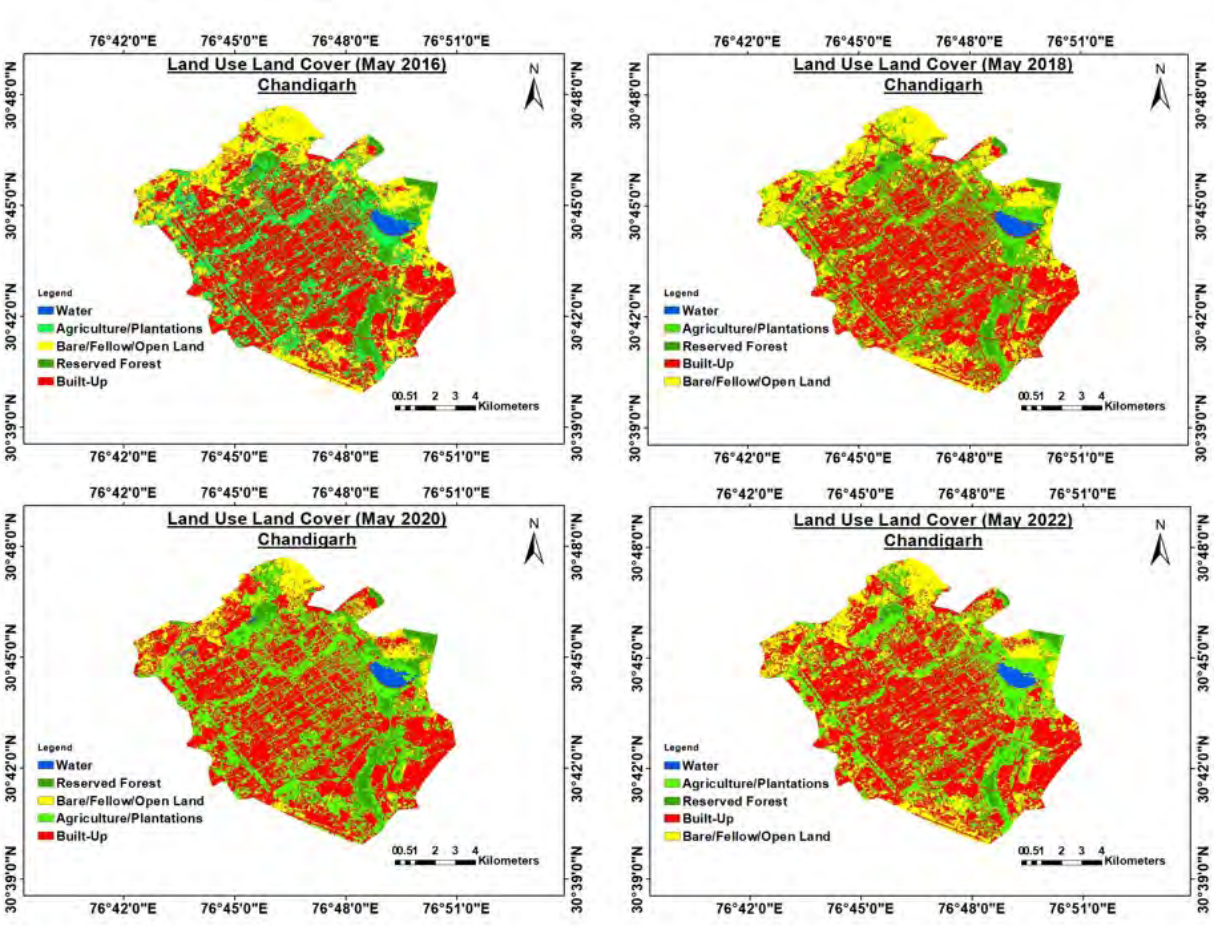

Figure 4. LULC changes for Chandigarh over May 2016, May 2018, May 2020 and May 2022.

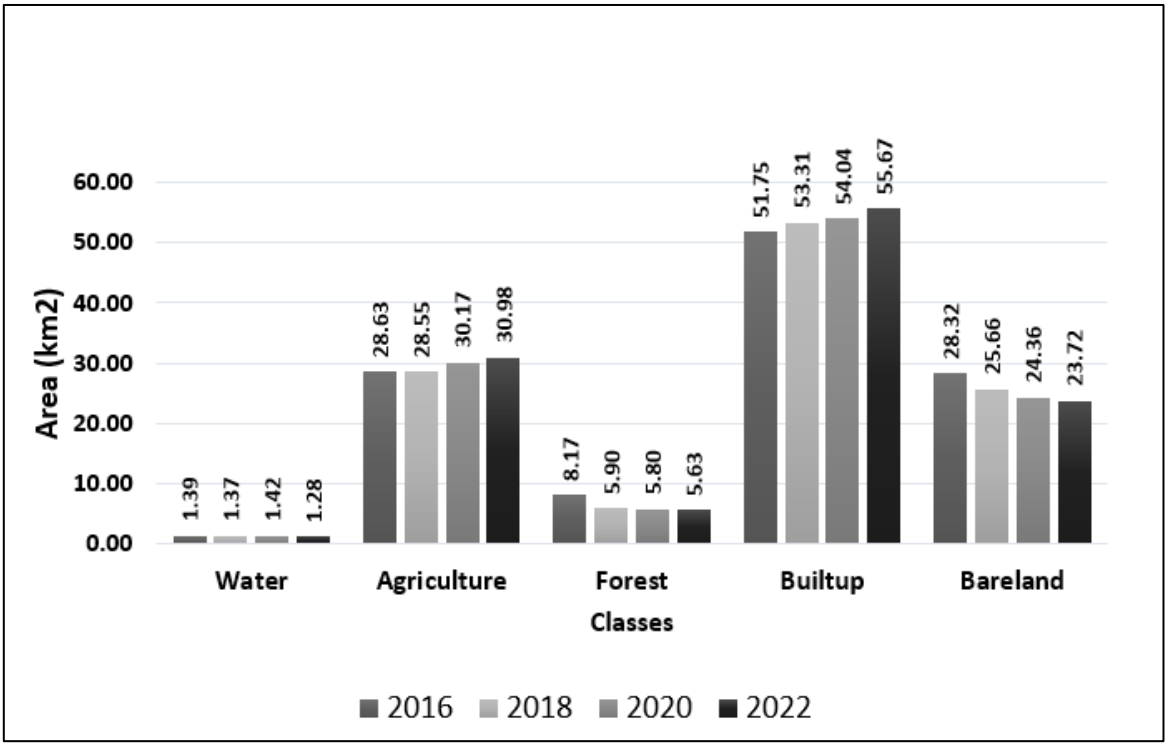

Figure 5. Statistical Analysis of changes in each class of LULC

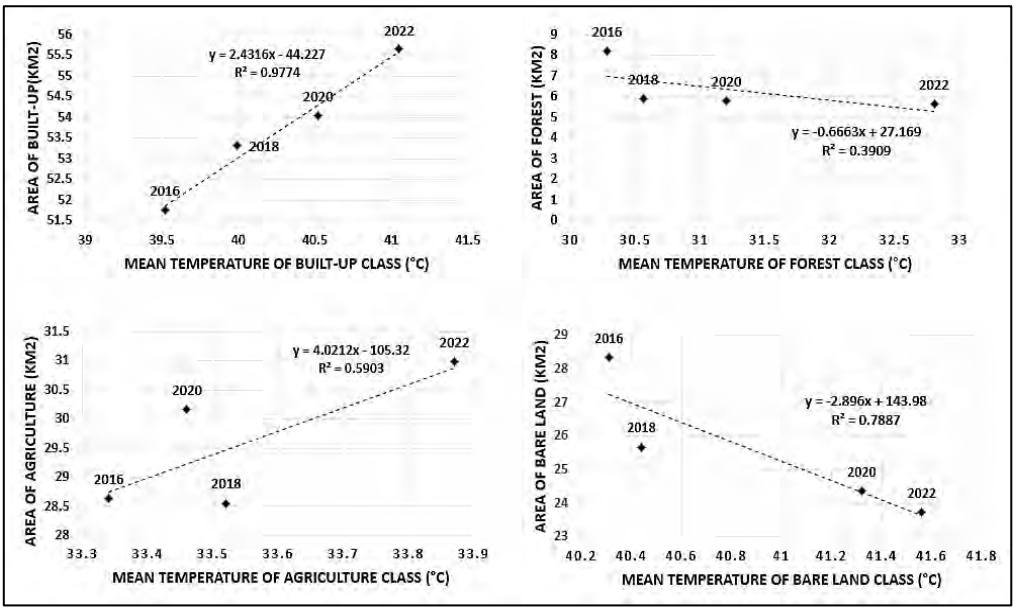

Figure 6. Relation between changes in LULC and LST

Table 4. User Accuracy (UA) and Producer Accuracy (PA) for LULC classification using MLC

Class	UA	PA	UA	PA	UA	PA	UA	PA
	2016		2018		2020		2022	
Water	100%	100%	100%	100%	100%	100%	100%	83.33%
Agriculture/Plantation	82.35%	75%	73.68%	82.35%	82.6%	76%	87.5%	77.77%
Reserved Forest	90%	81.81%	100%	76.925	90%	66.25%	100%	83.33%
Built-Up	87.09%	90%	97.5%	90.32%	78.57%	100%	82.14%	88.46%
Bare Land	81.25%	100%	86.66%	86.67%	80%	100%	79.23%	100%

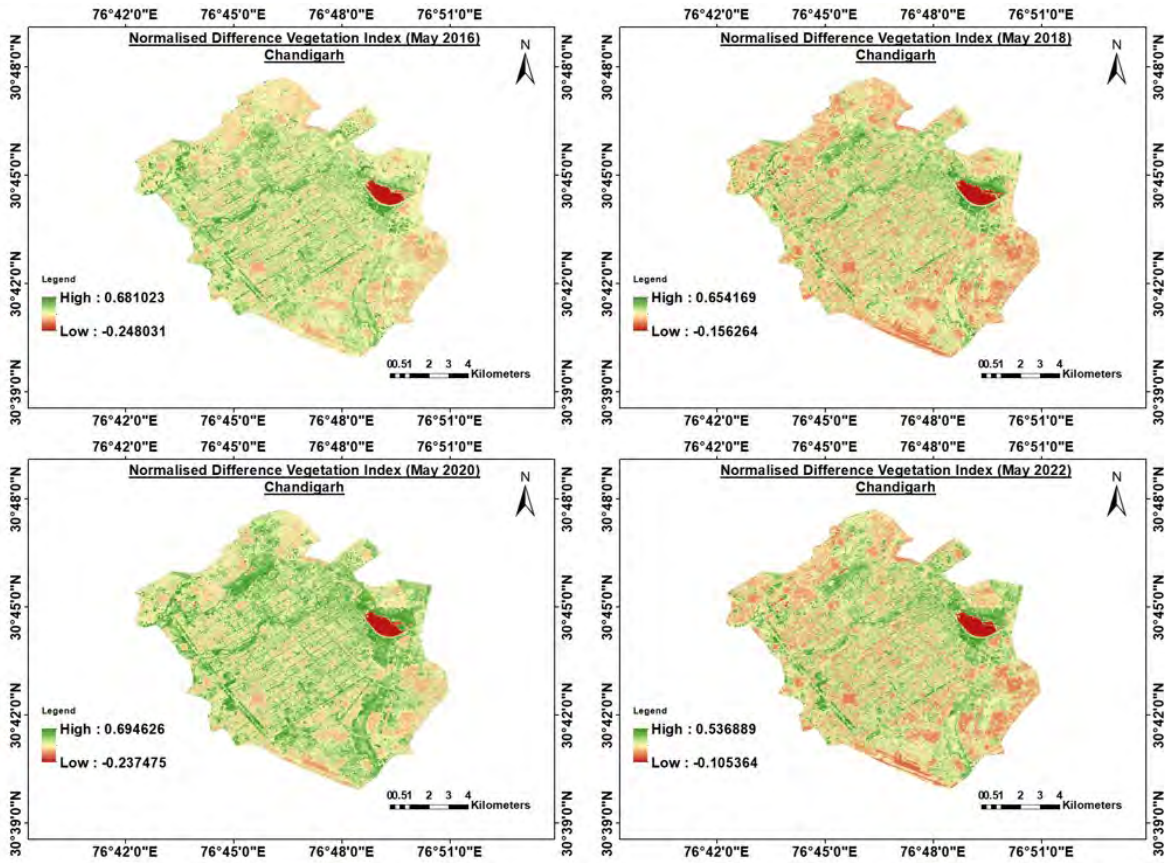

Figure 7. NDVI extraction for May 2016, May 2018, May 2020 and May 2022

Table 5. Overall Accuracy and Kappa coefficient for LULC classification

Year	Overall Accuracy	Kappa coefficient
2016	86.71%	0.795
2018	88.2%	0.82
2020	84.95%	0.78
2022	86.9%	0.799

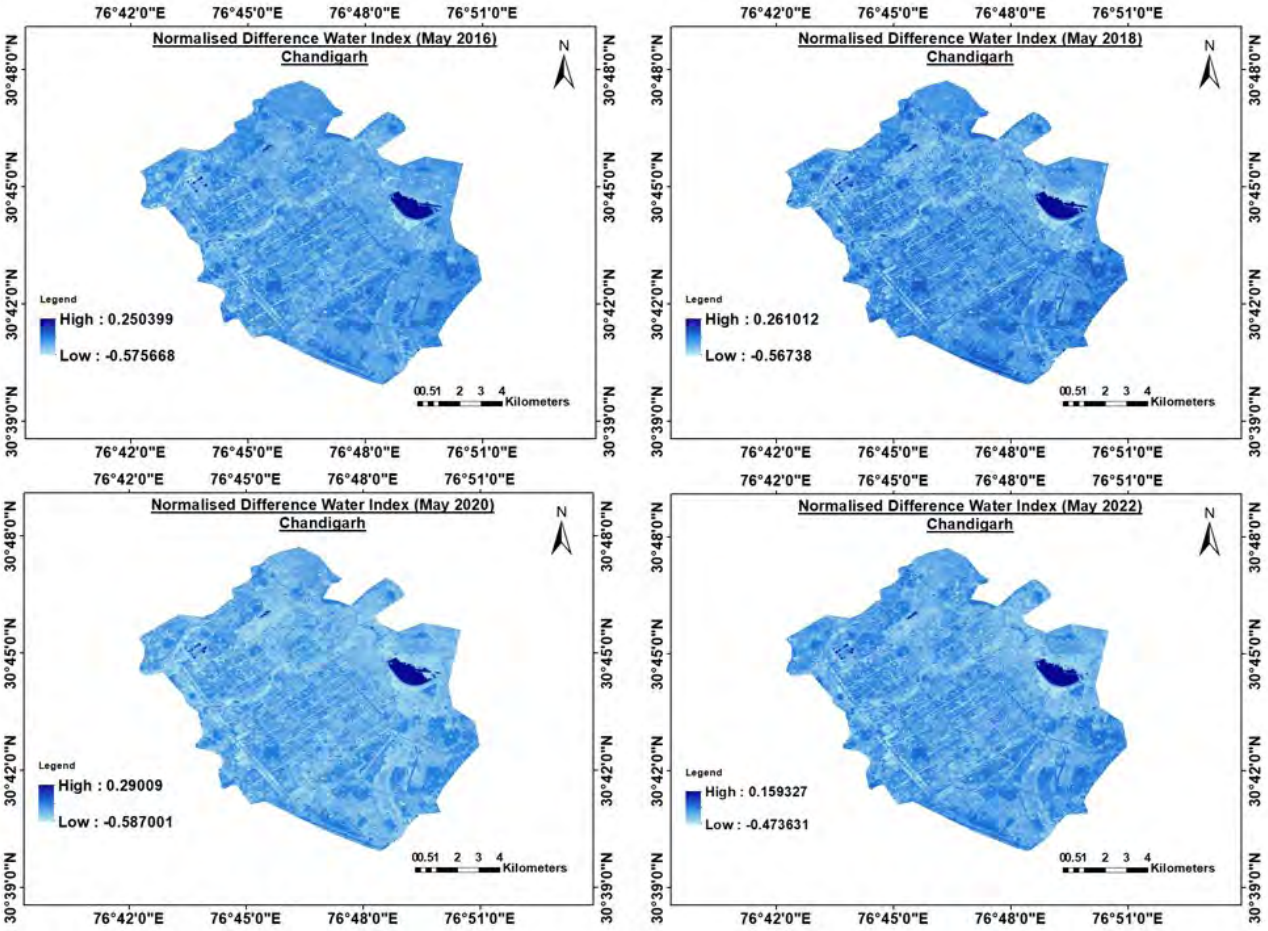

Figure 8. NDWI extraction for May 2016, May 2018, May 2020 and May 2022.

4.3 Accuracy Assessment

Error matrix or confusion matrix was computed to derive accuracy for the above classification. Stratified random sampling approach was used to select sample for each class. Highest overall accuracy of 88.20% was observed for the year 2018 with kappa coefficient of 0.82. The lowest accuracy for the year 2020 could be accounted for the misclassification of pixel points between vegetation and reserved forest class. The accuracy assessment has been summarised in Table (4) and Table (5).

4.4 Spatial-Temporal Analysis of Spectral Indices

Indices for four major classes, that is, NDVI for vegetation, NDWI for open water, NDBI for built-up and NBLI for bare lands have been considered and regression analysis along with correlation has been carried out. As can be observed from figure (7), NDVI is high (>0.3) for agricultural and forested areas. NDVI is a significant factor to consider with respect to LST as NDVI is directly employed for determination of LST. Correspondingly, LST in low in these areas.

The yearly variation of NDWI for the month of May is shown in Figure (8). NDWI is highest for Sukhna lake and Dhanas lake (>0.25) and LST for these regions is lowest. The yearly variation of NDBI for the month of May is shown in Figure (9). Highest NDBI can be observed for the central city and outskirts of the city (>0.5). Figure (10) shows yearly variations for the month of May for Chandigarh. Significant NBLI s observed in outskirts of the city.

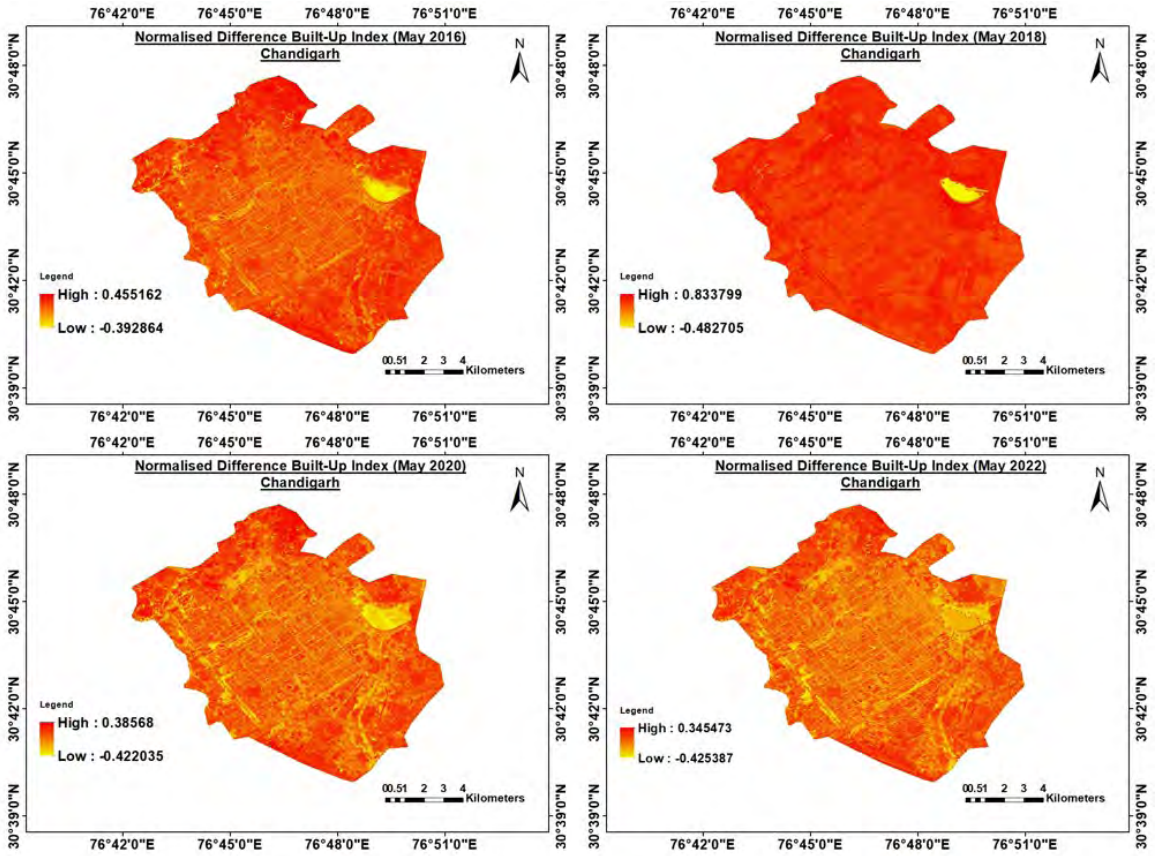

Figure 9. NDBI extraction for May 2016, May 2018, May 2020 and May 2022

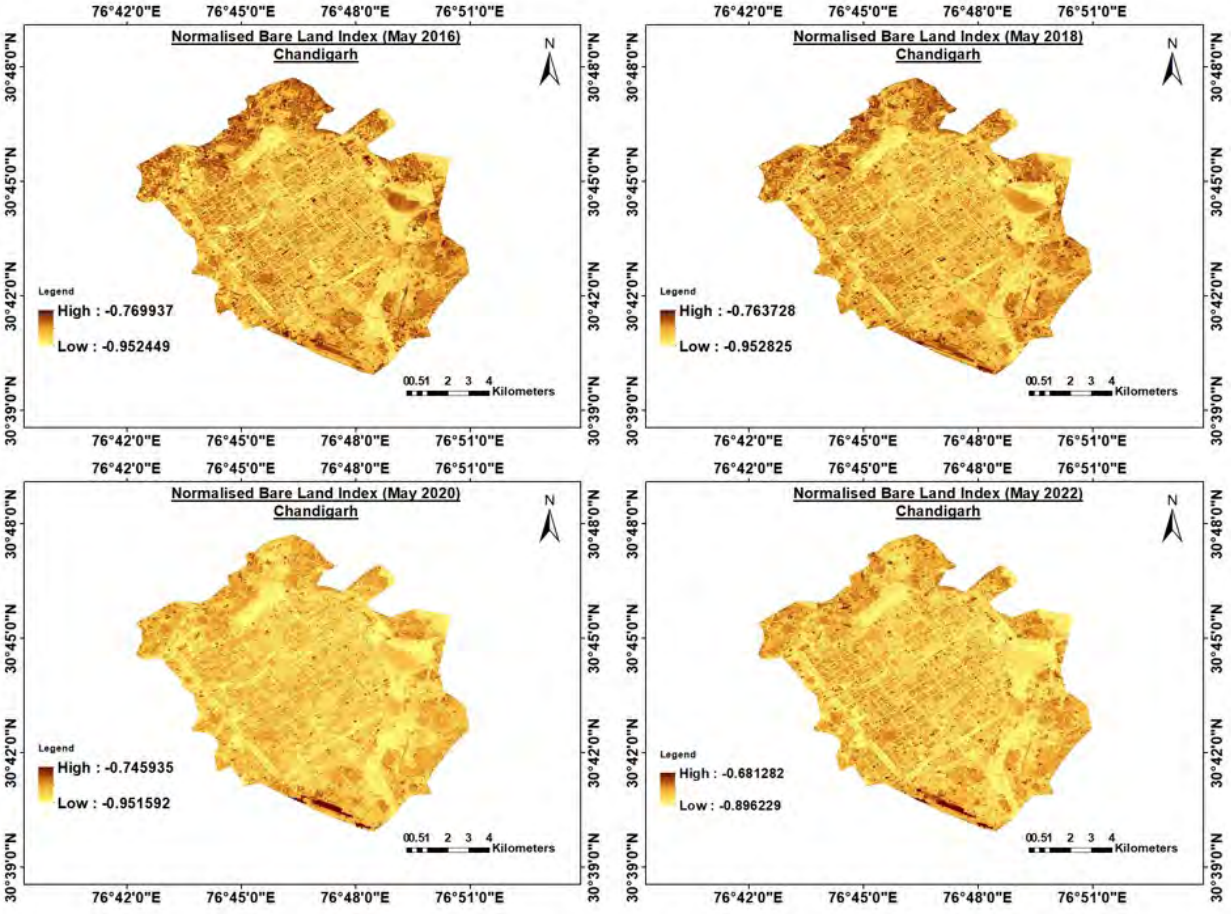

Figure 10. NBLI extraction for May 2016, May 2018, May 2020 and May 2022

4.5 Pearson's Correlation

A correlation analysis to establish relationship between surface temperature and spectral indices done and the results are summarised in Table (6). The Pearson correlation coefficient (r) measures the strength and direction of the linear relationship between two variables. A positive value of r (r>0) indicates an increasing trend between the two variables, whereas a negative value of r (r<0) indicates that when one variable is increasing, the other is decreasing. If r=0, it indicates little to no correlation between the variables. Indices for four major classes, that is, NDVI for vegetation, NDWI for open water, NDBI for built-up and NBLI for bare lands have been considered and regression analysis along with correlation has been carried out. A total of 2048 sample points each for NDVI, NDWI, NDBI and NBLI were utilised to establish the correlation with LST.As can be observed from figure (11), NDVI is high (>0.3) for agricultural and forested areas. NDVI is a significant factor to consider with respect to LST as NDVI is directly employed for determination of LST. Correspondingly, LST in low in these areas. This establishes the fact that there is a negative correlation between NDVI and LST. LST and NDVI shows a significantly negative correlation for May 2016 (-0.25), May 2018 (-0.29), May 2020 (-0.31) and May 2022 (- 0.352). In May 2022, there is a stronger negative relationship between NDVI and LST compared to all the previous years. This indicates that areas with more vegetation have a significant cooling effect on land surface temperatures during this period. Higher vegetation levels are associated with lower land surface temperatures. A weak negative correlation between NDVI and LST can be accounted for the dry month of May as the dry months tend to reduce the strength of regression (Guha and Govil 2021).

Table 6. Correlation between LST and spectral indices

LST	NDVI	NDWI	NDBI	NBLI
May 2016	-0.25	-0.015	0.44	0.324
May 2018	-0.29	0.212	0.51	0.348
May 2020	-0.31	0.159	0.53	0.421
May 2022	-0.352	0.110	0.59	0.477

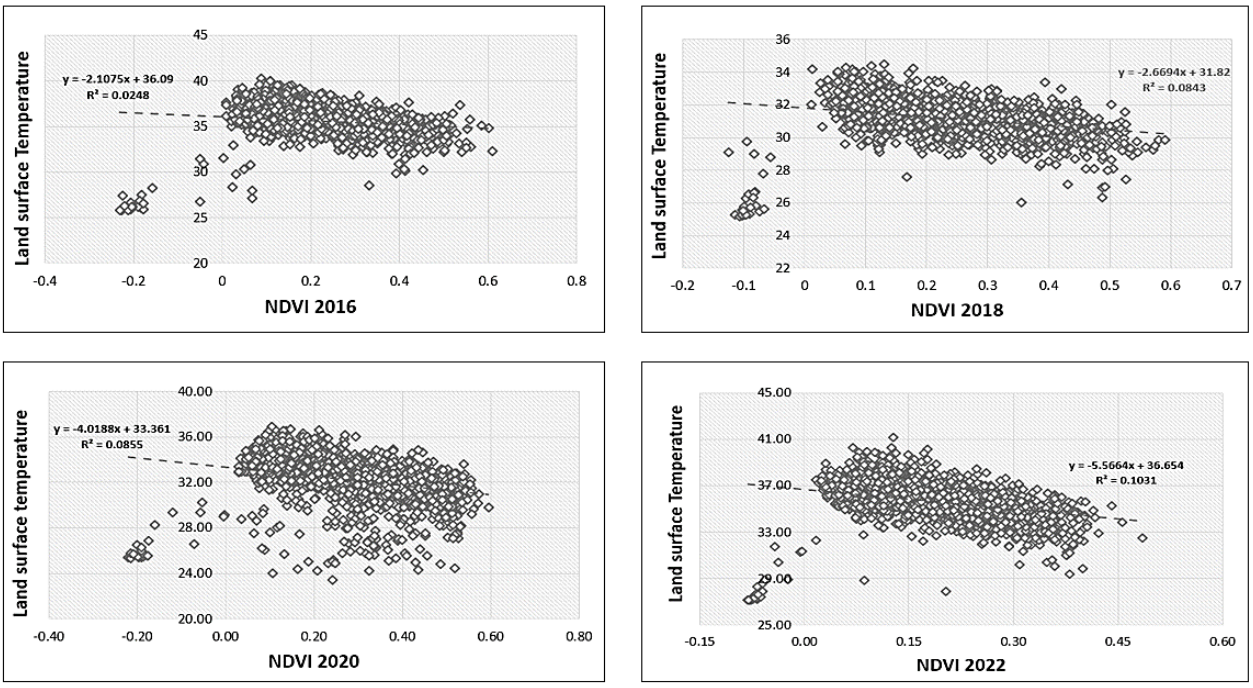

Figure 11. Correlation between NDVI and LST

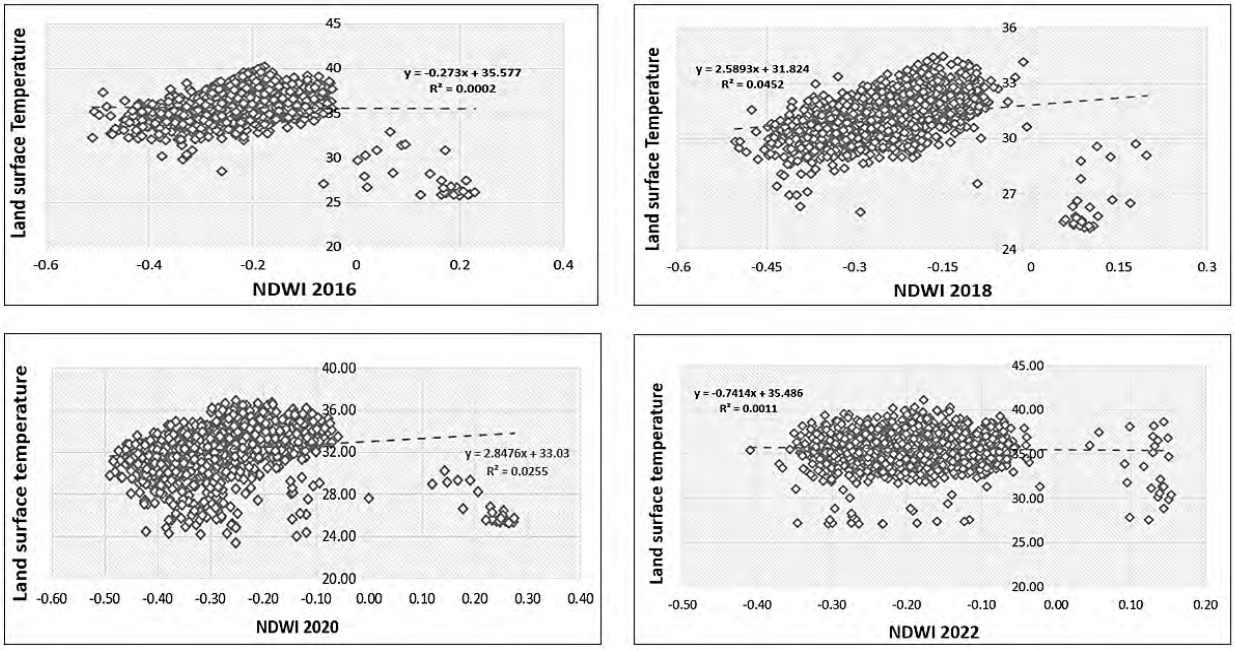

Figure 12. Correlation between NDWI and LST

Figure (12) shows correlation of LST and NDWI. The best LST-NDWI correlation can be observed for May 2018 (0.212), followed by May 2020 (0.159), May 2022 (0.11) and May 2016 (-0.015). From the analysis, it can be established that LST and NDWI build an insignificant correlation and can be considered as neutral.

Figure (13) shows correlation of LST and NDBI. The best LST-NDBI correlation can be observed for May 2022 (0.59), followed by May 2020 (0.53), May 2018 (0.51) and May 2016 (0.44). From the analysis, it can be established that LST and NDBI has a strong positive correlation and are highly correlated to each other. The correlation coefficients consistently indicate a positive correlation between NDBI (built-up areas) and LST across all the time periods. This suggests that urbanization and built-up areas have a substantial impact on increasing land surface temperatures during this period. The strength of this positive relationship varies but becomes notably stronger in more recent years for Chandigarh. This corresponds to building materials like asphalt and concrete which have low albedo and contribute to higher temperatures. One disadvantage of NDBI is that the tonal differences between built-up and bare land is unclear as one is not able to distinguish between bare land and built-up in the outskirts of the city. For this, another index called NBLI is considered.

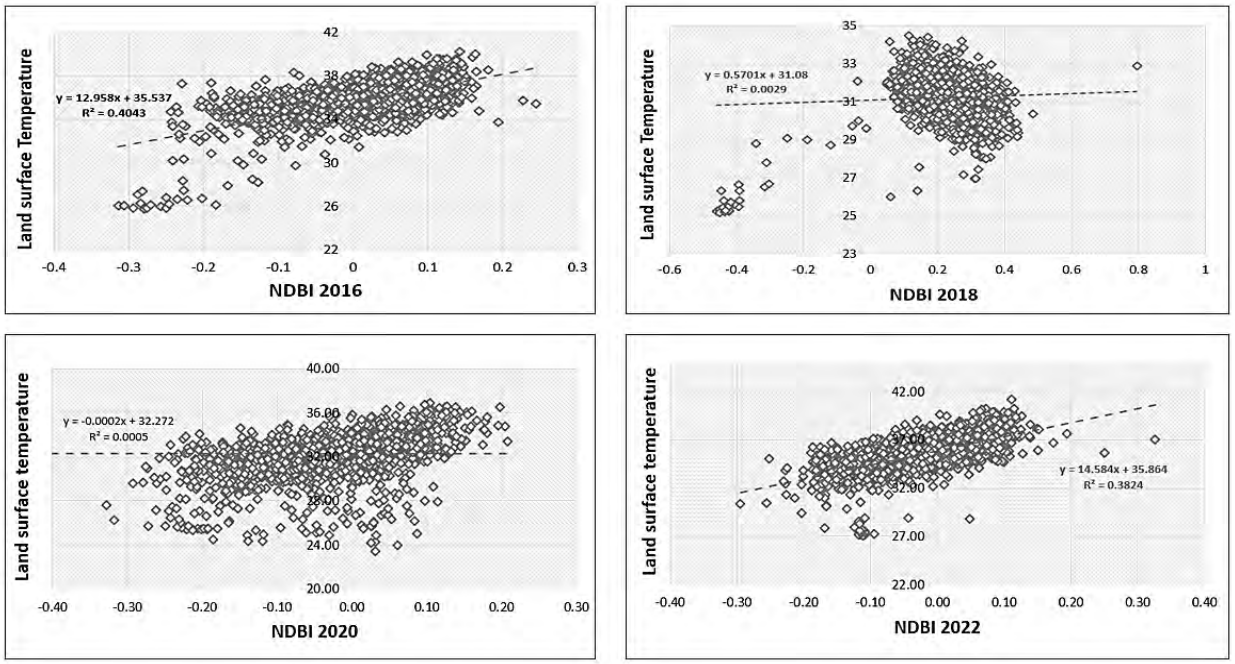

Figure 13. Correlation between NDBI and LST

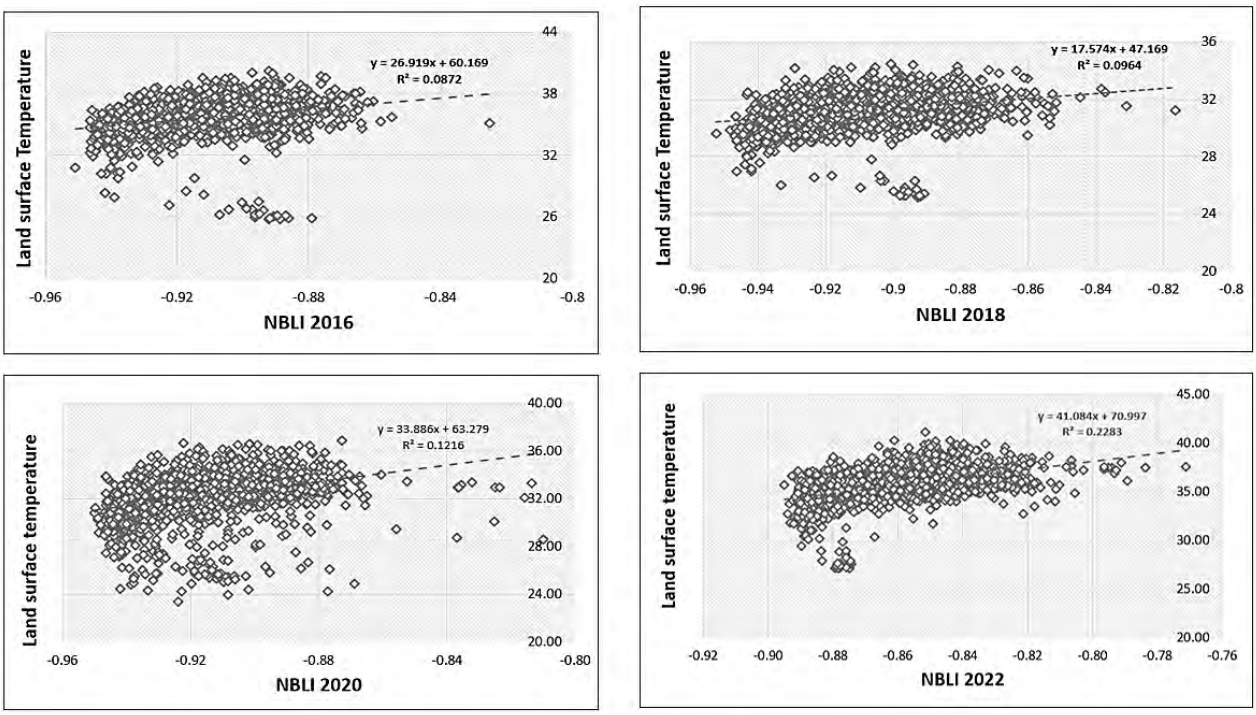

Figure 14. Correlation between NBLI and LST

The relation between LST and NBLI is shown in Figure (14). The best LST-NBLII correlation can be observed for May 2022 (0.477), followed by May 2020 (0.421), May 2018 (0.348) and May 2016 (0.324). The correlation coefficients consistently indicate a positive correlation between NBLI (bare lands) and LST across all the time periods. This suggests that areas with a high proportion of bare land experience a substantial increase in land surface temperatures during this period. The moisture present in the soil also plays a significant role in influencing the local temperature. Due to low moisture content of soil in the dry month of May, it is likely that sand absorbs more heat thus increasing the local surface temperature. The strength of this positive relationship varies but becomes notably stronger in more recent years, especially in 2022. This underscores the significant impact of bare land and the absence of vegetation on local land surface temperatures in Chandigarh during the study period.

The results obtained using correlation analysis indicate that in urban areas with high building density (as indicated by NDBI) and limited vegetation (low NDVI), there tends to be a positive correlation between LST and indices like NDBI and NBLI. Urban areas typically have higher temperatures due to the absorption and retention of heat by buildings and pavement, leading to increased LST, a phenomenon commonly referred to as Urban Heat Island Effect.

5. Conclusion

In this study, a comprehensive statistical analysis was conducted to examine the intricate relationship between Land Surface Temperature (LST) and Land-Use Land Cover (LULC) patterns within the urban context of Chandigarh city. LST was derived from Landsat-8 thermal and optical data using the mono-window method. Notably, our findings revealed a discernible increasing trend in LST, particularly within the categories of built-up and bare land, over the period spanning from 2016 to 2022. The mean LST exhibited a notable increment of approximately 2.5°C during this time frame. The utilization of Sentinel-2 Level 2A data was instrumental in enabling comprehensive analysis and investigation for LULC analysis. LULC classification was performed utilizing the Maximum Likelihood Classifier (MLC), which indicated an expansion of the built-up area within the city from 2016 to 2022, accompanied by a reduction in forest cover and bare land. Conversely, the water bodies and plantations remained relatively stable in terms of their spatial extent. A strong positive correlation can be seen between increase in built-up and LST, whereas a negative correlation can be seen for decreased forest cover and LST. Spectral indices have been derived using Sentinel 2 optical data. Analysis has been done to correlate LST with different spectral indices like NDVI, NDWI, NBLI and NDBI. A moderate negative correlation was discerned between LST and NDVI, underscoring the cooling effect of vegetation on local land surface temperatures. Conversely, the correlation between NDWI and LST was found to be insignificant for the Chandigarh region. Notably, NDBI exhibited a robust positive correlation with LST, further substantiating the heightened land surface temperatures in areas with increased urbanization and built-up structures. Additionally, a moderately positive correlation was observed between LST and NBLI, affirming the influence of bare land on elevating land surface temperatures. Furthermore, it was observed that the presence of water bodies, as indicated by NDWI, consistently led to negative correlations, underlining the cooling influence of water bodies in mitigating LST. These findings are influenced by a multitude of factors including the local climate, geographic characteristics, and topographical attributes. Urban canyons, characteristic of a city like Chandigarh, may experience positive correlations owing to heat-

trapping phenomena. While correlations provide valuable insights into relationships between variables, they do not indicate a direct cause-and-effect relationship. Consequently, these findings hold substantial utility in guiding informed environmental planning and policymaking for urban areas. Chandigarh, as a meticulously planned city, has shown a notable surge in plantation efforts in recent years. Transforming barren lands into eco-parks or wetlands represents a constructive avenue for urban planners and policymakers to mitigate the Urban Heat Island (UHI) effect and contribute positively to climate change mitigation efforts.

References

Alexander, Paul J., and Gerald Mills. 2014. "Local Climate Classification and Dublin's Urban Heat Island." Atmosphere 5(4):755–74. doi: 10.3390/atmos5040755.

Awuh, M. E., M. C. Officha, A. O. Okolie, and I. C. Enete. 2018. "Land-Use/Land-Cover Dynamics in Calabar Metropolis Using a Combined Approach of Remote Sensing and GIS." Journal of Geographic Information System 10(04):398–414. doi: 10.4236/jgis.2018.104021.

Awuh, M. E., P. O. Japhets, M. C. Officha, A. O. Okolie, and I. C. Enete. 2019. "A Correlation Analysis of the Relationship between Land Use and Land Cover/Land Surface Temperature in Abuja Municipal, FCT, Nigeria." Journal of Geographic Information System 11(01):44– 55. doi: 10.4236/jgis.2019.111004.

Chang, Chi Ru, Ming Huang Li, and Shyh Dean Chang. 2007. "A Preliminary Study on the Local Cool-Island Intensity of Taipei City Parks." Landscape and Urban Planning 80(4):386–95. doi: 10.1016/j.landurbplan.2006.09.005.

Faridatul, Mst Ilme, and Bo Wu. 2018. "Automatic Classification of Major Urban Land Covers Based on Novel Spectral Indices." ISPRS International Journal of Geo-Information 7(12). doi: 10.3390/ijgi7120453.

Guha, Subhanil, and Himanshu Govil. 2020. "Land Surface Temperature and Normalized Difference Vegetation Index Relationship: A Seasonal Study on a Tropical City." SN Applied Sciences 2(10). doi: 10.1007/s42452-020-03458-8.

Guha, Subhanil, and Himanshu Govil. 2021. "A Long-Term Monthly Analytical Study on the Relationship of LST with Normalized Difference Spectral Indices." European Journal of Remote Sensing 54(1):487–511. doi: 10.1080/22797254.2021.1965496.

Gupta, Kshama, Pushplata Garg, and Tanya Rajwal. 2017. Investigating the Relationship of Urban Form and Function with Surface Temperature Patterns: A Case Study of Chandigarh.

Gupta, Neha, Aneesh Mathew, and Sumit Khandelwal. 2019. "Analysis of Cooling Effect of Water Bodies on Land Surface Temperature in Nearby Region: A Case Study of Ahmedabad and Chandigarh Cities in India." Egyptian Journal of Remote Sensing and Space Science 22(1):81–93. doi: 10.1016/j.ejrs.2018.03.007.

He, Chunyang, Peijun Shi, Dingyong Xie, and Yuanyuan Zhao. 2010. "Improving the Normalized Difference Built-up Index to Map Urban Built-up Areas Using a Semiautomatic Segmentation Approach." Remote Sensing Letters 1(4):213–21. doi: 10.1080/01431161.2010.481681.

Jiang, Yitong, Peng Fu, and Qihao Weng. 2015. "Assessing the Impacts of Urbanization- Associated Land Use/Cover Change on Land Surface Temperature and Surface Moisture: A Case Study in the Midwestern United States." Remote Sensing 7(4):4880–98. doi: 10.3390/rs70404880.

Li, Erzhu, Peijun Du, Alim Samat, Junshi Xia, and Meiqin Che. 2015. "An Automatic Approach for Urban Land-Cover Classification from Landsat-8 OLI Data." International Journal of Remote Sensing 36(24):5983–6007. doi: 10.1080/01431161.2015.1109726.

Li, Hui, Cuizhen Wang, Cheng Zhong, Aijun Su, Chengren Xiong, Jinge Wang, and Junqi Liu.2017a. "Mapping Urban Bare Land Automatically from Landsat Imagery with a Simple Index." Remote Sensing 9(3). doi: 10.3390/rs9030249.

Li, Hui, Cuizhen Wang, Cheng Zhong, Zhi Zhang, and Qingbin Liu. 2017b. "Mapping Typical Urban LULC from Landsat Imagery without Training Samples or Self-Defined Parameters." Remote Sensing 9(7). doi: 10.3390/rs9070700.

McFeeters, S. K. 1996. "The Use of the Normalized Difference Water Index (NDWI) in the Delineation of Open Water Features." International Journal of Remote Sensing 17(7):1425– 32. doi: 10.1080/01431169608948714.

Nimish, G., M. C. Chandan, and H. A. Bharath. 2018. "Understanding Current and Future Landuse Dynamics with Land Surface Temperature Alterations: A Case Study of Chandigarh." Pp. 79–86 in ISPRS Annals of the Photogrammetry, Remote Sensing and Spatial Information Sciences. Vol. 4. Copernicus GmbH.

Norovsuren, B., B. Tseveen, V. Batomunkuev, T. Renchin, E. Natsagdorj, A. Yangiv, and Z. Mart. 2019. "Land Cover Classification Using Maximum Likelihood Method (2000 and 2019) at Khandgait Valley in Mongolia." in IOP Conference Series: Earth and Environmental Science. Vol. 381. IOP Publishing Ltd.

Qin, Zhihao & Karnieli, Arnon & Berliner, Pedro. 2010. "A Mono-Window Algorithm for Retrieving Land Surface Temperature from Landsat TM data and its Application to the Israel-Egypt Border Region." International Journal of

Remote Sensing. 22. 3719-3746. 10.1080/01431160010006971.

Pandey, Bhartendu, and P. K. Joshi. 2015. "Numerical Modelling Spatial Patterns of Urban Growth in Chandigarh and Surrounding Region (India) Using Multi-Agent Systems." Modeling Earth Systems and Environment 1(3). doi: 10.1007/s40808-015-0005-6.

Saini, Varinder, and Reet Kamal Tiwari. 2019. Remote Sensing Based Time-Series Analysis for Monitoring Urban Sprawl: A Case Study of Chandigarh Capital Region Study of Glacier Dynamics Using Advanced Remote Sensing Techniques View Project Remote Sensing for Agroinformatics View Project Remote Sensing Based Time-Series Analysis for Monitoring Urban Sprawl: A Case Study of Chandigarh Capital Region. Vol. 13.

Shivakumar, B. R., and S. v. Rajashekararadhya. 2018. "Investigation on Land Cover Mapping Capability of Maximum Likelihood Classifier: A Case Study on North Canara, India." Pp. 579–86 in Procedia Computer Science. Vol. 143. Elsevier B.V.

Tucker, Compton J. 1979. Red and Photographic Infrared Linear Combinations for Monitoring Vegetation. Vol. 8.

Zha, Y., J. Gao, and S. Ni. 2003. "Use of Normalized Difference Built-up Index in Automatically Mapping Urban Areas from TM Imagery." International Journal of Remote Sensing 24(3):583–94. doi: 10.1080/01431160304987

Journal of Geomatics Vol. 17, No. 2, October 2023

Identification of Urban Centre and Rural Growth Centres Around Guwahati and Its Surrounding Rural Region Using Hierarchical Settlements, Nested Hexagons, Remote Sensing and GIS

Jeni Bhattacharjee[1,*], Swapna Acharjee[2] and Sudisht Mishra[1]
[1]NERIST, Itanagar Arunachal Pradesh, 791109
[2]State Remote Sensing Application Centre (DST), Itanagar Arunachal Pradesh,
*E-mail: jenibhattacharjee@gmail.com

(Received: 10 April 2023; in final form 16 May 2023)

DOI: *https://doi.org/10.58825/jog.2023.17.2.67*

Abstract: Guwahati city is the highest order urban center of Assam and is an important gateway to the north eastern region of India. In this study, a 50km buffer from the master plan boundary of Guwahati Metropolitan Development Authority (GMDA) is selected for identifying potential urban centers and rural growth centers (URGC) of different order for decentralized planning and inter and intra-administrative cooperation around the city using multi-parametric criteria. This includes central place theory, nested hexagon method and thematic information on groundwater potential zones, land use/land cover, flood prone and landslide susceptible zones. Out of the 32 identified potential villages, 15 are proposed for new urban centers and 17 are proposed for development as rural growth centers. 9 towns are also proposed for up-gradation to higher order for proper spatio-functional interaction. However, several suggestions and preventive measures were made before initiating developmental expansion which needs to be considered. The findings of this study would be useful for decentralized planning to minimize the economic imbalances, rural migration and sustainable development of the region.

Keywords: GMDA, GIS, Hierarchical settlements, Nested hexagons, Remote sensing, URGC

1. Introduction

Urbanization in India is characterized by demographic changes like natural population growth and rural urban migration which stimulates growth (Taubenbock & Esch 2011). Over the years, unplanned urbanization and expansion of cities have burdened the poor and marginalized, bio-diversity and economy with stresses and strains (NITI Ayog 2021). Urban settlements in India have experienced rapid growth and population has increased from 14 percent at the time of independence to 31.8 per cent as per 2011 census of India (MoHUA 2020). These urban growths with increasing population in cities, towns and their suburbs have two dimensions. When it grows upwards, we mean increase in density and when it grows outwards it means area expansion. As the city expands outwards, a portion of the rural population is automatically transformed into urban one, but when the city grows upwards its demographic changes are profound (Richardson 1971; Ganguly 1995). Rural areas lack access to economic activities and basic amenities as compared to urban areas which has higher pull factors. Thus, migration from rural to urban areas are stimulated by the forceful 'push-pull factors' in rural settlements arising out of improper distribution of government schemes, inefficient monitoring of development activities, lack of infrastructures on agriculture, health, training & education facilities which restricts their capabilities and hence their services and products are marginally paid. Therefore, to minimize the rift between rural and urban sector, rural areas need to be integrated with urban centers. This integration between rural and urban sectors will lead to regional as well as sustainable development (Mishra & Deodhar 2009). The urbanization process has contributed to the mixture of land uses between rural and urban areas. Such co-existence has helped rural areas to increase their income by generating various opportunity. Similarly, urban sector was also benefitted through local ecosystem and food security. The integration between rural villages and towns will generate employment and markets facility for both farm and non-farm sector. This linkage will help in building the interdependency between urban-rural field in planning and resource management sector (Kim 2015). As per census 2011, urban population in India has an average decadal growth rate of 31.6 percent from 2001-2011. The small and medium towns (class II to VI) have also shown a growth rate of 48.6 percent to 185.7 percent. It is also estimated that by 2051 urban population will increase by 50 percent (MoHUA 2020). North East India is the country's gateway to south east Asian countries and covering 8 percent of India's land and 3.1 percent of India population. Today Guwahati is not only the principal city of Assam but also provide access to six-sister states in Northeast India (KPMG FICCI 2015). Although the urbanization level in North-east India is low but the rate of urbanization is high (Ray et al, 1999). It was therefore expected that small and medium sized towns would emerge. Besides, in the hilly areas, topography warrants that the small and medium sized towns rather than large cities would be the vehicle of urbanization. Growth of urban centers in the entire north eastern region is slow which is mainly due to its rural economy and poor level of industrialization. However, these small towns play a greater role in socio-economic development of the region and securing a better quality of life. The linkage between smaller towns and their rural hinterland provides connections between human, financial and marketing sector. Therefore, before initiating any developmental work for these small and medium towns, proper regional planning framework for the surrounding rural areas along with economic development and infrastructure planning must be incorporated (Sahasranaman 2012). Further, over

the years due to increasing needs and demands for water has caused water stress condition and exploitation. This situation calls for a proper cost-effective evaluation and planning for groundwater resources. Ground water is an important resource for any developmental initiatives which supports health, economic development and ecological diversity (Waikar & Nilawar 2014). Groundwater resources are an important and dependable source of water supply in both urban and rural areas.

The Guwahati city might see an increase in population to about 2.1 million by 2051. Hence to accommodate such growing population, Guwahati Metropolitan Development Authority (GMDA) is reviewing their existing master plan 2025 for possible expansion of present boundary (Hemani & Das 2015). As the city expands due to challenges in civic infrastructures and service delivery capabilities, small and medium towns/urban centers all around start to grow and develop because they act as an interface between agriculture and urban market and their position in rural urban linkages and economic development. Small and medium towns have predominantly rural economic base and most of the workforce are engaged in agriculture. Agriculture is space consuming and labor intensive and requires storage facilities, distribution depot, fertilizers, processing plants, and marketing needs. It is to be noted that small towns appear in a hierarchy because there are different grades of demands from the villages and each having a different threshold of population and ranges of goods. Such a hierarchy should be properly developed without gaps so that every area and everyone gets equal opportunities. Therefore, stress should be given to the small towns/urban centers because they are closer to rural people and will have a greater impact on the lower strata of the society (Ray et al, 1999). Further to achieve national growth along with human development, there is an urgent need to transform the rural landscape of India, bringing them at par with their urban counterparts in terms of amenities and opportunities, while preserving the soul of the village. Further, unplanned urban expansion, economic development and population growth contribute to natural hazards, especially floods, landslides etc. In the state of Assam, one of the most frequent and devastating disaster is flood which causes economic damages, social damages and loss of life and properties. Guwahati city suffers mostly from urban flooding which has become very costly and difficult to manage especially because of high concentration of people and property. Flood has long-term direct and indirect consequences such as loss of educational opportunities, diseases, and reduced nutrition apart from mobility and transportation hazards which impedes the achievement of developmental goals. Similarly, during monsoons, landslides also contribute to various challenges to the people and infrastructure. The present study assumes significance to identify urban centers and rural growth centers as cluster of venues which are geographically close to each other and serve multiple functions to full fill the diverse demand of residents both rural and urban. This study aims to use GIS and remote sensing together with nested hexagon structure and central place theory to identify urban and rural growth center using hierarchical settlement to achieve proper balance between urban and rural areas. Central place theory was developed by Christaller, (1933) and Losch, (1944) to describe the spatial pattern of urbanization and hierarchy of urban center. Their focus was mainly on organizing a city and its surrounding rural areas through geometric and hexagonal model called as nested hexagon. They also stated that the areas falling at the center of nested hexagon will be the main hinterland for its surrounding areas. Combining them with Guttman scalogram scale will help in grouping the settlements into different level of hierarchy of development. The Guttman scalogram can be used to rank the settlement on the basis of function located within them (Rondinelli 1980).

1.1 Study Area

Guwahati city is located in the northeastern part of India surrounded by the hills on the east, west and south and the river Brahmaputra on the north and supports a population of 9, 68, 549 in 2011 (TERI 2013) with a decadal growth of 18.29 percent. The study area was selected by taking a 50km buffer from GMDA master plan boundary comprising a total area of 13013.6km^2 that includes 328km^2 (without Brahmaputra River) GMDA area for identification of urban center and rural growth centers for potential inter- and intra- administrative cooperation in the region. The study area consists of ten districts of Assam namely Kamrup Rural (partial), Kamrup Metro (full), Nalbari (full), Morigaon (partial), Darrang (partial), Barpeta (partial), Goalpara (partial), Baksa (partial), Udalguri (partial) and West Karbi Anglong (partial) besides two districts of Meghalaya state namely Ri Bhoi (partial) and West Khasi Hills (partial) districts for decentralized planning. Figure 1 shows the demarcated study area over Landsat 8 OLI imagery and figure 2 and figure 3 shows population variation and decadal growth of the districts within the study area.

2. Database and Software

In this study GMDA boundary was obtained from the office of GMDA. For identification of the hierarchical order of settlements, urban centers and rural growth centers, villages having population of 5000 & above were selected in the state of Assam, and villages having population of 1000 & above were selected in the state of Meghalaya since in the hilly regions, it is difficult to get villages having population of 5000 and above. Further census villages and municipal town data were also collected from census of India (https://censusindia.gov.in.). Apart from the above, villages with less population but representing Block development office and primary health centers in the state of Assam were also considered so as to cover entire study area and proposed for decentralized planning. ArcGIS 10.3 and QGIS 3.24 software were used for the creation of base map, digitization of vector layers and creation of thematic maps. Population data of villages and towns and their amenities were obtained from census of India village and town directory. From the total sample of 10760 villages in the study area, 154 villages were identified and selected apart from 55 towns from census data which were falling within the 50km buffer region.

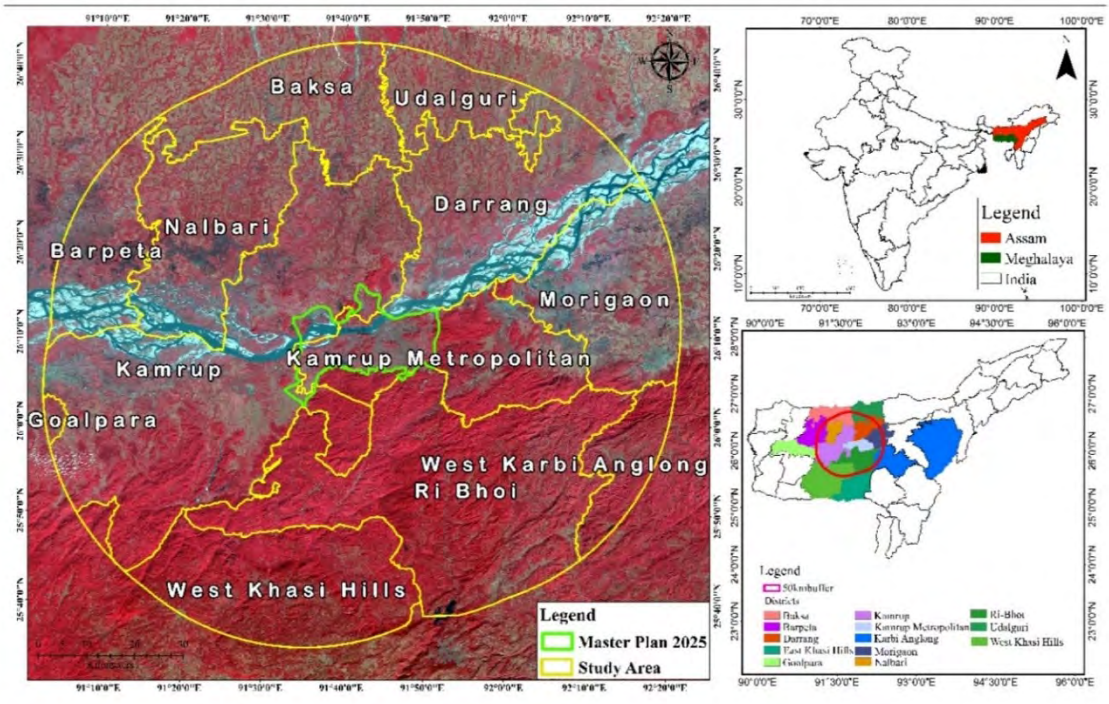

Figure 1. Study Area over Landsat 8 imagery

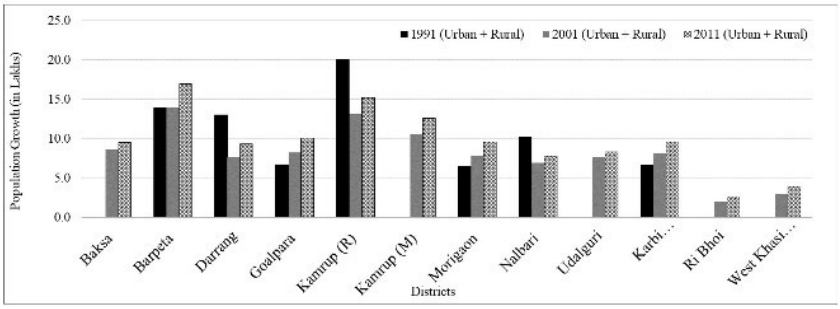

Figure 2. Populations Variation of districts year wise

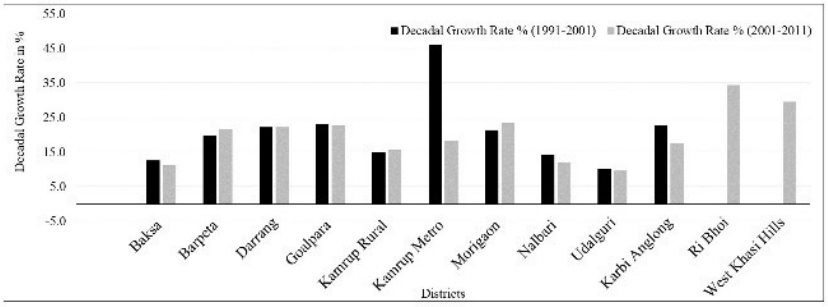

Figure 3. Decadal growth rates of districts

The geographical location of the villages and towns and administrative centers were obtained from Gram manchitra (https://panchayatonline.gov.in), Bhuvan panchayat (https://bhuvan-panchayat3.nrsc.gov.in) and ASDMA GIS portal (http://sdmassam.nic.in). Landsat 5 TM satellite imageries from U.S. Geological Survey (USGS) Earth explorer (https://earthexplorer.usgs.gov) were extracted for mapping land use land cover. The information on ground water potential zones, thematic layer was collected from North Eastern District Resource Plan (NEDRP) of North Eastern Space Application Centre (NESAC), Umiam, Meghalaya and information on flood prone areas was obtained from Bhuvan web portal. Further, the landslide susceptibility map of the study area was also obtained from global landslide susceptibility map from NASA for this study and analysis.

3. Methodology

The methodology to identify the potential centers in the study area involves following steps:

3.1 Creation of Base Map

The base map is generated in 1:50k scale in GIS software. Road network, railway line and water bodies like river and streams were digitized from Landsat 8 OLI satellite

imagery and google earth and later were verified and updated from north eastern district resource plan (NEDRP) portal.

3.2 Identification of Hierarchical Settlements

3.2.1 Determination of Centrality score and weightage of villages

Centrality score measures the importance of a settlement based on its socio-economic facilities and services irrespective of its hierarchy and location (Mishra & Deodhar 2009). In order to calculate the centrality scores, weightage of all the facilities at the villages were calculated first. Thereafter, it was multiplied with the number of times the facility available in the villages. Then the values were added up to calculate the centrality score of that particular village. The weightage calculated using Equation 1 (Rondinelli 1980; Mishra & Deodhar 2009; Rahman & Noor 2005).

$$W_f = \frac{N}{F_f} \quad (1)$$

Here N is the total number of villages, F_f is the total number of villages having that facility and W_f is the weightage of the particular facility. The Centrality Score can be obtained using Equation 2, (Rondinelli 1980; Mishra & Deodhar 2009; Rahman & Noor 2005)

$$\mathrm{CS} = \sum N_f \times W_f \quad (2)$$

Here CS is the centrality Score of the village, N_f is the number of a particular facility in the village.

The facilities and functions considered for calculation of centrality score for settlements are pre-primary school, primary school, middle school, secondary and senior-secondary school, degree college, government vocational /ITI centers, community health centers, primary health center, primary health sub-center, hospital, dispensary, family welfare center, anganwadi centers, ASHA, veterinary hospital, public bus service, railway station, post office, post & telegraph office, telephone (landlines), banking service ,self-help group, domestic, agriculture, commercial, all users for power supply.

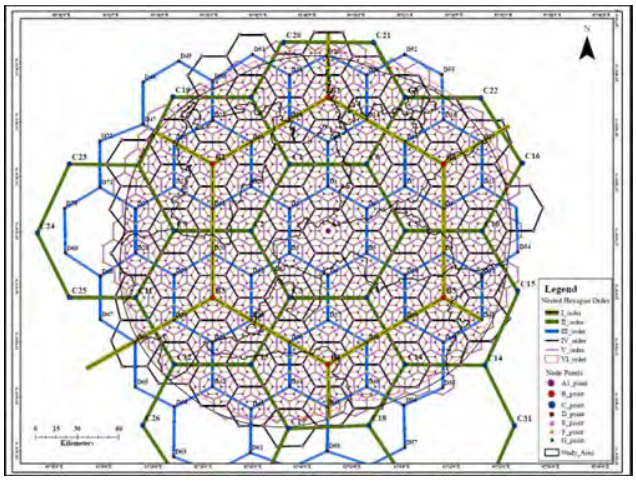

Figure 4. Nested Hexagon model with Guwahati as centre (A1)

3.2.2 Nested Hexagon

Figure 4 shows the nested hexagon covering the entire study and keeping Guwahati at its centre.

3.2.3 Identification of Potential Urban centres and Rural growth Centres:

The potential centers will be selected based on following criteria:

i) Population of the proposed urban center settlements must be 5000 and above.
ii) Rural growth centers to be proposed based on nested hexagon model even if it has population less than 5000.
iii) If two or more villages are at a close distance with each other, then on the basis of its centrality score suitable settlements will be selected.
iv) If settlements are already near to any existing urban center at a distance of 5km, then that settlement will not be proposed for urban centers.
v) Proximity of the settlements to road network.
vi) Potential ground water zones of the area.
vii) Flood prone and landslide susceptible zones within the study area.

4. Results and Discussion

4.1 Creation of Base Map

The primary approach for any analysis requires generation of base map. The base map of the entire study area was generated at a scale of 1:50k and contains information on geographical location of towns and villages and administrative units falling within the study area (Figure 5).

4.2 Hierarchy of the Village and Town Settlements over Nested Hexagon

The identified village settlements were overlaid on nested hexagonal structure to propose decentralized hierarchical settlement of different orders. But for town settlements, hierarchical order is given as per census class. The Figure 6 shows the existing settlements in the study area overlaid on nested hexagon. Altogether 209 settlements were identified including village settlements and existing towns for the proposal of hierarchical settlement. Out of these 209 settlements, 55 villages are having population more than 5000 and 99 villages having population less than 5000 and remaining 55 are already existing towns. The settlements falling outside the study area were not considered for this proposal.

The existing 55 towns are ordered as per their existing census order and shown in Figure 6. As per the census class, Guwahati is the only settlement that falls in the first order or class I category. No second order town settlement falls within the study area as per census 2011. Table 1 represents the number of town settlements and their respective census class. As per the nested hexagon pattern, out of 154 identified villages, none of the villages are falling in the first order of hierarchical order. Table 2 represents the existing order of the village settlements as per nested hexagon

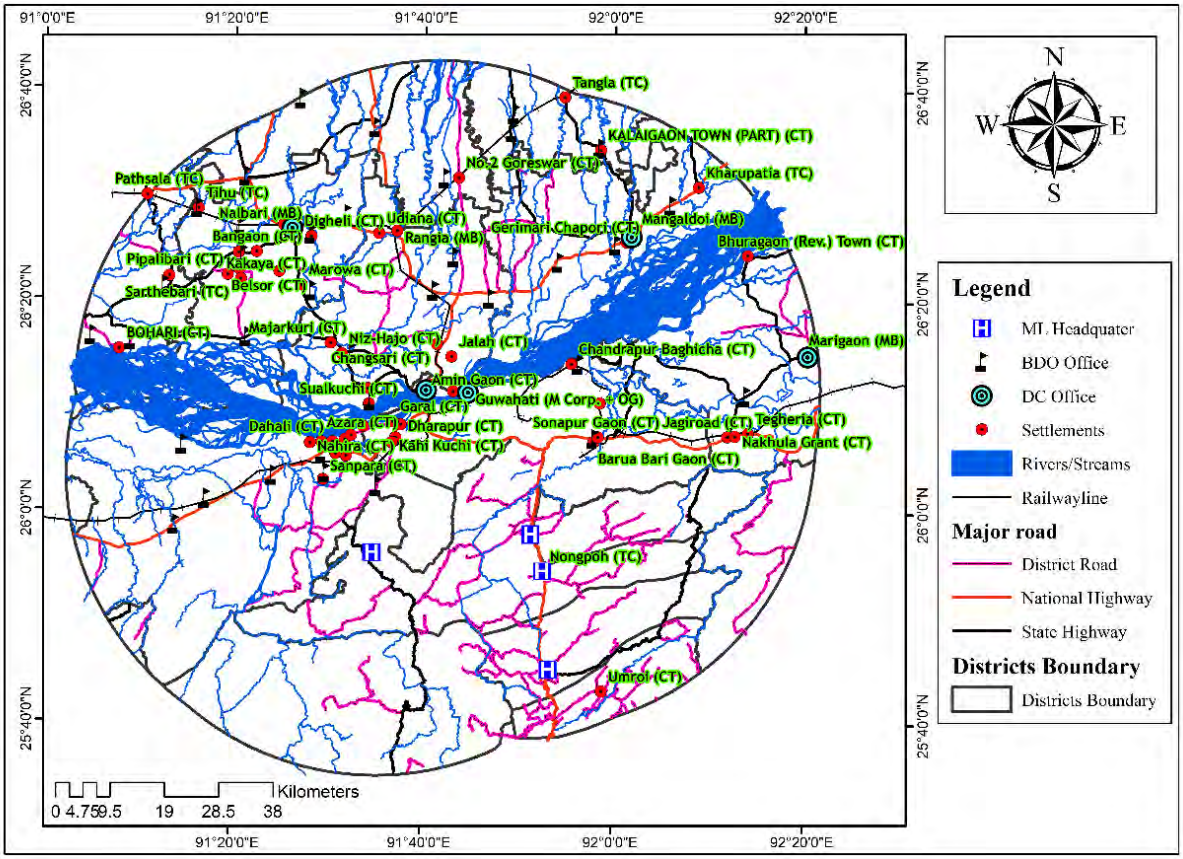

Figure 5. Base map of Study area

.Table 1. Existing Hierarchical order of Town settlement

No of Settlements	Census Order/Class
1	I Class
4	III Class
10	IV Class
28	V Class
12	VI Class

Table 2. Existing Hierarchical order of village settlement

No. of settlements	**Hierarchical order**
2	II order
7	III order
28	IV order
45	V order
72	VI order

Table 3 Population Size of settlement

Sl. No	Population size	Number of Settlements
1.	Less than 1300	45
2.	1300-2300	37
3.	2300-4000	16
4.	4000-11000	53
5.	More than 11000	3

Table 4 Centrality score of Village settlements

Centrality score	**No of Village settlements**
4-13	31
14-21	48
22-31	29
32-47	23
48-78	18
79-151	5

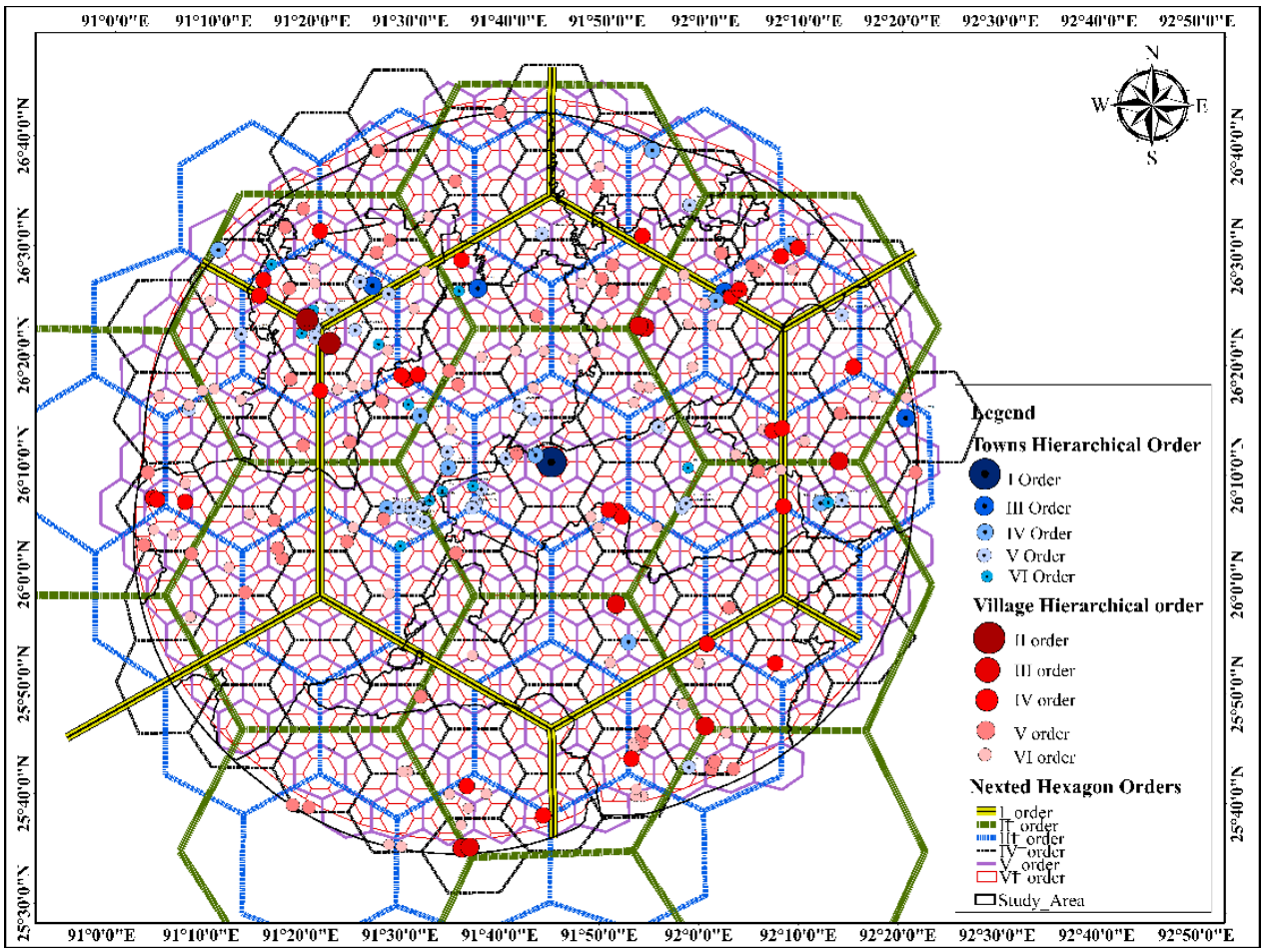

Figure 6. Existing Village and towns over nested hexagon

4.3 Identification of Potential Centres

To identify potential centers, some criterion has been selected which are illustrated below

4.3.1 Population

As per Urban and regional development plan formulation and implementation (URDPFI) guidelines 2015, Government of India, places having population **Table 3** *Population Size of settlement* of 5000 to 20000 are classified as small towns under the sub category of small town I and population ranging from 20000-50000 are classified under sub category small town II. However, any urban centers even if has less than 5,000 population may be given a statutory status and be called as a statutory town. Accordingly, 97 settlements were identified in the study area of which 55 are having population of more than 5000 in the ten districts of Assam and 42 settlements with population more than 1000 but less than 5000 in the two districts of Meghalaya state. For decentralized planning, another 57 settlements were identified which are having block development office and primary health centres having population less than 5000 (Figure 7). The settlements falling outside the buffer region are not included in this study.

4.3.2 Centrality Score

The result (Table 4) shows the centrality score of the settlements ranging from lowest to the highest and the calculation is based on amenities and functions. This reflects settlements with high centrality score have more functional capacity to serve the needs and demands of the surrounding regions. The centrality score of the 55 towns have also been calculated purely based on amenities and functions. The result indicates that out of all the 55 towns, only 1 town i.e., Guwahati (M Corp. + OG) with highest centrality score. After Guwahati, 7 towns are having second highest centrality score ranging from 37-51. Thereafter, 11 towns having centrality score ranging from 26-36. Similarly, centrality score of 12 towns is ranging from 18-25, 16 towns are having centrality score between 13-17 and 8 towns are having score ranging from 7-12.

4.3.3 Distance of selected villages from existing urban centres/towns

Under this criterion, a buffer ring of 5km was generated from existing towns in GIS software for analysis. The villages which are not close to existing towns or any urban centres are selected for further analysis.

4.3.4 Road connectivity

Road connectivity is another very important criterion for the selection of potential urban centres and rural growth centres which is carried out and shown below. Road connectivity helped us to identify the centres having proper communication network with neighbouring rural as well as urban areas.

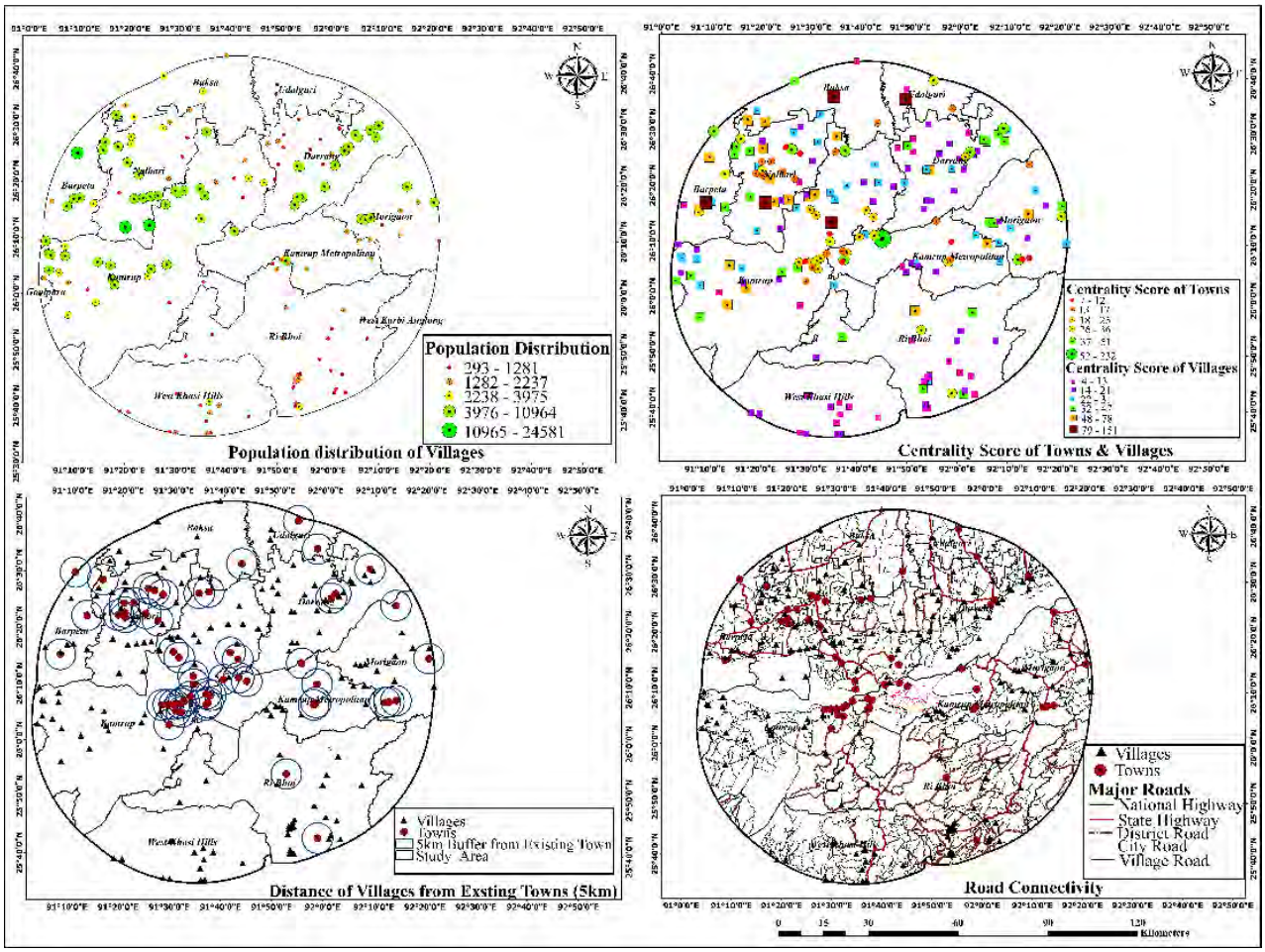

Figure 7. Criteria Map

Figure 7 shows the criteria map such as population distribution of villages, centrality score of towns and villages, distance of villages from existing towns and road connectivity to identify potential centers for decentralized planning and development within the study area.

4.4 Suitability Assessment of Identified Urban Centres, Rural Growth Centres and Towns using Multiple Parameters

After analyzing various multiple parameters, 34 village settlements and 10 existing towns were selected for suitability assessment. These were then overlaid over multiple thematic layers (Figure 8) such as land use land cover, ground water potential zones, flood prone zones and landslide susceptible zones. Land use land cover of 2011 was generated using Landsat 5 imagery and various classes were digitized following NRSC Land use/Land cover mapping guidelines and categorized into agriculture land, built-up, forest, grassland/grazing land, tree clad, shifting cultivation, wasteland, water bodies and wetland.

Land use land cover map shows an upsurge in developed areas within the Guwahati metropolitan region which is expanding towards the eastern, western and northern areas. Guwahati metropolitan region is already congested and densely built; hence it is essential and felt necessary to identify more urban centers and rural growth centers to reduce the pressure on Guwahati city. The ground water prospect (GWP) map was downloaded in raster format from open source NEDRP except West Khasi hills district in Meghalaya falling in the study area due to its non-availability. The GWP maps were categorized into excellent, good, moderate, nil, poor, very good, high and low prospect areas. Further, in absence of village boundary, a hexagonal bin of 5km was generated and 34 villages as identified were overlaid on this hexagonal bin and then on land use/land cover, flood hazard zones (BHUVAN, NRSC), landslide susceptible zones (Stanley and Kirschbaum 2017) and Ground water prospect zones (NEDRP) (Figure 10) for suitability assessment. The landslide susceptible map of the study area shows the villages falling within slight, moderate or severe zones. The flood prone zones (Figure 11) were used for analyzing and ascertaining whether the identified centers are falling into the different categories namely (Figure 8) very low, low, moderate, high, very-high, and no data zones in the study area. The table 5 and table 6 below showing suitability of selected 34 settlements of different orders for the proposed new urban centers and rural growth centers based on the selected parameters.

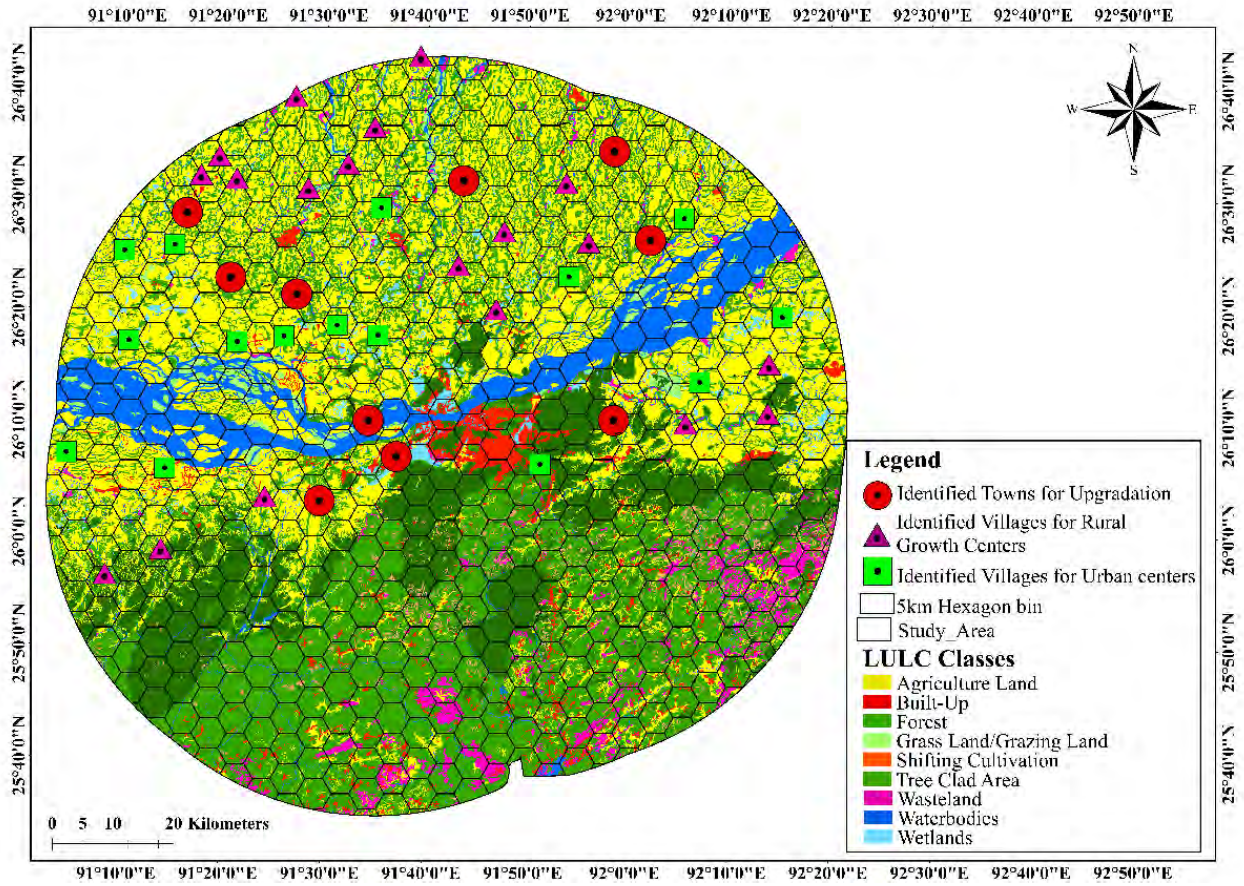

Figure 8. Identified Villages and Towns over LULC

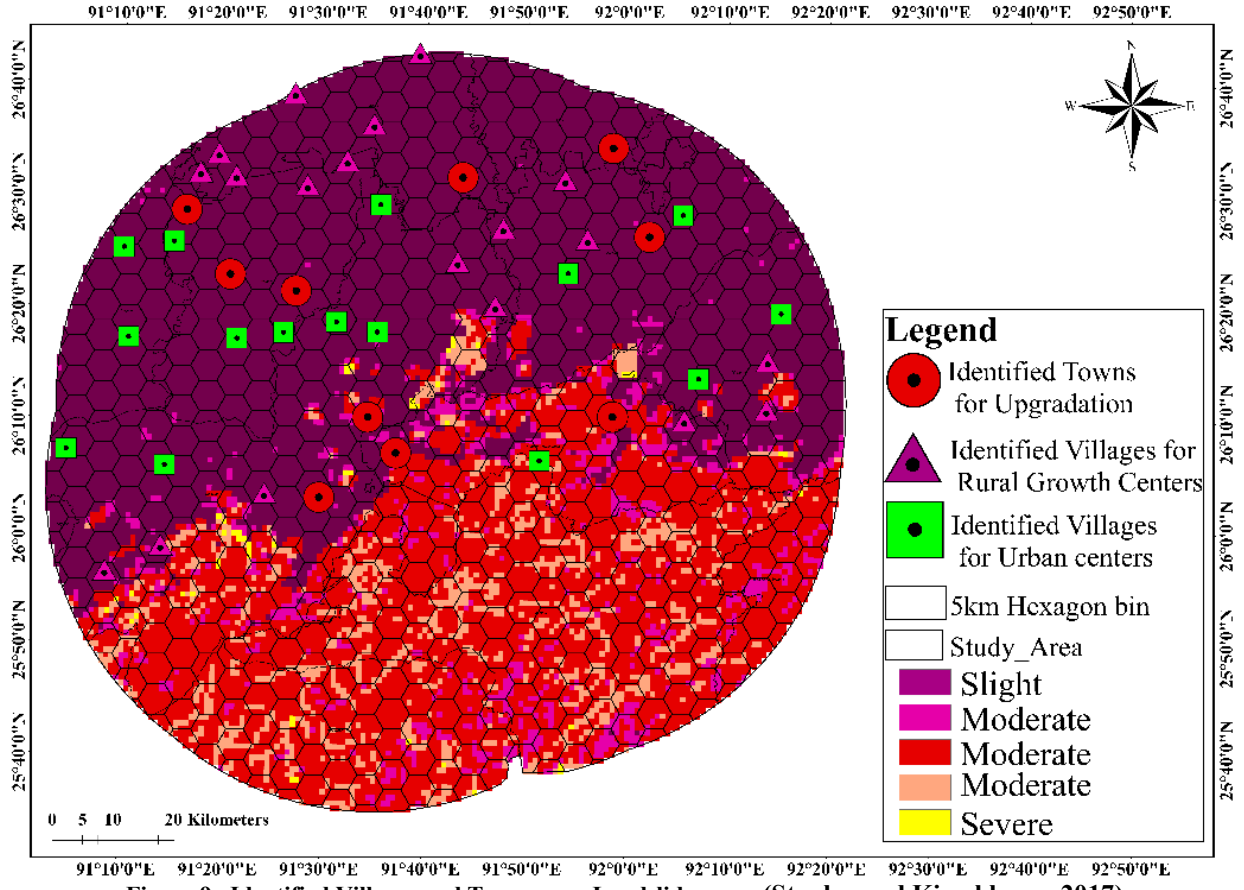

Figure 9. Identified Villages and Towns over Landslide zones (Stanley and Kirschbaum 2017)

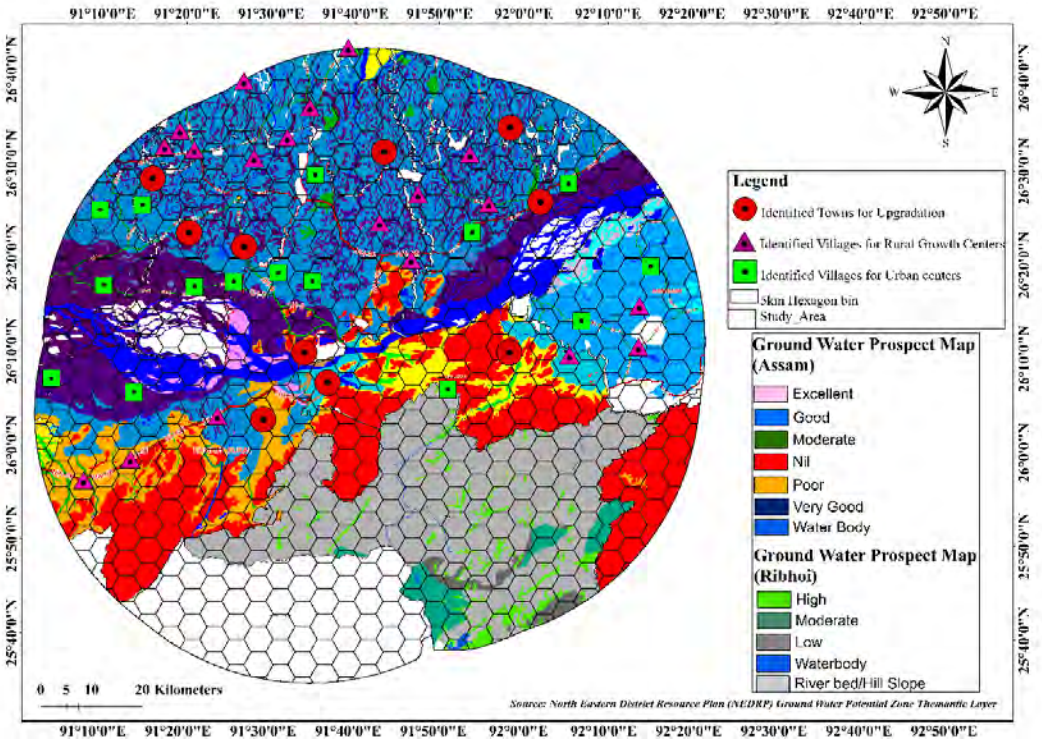

Figure 10. Identified Villages and Towns over Ground Water prospect zones (NEDRP)

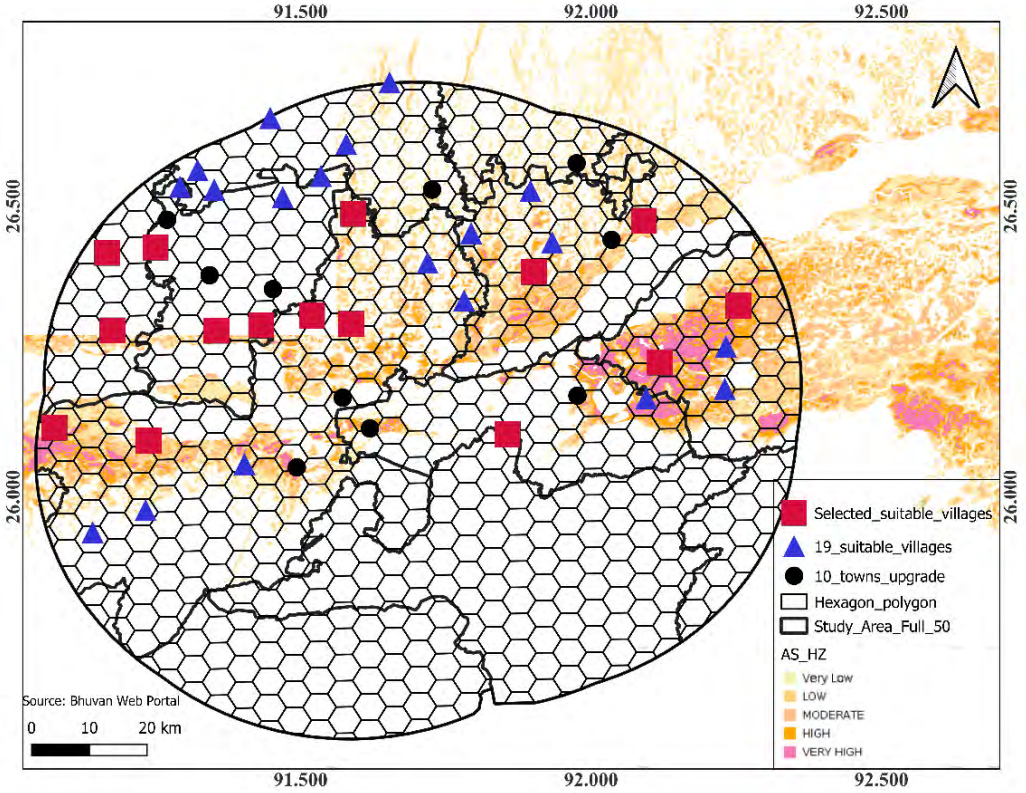

Figure 11. Identified Villages and Towns over Flood Hazard zones (Bhuvan)

From, Table 5 and Table 6, it is found that two village settlements namely Dhopguri and Dakua para from Kamrup rural district and one town namely Digaru Gaon (Digarubar Gaon) (CT) from Kamrup metropolitan district falls in poor ground water zones. Hence, these settlements were not proposed further for development of new rural growth centers and class upgradation. Finally, 15 urban centers and 17 rural growth centers along with nine towns of different hierarchical order were identified and overlaid on the nested hexagon (Figure 9). However, certain preventive measures are required to be taken and suggested for the proposed settlements from the purview of urban expansion which are as follows

Table 5. Settlements of different orders Proposed for Urban centre and Rural growth centre

AA	BB	CC	DD	EE	FF	GG	HH	II	JJ
Morigaon	Bhakat Gaon	1993	III	RGC	GD	MD	SL	AG/PTC	S
Darrang	Bhuktabari	5400	III	UC	VG	VL-MD	SL	AG/PTC	S
Kamrup (M)	Amerigog N.C.	5348	IV	UC	NL	VL	MD	BU/FFL	S
Morigaon	Burha Buri	5875	IV	UC	GD	VL-HH	SL	AG/PTC	S
Morigaon	Kalikajari	7266	IV	UC	GD	LW-HH	SL	WL/AG	S
Baksa	Kaljhar	2867	IV	RGC	VG	VL	SL	BU/AG/PTC	S
Kamrup_Rural	Khopani Kuchi	5244	IV	UC	GD	VL-MD	SL	AG/PTC	S
Nalbari	Khudra Makhibaha	5052	IV	UC	VG	VL-MD	SL	AG/PTC	S
Nalbari	Narayanpur	5748	IV	UC	VD	LW	SL	BU/ AG /PTC/WB	S
Darrang	Sanapatipara (Sentipukhuri)	1122	IV	RGC	VG	VL	SL	AG /PTC	S
Kamrup (R)	Tulsibari	7214	IV	UC	VG	VL	SL	BU/ AG /PTC /WB	S
Kamrup_Rural	Tupamari	10964	IV	UC	VG	VL-HH	SL	AG	S
Baksa	Baganpara	3211	V	RGC	VG	VL	SL	AG /PTC	S
Nalbari	Balitara No.4	1584	V	RGC	VG	VL	SL	AG /PTC /WB	S
Darrang	Bar - Satra	1095	V	RGC	VG	LW	SL	AG /PTC	S
Baksa	Bareigaon	2812	V	RGC	VG	VL	SL	AG /PTC /WB	S
Baksa	Bhalukdonga	2099	V	RGC	VG	VL	SL	BU/ AG /PTC	S
Baksa	Bhawraguri	1441	V	RGC	GD	VL	SL	AG /PTC /WB	S
Kamrup_Rural	Dakuapara	3016	V	RGC	PR	VL	SL-MD	BU/ AG/ PTC	US
Kamrup_Rural	Jajikona	1903	V	RGC	VG	LW	SL	AG /PTC/WB	S
Darrang	Khataniapara	5968	V	UC	VG	LW	SL	AG /PTC	S
Kamrup_metro	Maloibari Pathar	1521	V	RGC	GD	VL-VH	SL	AG /PTC /WB	S
Kamrup_Rural	Manah Kuchi	6290	V	UC	VG	VL-MD	SL	AG/ PTC	S
Nalbari	Niz-Namati	4784	V	RGC	VG	LW	SL	BU/ AG /PTC	S
Kamrup_Rural	Nowapara	3596	V	RGC	GD	VL-HH	SL	BU/AG/PTC	S
Morigaon	Sarubori	1350	V	RGC	GD	VL-VH	SL	AG	S
Nalbari	Bangaon	1409	VI	RGC	VG	VL	SL	AG/PTC/WB	S
Kamrup_Rural	Bezera	2434	VI	RGC	VG	VL-MD	SL-MD	AG /PTC	S
Kamrup_Rural	Dhopguri	3889	VI	RGC	PR	VL	SL	AG /PTC	US
Barpeta	Kawaimarikaragari Reserve	24581	VI	UC	VG	VL- HH	SL	AG	S
Nalbari	Loharkhatha	6384	VI	UC	VG	VL-MD	SL	AG/ PTC /WB	S
Barpeta	Muchalman Gaon	6385	VI	UC	VG	VL- MD	SL	AG/ PTC /WB	S
Darrang	Salikajhar	2032	VI	RGC	VG	VL	SL	AG/ PTC	S
Kamrup_Rural	Tukura Para	7166	VI	UC	VG	LW	SL	BU/AG	S

Table 6. Proposed towns for upgradation to higher order from its current status class/order

AA	BB'	CC	DD'	EE'	FF	GG	HH	II	JJ
Darrang	Mangaldoi (MB)	25989	III	UG-II	VG	VL-MD	SL	BU/AG/ PTC	S
Kamrup	Sualkuchi (CT)	13898	IV	UG-III	VG	LW	SL-MD	BU/WB	S
Baksa	No.2 Goreswar (CT)	5631	V	UG-II	VG	VL	SL	BU/AG/ PTC	S
Kamrup Metropolitan	Azara (CT)	8780	V	UG-IV	GD	VL-HH	SL	BU/AG/WL	S
Nalbari	Belsor (CT)	8523	V	UG-II	VG	VL-MD	SL	AG/ PTC	S
Udalguri	Kalaigaon Town (Part) (CT)	5112	V	UG-III	GD	VL	SL	BU/AG/ PTC	S
Kamrup	Sanpara (CT)	4534	VI	UG-IV	GD	VL-VH	SL	BU/AG/ PTC	S
Kamrup (M)	Digaru Gaon (Digarubar Gaon) (CT)	3207	VI	UG-III	PR	VL	MD	FL/AG	US
Nalbari	Tihu (TC)	4599	VI	UG-IV	VG	MD	SL	BU/AG/ PTC	S
Nalbari	Marowa (CT)	4004	VI	UG-V	VG	LW	SL	AG/ PTC	S

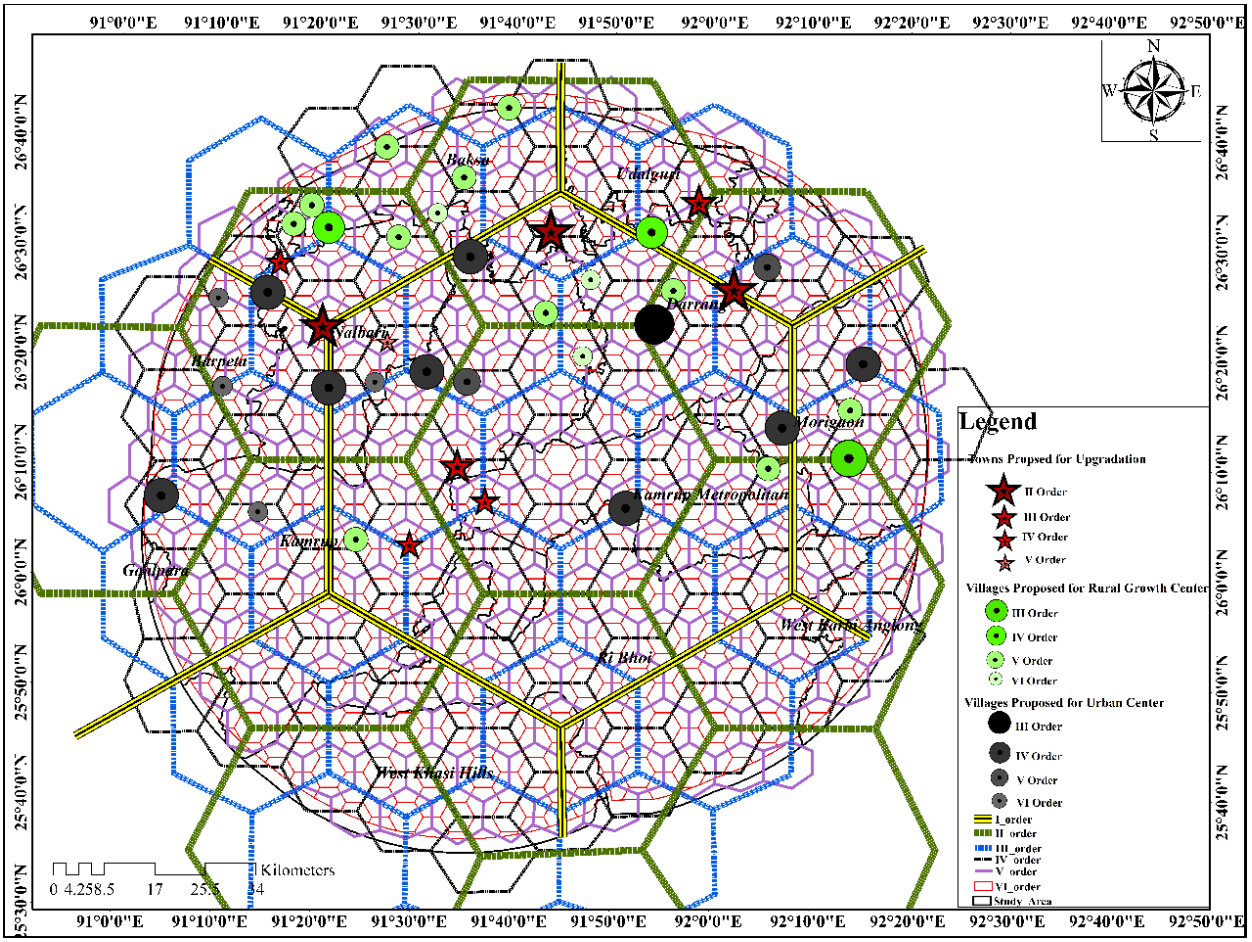

Figure 12. Hierarchy of settlements

i) Adequate vegetative and structural protection measures are suggested for the proposed URGC settlements which are having moderate to high flood prone and landslide susceptible areas.
ii) Expansion should be avoided in areas which are covered with wetlands.
iii) Rivers and streams need to be taken care of during expansion process.
iv) Adequate groundwater recharge structure and rainwater harvesting is suggested for the existing unsuitable settlements due to poor groundwater potential.
v) Settlements with available surface water supply from river and streams were proposed for urban centres within the study area.

5. Conclusion

This study identifies potential urban centers and rural growth centers using central place theory, nested hexagon model, GIS and remote sensing around the city of Guwahati for which multiple criteria were determined. The criteria although includes population of 5000 and above but for wider coverage of the study area villages with less than 5000 population is proposed for Rural Growth Centers. A total of 209 settlements were selected for identification of urban centers and rural growth centers. Further, based on multiple criteria, 34 villages and 10 existing towns were identified for the proposal of urban centers and rural growth centers and up gradation of towns to higher order. These selected 34 centers were further analyzed for suitability assessment by generating a 5km hexagonal bin which was overlaid on ground water potential zones, flood prone areas, land use land cover and landslides susceptibility of the area to assess suitability. After suitability assessment, out of identified 10 towns, nine towns have been selected and proposed for up gradation to higher order. Out of 34 village settlements, 15 villages were proposed for new urban centers and 17 villages were proposed for rural growth center within the study area for decentralized planning. After considering all the parameters and pre-determined criteria, two village settlements were not proposed since they were falling within poor ground water potential zones. Thus, a total of 32 settlements were finally selected for development as new urban centers and rural growth centers (URGC) within the study area. However, several suggestion and preventive measures were made which needs to be considered before initiating developmental expansion. In this study, an attempt has been made to identify potential urban centers and rural growth centers for decentralized planning with proper integration and co-relation between urban and rural sectors that will fulfill aspirations of people and achieve sustainable development of the region.

Abbreviations

***RGC*=**	**Rural Growth Centre**	**AA'=**	**District**
***UC* =**	**Urban Centre**	**BB=**	**Name of village settlement**
***VG* =**	**Very Good**	**BB′=**	**Name of Town settlement**
***GD* =**	**Good**	**CC=**	**Population**
***MD* =**	**Moderate**	**DD=**	**Hierarchical order as per nested Hexagon**
***NL* =**	**Nil**	**DD′=**	**Existing Orders as per Census data**
***PR* =**	**Poor**	**EE=**	**Proposed new Urban Centers/Rural Growth Centers**
***VH* =**	**Very High**	**EE′=**	**Proposed Towns for Upgradation to higher order as per Nested Hexagon**
***HH* =**	**High**	**FF=**	**Ground Water Prospect Zones**
***LW* =**	**Low**	**GG=**	**Flood Prone Zones**
***VL* =**	**Very Low**	**HH=**	**Landslide susceptible Zones**
***SL* =**	**Slight**	**II=**	**Land use/ Land Cover (within 5 km Hexagon zone)**
***SV* =**	**Severe**	**JJ=**	**Remarks**
***AG* =**	**Agriculture**		
***PTC*=**	**Patches of Tree Clad**		
***FFL* =**	**Forest Fringe Land**		
***FL* =**	**Forest Land**		
***BU* =**	**Built-Up**		
***WL*=**	**Wetland**		
***WB*=**	**Waterbodies**		
***S* =**	**Suitable**		
***US* =**	**Un-Suitable**		
***UG* =**	**Upgrade**		

Conflict of Interest The author(s) declared no potential conflicts of interest with respect to the research, scholarship, and/or publication of this article.

References

Bhuvan Geo-Portal and Web Service Group National Remote Sensing Centre (NRSC), Indian Space Research Organisation. Government of India. Hyderabad. https://bhuvan.nrsc.gov.in.

Census of India 2011. Office of the Registrar General & Census Commissioner, India. https://censusindia.gov.in.

Christaller W. (1933). Die zentralen Orte in Suddeutschland. – Eine Okonomisch-Geographische Untersuchung Uber die GesetzmaXigkeit der Verbreitung und Entwicklung der Siedlungen Mit Stadtischen Funktionen (English transl. 1967, Central Places in Southern Germany. Englewood Cliffs, NJ: Prentice-Hall). Jena: G. Fischer.

Emerging North East India. *Economically And Socially Inclusive Development Strategies*. 2015. KPMG FICCI. https://assets.kpmg.

Formulation of GIS based Master Plans for Small and Medium Towns: Design & Standards for Application of Drone/ UAV Technology (2020*)*. Town & Country Planning Organisation, Ministry of Housing and Urban Affairs, MoHUA. Government of India. http://www.tcpo.gov.in.

Ganguly J.B. (1995) Urbanization and Development in North-East India Trends and Policy Implications. Deep and Deep Publication, New Delhi.

Hemani S. and A.K. Das (2015). City Profile: Guwahati. *The International Journal of urban policy and planning*. 137-157.

Kim S.M. (2015). An Empirical Analysis on Urban-Rural Linkage in Mumbai Metropolitan Area. *The Journal of Development Practice*. 2, 20-25.

Losch A. (1944). Die Raumliche Ordnung der Wirtschaft (English transl. 1954, The Economics of Location. New Haven, CT: *Yale University Press*. Jena: G. Fischer.

Mishra S. and S.V. Deodhar (2009). Urban -Rural Interface and Sustainable Development -A Case Study of Kosi Command Area. *Journal of Rural development*. 28(3), 343-356.

North Eastern District Resource Plan (NEDRP) Geo Explorer. North Eastern Space Application Centre Umiam Meghalaya (NESAC). https://nesac.gov.in/portals-geo-portals/.

Office of the Register General and Census Commissioner, India. Ministry of Home Affair. Government of India. https://censusindia.gov.in.

Rahman K.U. and S. Noor (2005). Central Functions and Centrality in Rural Settlements of Sargodha District. *Pakistan Geographical Review*. 60 (2), 70-79.

Ray B.D., A.K. Neog and H.K. Mazhari (1999*)*. Urban Development in North East India Potentiality and Problems. *Reliance publishing house. New Delhi.*

Reforms In Urban Planning Capacity in India (2021). Niti Aayog, Government of India. https://www.niti.gov.in.

Risk Assessment and Review of Prevailing Laws, Standards, Policies and Programmes to Climate Proof

Cities- Synthesis Report for Guwahati. TERI, 2013. https://www.teriin.org.

Richardson H.W. (1971) Urban Economics, Penguin.

Rondinelli D.A. (1980). Spatial Analysis for Regional Development A Case Study in the Bicol River Basin of the Philippines. The United Nation University.

Sahasranaman A. (2012). Financing the Development of Small and Medium Cities. *Economic & Political Weekly*. 47 (24), 59-66. https://www.epw.in/.

Stanley T. and D.B. Kirschbaum (2017), A heuristic approach to global landslide susceptibility mapping, Nat. Hazards, 1–20, doi:10.1007/s11069-017-2757-y

Taubenbock, H., and T. Esch (2011). Remote sensing -An effective data source for urban monitoring. *Oceanic engineering society*.

Urban And Regional Development Plans Formulation and Implementation (URDPFI) Guidelines. Town & Country Planning Organisation. Ministry of Urban Development. https://mohua.gov.in.

Waikar M.L. and A.P. Nailawar (2014). Identification of Groundwater Potential Zone Using Remote Sensing and GIS Technique. *International Journal of Innovative Research in Science, Engineering and Technology*. 3 (5), 12163-12174.

Journal of Geomatics Vol. 17, No. 2, October 2023

Development of Machine Learning based Models for Multivariate Prediction of Wheat Crop Yield in Uttar Pradesh, India

Sukirti[1]. Kamal Pandey[2*], Abhishek Danodia[3], . Harish Chandra Karnatak[2]
[1]Indian Institute of Remote Sensing (IIRS), Dehradun
[2]Department of Geoweb Services, IT and Distance Learning, IIRS, ISRO, Dehradun
[3] Agriculture and Soils Department, IIRS, Dehradun
*kamal@iirs.gov.in

(Received: 21 April 2023; in final form 27 November 2023)

DOI: *https://doi.org/10.58825/jog.2023.17.2.70*

Abstract: The consequences of climate change have a substantial impact on agricultural crop production and management. Predicting or forecasting crop yields well in advance would help farmers, agriculture corporations and government agencies manage risk and design suitable crop insurance plans. Ground survey is the traditional way of determining yield, which is subjective, time-consuming, and expensive. While Machine Learning (ML) techniques make yield prediction less expensive, less time taking and more efficient. In this study, thirteen years of meteorological parameters and wheat yield data (2001-2013) of Uttar Pradesh were used to train and analyze three Machine Learning Regression models viz. Support Vector Regression, Ordinary Least Squares, and Random Forest. Each model's performance was assessed using Mean Absolute Error (MAE), Mean Squared Error (MSE), and Root Mean Squared Error (RMSE). Results revealed that the Random Forest model with a MAE of 0.258 t/ha, MSE of 0.096 t/ha and RMSE of 0.311 t/ha proved to be the best model in the yield prediction of wheat when results are statistically compared with others. Researchers and decision-makers can use the findings to estimate pre-harvest yields and to ensure food security.

Keywords: Meteorological parameters, Wheat, Multivariate, Yield prediction, Machine Learning, Random Forest.

1. Introduction

India has a long history of agriculture (Madhusudan, 2015) dating back to the Indus Valley Civilization. Agriculture sector is very important for India's socioeconomic structure as it is one of the largest economic sectors in terms of population diversity. The inability to integrate technology to provide the intended results is one of the biggest challenges Indian agriculture is facing (Nigam et. al., 2019). Due to the uneven climatic trends brought on due to the negative impacts of global warming, which has affected crop production as well, farmers find it challenging to precisely predict temperature and rainfall patterns for their agricultural practices. Farmers play important role to ensure food security for the human civilization. Food security is provided through agriculture, and is crucial for a nation's economic growth (Barman, 2020). Since the launch of Earth Observation (EO) satellites and the explorer missions that followed, satellite remote sensing has enabled us gather remote sensing data at improving scales (Karthikeyan et. al., 2020; Shetty et. al., 2021; Virnodkar et. al., 2020; Feizizadeh et. al., 2023; Jamali 2019; Chatziantoniou et. al., 2017; Ienco et. al., 2019.

Global temperature is rising as a result of the continuing rise in greenhouse gas emissions. Some effects of climate change include shifting seasons, melting glaciers, increasing precipitation, rise in extreme weather occurrences, and so on. World population and socioeconomic growth, along with climate change, represent a danger to food security. An extremely high rate of land degradation brought on by climate change is creating accelerated desertification and nutrient-deficient soils. The problem of land degradation is said to be a serious global threat and is getting worse day by day (Arora 2019). Rising temperature is also leading to gradual decline in annual crop yield. Crop failures are more likely to occur in the short term as a result of altered precipitation patterns, and diminished crop productivity \(Poudel and Shaw 2016).

Until recently, yield prediction was being done by considering the farmer's knowledge of a particular area and crop. Empirical and crop growth models (Jørgensen, 1994) were created using meteorological data to for the yield prediction, but these techniques also have a lot of problems owing to the spatial distribution of the weather stations. The outputs from these operations are accessible only after the crops have been harvested,. Therefore, it is essential to decrease expenses and longer waits involved in the traditional practices while also improving yield prediction accuracy. For this purpose, machine learning techniques provide an alternate option with improved and proven performance matrix. (Nigam et. al., 2019; Jaafar and Mourad 2021; Cunha et. al., 2018; Pantazi et. al., 2016).

Researchers across the globe have attempted and developed machine learning techniques for crop yield forecasting. Preseason forecasting was a technique developed that used a machine learning-based system to predict soybean yields before the start of the crop season (Cunha et. al., 2018). The system was based on a recurrent neural network (RNN) that was trained using historical data on municipal-level soybean and/or maize yields as well as parameters such as precipitation, temperature, and soil conditions. A reanalysis-based seasonal forecast product of temperature and precipitation, which enabled predicting up to seven months in advance, providing the meteorological data operationally (Cunha et. al., 2018). The findings were on par with, and in some cases better than, similar models that are limited to early season

forecasting due to the need for remote sensing data across the farm. This study concentrated on the quantification of machine learning algorithms and their practical application. The method mentioned also considered the unpredictable rainfall and temperature in order to obtain a steady trend. On the basis of mean absolute error, the results of different algorithms were compared. The most accurate regressor for predicting yield was found to be the Random Forest Regressor. A sequential model called Simple Recurrent Neural Network performed better at forecasting rainfall than the LSTM for forecasting the temperature (Nigam et. al., 2019).

A technique to anticipate agricultural yield based on historical data was designed and implemented by Bondre et al (2019) Using agricultural data, machine learning methods like Support Vector Machine and Random Forest were used to determine the recommended fertiliser for a number of crops (Bondre and Mahagaonkar 2019). It concentrated on developing a prediction model that may be applied to crop yield forecasting in the future. Different sources were used to collect a variety of datasets, including those for crops, crop yield, geography, soil and crop nutrients, and fertiliser.

Haque et al (2020) suggested two distinct Machine Learning (ML) algorithms in their study to examine the crop yield (Haque et.al., 2020). With 140 data points collected, the Support Vector Regression (SVR) and Linear Regression (LR) algorithms proved to be quite effective for evaluating the performance of the parameters involved in the forecast. The Mean Square Error (MSE) and Coefficient of Determination were used to calculate the error rate (R^2) and the same dataset was used to directly compare the results obtained from the ML models. Pantazi et al (2016) attempted a study wherein online multi-layer soil data and crop growth parameters from satellite imagery were used to forecast within-field variation in wheat yield. An unsupervised learning system was combined with supervised self-organizing maps that could handle data from numerous soil and crop sensors. The effectiveness of XY-fused Networks (XY-Fs), Supervised Kohonen Networks (SKNs), and Counter-Propagation Artificial Neural Networks (CP-ANNs) for predicting wheat production in a field in Bedfordshire, UK, was compared during a single cropping season (Pantazi et. al., 2016).

In the field of crop yield analysis, machine learning (ML) is a new topic of research. By providing inputs for growing the best possible crop and anticipating the yields, ML has the potential to transform agriculture (Nigam et. al., 2019) to new dimension. In order to help farmers for selecting a suitable crop for cultivation to obtain maximum yield, ML model takes into consideration parameters like temperature, rainfall, area, etc. The ML based approaches has the potential to improve the expanding agricultural industry of countries like India and, taken together, raise the living standard of farmers. The objectives of the presented study are in line with the above argument viz. (i) To develop machine learning models to predict yield of wheat for the state of Uttar Pradesh, and (ii) To compare the performance of different models and to find out the best one for multivariate analysis of yield prediction. The study aims to promote wide spread use of ML models in decision making in a farming sectors for the countries like India where agriculture has a majoe share in economy.

2. Materials and Methods

2.1 Study Area

Uttar Pradesh (UP) is the fourth largest state of India with an area of 240,928 km^2. UP is the most populous state of India. It is located between latitude 24º to 31º North and longitude 77º to 84º East (Figure 1).

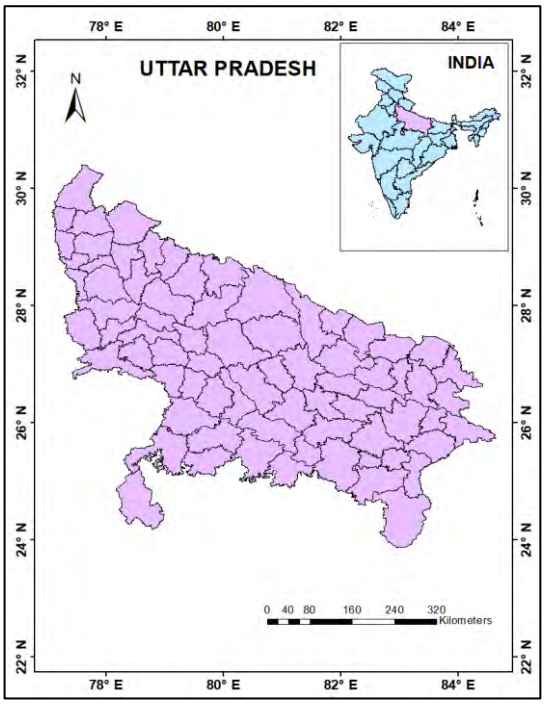

Figure 1. Map of Study Area (Uttar Pradesh)

There are 18 divisions and 75 districts in Uttar Pradesh. Due to the predominately agrarian economy, Uttar Pradesh is prominently dependent on the performance of industries like agriculture, horticulture, animal husbandry, dairy, fishery, etc. With four distinct seasons, Uttar Pradesh has a humid subtropical climate. The state receives an average of 650 mm of rainfall per year in the southwest and 1000 mm in the eastern and south eastern regions (Nihar et.al., 2022).

Approximately 47% of the population is directly dependent on agriculture for their livelihood, and climate is the primary factor affecting the production. Given the size of the state's geographic area and the access to the fertile Indo-Gangetic plains, UP makes a considerable contribution to the country's food security. The state produces about 12% of India's rice and 28% of it is wheat. Additionally, a significant amount of sugarcane is produced, making up 44% of the nation's total output (Gulati et.al., 2021). The major crops of the state are rice, wheat, maize, sugarcane, chickpea and pigeon pea. About 24% of the state's agricultural area is used to grow wheat throughout the state.. On an average the total geographical area under wheat crop is 9730.60 ha, total production is 32799.71 tons and total yield is 3371 kg/ha.

2.2 Data Used

Wheat yield was predicted using net sown area, and meteorological variables such as mean rainfall, mean temperature, mean relative humidity, mean wind speed, mean wind direction, and surface net solar radiation (for Rabi Season). The Indian government website (data.gov.in) provided historical district-level wheat yield data (2001-2013). The Climate Change Service (https://climate.copernicus.eu/), a website run by the ECMWF as part of The Copernicus Program, was used to collect all the meteorological data for the time period of 2001-2013. The datasets were gridded with hourly temporal resolution and a horizontal resolution of 0.5° x 0.5°. The ECMWF Copernicus services provide ever-changing datasets by continuously monitoring the climate and atmospheric composition and using climate and atmosphere reanalysis..

2.3 Data Pre-processing

The crop production data that were downloaded from data.gov.in were district- and season-specific, and they date back to 1997. Required yield data of wheat crop of Uttar Pradesh from 2001-2013 was extracted from the downloaded dataset. The collected data was organized in a Comma Delimited (CSV) format before being used with other meteorological parameters to form the dataset used for this study.

2.3.1 Principal Component Analysis

In order to study, model, and explain complex multivariate real-world systems, various statistical methods are available and Principal Component Analysis (PCA) is one of the widely used method to study the collinearity among the parameters . It is a useful tool for conducting data analysis on huge data sets and for identifying the main trends and the variables that influence them. It can quickly determine which primary components contribute the most to data variability. Instead of performing the whole process of attempting to estimate which of the variables might be of the most relevance, effort might instead be spent on trying to find and comprehend these few most critical components (Bloomer and Rehm 2014). In this research study, PCA was used to identify and address multicollinearity issues.

2.3.2 Data Splitting

The primary requirement of any ML model is data splitting, and the available dataset must be divided into three parts:

a. Using the **training set**, the model is trained or fitted. The optimal weights or coefficients for ML models can be found using the training set.
b. The **validation set** is utilised to improve the model performance by adjusting the the hyperparameters used in the model. For each potential setting of the hyperparameters, the model is fitted using the training set, and the performance is assessed using the validation set.
c. The **test set** is necessary for a fair assessment of the final model..

In cases where the dataset is less complicated and tuning of hyperparameters is not required , only the training and test sets can be used. Accordingly, the data array was divided into two subsets, one for training and the other for testing, using the Sklearn library's data splitting function known as train test split. By default, it divides the two subsets into random divisions. In this study, 80% of the data were used for training, with the remaining data being utilised to test the algorithm's performance..

2.4 Machine Learning Algorithms

The models were built using long-term datasets for the years from 2001 to 2013. The presented research work is focused on developing yield estimation models for wheat using the three ML models viz. Random Forest (RF), Ordinary Least Squares (OLS), and Support Vector Regression (SVR),.. The performance of these models were further compared to select the best performing model.

2.4.1 Random Forest

Random Forest is an ensemble based ML model wherein multiple decision trees are combined for producing aggregated output.. Ensemble learning is the process of combining the predictions or classifications of different models that have all been trained on the same data. The underlying principle of ensemble learning is that each model's errors—in this case, the errors of a decision tree—are separate and unrelated to one another. A Random Forest model's forecast is produced by averaging the predictions of various decision trees and hence there isn't a single equation that summarizes the RF model.

Similar study has been done in which Random Forests and Multiple Linear Regressions were compared, for crop production prediction, for wheat, maize, and potato at global and regional scales in response to meteorological and biophysical variables. They trained the RF models to predict crop yield using a variety of biophysical predictors (Jeong et. al., 2016).

2.4.2 Ordinary Least Squares

Ordinary Least Square is one of the popular regression model in ML. Building a model that lowers the overall squared deviations between the expected and actual data is an approach used to estimate unknown parameters. OLS tries to reduce this sum (Brinkhoff and Robson 2021). It is a linear regression method that aims to minimize the sum of squared residuals between the predicted values and the actual values. The equation (1) for OLS is:

$$y = w_0 + w_1x_1 + w_2x_2 + ... + w_nx_n + \varepsilon \quad (1)$$

Here, y is the predicted output, x_1, x_2,..., x_n are the input variables, w_0, w_1, w_2,..., w_n are the coefficients (weights) to be learned, and ε represents the error term. The study carried out by Sharma and team (2013) utilized OLS for the yield prediction of rainfed maize and soyabeans crops and reported the outputs with high accuracy. (Sharma et. al., 2013).

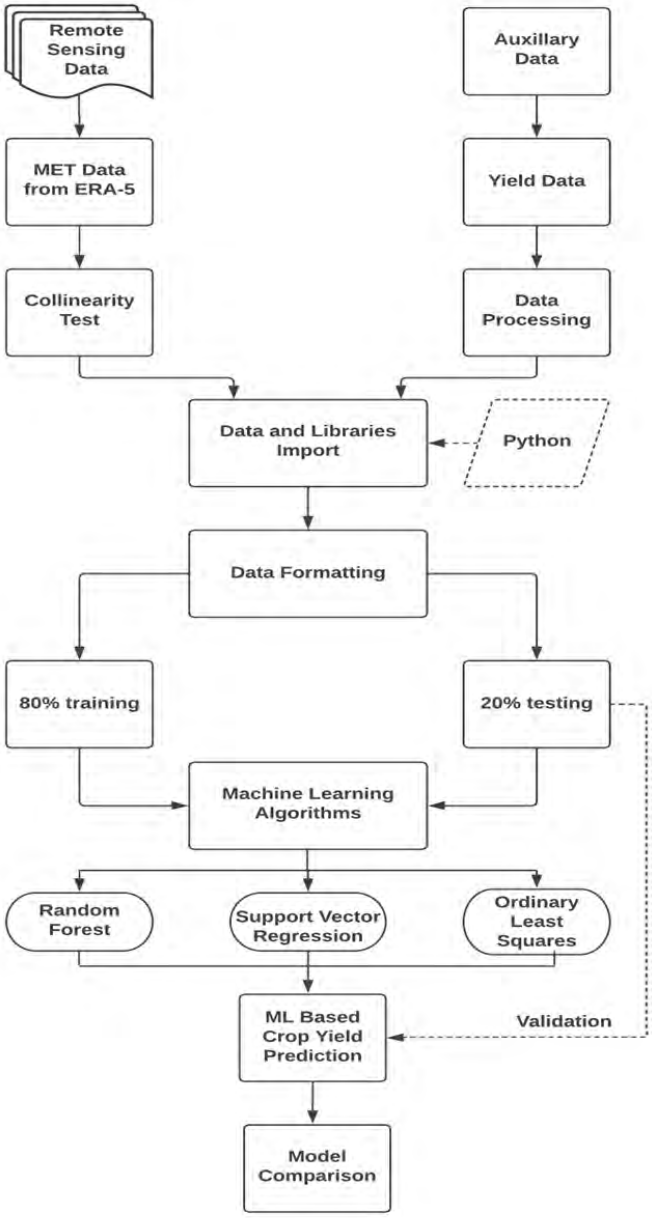

Figure 2. Flowchart of Methodology

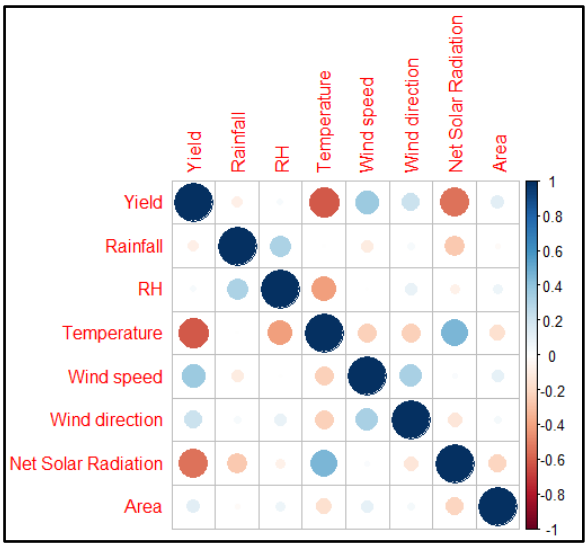

Figure 3. Correlation Matrix of Independent Variables

2.4.3 Support Vector Regression

A well-known machine learning approach called Support Vector Machine (SVM) is widely utilized in both classification and regression. The Support Vector Regression (SVR) aims to fit the best line within a threshold value, in contrast to other regression models that aim to minimize the difference between the actual and predicted value. Equation (2) is the generic representation for the line in support vector regression:

$$y = wx+b \quad (2)$$

SVR has been used in similar studies, a study in Andhra Pradesh, India which concentrated on the forecasting of important Kharif crops employed modular artificial neural networks to first anticipate the quantity of monsoon rainfall before applying support vector regression and rainfall data to calculate the potential yield of the main kharif crops. They concluded that the proposed strategy outperformed earlier machine learning algorithms in estimating kharif crop production after comparing their study with other ML methods (Khosla et.al., 2020).

3. Results and Discussion

3.1 Correlation Analysis

Collinearity check among the participating parameter is carried out before developing a predictive model in order to reduce the redundancy. If the correlation among different variables is high, it gives rise to multicollinearity problems and estimates are unstable. Therefore, to examine the co-linearity between the independent variables and prevent the multicollinearity issue, principal component analysis (PCA) is used in the present study. It was found that there was no significant correlation between the variables as shown in Figure 3..

3.2 Importance of Predictor Variables

The significance of these predictor variables was examined using the Random Forest model's characteristics. These factors were ranked according to their importance, and it was observed that each variable has its importance for yield estimation differently (Figure 4). Surface net solar radiation is observed to be the most crucial factor in the yield estimation, followed by mean temperature, mean wind speed, and area. Since wheat is a rabi (winter) crop, temperature and net solar radiation both have a significant impact on the crop's ability to grow. Strong winds can lead to lodging of the crop and hence mean wind speed also plays very important role in for the overall crop yield.

3.3 Model Comparison

The density scatter plots for each algorithm are shown in Figures 5. Among the models, RF demonstrated the highest predictive accuracy, as evidenced by its scatter plot exhibiting the strongest alignment between observed and predicted yield. The data points are closely clustered around a central line, with only a few outliers indicating a robust relationship between the two variables. This was further supported by the highest coefficient of determination (R^2) achieved by the RF model. On the other hand, SVR performed relatively poorly as compared to the other models and as evident in its scatter plot. The lower R^2 value associated with the SVR model indicated a weaker correlation and less accurate predictions. These findings highlight the superior performance of the RF model in predicting crop yield, while underscoring the limitations of SVR in this particular context.

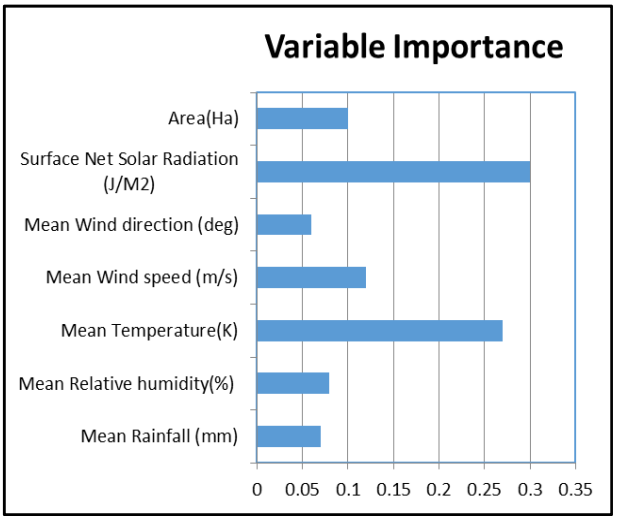

Figure 4. Importance of Predictor Variables

Mean Squared Error (MSE), and Root Mean Squared Error (RMSE) of yield forecasts were estimated for the ML models and out of all three models, RF showed the best predictive capability for wheat yield ($R^2 = 0.72$).

3.3 Discussion

The ability of these ML models (RF, OLS, and SVR) to predict the yield of wheat in Uttar Pradesh was tested using Mean Absolute Error (MAE), Mean Squared Error (MSE), and Root Mean Squared Error (RMSE). Results for the ML models are summarized in Table 1. Random forest successfully predicted the wheat yield and was compared against the test data, which was not used in training the model. Comparison between the observed and predicted yield (Figure 5a) produced an R^2 of 0.72. The model was able to explain with MAE value of 0.258 t/ha, MSE value of 0.096 t/ha and RMSE value of 0.311 t/ha.

The method we followed in this study was found similar to the method adopted by Schwalbert et al 2020. They found that combining meteorological information with multi-temporal satellite imagery could produce useful data, thus enabling the creation of more precise yield forecast models, which is consistent with our work. Using a regression model between historical meteorological data and yield data for food crops, the effects of climate change were investigated in the mountainous regions of Nepal. They came to the conclusion that different crops' yield is affected differently by climate variables. However, the current climate trends have a negative impact on winter crops (Poudel and Shaw 2016).

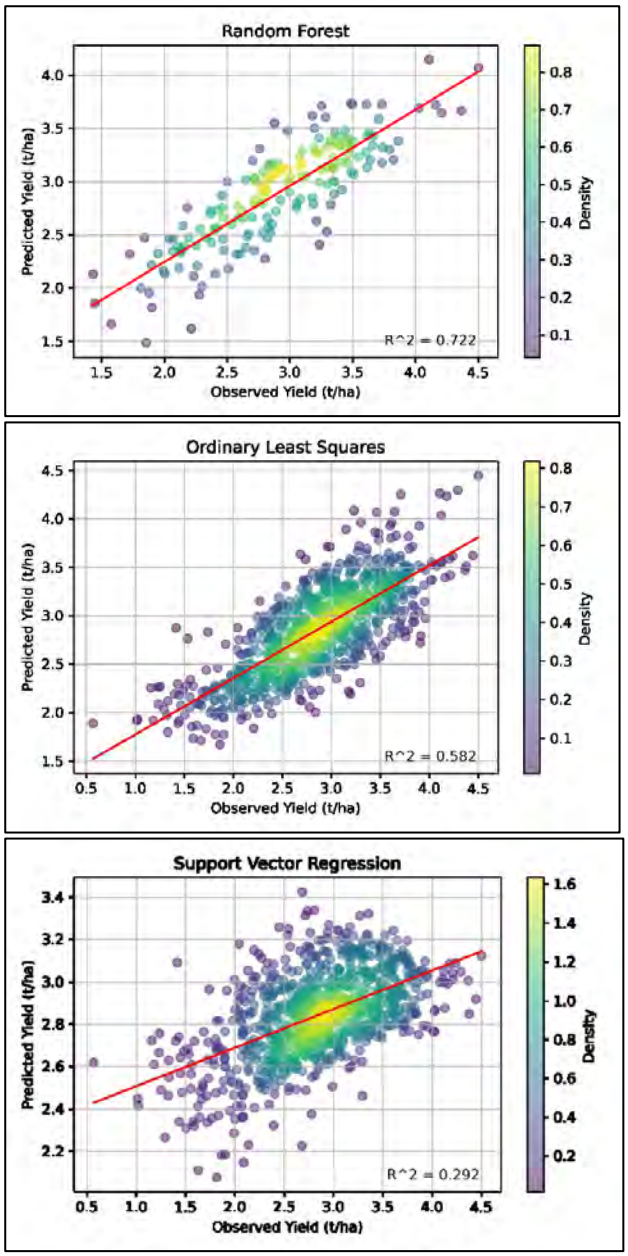

Figure 5. Scatter plot of Predicted yield against Observed Yield for (top) Random Forest, (middle) Ordinary Least Squares. And (bottom) Support Vector Regression

Table 1. Prediction Performance of Different Algorithms

Algorithm	MAE (t/ha)	MSE (t/ha)	RMSE (t/ha)
Random Forest	0.258	0.096	0.311
Support Vector Regression	0.439	0.304	0.552
Ordinary Least Squares	0.312	0.156	0.395

Cabas et al 2010 concluded in their study that the non-climatic variables had a relatively minor impact on the yield distribution, indicating that climatic factors should dominate this relationship (Cabas et. al., 2010). A system to forecast agricultural yield based on historical data has also been proposed by Bondre and Mahagaonkar (Bondre and Mahagaonkar 2019). They used agriculture data and machine learning techniques like Support Vector Machine and Random Forest and obtained the accuracy of 99.47% and 97.48% for . SVM and RF respectively. Therefore, SVM method was found to be good for agricultural yield prediction as opposed to our result. This might be due to the difference in predictor variables.

4. Conclusion

. With the help of machine learning algorithms and publicly available data, this study established a methodology for estimating winter wheat production on a regional scale that might possibly be used to estimate crop yield globally and in regions with low frequency of observed data. By merging crop models with additional data for crop yield estimation, forecasting, and catastrophe monitoring in vast areas, the framework can be further enhanced. In order to estimate winter wheat yield from 2001 to 2013 along with 07 parameter of winter season viz. mean temperature, mean relative humidity, mean pressure, mean wind speed, mean wind direction, mean precipitation and mean solar radiation, three ML models (Support Vector Regression, Ordinary Least Squares, and Random Forest) were used in this study. Using three error metrics—Mean Absolute Error (MAE), Mean Squared Error (MSE), and Root Mean Squared Error (RMSE)—accuracy was compared to assess each model's performance. Overall, all three models performed well but RF model performed the best. With MAE values of 0.258,

MSE values of 0.096, and RMSE values of 0.311, it was found that RF outperformed SVR and OLS. The poorest result was obtained by SVR. This study has the potential to open up new possibilities for productive research on agricultural production prediction utilizing a variety of meteorological factors. It will encourage and promote research into the use of machine learning techniques for yield forecasting.

Acknowledgements:
Authors express their sincere thanks to Copernicus (https://scihub.copernicus.eu/) for providing satellite data at no cost. The authors are also thankful to the Indian Institute of Remote Sensing for providing the laboratory facilities for the completion this work.

Competing Interests: We, the authors declare that we have no competing interests.

References

Arora N.K. (2019), "Impact of climate change on agriculture production and its sustainable solutions," *Environ. Sustain.*, vol. 2, no. 2, pp. 95–96, doi: 10.1007/s42398-019-00078-w.

Barman S. (2020), "The Political Economy of Food Security in India: Evolution and Performance, International Journal of management, 11(12), pp 1156-1162"

Bloomer C. and G. Rehm (2014), "Using principal component analysis to find correlations and patterns at diamond light source," *IPAC 2014 Proc. 5th Int. Part. Accel. Conf.*, pp. 3719–3721

Bondre D. and S. Mahagaonkar (2019), "Prediction of crop yield and fertilizer recommendation using machine learning algorithms," International Journal of Engineering, Applied Science and technology vol. 4(5), pp. 371–376

Brinkhoff J. and A. J. Robson (2021). "Block-level macadamia yield forecasting using spatio-temporal datasets," *Agric. For. Meteorol.*, vol. 303, doi: 10.1016/j.agrformet.2021.108369.

Cabas J., A. Weersink and E. Olale (2010). "Crop yield response to economic, site and climatic variables," *Clim. Change*, vol. 101, no. 3, pp. 599–616, 2010, doi: 10.1007/s10584-009-9754-4.

Chatziantoniou A., G. P. Petropoulos and E. Psomiadis (2017). "Co-Orbital Sentinel 1 and 2 for LULC mapping with emphasis on wetlands in a mediterranean setting based on machine learning," *Remote Sens.*, vol. 9, no. 12,

Cunha R.L.F, B. Silva and M. A. S. Netto (2018). "A scalable machine learning system for pre-season agriculture yield forecast," *Proc. - IEEE 14th Int. Conf. eScience, e-Science* pp. 423–430, doi: 10.1109/eScience.2018.00131.

Feizizadeh B., D. Omarzadeh, M. Kazemi Garajeh, T. Lakes and T. Blaschke (2023). "Machine learning data-driven approaches for land use/cover mapping and trend analysis using Google Earth Engine," *J. Environ. Plan. Manag.*, vol. 66, no. 3, pp. 665–697, doi: 10.1080/09640568.2021.2001317.

Gulati A., P. Terway and S. Hussain (2021) "Performance of agriculture in Uttar Pradesh", In: A. Gulati, R. Roy and S. Saini (eds) Revitalizing Indian Agriculture and Boosting Farmer Income. Indian Studies in Business and Economics, Springer

Haque F.F., A. Abdelgawad, V. P. Yanambaka and K. Yelamarthi (2020). "Crop Yield Analysis Using Machine Learning Algorithms," *IEEE World Forum Internet Things, WF-IoT 2020- Symp. Proc.*, doi: 10.1109/WF-IoT48130.2020.9221459.

Ienco D., R. Interdonato, R. Gaetano and D. Ho Tong Minh (2019). "Combining Sentinel-1 and Sentinel-2 Satellite Image Time Series for land cover mapping via a multi-source deep learning architecture," *ISPRS J. Photogramm. Remote Sens.*, vol. 158, pp. 11–22, doi: 10.1016/j.isprsjprs.2019.09.016.

Jaafar H. and R. Mourad (2021). "Gymee: A global field-scale crop yield and et mapper in google earth engine based on landsat, weather, and soil data," *Remote Sens.*, vol. 13, no. 4, pp. 1–30, doi: 10.3390/rs13040773.

Jamali A. (2019). "Evaluation and comparison of eight machine learning models in land use/land cover mapping using Landsat 8 OLI: a case study of the northern region of Iran," *SN Appl. Sci.*, vol. 1, no. 11, doi: 10.1007/s42452-019-1527-8.

Jeong J.H, J.P. Resop, N.D. Mueller, D.H. Eleisher, K. Yun, E.E. Butler, D.J. Timlin, K. Shim, J.S. Gerber, V.R. Reddy and S. Kim (2016). "Random forests for global and regional crop yield predictions," *PLoS One*, vol. 11(6), doi: 10.1371/journal.pone.0156571.

Jørgensen S.E. (1994). "Models as instruments for combination of ecological theory and environmental practice," *Ecol. Modell.*, vol. 75–76, no. C, pp. 5–20, doi: 10.1016/0304-3800(94)90003-5.

Karthikeyan L., I. Chawla and A.K. Mishra (2020). "A review of remote sensing applications in agriculture for food security: Crop growth and yield, irrigation, and crop losses," *J. Hydrol.*, vol. 586, 2020, doi: 10.1016/j.jhydrol.124905.

Khosla E., R. Dharavath and R. Priya (2020). "Crop yield prediction using aggregated rainfall-based modular artificial neural networks and support vector regression," *Environ. Dev. Sustain.*, vol. 22, no. 6, pp. 5687–5708, doi: 10.1007/s10668-019-00445-x.

Madhusudan L. (2015). "Agriculture role on Indian..Economy. - *Business and economics journal*, vol 6, no. 4

Nigam A., S. Garg, A. Agrawal and P. Agrawal (2019) "Crop yield prediction using machine learning algorithms," Fifth International Conference of Image Information Processing. Shimla, 125-130

Nihar A., N. R. Patel and A. Danodia, (2022). "Machine-Learning-Based Regional Yield Forecasting for Sugarcane Crop in Uttar Pradesh, India," *J. Indian Soc. Remote Sens.*, vol. 50, no. 8, pp. 1519–1530, doi: 10.1007/S12524-022-01549-0.

Pantazi X.E., D. Moshou, T. Alexandridis, R. L. Whetton and A. M. Mouazen (2016). "Wheat yield prediction using machine learning and advanced sensing techniques," *Comput. Electron. Agric.*, vol. 121, pp. 57–65, doi: 10.1016/j.compag.2015.11.018.

Poudel S. and R. Shaw (2016). "The relationships between climate variability and crop yield in a mountainous environment: A case study in Lamjung District, Nepal," *Climate*, vol. 4, no. 1, doi: 10.3390/cli4010013.

Schwalbert R.A., T. Amado, G. Corassa, L.P. Pott, P.V.V. Prasad and I.A. Ciampitti (2020). "Satellite-based soybean yield forecast: Integrating machine learning and weather data for improving crop yield prediction in southern Brazil," *Agric. For. Meteorol.*, vol. 284, doi: 10.1016/j.agrformet.2019.107886.

Sharma V., D. R. Rudnick and S. Irmak, (2013). "Development and evaluation of ordinary least squares regression models for predicting irrigated and rainfed maize and soybean yields," *Trans. ASABE*, vol. 56, no. 4, pp. 1361–1378, doi: 10.13031/trans.56.9973.

Shetty S., P.K. Gupta, M. Belgiu and S. K. Srivastav (2021). "Assessing the effect of training sampling design on the performance of machine learning classifiers for land cover mapping using multi-temporal remote sensing data and google earth engine," *Remote Sens.*, vol. 13, no. 8, doi: 10.3390/rs13081433.

Virnodkar S.S., V. K. Pachghare, V. C. Patil and S. K. Jha (2020). "Remote sensing and machine learning for crop water stress determination in various crops: a critical review," *Precis. Agric.*, vol. 21, no. 5, pp. 1121–1155, doi: 10.1007/s11119-020-09711-9.

Journal of Geomatics Vol. 17, No. 2, October 2023

Monitoring Dynamics of Sprawling Bhopal "An Emerging Metropolitan"

Durgesh Kurmi*[1], Divya Patel[2]
[1]Department of Geography, Institute for Excellence in Higher Education, Bhopal, M.P.
[2]Department of Chemistry, Swamy Vivekanand Government P.G. College, Narsinghpur, M.P.

(Received: 22 May 2023; in final form 9 August 2023)

DOI: *https://doi.org/10.58825/jog.2023.17.2.87*

Abstract: Urban growth is a spatial and demographic process. Hasty rate of urban expansion pose endangerment to surrounding natural escape which is termed as sprawl. Data extracted from Landsat 5 TM 1991, Landsat 5 TM 2001, Landsat 7 ETM 2011, Landsat 8 OLI 2020 imageries was utilized to quantify urban expansion of the Bhopal city, with respect to direction and pattern, from 1991-2021. A direct relationship between population and built-up area is established, which reflects urban sprawl. Statistical study and spatio-temporal analysis of the data is done to account for these changes. The research revealed that Bhopal City has majorly spread towards south and south-east directions in an uncontrolled manner, engulfing used productive cropped areas. Sprawling pattern has evolved from radial to leap-frogging, with time.

Keywords: Sprawl, Population, Built-up Area, GIS, Quantification, Bhopal.

1. Introduction

The term urban sprawl is largely used by scholars dealing with urban development and its pattern. Researchers including environmental activists, town planners, demographers and geographers show keen interest in study of sprawl because of its multidisciplinary impacts (Ansari 2000; Franz et al. 2005). Smart cities as identified by Govt. of India, city capitals, cities with historical value and metropolitan cities are major centre of attraction, as they grow faster than other cities. Bhopal being a state capital, smart city and area of historical value has many attributes which makes it a desirable location to be identified for study, but still it credits very limited literature with regard to its sprawling (Aithal et al. 2014; Aithal et al. 2016; Bhattacharya et al. 2017;). Bhopal is the second largest city of the state of Madhya Pradesh (Pandey & Pandey 2016), built on a hilly area, having varied cultural and historical heritage. After Bhopal was made the capital of the state of MP in 1956 a number of central and state govt. offices were established and migration of people started (Census 1991). To make room for the offices and to develop residential accommodation, new constructions began in the area (Dhivya et al. 2015). Geographical expansion and socio-economic development of Bhopal, termed as urban sprawl, turned Bhopal into a vast metropolitan city. Sprawl is a broad topic which emphasizes on the outgrowth of a city on its border regions. This growth (sprawl) is unauthorized, low density, haphazard and auto-dependent (Banai et al. 2014). The area under urban sprawl is characterized by a condition where urban development unfavourably hampers with urban environment which is neither tolerable urban situation nor pertinent for an agricultural rural environment (Chandrasekar et al. 2010; Tiwari et al. 2017). Study of sprawl and its types gives a detailed picture about spatial forms of urban footprint.

Sprawl is observed to obstruct regional sustainable development and thus raise wide social concern (Bruegmann 2005). This topic is very relevant in current scenario as it deals with the development, growth and size of urban centres of Bhopal. The rapid growth of population has given rise to the increasing pace of urbanization, by which there has been a significant migration of population from rural areas to urban areas in search of better livelihood (Aithal et al. 2016). This phenomenon has completely changed the demographic, social, physical and cultural landscape.

With time, techniques to analyze sprawl have evolved from manual mapping to GIS (Geographical Information system). GIS has developed rapidly, bringing many new capabilities and innovations in spatial planning (Epsteln et al. 2002; Bhatta et al. 2012). GIS has literally brought the world in our pockets. GIS is explored for planning and community development (Bhatta et al. 2009). Mapping population density and spatial distribution based on Satellite imagery facilitates in population planning (Batty et al. 2001; Bhatta et al. 2010). These advanced techniques are implied in this work to make accurate analysis about the spatial expansion of Bhopal city in the period of 1991 to 2021. The study further aims to do calculative analysis of sprawl and study the causative factors responsible for urban sprawl. In our previous work, the effect of sprawl on health and environment has been studied, now we have taken the study of the impact of sprawl to some other walks of human life and environment viz demographic, social, cultural and economic characteristics of the city.

Database – Secondary and tertiary (RS data) data have been used for the present study. However, field observations were also undertaken for verification of ground level realities. The following is the list of data sources employed in this study:

- Survey of India Toposheet No. F43/F7, F8, scale 1:50,000
- Census of India, 1991, 2001, 2011.
- Gazetteers of Bhopal District
- Town and Country Office record, Bhopal
- Municipality Corporation Office record, Bhopal
- Department of Statistic record, Bhopal
- Town Directory record, Bhopal
- Master Plan of Bhopal 1991, 2005, 2031 (Draft)
- LANDSAT 5 TM 1991, LANDSAT 5 TM 2001 and LANDSAT 7 ETM 2011, LANDSAT OLI 2020 (USGS portal)
- Google Earth Imagery

2. Methodology

The study is spread over a period of 30 years from 1991 to 2021. An integrated geo-spatial approach i.e. Remote sensing and GIS in conjunction with secondary data has been adopted in the study. The remote sensing and GIS data were handled with the help of ERDAS Imagine (Product developed by Leica Geosystems) and ArcGIS (Product developed by ESRI).

To create the maps of Bhopal for different decades, demarcating sprawling of Bhopal, toposheets were downloaded from website of Survey of India. Landsat Imageries were acquired from USGS portal and Bhopal Master Plan was procured from department of Town and Country Planning, Bhopal. The Survey of India toposheet no. F43/F7 & toposheet no. F43/F8 with scale of 1:50,000 were scanned. Using these toposheets, georeferencing of satellite imageries viz. Landsat 5 TM 1991, Landsat 5 TM 2001, Landsat 7 ETM 2011, Landsat 8 2020 were performed, followed by geometric correction using ERDAS Imagine 9.2 software. Approximately, 40 ground control points were selected in order to register the images to the Universal Transverse Mercator (UTM) coordinate system WGS 84 Datum. The shapefile was then created in ArcGIS. Thus, Geo-database for needed data was created. Images were then pre-processed including Image Rectification, Image Enhancement, Atmospheric Error correction and Image Destriping. Post processing of images they were classified using unsupervised methods creating signature file. Then, supervised classification was carried out using land use and land cover variable. Further ground truth reality was verified by Earth Google and the overall result was drawn. Finally, maps depicting sprawl of Bhopal metropolitan were prepared and decadal changes were studied. The detailed methodology is demonstrated in Figure 1.

3. Study Area

Bhopal is situated along 77º 25’ E longitude and 23º 15’N latitude (Bhopal Master Plan, 2005). It is located in Huzur tehsil of Bhopal district. The city consists of old city, Tatya Tope Nagar, Bairagarh, Bharat Heavy Electrical Limited and a large number of nearby villages. Situated at an elevation of 550-600m (Bhopal Master Plan, 2005) above sea level, the city has a beautiful surroundings of low hills and large lakes. Location of Bhopal city is shown in Figure 2. Most of the city is situated on the Malwa plateau and to the south lies the main line of the Vindhyas, with the fertile valley of the Narmada beyond it. Having 85 wards, covering a gross area of ~285 km^2 (Bhopal Municipal Corporation) including the lakes and hills, the city is a low-density city of 50 persons per hectare (PPH). Even if the areas of steep hills and the lake area of 38 km^2 are discounted, the density on habitable land remains low at 80 PPH (Dasgupta et al. 2013).

Bhopal as we see now has seen many phases of development under different rulers beginning from Raja Bhoj (Bhopal-State-Gazetteer-Vol-III.), passing on to Nawabs and the British Rule. King Vikramaditya desired to develop Bhopal around the Om Valley, but the development shifted towards the lake (Bhopal-State-Gazetteer-Vol-III). Old Bhopal as we see now, including Islamnagar, Jahangirabad, Peer Gate etc. was developed in the reign of Nawabs. Post-independence, after Bhopal was carved out as the capital of the state of Madhya Pradesh, TT Nagar, Govindpura, BHEL etc. were developed. This development marks the beginning of expansion of Bhopal, or sprawling of Bhopal. At the time of the preparation of the Bhopal Development Plan 1991, the city had already expanded to the north and the southeast.

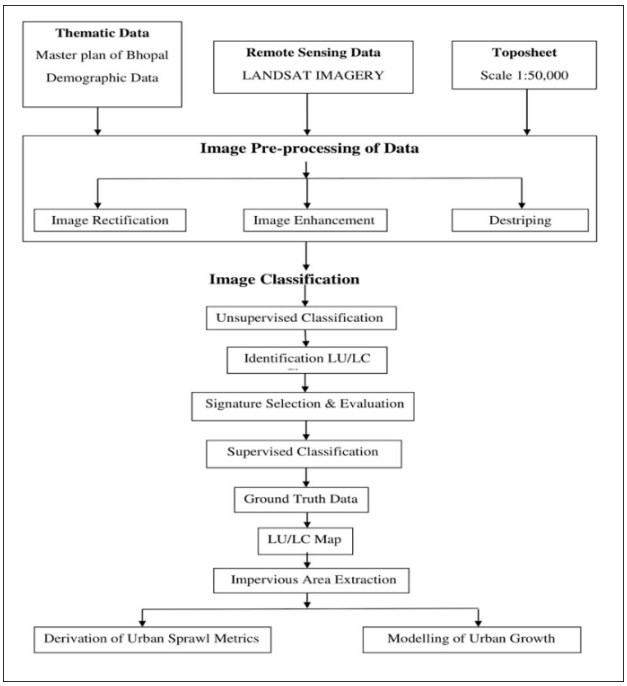

Figure 1. Flowchart explaining the steps followed to construct spawal and landuse map from GIS software

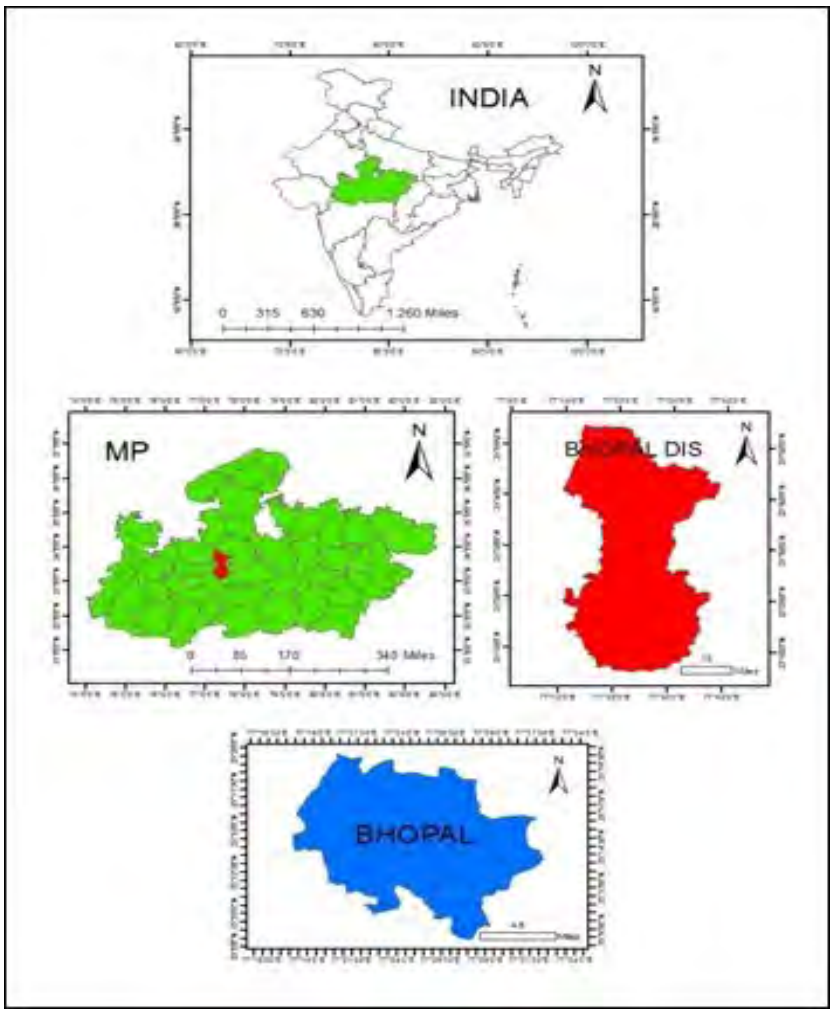

Figure 2. Location map of Bhopal district

4. Result and Discussion

Human built-up environment and natural environment, altogether makes ecosystem. Urban sprawl can be broadly studied by analysis of these two basic parameters over a period of time. Analysis of built-up area along with urban and rural fringe is a potential and a precise parameter that indicates sprawling (Brueckner 2000). This is then influenced by other parameters such as, population growth rate, migration, industrial development (Pareta et al. 2015) etc. Sprawl is influenced by the population in a particular region. To have a better view of how the city grows over time, and to drive a statistical illustration of urbanization, there is need to choose quantitative measures (Deal et al. 2004), which will summarize one or more characteristics that define urban sprawl. Quantification of sprawl is done by calculating the ratio of total population to the total built-up of the area under study, in a defined time zone.

In the present study, the analysis of expansion has been done on census year or decadal basis, in which population related data has been calculated from population district census handbook and construction area through GIS. Built-up area boundary is calculated from Master plan of Bhopal and Satellite data for 1991, 2001, 2011 and **2020**. The built up areas and population for all three time periods is represented in Table 1. This data depicts clear and better illustration of urban statistics of Bhopal city.

Post emergence of Bhopal as state capital in 1956, built-ups kept growing continuously with every decade, however, the growth reported was highest in the time frame of 1991-2001. By the year 2011, Bhopal had expanded horizontally with growth in built-up area. The population growth rate declined in this decade by -8.19%, mainly due to the formation of the state of Chhattisgarh from the state of Madhya Pradesh. Emergence of a new state capital caused migration from Bhopal metropolis to newly formed state of Chhattisgarh. There has been a rapid growth in the construction sector during this decade, showing a speedy sprawl. Growth rate for last decade seems to be nearly constant, both for population and built-up land. In these 10 years, the construction area of the city has increased at the average rate of 14.24 km^2 per year, which is the highest decadal increase so far.

Later from 2001-2011 the change in built-up area was comparatively low and nearly constant for the next two decades, viz. 100.63% & 107.38%, respectively, indicating rise in vertical growth along with horizontal expansion. Similar trend is observed for population growth in the last 2 decades. Population grew with time however the growth rate appears to be controlled in the later decades. This implied that growth in built-up areas was in commensurate with growth in population of the city.

Table 1 Built-up area of Bhopal city (1991-2001)

Decade	Built-up area (km^2)	Change in Built-up area from previous decade (km^2)	Percentage change w.r.t. previous decade	Population	Change in Total Population w.r.t. previous decade	Percentage change over the previous decade
1991	15.80	-	-	1,062,018	-	-
1991-2001	66	50.20	317.72	1,458,416	3,96,398	37.32
2001-2011	132.42	66.42	100.63	1,883,381	4,24,965	29.13
2011-2021	274.62	142.2	107.38	23,90,000*	5,06,619	26.89

Source: Population data – Census 1991, 2001, 2011 & Approximated data 2021 by Bhopal Master plan 2031

Table 2. Change in Built-up area and Population of Bhopal City (1991-2021)

Year		1991	2001	2011	2021
Total Built-up Area		15.8	66	132.42	274.62
Change in the Built-up Area from Base Year 1991	Area in sq km	-	50.2	116.42	258.82
	Area in percentage	-	317.72	736.83	1638.10
Total Population		1,062,018	1,458,416	1,883,381	23,90,000*
Change in the Population from Base Year 1991	Population	-	396,398	821,363	1,327,982
	Population in percentage	-	37.32	77.34	125.04

Source: Population data – Census 1991, 2001, 2011 & Approximated data 2021 by Bhopal Master plan 2031

A comparative analysis of Table 2 clearly shows that- rise in population appears to be quite insignificant as compared to built ups, percentage wise, but it's comparable when the figures are equated. This can be understood by studying per capita land consumption in the respective time scales. Overall in 30 years the population increased by 13, 27, 982 with an average change of 44, 266.06 person per year. In this line, another parameter of sprawl, i.e., built up land increased by 258.82 km^2 from 1991 to 2021, and urban area stretched annually by about 8.62 km^2 in the period of our study. Growth in the construction sector is synonymous with urban expansion. The fact that urban expansion is influenced by population growth is established. Population rise is a clear reason for rise in built-up areas, an indicator of sprawl. To support this fact, statistical analysis of the above data has been made.

4.1 Statistical Analysis -

A linear graph has been drawn for the effectual understanding of the built-up and demographic dynamics of Bhopal in spatio-temporal context. Above stated factors are further supported by these graphs. Discussing first about the change in built-up area, the deviation of slope from a perfect straight line ($R^2 < 1$) explains inconsistent change in built-up area with time. When we see the decadal change in built-ups, in the first decade it increased more than 4 times of the initial area available, accounting for highest % change i.e. 317.72%. After that in each decade built-up land of Bhopal almost doubled, i.e. 100% increase, to cater its growing needs. A sudden burst in built-up area by 50 km^2 from 1991 to 2001 can be devoted to development of Upper Lake for tourism purposes in the western side of the city on the highway connecting Bhopal with Indore. Also, new residential areas came into existence during this time. Although the city has expanded in all directions, the main growth was along the eastern parts of the city along National Highway No. 46. In the south east direction an industrial area was developed by the State govt. of the city. The Madhya Pradesh State Industrial, and Infrastructure Development Corporation has developed an Industrial Model Township on the Southern side of the city, a region which was prevented from development till 2001 due to its geographical design.

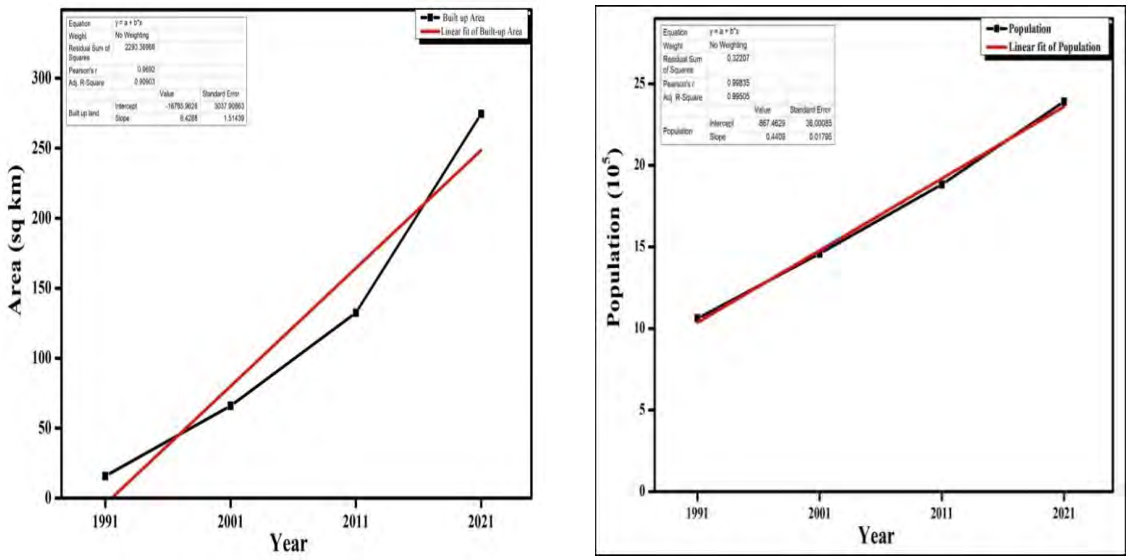

Figure 3. Comparative trend of built-up area and population

Study of slope value (8.4288) from 2011-2021 is highest than others, indicating that in last 10 years the built-up area has increased phenomenally i.e. ~142km^2 which is maximum in the 3 decades. Although growth rate was highest for the first decade, but from 2011-2021, Bhopal's potential was explored the most in all fields. Before this period although being a capital, Indore was preferred more by people of the state for job and educational purposes. By 21st century Bhopal became a city of choice for industrial, educational and service sectors.

Population of Bhopal has increased almost constantly with time, showing a perfect linear fitting, with a R2 value of 0.999. This means average population change does not show much variation. The tentative population change for 2021 is also supposed to follow this trend, and fall in this same line.

Rate of population growth is plotted against different decades in Figure 3 This is however a declining graph, where slope value is 0.4409 with regression coefficient (R2) equals to 0.99505 Though population has increased decade by decade, but the rate is slower in comparison with its previous decade. In relation to constantly rising population in these decades the positive aspect was that the growth rate did not rise instead it decreased with every decade. The population growth rate for the last decade based on the estimated population deviates from this slope. Although the growth rate is lesser than the previous decade, contrary to this it has dropped with a slower pace. From 2001-2011 population growth rate dropped by 8%, whereas from 2011-2021 it is estimated to drop only by 3% approximately. However, even with the falling growth rate, the population increase was huge enough to invoke urban expansion and consecutive sprawling of Bhopal city. Socio-ecological factors are equally valuable for accounting population change. Like, Bhopal gas tragedy in 1984 caused a huge mortality rate (Litt et al. 2017), thereby bringing a downfall in 1991 population count. The steepness of slope changes for next decade, showing a greater declining growth rate in 2001, is awarded to the state of Chhattisgarh being carved out and separated from Madhya Pradesh prompting migration of many government employees to the newly formed state.

Spatial and Temporal Changes: Urban sprawl is characterized by change in spatio-temporal characteristics of the area. Its overall a spatial and demographic phenomenon, occurred due to concentration of population within a specific society and economy (Li et al. 2012). Population trends in the city and urban sprawl refer to the area expansion of urban concentration beyond what they have been. This rise in population in turn demands more residential land and hence affects land cover within and around the urban area including forest cover, green cover, agricultural land, waste land, water bodies etc. (Alaguraja, P., et al. 2010) This demand is compensated either by discrete construction in urban fringes or multi-storied constructions within the city and filling the gaps in the urban space. The job of accommodating the growing population and making enough space for all is carried out by the department of town planning. The team based on GIS data and Remote Sensing images, prepares a future map to deal with the future needs, and this involves study of spatial and temporal structures in morphology of the city. Sprawling of Bhopal in terms of built-up area and land cover for different decades is shown in Figure 4.

.

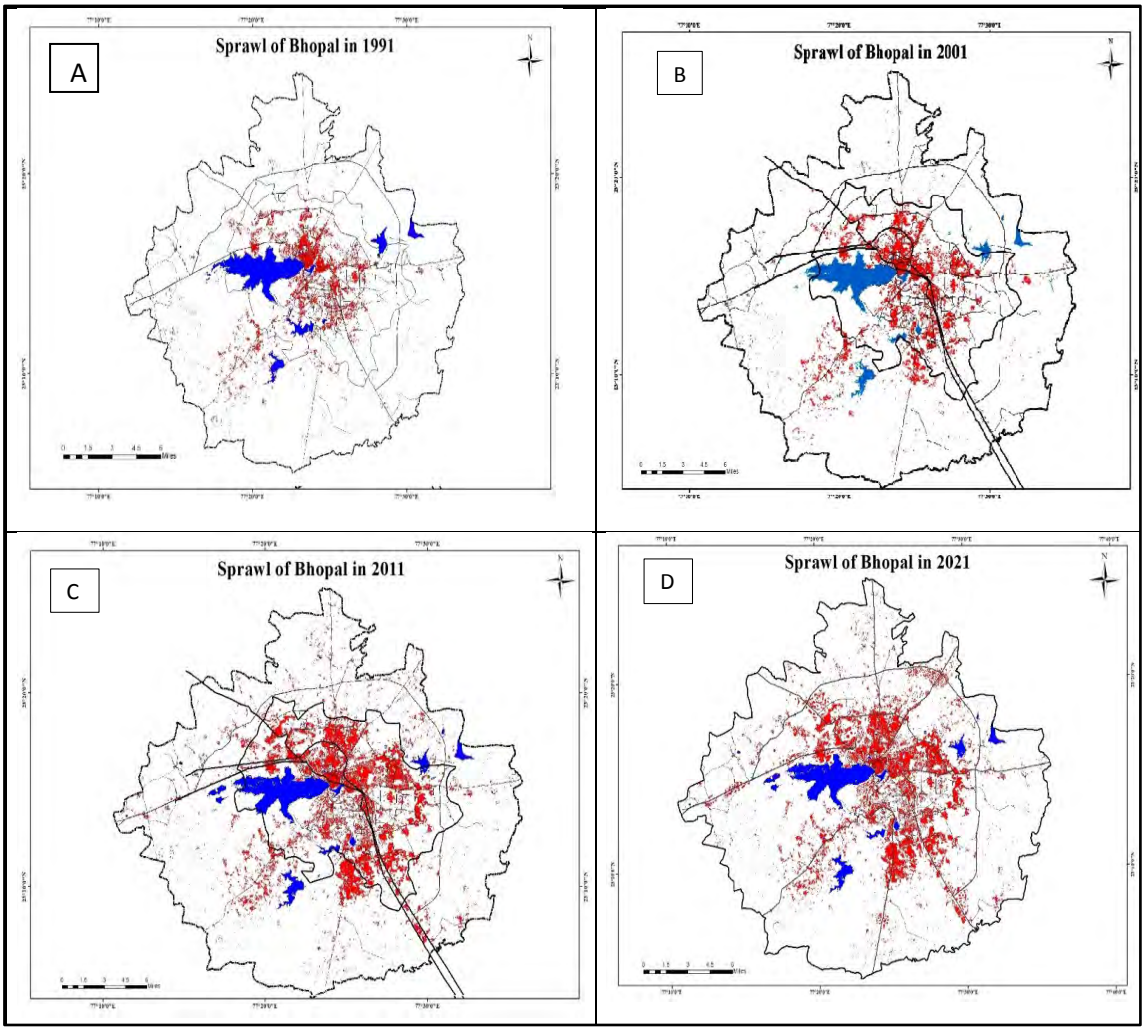

Figure 4. Decadal Change in Built-up Area

Sprawling pre-1991: Till 1991, the total population of city - 1,062,018 was spread over total built-up area of 15.8 km^2, as reported. Remote sensing images of Bhopal district display semi-radial development around CBD, until 1991. The pressure of continuously expanding city centres, when gradually affects the associated environment and neighbourhoods, around the edge of the core, is termed as radial contiguous sprawl. Often, CBD is the urban area which is most densely populated. Old Bhopal was the only CBD of the city. In radial sprawling, development of the peripheral area of the CBD (Central business district) takes place coupled with city roads. An excessive construction work from Old Bhopal towards the outer boundary demarcates urban expansion in pre-1991.

All sorts of facilities viz residential, commercial, health, entertainment etc. got concentrated in the core of the city. The area in and around city centre became densely populated. Rise in degree of residential inaccessibility served as an impetus for people to settle at urban fringes of the Bhopal district. To cater the lack of functional space initially, new colonies began to develop in unplanned and isolated form known as termed as breed or diffusion growth

Spatial temporal Sprawl: From 1991 to 2001 – There has been a rapid growth in the construction sector during this decade. Where the total built up area was 15.8 sq km in 1991, it increased to 66 sq km in 2001, showing rapid expansion of the city. Data table and GIS images altogether display that during 1991 to 2001, the built-up area grew at the rate of 5.02 sq. km per annum with a tenuous growth of 317.72 percent. The main reason for the rapid expansion during this period was the successful implementation of Bhopal Development Plan 1991 by the state government. Many development schemes were implemented in the city, as a part of the Development Plan which became the reason for prompt expansion.

The construction work before 1991 was mainly unplanned, except for that in the BHEL residential area. After 1991 BHEL stretched in the east towards Raisen Road, in the North East towards Vidisha Road (bypass); and in the southeast towards Misrod along the Hoshangabad Road fragmented expansion of the city is observed. The direction of enlargement of the city is determined by its geographical distribution. Presence of lake in the south-west hindered growth of city in that direction.

Satellite imageries of Bhopal for 1991 to 2001 confirmed the major developments took place alongside the lower lake. In the southern periphery Berasia road, in south east direction Pratap Nagar and Old Subhash Nagar on the Hoshangabad road alongwith NH-12 were affected by

expansion of Old Bhopal. This semi-circular development occupied BHEL Township in East and Sagar-Raisen road (NH-86) in North East of Bhopal. Growth of Lalghati from Old city besides the upper lake in the north-west completes the semi-radial pattern of development.

Spatial temporal Sprawl: 2001-2011 - A decadal growth of 100.63 per cent is observed in this decade. The total construction area during this period increased to 132.42 sq km with an increase of 66.42 sq km at the rate of 6.64 sq km per annum. As stated before, declined growth rate in this decade, is mainly due to the division of the state of Chhattisgarh from the state of Madhya Pradesh. Due to this, the state capital was changed, resulting in the migration of people from Bhopal metropolis to Raipur, also there was a decline in rural migration towards Bhopal.

Studying the spatio-temporal changes from 2001 to 2011, by aid of remote sensing images show that in south eastern direction development took place along NH-12 from Railway colony to Misrod and in northwest this highway extended besides lake along Vallabh Nagar. In the south eastern side of Bhopal sprawl is visible in Avadhpuri, Jharkheda, Shobhapur, Toomda, Mandideep, Obaidullaganj and ThunaKalan areas. Development was also observdbeside Kolar road marks expansion in the southern direction. NH 86 was also hit by sprawling in the northeast face as a consequence to whichKainchiChola, Navjivan Colony, Nawab Colony, Devki Nagar, NariyalKheda along by-pass and area around Trilanga were affected by it. NH-18 in the western direction of Bhopal spread across Lalghati into Pooja Shree Nagar, Hemu Colony etc.

Spatial temporal Sprawl: 2011-21 - There was a decadal growth of 107.38% during this time period. In this time, the construction area of the city has increased at the rate of 14.24 sq. km per year, which is the highest increase in decades so far. The total construction area during this period increased to 274.62 sq km with an increase of 142.2 sq km. Many new urban settlements have come out of Bhopal city and are part of the city. These small or big new urban centers are clear results of the leapfrogging expansion of the Bhopal city.

Misrod, Mandideep Industrial Hub, Kolar, Kotra Sultanabad, Anand Nagar, Lalghati, Bairagarh etc. are the areas which are result of sprawling in previous decade and have become so densely populated that they itself popped out as core areas for further stretching out of the city. For example, Golden city, Shri Ram Colony, Sneh Nagar, Bhairopur have developed around Misrod expanding the south western boundary of Bhopal along NH-12. Another well-known characteristic of this sprawl is it favours development of parcels located further out in the counties over the empty lands adjacent to existing development (Torrens et al. 2000). A few developments around Kolar in the South can also be named out from the map- Sarvadharam colony, Mahabali Nagar, Shridipuram, Banjari, GehunKheda, Rajharsh colony etc. Kamla Nagar, Gomti Colony, Type-9, C-Sector, Dwarikapuri colony are the areas developed with respect to Kotra Sultanabad along Bilkisganj road. The eastern boundary of the city has expanded around Anand Nagar area in the form of Siddharth Lake City, Press colony, Gopalnagar, Sukhsagar etc. NH-18 in the northwest side of Bhopal also shows immense growth.

Leapfrogging creates functional decentralization and haphazard development patterns in fringe areas. This development consumes large amount of land and causes land fragmentation. This growth is characterized by dispersed development of residential, semi-public and industrial area. With the advancement in time, these sprawling patterns show interconversion due to rapid growth. Here we can see how radial contiguous sprawl in 2001 and ribbon development in 2011 has converted to leapfrog development in 2021 for the case of Bhopal city.

5. Conclusion

This research conceptualized urban sprawl from a geographic perspective in order to assess the spatial distribution of sprawl patterns. In this work, with the use of GIS and remote sensing technology an attempt has been made to study the criteria and patterns of expansion of state capital of Madhya Pradesh with respect to direction in the recent three decades. An alteration in spatial-temporal pattern of urban area from radial to leap-frogging via linear is seen. It also helped to understand the need of built up area for the growing city and the way in which the demand is being fulfilled. Bhopal has proved to be good example for quite a planned expansion compatible with sustainable development. However, there is further need to zoom in this study to particular targeted areas, to understand the nature of development of those locations. Apart from population and built-up land, there are many other reasons which visibly support this phenomenon- such as rise in expenditure, capacity, living standard, transportation cost etc. Future study could be directed towards studying these supporting factors and widespread effects of sprawl. There is further scope to analyze changes in land use pattern as a consequence of urban sprawl. This will give a clear idea of how demographic transitions have lead to the shaping of the city into this present metropolitan landscape.

References

Aithal H.B., K.T.K. Kalal, V. Rao and T.V. Ramachandra (2014), Modelling of Urban Dynamics in Bhopal, Sahyadri Conservation Series 47. http://ces.iisc.ernet.in/energy

Aithal H.B.S. and T.V. Vinay Ramachandra (2016), Agent Based Modelling Urban Dynamics of Bhopal, India, Journal of Settlement and Spatial Planning, 7, 1-14.

Alaguraja P., S. Durairaju, D. Yuvaraj, M. Sekar, P. Muthuveerran, M. Manivel and A. Thirunavukkarasu (2010), Land use and land cover mapping-Madurai District, Tamilnadu, India using remote sensing and GIS techniques. International Journal of Civil and Structural Engineering, 1(1), 91–100.

Ansari A.S. (2000), Urban renewal and development: A case of Hyderabad, Rawat Publication, Jaipur, 25-31.

Banai R. and T. DePriest (2014), Urban Sprawl: Definitions, Data, Methods of Measurement and

Environmental Consequences, Journal of Sustainability Education, Vol. 7, 22.

Batty M. and D. Howes (2001), Predicting Temporal Patterns in Urban Development from Remote Imagery in Donnay, J.P., Barnsley, M.J., Longley, P.A. (eds.), Remote Sensing and Urban Analysis, 185–204, Taylor and Francis, London.

Bhatta B. (2012), Urban Growth Analysis and Remote Sensing: A Case Study of Kolkata, India 1980-2010, Springer Science & Business Media, Publishing Press, 103.

Bhatta B. (2010), Analysis of Urban Growth and Sprawl from Remote Sensing Data, Advance in Geographic Information Science, Heidelberg, New York.

Bhatta B. (2009), Analysis of Urban Growth Pattern Using Remote Sensing and GIS: A Case Study of Kolkata, India, International Journal of Remote Sensing, Volume 30 (18) 4733-4746.

Bhattacharya A. and R. Shubhangi (2017), Dynamic Growth of Bhopal City Core: A Conceptual and Legal Approach, International Journal on Emerging Technologies, 8(1), 608-613.

Bhopal Development Plan (1991), Directorate of Town & Country Planning, Madhya Pradesh.

Bhopal Development Plan (2005), Directorate of Town & Country Planning, Madhya Pradesh.

Bhopal Development Plan (2031), Directorate of Town & Country Planning, Madhya Pradesh.

Bhopal State Gazetteer 2015, Vol-III, Calcutta Superintendent Government Printing, India, 123735.

Bhopal Municipal Corporation, DIMTS, (2012), Draft Report on Comprehensive Mobility Plan for Bhopal.

Bruegmann R. (2005), Sprawl: A Compact History, The University of Chicago Press, Chicago and London, (6), 301.

Brueckner J. (2000), Urban Sprawl: Diagnosis and Remedies, International Science Regional Review, (23) 160-171.

Census of India (1991), District Census Handbook, Directorate of Census Operations, Bhopal, MP.

Census of India (2001), District Census Handbook, Directorate of Census Operations, Bhopal, MP.

Census of India (2011), District Census Handbook, Directorate of Census Operations, Bhopal, MP.

Chandrasekar N., P. Sivasubramanian and J.P. Soundranayagam (2010), Ecological Consequences of Rapid Urban Expansion: Tirunelveli, India, African Journal of Basic and Applied Sciences, 2 (5-6), 167-176.

Dasgupta T. (2013), Waste Management in Bhopal Municipal Corporation Issues and Perspective, International Journal of Scientific Engineering and Technology, 2 (9), 807-810.

Deal B. and D. Schunk (2004), Spatial Dynamic Modeling and Urban Land Use Transformation: A Simulation Approach to Assessing the Costs of Urban Sprawl, Ecological Economics, 51(1–2), 79–95.

Dhivya B., S.S. Niranjan, J. Sarup and K. Dharavath (2015), Mapping of Impervious Surface Using Spectral Angle Mapper (SAM) and NDVI Techniques, Case Study: Bhopal City, Indian Journal of Science and Technology, (8) 28.

Epsteln J., K. Payne and E. Kramer (2002), Techniques for Mapping Suburban Sprawl, Photogrammetric Engneering & Remote Sensing, 63(9), 913–918.

Franz G., G. Maier and P. Schröck (2005), Urban Sprawl How useful is this concept ?, European Regional Science Association., 1–29.

Li F. and A. Nanjing (2012), Investigation of Urban Sprawl on the Basis of Remote Sensing Data - A Case Study in Jiangning , Nanjing City , China, Unpublished.

Litt L.S.D. and R. Kumar (2017), Emerging Pattern of Urbanization and Economic Development in Madhya Pradesh, International Journal on Arts Management and Humanities. 6(2), 97–105.

Pandey A.K. and A. Pandey (2016), Madhya Pradesh Samany Gyan Sandarbh, Madhya Pradesh Hindi Granth Academy, 2nd Edition, 71.

Pareta K. and U. Pareta (2015), Urban Sprawl Mapping using Multi-Sensor and Multi-Temporal Satellite Remote Sensing Data & GIS, International Journal of Scientific Research in Science, Engineering and Technology. 1(1), 263–271.

Tiwari A. and V. Goel (2017), URBAN SPRAWL Causes, Effects and Remedies for Indian cities, IOSR Journal of Environment Science, Toxicology and Food Technology, 11(11), 61–67.

Torrens P.M. (2000), Measuring Sprawl, Centre for Advanced Spatial Analysis, University College, London, Casa, 6-7

A comparative analysis of machine learning algorithms for land use and land cover classification using google earth engine platform

Abhijit Patil[1]* and Sachin Panhalkar[1,2]
[1]Department of Geography, Shivaji University, Kolhapur, India.
[2]Center for Climate Change and Sustainability Studies, Shivaji University Kolhapur, India
*Email: abhijitpatil8893@gmail.com

(Received: 4 June 2023; in final form 17 October 2023)

DOI: *https://doi.org/10.58825/jog.2023.17.2.96*

Abstract: This study evaluates different machine learning algorithms for land use and land cover classification using Sentinel-2 Level-1C data with 10-meter spatial resolution. The algorithms include Random Forest (RF), Classification and Regression Trees (CART), Support Vector Machines (SVM), Naive Bayes (NB), and Gradient Boosting (GTB). The classification was performed on the Google Earth Engine (GEE) platform. Results highlight variations in land cover classification among algorithms, with RF and CART identifying cropland as dominant, SVM indicating fallow land presence, NB revealing significant forest cover, and GTB emphasizing cropland importance. Accuracy assessment was performed to evaluate the performance of the algorithms, considering metrics such as producer accuracy, consumer accuracy, overall accuracy, and Kappa coefficient. SVM demonstrates the highest overall accuracy and agreement with reference data. The study contributes insights for land management and planning, and GEE proves valuable for LULC classification.

Keywords: LULC, GEE, Machine Learning, Kolhapur

1. Introduction

Land Use and Land Cover (LU/LC) classification is a pivotal aspect of understanding the dynamic changes occurring on Earth's surface. Over the years, these changes have been influenced by a multitude of factors, including urbanization, agricultural expansion, industrialization, and climate variations (Turner et al., 2015). Accurately mapping and monitoring these transformations are crucial for informed decision-making in fields such as urban planning, environmental management, and natural resource conservation (Foody et al., 2013). This paper aims to shed light on the evolution of LU/LC classification methodologies, highlighting the pivotal role of remote sensing technology and the recent advancements in machine learning algorithms.

The advent of remote sensing technology has revolutionized the field of LU/LC classification. It has enabled researchers to collect and analyze vast amounts of data, providing a comprehensive view of Earth's surface across various temporal and spatial scales (Xie et al., 2019). Remote sensing data, acquired through satellites such as Landsat, MODIS, and Sentinel, have become invaluable sources for extracting critical information about land cover and its changes over time (Roy et al., 2014; Wulder et al., 2016; Gómez et al., 2016). These datasets offer a rich and diverse source of information, facilitating detailed analysis and monitoring of LU/LC patterns.

Over the past few decades, researchers have successfully harnessed the power of remote sensing imagery to create accurate and up-to-date LU/LC maps, capitalizing on its wide availability, comprehensive coverage, and ease of use (Stromann et al., 2019). However, generating such maps for large regions has presented challenges, including the need for substantial data storage, processing capacity, and diverse analytical approaches (Xie et al., 2019). Addressing these challenges led to the emergence of platforms like Google Earth Engine (GEE).

Before the introduction of GEE, various platforms were employed for LU/LC mapping, each with its own set of limitations. For example, while some platforms offered extensive datasets, they often lacked the computational power required for efficient processing (Shelestov et al., 2017; Pimple et al., 2018). Others provided robust processing capabilities but had limited access to high-quality remote sensing data sources. These constraints hindered the ability to produce accurate and timely LU/LC maps.

GEE was introduced as a game-changer in the realm of LU/LC mapping. This cloud-based platform seamlessly integrates an extensive collection of Earth observation data from various sources with high-performance computing services, enabling efficient processing of satellite imagery (Gorelick et al., 2017; Sidhu et al., 2018; Kolli et al., 2020). GEE offers access to a wide array of freely available satellite imagery, including datasets from sources such as Landsat, Sentinel, and MODIS (Shelestov et al., 2017; Pimple et al., 2018). It provides user-friendly interfaces in JavaScript and Python, facilitating the development and implementation of customized algorithms for satellite imagery processing and LU/LC mapping.

In light of these considerations, this study aims to leverage the power of GEE and conduct a comparative analysis of various machine learning algorithms for LU/LC classification using Sentinel-2 Level-1C data with a 10-meter spatial resolution. The research focuses on elucidating how different algorithms capture LU/LC variations and contribute to the advancement of mapping techniques. It seeks to address the critical question of which machine learning algorithm achieves the highest

accuracy in LU/LC classification, offering valuable insights for land management, planning, and environmental monitoring.

In this context, it is essential to explore and compare the performance of different machine learning algorithms in LU/LC classification (Level 1), with a focus on the area of interest in the present study, the Kolhapur City Region. By assessing the advantages and limitations of these algorithms, this research seeks to provide valuable insights for land management, planning, and environmental monitoring.

Through this investigation, we intend to demonstrate not only the efficacy of machine learning algorithms but also the importance of platforms like GEE in harnessing the full potential of remote sensing technology for LU/LC classification in a dynamic world.

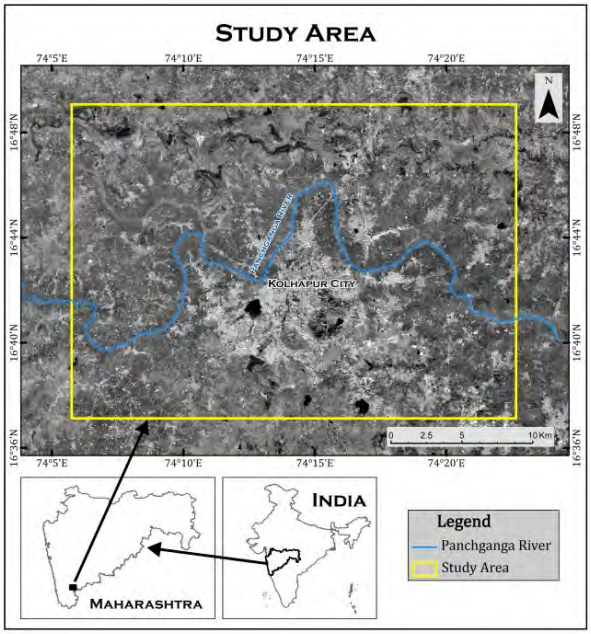

Figure 1. Location of study area

2. Study Area

The study area selected for this research comprises the surrounding region of Kolhapur city, situated in the south-western part of Maharashtra state, India. This region extends between 16° 37' 8" to 16° 49' 4" North latitude and 74° 5' 45" to 74° 22' 39" East longitude (Figure.1), covering an approximate area of 662 km².

Kolhapur city, renowned for its historical and cultural heritage, is strategically located on the southern bank of the Panchganga River within this study area. It serves as the central urban hub, experiencing rapid growth and urbanization. The choice of Kolhapur as the area of interest in this study is driven by its significance as a dynamically evolving urban center in the region.

In addition to the urban and agricultural areas, the study area includes significant natural features such as forests, water bodies, and barren land. These natural areas play a vital role in biodiversity conservation and maintaining ecological balance by providing habitat for a diverse range of plant and animal species.

The study area experiences distinct seasonal variations in rainfall, with the monsoon season typically extending from June to September. The annual average rainfall of this region is 1010mm. It is important to note that rainfall is a pivotal factor influencing land use and land cover dynamics in the region. It impacts agricultural practices, water availability, and natural ecosystems.

Regarding the physiography of the study area, it includes a diverse range of landscapes, from urban and agricultural plains to natural features such as forests and water bodies. The rapid growth of Kolhapur city and the surrounding region contributes to the changing physiography, making it an ideal location for studying land use and land cover dynamics.

3. Data and Methods

The systematic flow of the research methodology is depicted in Figure 2, illustrating the sequential steps undertaken in the study.

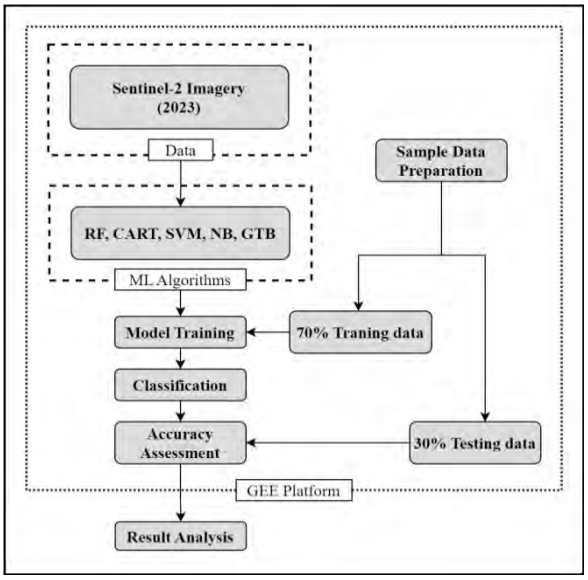

Figure 2. Research methodology

3.1 Data

The cloud-based GEE platform stores an extensive collection of Earth observation data (EOD) spanning over the past four decades. This vast dataset includes satellite images from platforms like Sentinel, Landsat, and MODIS, as well as other geospatial data such as climate and demographic information. Within the GEE platform, users have access to a wide range of EOD, including Sentinel data. This comprehensive data repository allows researchers to leverage a diverse array of satellite imagery and ancillary data to analyze and understand various aspects of the Earth's surface.

In the present study, Sentinel-2B (MSI) Level-1C satellite imagery from 05-03-2023 was utilized. To ensure data quality, only datasets with minimal cloud cover, constituting less than 10 percent of the total data, were

selected for analysis. For image classification purposes, three specific bands, namely Green (B3), Red (B4), and Near-Infrared (B8), from the Sentinel-2 dataset were employed. These bands have a spatial resolution of 10 meters, allowing for detailed and accurate classification of land use and land cover patterns within the study area.

3.2 Sample Selection

In supervised learning, training data plays a vital role, and a significant number of samples are typically required for most machine learning algorithms. However, obtaining accurate reference data from satellite imagery can be a challenging and complex task (Chi et al., 2008). The process of delineating and acquiring reference data involves identifying and labeling specific land cover classes within the satellite imagery, which can be a time-consuming and labor-intensive process.

In recent literature, the practice of utilizing separate training and testing datasets is widely adopted in the development of LULC classification models. Typically, a common ratio of 70% training data and 30% testing data is followed (Naceur et al., 2022; Huang et al., 2022; Wang et al., 2020). These reference sample points were generated based on high-resolution Google Earth images. For the current study, a total of six land cover classes were identified, and a total of 300 sample points were collected, with 50 sample points per class. Out of these, 35 sample points (Figure 3a) were designated for training the models, while the remaining 15 sample points (Figure 3b) were kept aside for the purpose of accuracy assessment. This practice ensures that the models are trained on a substantial amount of data, allowing them to learn the patterns and characteristics of the land cover classes. The testing dataset, comprising unseen data points, is used to evaluate the performance and generalization capability of the trained models.

3.3 Methods for Classification

The present study utilized the GEE platform to train classifiers for Sentinel-2 imagery by employing five different machine learning algorithms: Random Forest (RF), Classification and Regression Trees (CART), Support Vector Machine (SVM), Naive Bayes (NB), and Gradient Tree Boosting (GTB).

CART is a binary decision classification tree algorithm developed by Breiman (Breiman et al., 1984). It is a popular machine learning algorithm that enables straightforward decision-making in logical if-then scenarios. CART is a decision tree-based algorithm that recursively splits the data based on selected features to create a tree structure for classification or regression tasks. CART is advantageous for its interpretability and simplicity in visualizing and understanding the decision-making process. In the current study, the "*ee.Classifier.smileCart*" technique, GEE library, was employed to perform CART classification.

RF is an ensemble learning algorithm that combines multiple decision trees to make predictions. It is widely recognized for its ability to handle high-dimensional data and capture complex relationships between features and classes. The algorithm was first proposed by Leo Breiman (Breiman, 2001). One of the main advantages of Random Forest is its ability to reduce overfitting and improve generalization. In RF, the number of parameters and trees are two important factors that significantly impact the performance of the algorithm. These parameters are user-defined and can be adjusted based on the specific problem and dataset. The literature suggests that the optimal number of trees in a Random Forest typically ranges from 100 to 500 (Belgiu & Dragu, 2016). Having a larger number of trees can improve the model's accuracy, but there is a diminishing return as the number of trees increases. In the present study, 300 trees were selected as a compromise between computational efficiency and achieving a sufficiently accurate classification. In the current study, "*ee.Classifier. smileRandomForest*" technique as a GEE library, was employed to perform RF classification.

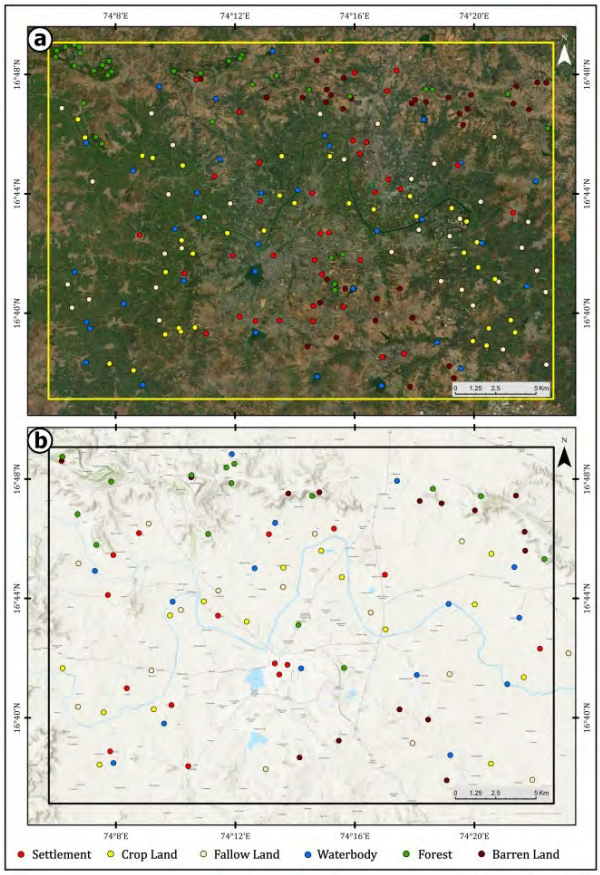

Figure 3. Training Samples (a) Testing Samples (b)

SVM is a machine learning technique that leverages the statistical learning theorem to identify an optimal higher-dimensional space by mapping the original input space. SVM finds an optimal hyperplane to separate different classes by maximizing the margin between them. This technique was initially introduced by Vapnik (Vapnik, 1995) and further developed by Cortes and Vapnik (Cortes & Vapnik, 1995) in the same year. The main parameters for selecting support vectors are the cost parameter C, Gamma, and kernel functions (Hsu et al., 2003). SVM offers several advantages for LULC classification. It can effectively handle non-linear relationships between input features and land cover classes by utilizing kernel

functions. In the current study, "*ee.Classifier.libsvm*" technique as a GEE library, was employed to perform SVM classification.

NB is a probabilistic classifier that assumes independence among features given the class and calculates the probability of each class given the input features using Bayes' theorem. Despite its simplicity, NB can perform well in various classification tasks, especially when the independence assumption holds reasonably well (John & Langley, 1995). NB is computationally efficient and can handle large datasets with high-dimensional feature spaces. It remains a popular choice for classification tasks, including LULC classification, due to its computational efficiency and effectiveness in certain scenarios. In the present study, "*ee.Classifier.smileNaiveBayes*" technique as a GEE library, was employed to perform NB classification.

GTB is a machine learning algorithm proposed by Jerome Friedman (Friedman, 1999). GTB is a boosting algorithm that combines multiple weak classifiers, usually decision trees, to create a strong ensemble model. GTB iteratively adds new trees to correct the errors made by previous trees, resulting in improved predictive accuracy. GTB is particularly effective in handling complex relationships and can capture non-linear interactions between features. In the present study, "*ee.Classifier.smileGradientTreeBoost*" technique as a GEE library, was employed to perform GTB classification.

3.4 Accuracy Assessment

Accuracy assessment is an essential step in evaluating the performance of LULC classification models. In this study, several metrics were used to assess the accuracy of the classification results, including producer accuracy, consumer accuracy, overall accuracy and Kappa coefficient. A total of 90 samples, with 15 samples for each class, were utilized for accuracy assessment purposes. These metrics allow for a comprehensive evaluation of the classification performance and provide insights into the reliability and effectiveness of the LULC classification models.

4. Result and Discussion

4.1 LULC Classification using GEE

This study investigated the performance of different machine learning techniques for land use and land cover (LULC) classification using Sentinel-2 Level-1C data with a spatial resolution of 10 meters. Figure 4 demonstrate how machine learning algorithms such as RF, CART, SVM, NB and GTB were used for the classification of LULC maps for 2023 on the GEE platform. The LULC classification focused on six major classes: settlement, cropland, fallow land, waterbodies, forest and barren land. The RF classification revealed that cropland occupied a significant land area of 266 square kilometers, accounting for 40% of the total area. This highlighted the agricultural dominance in the study area. However, compared to the other algorithms, RF had the second lowest land area for cropland. Waterbodies accounted for only 8 square kilometers (1% of the total area), indicating limited water resources in the study area. The CART classification showed an even larger land area dominated by cropland, covering 371 square kilometers (56% of the total area). This result further emphasized the agricultural dominance. Similar to the RF classification, waterbodies accounted for only 7 square kilometers (1% of the total area). The SVM classification identified a higher land area for the fallow land class, covering 120 square kilometers (18% of the total area). This indicated a significant presence of fallow land in the study area. Conversely, the settlement class had a relatively smaller land area of 99 square kilometers (15% of the total area). The NB classification produced a higher land area for the forest class, covering 219 square kilometers (33% of the total area). This indicated a significant presence of forests in the study area. However, the fallow land class had a relatively smaller land area of only 14 square kilometers (2% of the total area). It is important to note that the NB algorithm tends to classify fallow land into other classes, resulting in a lower land area for this category. The GTB classification revealed that cropland occupied a significant land area of 326 square kilometers (49% of the total area), making it the highest among all the algorithms for this class. Waterbodies accounted for 9 square kilometers (1% of the total area), representing the lowest land area among all the algorithms for this class.

The results of the LULC classification using different machine learning algorithms provided valuable insights into the land cover distribution in the study area (Figure 5). The RF and CART classifications consistently identified cropland as the dominant land cover class, highlighting the agricultural dominance in the region (Table 1). The SVM classification showcased a significant presence of fallow land, indicating land management practices in the study area. The NB classification revealed a substantial forest cover, while the GTB classification confirmed the importance of cropland in the landscape.

These variations in land cover classifications among the algorithms can be attributed to their inherent differences in modeling approaches and parameter settings. Each algorithm has its strengths and weaknesses in capturing specific land cover characteristics. Therefore, the choice of algorithm should be carefully considered based on the research objectives and the characteristics of the study area.

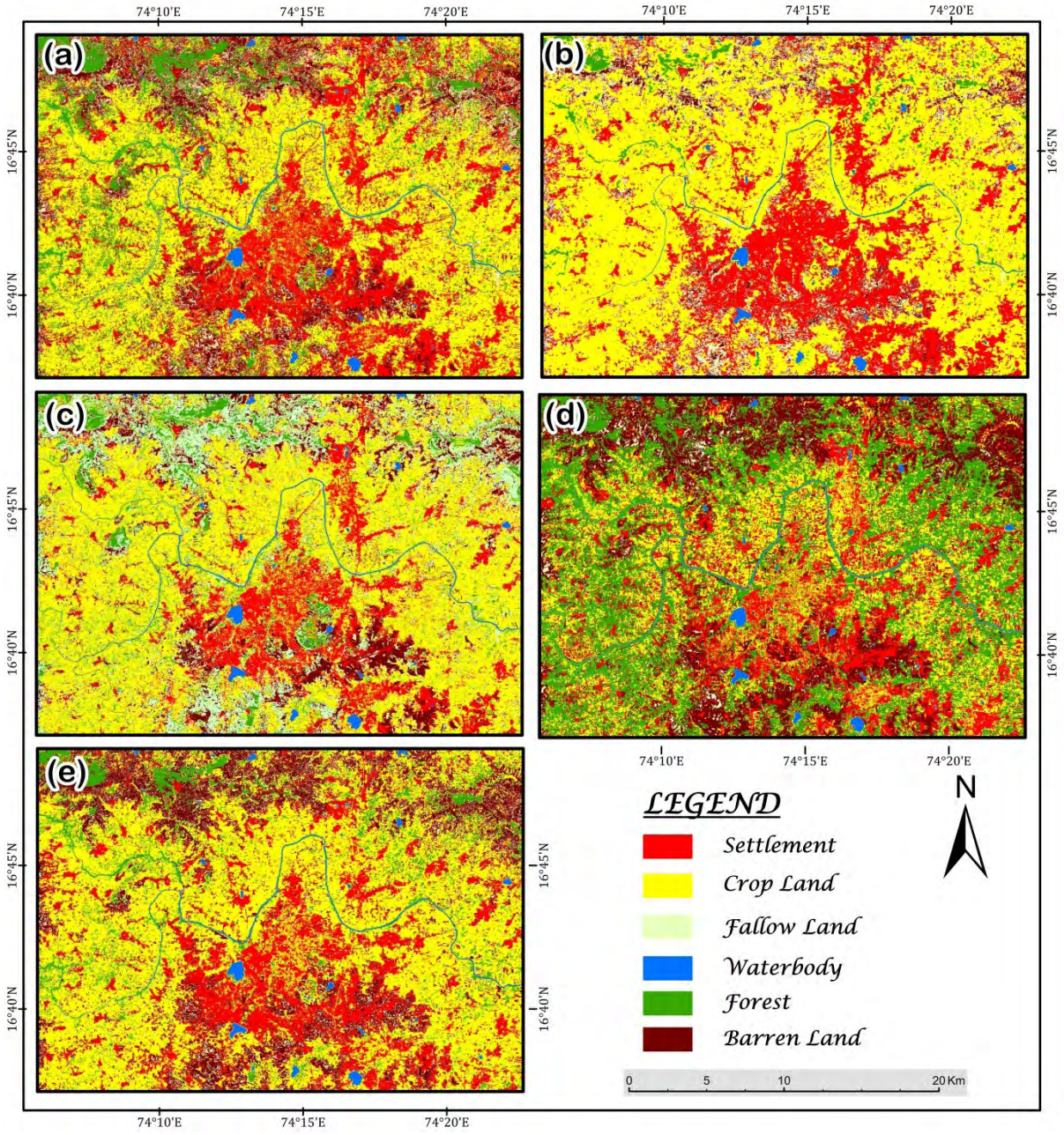

Figure 4. LULC classification (a) RF (b) CART (c) SVM (d) NB (e) GTB

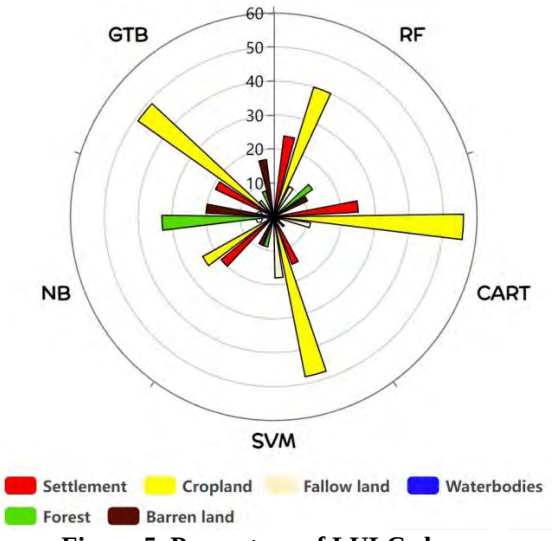

Figure 5. Percentage of LULC classes

4.2 Accuracy Assessment

The accuracy assessment was conducted to evaluate the performance of the machine learning algorithms in classifying land use and land cover (LULC) categories. The assessment involved calculating producer accuracy and consumer accuracy for each class, as well as overall accuracy and Kappa coefficient. Producer accuracy measures the correctness of classifying pixels belonging to a specific class. The results of the producer accuracy analysis for each algorithm are presented in Table 2. For the settlement class, RF, CART, SVM, and NB algorithms achieved high producer accuracy scores of 0.93, indicating accurate classification of settlement areas. GTB algorithm achieved a perfect producer accuracy score of 1. Cropland classification showed varied results among the algorithms. RF and SVM achieved high producer accuracy scores of 0.93, indicating accurate classification. CART had a relatively lower score of 0.8, while NB and GTB showed scores of 0.66 and 1 respectively.

Table.1: Percentage of LULC classes

Class/Algorithm	RF	CART	SVM	NB	GTB
Settlement	24.42	25.00	14.98	19.59	18.84
Cropland	40.16	56.10	47.96	24.43	49.27
Fallow land	9.84	11.01	18.18	2.06	5.93
Waterbody	1.14	1.05	1.13	1.18	1.32
Forest	13.81	2.40	8.84	33.07	7.59
Barren land	10.63	4.44	8.90	19.67	17.05
Total	**100**	**100**	**100**	**100**	**100**

Fallow land classification showed consistent high producer accuracy scores across most algorithms, ranging from 0.86 to 0.93. SVM achieved a perfect score of 0.93. Waterbodies were accurately classified by all algorithms, with producer accuracy scores ranging from 0.86 to 0.93. Forest classification results varied among the algorithms, with RF and SVM achieving high producer accuracy scores of 0.93 and 1 respectively. CART and NB showed lower scores of 0.73 and 0.53, while GTB achieved a perfect score of 1. Barren land classification had varied results, with RF achieving a producer accuracy score of 0.8, CART scoring 0.33, SVM scoring 0.93, NB scoring 0.86, and GTB scoring 0.6.

Consumer accuracy measures the correctness of classifying pixels that were labelled by reference data. The results of the consumer accuracy analysis for each algorithm are presented in Table 3. For the settlement class, RF, CART, and SVM algorithms achieved perfect consumer accuracy scores of 1, indicating accurate classification of settlement areas. NB and GTB algorithms achieved scores of 0.77 and 0.93 respectively. Cropland classification showed varied results among the algorithms. RF and SVM achieved relatively high consumer accuracy scores of 0.87 and 0.93 respectively. CART had a lower score of 0.63, while NB and GTB showed scores of 0.55 and 1 respectively. Fallow land classification showed varied results, with consumer accuracy scores ranging from 0.59 to 0.93. SVM achieved the highest score of 0.93. Waterbodies were accurately classified by all algorithms, with perfect consumer accuracy scores of 1. Forest classification results varied among the algorithms, with RF achieving a consumer accuracy score of 0.87, CART scoring 0.78, SVM scoring 0.93, NB scoring 0.8, and GTB scoring 0.88. Barren land classification had varied results, with RF achieving a consumer accuracy score of 0.92, CART scoring 0.71, SVM scoring 0.87, NB scoring 0.86, and GTB scoring 0.9.

Overall accuracy provides an assessment of the overall correctness of the classification results, while Kappa coefficient measures the agreement between the classification results and the reference data. Among the algorithms, SVM achieved the highest overall accuracy score of 0.94, indicating a high level of accuracy in classifying the LULC categories. RF, NB, and GTB algorithms achieved overall accuracy scores of 0.91, 0.8, and 0.9 respectively (Figure 6). CART algorithm had a lower overall accuracy score of 0.76. SVM also achieved the highest Kappa coefficient of 0.93, indicating a substantial agreement between the classification results and the reference data. RF, NB, and GTB algorithms achieved Kappa coefficients of 0.89, 0.86, and 0.88 respectively. CART algorithm had a lower Kappa coefficient of 0.72 (Figure 6).

These accuracy assessment results provide valuable insights into the performance of different machine learning algorithms for LULC classification. The SVM algorithm demonstrated the highest accuracy and agreement with the reference data, indicating its effectiveness in accurately classifying the LULC categories in the study area.

Table 2: Producer accuracy

Class/ Algorithm	RF	CART	SVM	NB	GTB
Settlement	0.93	1	0.93	0.93	1
Cropland	0.93	0.8	0.93	0.66	1
Fallow land	0.93	0.86	0.93	0.86	0.93
Waterbodies	0.93	0.86	0.93	0.93	0.86
Forest	0.93	0.73	1	0.53	1
Barren land	0.8	0.33	0.93	0.86	0.6

Table 3: Consumer accuracy

Class/ Algorithm	RF	CART	SVM	NB	GTB
Settlement	1	1	1	0.77	0.93
Cropland	0.87	0.63	0.93	0.55	1
Fallow land	0.82	0.59	0.93	0.86	0.73
Waterbodies	1	1	1	1	1
Forest	0.87	0.78	0.93	0.8	0.88
Barren land	0.92	0.71	0.87	0.86	0.9

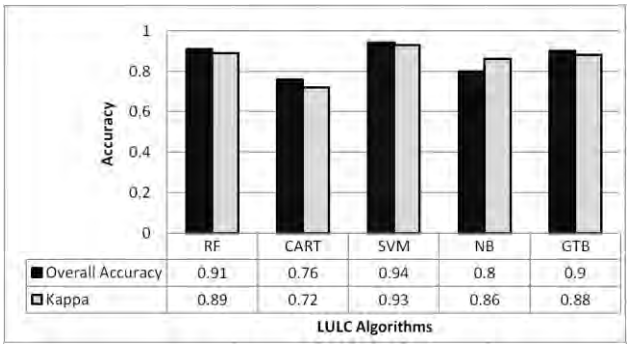

Figure 6. Overall accuracy and kappa coefficient

5. Conclusion

The primary objective of this study was to analyze the performance of various machine learning algorithms in the context of LU/LC classification using Sentinel-2 Level-1C data. Our findings shed light on the significant agricultural dominance within the study area, with cropland emerging as the dominant land cover class. Additionally, the study revealed the presence of fallow land, forests, and waterbodies, adding depth to our understanding of the landscape.

One of the key takeaways from this research is the pivotal role that the choice of algorithm plays in the classification outcomes. Our results underscore the importance of selecting the most suitable algorithm based on specific research objectives and the unique characteristics of the study area. It is evident that different algorithms excel in capturing distinct aspects of the landscape, which has implications for the accuracy and applicability of land cover classification results.

Furthermore, our accuracy assessment demonstrated the effectiveness of the SVM algorithm in accurately classifying the various land cover categories. This highlights the relevance of SVM in LU/LC classification tasks, but it should also encourage researchers to carefully consider algorithm selection for their own studies.
In conclusion, this research contributes valuable insights that hold significance for land management, urban planning, and environmental monitoring purposes. The dynamic interplay between machine learning algorithms and LU/LC classification results offers a fertile ground for further investigation and validation. Future research endeavors should aim to refine and expand upon these findings to enhance the accuracy and applicability of LU/LC classifications in diverse geographic regions.

Conflict of Interest
The authors confirm that there is no conflict of interest.

References

Belgiu M. and L.Dragu (2016). Random Forest in Remote Sensing: A Review of Applications and Future Directions. ISPRS Journal of Photogrammetry and Remote Sensing, 114, 24-31.

Breiman L. (2001). Random Forests. Machine Learning, 45, 5-32. https://doi.org/10.1023/A:1010933404324

Breiman L., J.H. Friedman, R.A. Olshen and C.J. Stone (1984). Classification and Regression Trees (1st ed.). London, UK: Routledge.

Chi M., R. Feng and L. Bruzzone (2008). Classification of Hyperspectral Remote-sensing Data with Primal SVM for Small-sized Training Dataset Problem. Advances in Space Research, 41(11), 1793-1799.

Cortes C. and V. Vapnik (1995). Support-Vector Networks. Machine Learning, 20(3), 273-297. https://doi.org/10.1007/bf00994018

Foody G.M., L. See, S. Fritz, M. Van der Velde, C. Perger, C. Schill, ... & F. Kraxner (2013). Assessing the accuracy of volunteered geographic information arising from multiple contributors to an internet based collaborative project. Transactions in GIS, 17(6), 847-860.

Friedman J.H. (1999). Greedy Function Approximation: A Gradient Boosting Machine. Annals of Statistics, 1189-1232.

Gómez C., J.C. White and M.A. Wulder (2016). Optical Remotely Sensed Time Series Data for Land Cover Classification: A Review. ISPRS Journal of Photogrammetry and Remote Sens, 116, 55-72.

Gorelick N., M. Hancher, M. Dixon, S. Ilyushchenko, D. Thau and R. Moore (2017). Google Earth Engine: Planetary-Scale Geospatial Analysis for Everyone. Remote Sensing of Environment, 202, 18-27.

Hsu C.W., C.C. Chang and C.J. Lin (2003). A Practical Guide to Support Vector Classification. Technical Report, Department of Computer Science and Information Engineering, University of National Taiwan, Taipei, Taiwan.

Huang W., M. Ding, Z, Li, J. Zhuang, J. Yang, X. Li, L. Meng, H. Zhang and Y. Dong (2022). An efficient user-friendly integration tool for landslide susceptibility mapping based on support vector machines: SVM-LSM Toolbox. Remote Sensing, 14(14), 3408. https://doi.org/10.3390/rs14143408

John G.H. and P. Langley (1995). Estimating Continuous Distributions in Bayesian Classifiers. In Proceedings of the Eleventh Conference on Uncertainty in Artificial Intelligence (pp. 338-345).

Kolli M.K., C. Opp, D. Karthe and M. Groll (2020). Mapping of Major Land-Use Changes in the Kolleru Lake Freshwater Ecosystem by Using Landsat Satellite Images in Google Earth Engine. Water, 12, 2493.

Naceur H. A., A.G. Hazem, I. Brahim, N. Mustapha, A. Hussein, A.A.D. Ahmed and A, Motrih (2022). Performance assessment of the landslide susceptibility modeling using the support vector machine, radial basis function network, and weight of evidence models in the

N'fis River basin, Morocco. Geoscience Letters, 9(1). https://doi.org/10.1186/s40562-022-00249-4

Uday P., S. Dario, S. Asamaporn, P. Sukan, L. Kumron, S. Henry , S. Jaturong , G. Valery and T. Sirintornthep (2018). Google Earth Engine Based Three Decadal Landsat Imagery Analysis for Mapping of Mangrove Forests and Its Surroundings in the Trat Province of Thailand. Journal of Computational Comm., 6, 247-264.

Roy D.P., M.A. Wulder, T.R. Loveland, C.E. Woodcock, R.G. Allen, M.C. Anderson, D. Helder, J.R. Irons, D.M. J ohnson, R. Kennedy, T.A. Scambos, C.B. Schaaf, J.R. Sc hott, Y. Sheng, E.F. Vermote, A.S. Belward, R. Bindscha dler, W.B. Cohen, F. Gao, J.D. Hipple and Z. Zhu (2014). Landsat-8: Science and Product Vision for Terrestrial Global Change Research. Remote Sensing of Environment, 145, 154-172.

Shelestov, A., L. Mykola, K. Nataliia, N. Alexei and S. Sergii (2017). Exploring Google Earth Engine Platform for Big Data Processing: Classification of Multi-Temporal Satellite Imagery for Crop Mapping. Frontiers in Earth Science, 5, 17.

Sidhu N., E. Pebesma E and G. Câmara (2018). Using Google Earth Engine to Detect Land Cover Change: Singapore as a Use Case. European Journal of Remote Sensing, 51, 486-500.

Stromann, O., A. Nascetti, O. Yousif and Y. Ban (2019). Dimensionality reduction and feature selection for object-based land cover classification based on Sentinel-1 and Sentinel-2 time series using Google Earth Engine. Remote Sensing, 12(1), 76.

Turner W., S. Spector, N. Gardiner, M. Fladeland, E. Sterling and M. Steininger (2015). Free and open-access satellite data are key to biodiversity conservation. Biological Conservation, 182, 173-176.

Vapnik V. (1995). The Nature of Statistical Learning Theory. https://doi.org/10.1007/978-1-4757-2440-0.

Wang G., L. Xinxiang, C. Chen, S. Himan and S. Ataollah (2020). Hybrid computational intelligence methods for landslide susceptibility mapping. Symmetry, 12(3), 325. https://doi.org/10.3390/sym12030325.

Wulder M.A., C.W. Joanne, R.L. Thomas, E.W. Curtis, S.W. Alan, B.C. Warren, A.F. Eugene, S. Jerad. G.M. Jeffrey and D.P. Roy (2016). The Global Landsat Archive: Status, Consolidation, and Direction. Remote Sensing of Environment, 185, 271-283.

Xie, S., L. Liu, X. Zhang, J. Yang, X. Chen, X. and Y. Gao (2019). Automatic Land-Cover Mapping Using Landsat Time-Series Data Based on Google Earth Engine. Remote Sensing, 11(23), 23.

Author Index (Vol. 17)

INDIAN SOCIETY OF GEOMATICS: AWARDS

National Geomatics Award for Excellence

This award has been instituted to recognize outstanding and conspicuously important contribution in promoting geomatics technology and applications at the country level. The contributions should have made major impact on the use of this technology for national development.
Areas of contribution considered for the award are:

1. Geographical Information System
2. Global Positioning System
3. Photogrammetry
4. Digital Cartography
5. Applications of Geomatics

The award shall consist of Rs. 50,000/- in cash, a medal and citation.

Eligibility

Any citizen of India, engaged in activities related to geomatics technology and its applications is eligible for this award. The prize is awarded on the basis of work primarily done in India.

The age limit for awardees is 45 years or above as on June 30 of the year of award.

Selection

A duly constituted Award Committee will evaluate all nominations received. The committee shall consist of eminent experts in the field of geo-spatial technology, to be identified by the Executive Council, ISG. The committee shall forward selected name/s to ISG – EC for approval and announcement. Apart from those persons, whose nominations have been received, the Committee may consider any person or persons who, in their opinion, have made outstanding contributions to development of geo-spatial technology and applications.

The award can be withheld in any year if, in the opinion of the committee, no candidate is found suitable in that particular year.

Presentation of the Award

The award shall be presented during the Annual Convention of ISG. Local Hospitality shall be taken care by ISG & Air fare (low cost) may be reimbursed if awardees request for it.

How to make Nomination

The nominations can be proposed by Head of a major research institute/ centre; Vice-Chancellor of a university; Secretary of Government Scientific Departments; President of a National Academy, President, Indian Society of Geomatics / Indian Society of Remote Sensing / Indian National Cartographic Association / ISG fellow or two life members of the society with more than 10 year old membership.

A candidate once nominated would be considered for a total period of two years. Nomination should be sent in the prescribed format to Secretary, ISG.

The last date for receiving nominations shall be September 30 or otherwise extended.

Format for nomination of Geomatics Award for Excellence

1. Name of the Nominee
2. Postal Address
3. Academic Background (Bachelor degree onwards)
4. Field of Specialisation
5. Important positions held (in chronological order)
6. Professional Experience including foreign assignments.
7. Important Awards / Honours
8. Important Publications/Patents: (A set of ten most important publications to be enclosed with this form)
9. Contributions of Nominee based on which the nomination is sent (in 1000 words, also provide a statement
   in 50 words which may be used for citation.):
10. Other Relevant Information:

Proposer:

Signature
Name
Address
Phone/ Fax
E-mail
Life Membership No. (in case of ISG Member):

Place & Date

Endorsed by (in case nomination is by 2 ISG Life members)

Signature
Name
Address
Phone/ Fax
E-mail
Life Membership No. (in case of ISG Member):

Place & Date
(The proposer should give a brief citation of the nominee's work)

National Geomatics Award

National Geomatics Award to be given each year: a) for original and significant contribution in Geomatics technology, b) for innovative applications in the field of Geomatics. Each award comprises a medal, a citation and a sum of Rs 25,000/- The guidelines for these awards are available on ISG website.

ISG Chapter Award for Best Performance

The best chapter award will be given to an active chapter of Indian Society of Geomatics, which has made significant contribution to further the mandate and goal of the society. The award consists of a citation and medal

President's Appreciation Medal for Contribution to the ISG

This award will be given to a member of the society, who has made noteworthy contribution to the growth of the ISG (its main body or any chapter). The Award consists of a Medal and a Citation.

Prof. Kakani Nageswara Rao Endowment Young Achiever Award

Indian Society of Geomatics instituted a new award from year 2013 named "Prof. Kakani Nageswara Rao Endowment Young Achiever Award", to encourage young researchers/scientists/academicians pursuing research in the field of geospatial technology/applications. The award carries a cash prize of Rs. 10,000/- along with a citation.

NATIONAL GEOMATICS AWARD

Indian Society of Geomatics has instituted two National Geomatics Awards to be given each year for (a) Original and significant contribution in Geomatics technology, (b) Innovative application(s) in the field of Geomatics. Each award comprises a medal, a citation and a sum of Rs. 25,000/-.

The guidelines for the award are as under

Areas of contribution considered for the award (both technology and applications)

1. Geographical Information System
2. Global Positioning System
3. Photogrammetry
4. Digital Cartography
5. Remote Sensing

Eligibility

Any citizen of India engaged in scientific work in any of the above-mentioned areas of research is eligible for the award.

The awards are to be given for the work largely carried out in India.

- First award will be given for original contribution in the field of Geomatics technology supported by publications in a refereed journal of repute.
- Second award will be given for carrying out innovative application(s). Supported by publications in rear reviewed Journals of repute.
- The contribution for the first award should have been accepted by peers through citation of the work.
- Work based on the applications of existing technologies will not be considered for the first award.
- The work should have made impact on the overall development of Geomatics.

How to Send Nomination

Nominations should be sent in the prescribed format, completed in all aspects to the Secretary, Indian Society of Geomatics, Space Applications Centre Campus, Ahmedabad 380 015 by August 31 of the year of award.

Selection Process

An expert committee, consisting of at least three members, constituted by the Executive Council of the Indian Society of Geomatics, will scrutinize the nominations and recommend the awardees' names to the Executive Council. The Council will decide on the award based on the recommendations.

FORMAT FOR AWARD NOMINATION

1. Name of the Candidate:
2. Present Position:
3. Positions held earlier (chronological order):
4. Academic qualifications (Bachelor's degree onwards):
5. Names of at least three Indian Scientists/Technologist in the area as possible referees *:
6. Brief write up on the work (500 words) for which award is claimed:
7. Publication(s) on the above work (reprint(s) to be enclosed):
8. List of other publications of the candidate:
9. Citation of the work for which award is claimed:
10. Impact of the work (for which award is claimed) on the development in the field of Geomatics (500 words):
11. Whether the work has already won any award? If so, give details:

The Applications in the above format (five copies) should be submitted (by Registered Post or Speed Post) to

The Secretary, Indian Society of Geomatics,
Space Applications Centre Campus,
Ahmedabad-380015

so as to reach by September 30 of the year of award

*ISG is, however, not bound to accept these names and can refer the nomination to other experts/peers

INDIAN SOCIETY OF GEOMATICS: FELLOWS

Shri Pramod P. Kale, Pune
Dr George Joseph, Ahmedabad
Dr A.K.S. Gopalan, Hyderabad
Dr Prithvish Nag, Varanasi
Dr Baldev Sahai, Ahmedabad
Shri A.R. Dasgupta, Ahmedabad
Dr R.R. Navalgund, Bengaluru
Shri Rajesh Mathur, New Delhi
Dr Ajai, Ahmedabad
Prof P. Venkatachalam, Mumbai
Dr Shailesh Nayak
Prof I.V. Murli Krishna
Prof SM Ramasamy, Tiruchirapalli
Dr Ashok Kaushal, Pune
Shri A.S. Kiran Kumar, Bengaluru
Prof. P.K. Verma, Bhopal
Maj. Gen. Siva Kumar, Hyderabad
Dr A S Rajawat, Ahmedabad
Dr Shakil Romshoo, Srinagar

INDIAN SOCIETY OF GEOMATICS: PATRON MEMBERS

P-1 Director, Space Applications Centre (ISRO), Jodhpur Tekra Satellite Road, Ahmedabad - 380 015
P-2 Settlement Commissioner, The Settlement Commissioner & Director of Land Records-Gujarat, Block No. 13, Floor 2, Old Sachivalay, Sector-10, Gandhinagar – 382 010
P-3 Commissioner, Mumbai Metropolitan Region Development Authority, Bandra-Kurla Complex, Bandra East, Mumbai - 400 051
P-4 Commissioner, land Records & Settlements Office, MP, Gwalior - 474 007
P-5 Director General, Centre for Development of Advanced Computing (C-DAC), Pune University Campus, Ganesh Khind, Pune - 411 007
P-6 Chairman, Indian Space Research Organization (ISRO), ISRO H.Q., Antariksha Bhavan, New BEL Road,Bengaluru 560 231
P-7 Director General, Forest Survey of India, Kaulagarh Road, P.O. I.P.E., Dehra Dun – 248 195
P-8 Commissioner, Vadodara Municipal Corporation, M.S. University, Vadodara - 390 002
P-9 Director, Centre for Environmental Planning and Technology (CEPT), Navarangpura, Ahmedabad - 380 009
P-10 Managing Director, ESRI INDIA, NIIT GIS Ltd., 8, Balaji Estate, Sudarshan Munjal Marg, Kalkaji, New Delhi - 110 019
P-11 Director, Gujarat Water Supply and Sewerage Board (GWSSB), Jalseva Bhavan, Sector – 10A, Gandhinagar - 382 010
P-12 Director, National Atlas & Thematic Mapping Organization (NATMO), Salt Lake, Kolkata - 700 064
P-13 Director of Operations, GIS Services, Genesys International Corporation Ltd., 73-A, SDF-III, SEEPZ, Andheri (E), Mumbai - 400 096
P-14 Managing Director, Speck Systems Limited, B-49, Electronics Complex, Kushiaguda, Hyderabad - 500 062
P-15 Director, Institute of Remote Sensing (IRS), Anna University, Sardar Patel Road, Chennai - 600 025
P-16 Managing Director, Tri-Geo Image Systems Ltd., 813 Nagarjuna Hills, PunjaGutta, Hyderabad - 500 082
P-17 Managing Director, Scanpoint Graphics Ltd., B/h Town Hall, Ashram Road, Ahmedabad - 380 006
P-18 Secretary General, Institute for Sustainable Development Research Studies (ISDRS), 7, Manav Ashram Colony, Goplapura Mod, Tonk Road, Jaipur - 302 018
P-19 Commandant, Defense institute for GeoSpatial Information & Training (DIGIT), Nr. Army HQs Camp, Rao Tula Ram Marg, Cantt., New Delhi - 110 010
P-20 Vice President, New Rolta India Ltd., Rolta Bhavan, 22nd Street, MIDC-Marol, Andheri East, Mumbai - 400 093
P-21 Director, National Remote Sensing Centre (NRSC), Deptt. of Space, Govt. of India, Balanagar, Hyderabad - 500 037
P-22 Managing Director, ERDAS India Ltd., Plot No. 7, Type-I, IE Kukatpalli, Hyderabad - 500 072
P-23 Senior Manager, Larsen & Toubro Limited, Library and Documentation Centre ECC Constr. Gp., P.B. No. 979, Mount Poonamallee Road, Manapakkam, Chennai - 600 089.
P-24 Director, North Eastern Space Applications Centre (NE-SAC), Department of Space, Umiam, Meghalaya 793 103
P-25 Progamme Coordinator, GSDG, Centre for Development of Advanced Computing (C-DAC), Pune University Campus, Pune – 411 007
P-26 Chief Executive, Jishnu Ocean Technologies, PL-6A, Bldg. No. 6/15, Sector – 1, Khanda Colony, New Panvel (W), Navi Mumbai – 410 206
P-27 Director General, A.P. State Remote Sensing Applications Centre (APSRAC), 8th Floor, "B" Block, Swarnajayanthi Complex, Ameerpet, Hyderabad- 500 038
P-28 Director, Advanced Data Processing Res. Institute (ADRIN), 203, Akbar Road, Tarbund, Manovikas Nagar P.O., Secunderabad –500 009
P-29 Managing Director, LEICA Geosystems Geospatial Imaging Pvt. (I) Ltd., 3, Enkay Square, 448a Udyog Vihar, Phase-5, Gurgoan- 122 016
P-30 Director, Defense Terrain Research Limited (DTRL), Ministry of Defense, Govt. of India, Defense Research & Development Organisation, Metacafe House, New Delhi – 110 054
P-31 Chairman, OGC India Forum, E/701, Gokul Residency, Thakur Village, Kandivali (E), Mumbai – 400 101
P-32 Managing Director, ML Infomap Pvt. Ltd., 124-A, Katwaria Sarai, New Delhi – 110 016
P-33 Director, Rolta India Limited, Rolta Tower, "A", Rolta Technology Park, MIDC, Andheri (E), Mumbai – 400 093
P-34 Director, State Remote Sensing Applications Centre, Aizawl – 796 012, Mizoram

Instructions for Authors

The journal covers all aspects of Geomatics – geodata acquisition, pre-processing, processing, analysis and publishing. Broadly this implies inclusion of areas like GIS, GPS, Photogrammetry, Cartography, Remote Sensing, Surveying, Spatial Data Infrastructure and Technology including hardware, software, algorithm, model and applications. It endeavors to provide an international forum for rapid publication of developments in the field – both in technology and applications.

A manuscript for publication must be based on original research work done by the author(s). It should not have been published in part or full in any type of publication nor should it be under consideration for publication in any periodical. Unsolicited review papers will not be published.

The Editorial Board or the Indian Society of Geomatics is not responsible for the opinions expressed by the authors.

Language

The language of the Journal will be English (Indian). However, manuscripts in English (US) and English (British) are also acceptable from authors from countries located outside India.

Manuscript Format

Each paper should have a title, name(s) of author(s), and affiliation of each of the authors with complete mailing address, e-mail address, an abstract, four to six keywords, and the text. The text should include introduction/background, research method, results, discussion, followed by acknowledgements and references. The main text should be divided in sections. Section headings should be concise and numbered in sequence, using a decimal system for subsections. Figures, images and their captions should be inserted at appropriate points of the text. Figures, images and tables should fit in two column format of the journal. If absolutely necessary, figures, images and tables can spread across the two columns. Figures and images, however, should not exceed half a page in height. A title should be provided for each Table, Image and Figure. All figures and images should be in 600 dpi resolution and sized as per column/margin width. Authors must ensure that diagrams/figures should not lose easy readability upon reduction to column size. The SI (metric) units and international quantities should be used throughout the paper. In case measurements are given in any other system, equivalent measurements in SI (metric) units should be indicated in brackets.

Use MS Word with English (UK/US) or English (Indian) dictionary. The page size should be A4 paper, with 2 cm margin on all sides. Title, authors and affiliation should be centred. Abstract should be justified across margins. The manuscript text should be in two columns of 8.2 cm each with a gutter of 6mm between them. Use only Times New Roman fonts. Title should be 12 points bold. Authors and affiliation should be 9 points. All other text including headings should be 10 points. Heading numbering scheme should be decimal e.g. 1, 1.1, 1.2.3, etc. Headings should be in bold.

Normally length of a published paper should be about 6-10 pages in A4 size including figures. Use of illustrations in colour should be restricted and resorted to only where it is absolutely necessary and not for enhancing the look of the paper. If the number of colour illustrations exceeds five, authors' institution may be asked to reimburse the extra cost involved, which at current rates is about Rs. 2500 per coloured figure/diagram/plate/illustration.

Submission of Manuscript

Submissions should be in electronic form via email. The manuscript may be sent by email to editorjogisg@gmail.com. In exceptional cases hard copy submission in camera ready form may be allowed with the prior permission of the Chief Editor. Submission in any other form will be returned to the author. To speed up the review process, authors are advised to provide a list of three probable reviewers with their institutional address and e-mail IDs.

Guidelines for Citing References

Names of all cited publications should be given in full. No abbreviations should be used. Following procedure is to be adopted.

Journal Publications

Bahuguna, I.M. and A.V. Kulkarni (2005). Application of digital elevation model and orthoimages derived from IRS-1C Pan stereo data in monitoring variations in glacial dimensions, Journal of the Indian Society of Remote Sensing, 33(1), 107- 112. (to be referred to in the text as Bahuguna and Kulkarni (2005) or if more than two sets of authors are to be referred to, as (Bahuguna and Kulkarni, 2005; Jain et al., 1994)) When more than two authors are to be referred to, use Jain et al. (1994). However, in References, all authors are to be mentioned.

Publication in a Book

Misra, V.N. (1984). Climate, a factor in the rise and fall of the Indus Civilization – Evidence from Rajasthan and Beyond in Frontiers of the Indus Civilization (B.B. Lal and S.P. Gupta: Chief Editors) Books and Books, New Delhi, pp. 461-489

Papers Published in Seminar/ Symposium Proceedings

Jain, A., A.R. Shirish, M. Das, K. Das, M.C. Porwal, and P.S. Roy (1994). Remote Sensing and Geographic Information System – An approach for the assessment of biotic interference in the forest ecosystem. Proceedings. 15th Asian Conference on Remote Sensing, Bangalore, November 17-23, 1994, pp. 65-72.

Books

Possehl, Gregory L. (1999). Indus Age: The beginnings. Oxford and IBH Publishing Corporation, New Delhi.

Reviewing

Each paper will be reviewed by three peers. Papers forwarded by members of the Editorial or Advisory Boards along with their comments would get processed faster and may be reviewed by two referees only.

Sample format for Authors is available in downloadable form at ISG website: www.isgindia.org/JOG/Sample_format.doc

Copyright

The copyright of the paper selected for publication will rest with the Indian Society of Geomatics. Corresponding author shall be required to sign a copyright assignment form, on behalf of all authors, once the paper is selected for publication. Authors are, however, at liberty to use this material elsewhere after obtaining permission from the Indian Society of Geomatics.

If the authors have used any copyright material in their manuscript, it is understood that they have obtained permission from the owner of the copyright material and they should convey the same along with the manuscript to the Chief Editor.

Certificate of Original Work

The authors will also provide a certificate that the paper is an original work, not published or being considered for publication elsewhere.

In the event the certificate turns out to be false, the Journal shall ban the author(s) from publishing in the Journal for a period of five years and inform the same to all other related publications.

Reprints

Authors will be allowed to download the (PDF) of their paper from ISG Website www.isgindia.org, No hard copy reprints will be provided.

Journal of Geomatics

Advertisement Rates

	1 Issue	4 Issues
Back Cover Page in colour	**Rs. 25,000**	**Rs. 80,000**
Inside Cover Page in colour	**Rs. 20,000**	**Rs. 64,000**
Full Page inside in colour	**Rs. 15,000**	**Rs. 48,000**
Full Page inside in B/W	**Rs. 10,000**	**Rs. 32,000**

Advertisement Details

Mechanical Details
Double Spread/Center Spread (42 x 29.7) cm
Full page bleed (21 x 29.7) cm
Full page non-bleed (19 x 27.7) cm

Art Requirements

Negatives: Art must be right reading, emulsion, down. Film must be supplied in one piece per color, each identified by color. Camera-ready art is accepted for black & White adds; however, film is preferred. Electronic Files are also accepted.

Electronic File Requirements: All material must be received before ad close dates.

Software: Adobe illustrator 9.0 (saved as EPS). Adobe Photoshop CS (saved as EPS or TIFF). Please convert higher versions down. If you can only supply an IBM format, the file must be in viewable EPS or TIFF format with fonts embedded as that format.

Colour Ads: Colour separations must be provided, right reading, emulsion down. Please note that files using RGB or Pantone colours (PMS) must be converted to CMYK before we receive files.

Journal of Geomatics Vol 17, No. 2, October 2023

To,
The Secretary, Indian Society of Geomatics
6202, Space Applications Centre (ISRO)
AHMEDABAD – 380 015. INDIA

Sir,
I want to become a Member/ Life Member/ Sustaining Member/ Patron Member/Foreign Member/Student Member of the Indian Society of Geomatics, Ahmedabad for the year _____. Membership fee of Rs._____/- is being sent to you by Cash/DD/Cheque. (In case of DD/Cheque No.____dated_____drawn on Bank.

_____ . I **agree to abide by the Constitution of the Society.**

Date:

Place: **Signature**

- Name: Mr/Ms/Mrs/Dr_____
- Address: _____

_____PIN: _____

- Phone:_____Fax:_____Email:_____
- Date of Birth _____
- Qualifications_____
- Specialisation: _____
- Designation: _____ Organisation. _____
- Membership in other Societies: _____
- Mailing Address: _____

_____PIN: _____

Proposed by:
(Member's Name and No)
Signature of Proposer

For Office Use: A/P/L Member No.		Receipt No.		Date:	

Indian Society of Geomatics (ISG), Room No. 6202 Space Applications Centre (ISRO), Ahmedabad-380015, Gujarat. Url: www.isgindia.org Phone: +91-79 26916202
Email: secretary@isgindia.org or sasharma@sac.isro.gov.in Fax +91-79-26916287

MEMBERSHIP FEES

Sr. No.	Membership Category	Life/Patron Membership fees ₹ Indian	Life/Patron Membership fees US $ Foreign	Annual Subscription ₹ Indian
1.	Annual Member	10	---	300
2.	Life Member a) Admitted below 45 years of age	2500	250	
	b) Admitted after 45 years of age	2000	200	
3.	Sustaining Member	---	---	2000
4.	Patron Member	50000	3000	---
5.	Student Member	10	---	100

MEMBERSHIP GUIDELINES

- Subscription for Life Membership is also accepted in two equal instalments payable within duration of three months, if so desired by the applicant. In such a case, please specify that payment will be in instalments and also the probable date for the second instalment (within three months of the first instalment).
- A Member of the Society should countersign application of membership as proposer.
- Subscription in DD or Cheque should be made out in the name of **'Indian Society of Geomatics'** and payable at Ahmedabad.
- Direct deposit in ISG A/Cs must include bank fee RS. 25/- for cash payment.
- Financial year of the Society is from April 1 to March 31.
- For further details, contact Secretary, Indian Society of Geomatics at the address given above.
- ISG has chapters already established at the following places. Ahmedabad, Ajmer, Bhagalpur, Bhopal, Chennai, Dehradun, Delhi, Hissar, Hyderabad, Jaipur, Ludhiana, Mangalore, Mumbai, Mysore, Pune, Shillong, Trichi, Srinagar, Vadodara, Vallabh Vidya Nagar, Visakhapatnam and Trivandrum. Applicants for membership have the option to contact Secretary/Chairman of the local chapter for enrolment. Details can be found at the website of the Society: www.isgindia.org.
- Journal of the Society will be sent to Life Members by softcopy only.

Indian Society of Geomatics (ISG), Room No. 6202 Space Applications Centre (ISRO),

Ahmedabad-380015, Gujarat. Url: www.isgindia.org Phone: +91-79 26916202

Email: secretary@isgindia.org or sasharma@sac.isro.gov.in Fax +91-79-26916287

Geomatics Revealed

IGiS

Integrated GIS & IP Software

VERSION 2.0

MAKE IN INDIA

National Awards on Technology
By The Former President of India,
Dr. A. P. J. Abdul Kalam

Launch of IGiS Version 2.0
By Padam Shri AS Kiran Kumar, Chairman, ISRO and
Shri Tapan Mishra, DIRECTOR, SAC, ISRO.

What's new in IGiS

IGiS Version 2.0 is full of enhancements which you'll appreciate every day. New advanced GIS/IP and SAR modules are vital now a days. New COM Based Architecture makes you even more productive. The more you do with IGiS Version 2.0, the more you'll wonder how you ever did without it.

Enhancements in IGiS Version 2.0

- Advanced GIS / Image Processing
- Microwave SAR Analysis
- Meteorological Analysis
- COM Based Scalable Architecture
- New Ribbon Bar GUI
- Python Customization
- OGC Standards

Product Development Partner

इसरो isro
Government of India | Department of Space
Indian Space Research Organisation - (ISRO)

SGL Scanpoint Geomatics Ltd.
www.scanpointgeomatics.com

Scanpoint Geomatics Ltd.
Corporate Office : 12, Abhishree Corporate Park, Iskcon - Ambli Road, Ahmedabad - 380 058. Gujrat (India)
[P] +91 2717 297096-98 [F] +91 2717 297039 [E] info@scanpointgeomatics.com [W] www.scanpointgeomatics.com

INDIAN SPACE RESEARCH ORGANISATION
GOVERNMENT OF INDIA

nrsc

इसरो isro

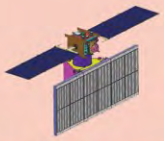

Only Organization in the Country
to Acquire & Supply
Satellite Data to Users

Aerial Acquisition for Specific
User Demands &
Disaster Management Support

Open Data & Value Added
Products Dissemination
Through Bhuvan

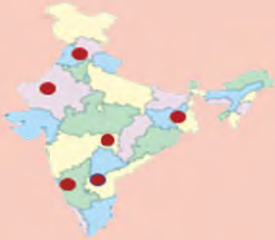

Region Specific Solutions

Capacity Building in
Remote Sensing Applications

A Smart Destination For Geospatial Solutions

National Remote Sensing Centre
Hyderabad, India
www.nrsc.gov.in
www.bhuvan.nrsc.gov.in
data@nrsc.gov.in